
Doctoral Dissertations

Student Theses and Dissertations

Spring 2018

Shear performance and behavior of long carbon fiber reinforced concrete

Benjamin Paul Gliha

Follow this and additional works at: https://scholarsmine.mst.edu/doctoral_dissertations



Part of the [Civil Engineering Commons](#)

Department: Civil, Architectural and Environmental Engineering

Recommended Citation

Gliha, Benjamin Paul, "Shear performance and behavior of long carbon fiber reinforced concrete" (2018). *Doctoral Dissertations*. 3094.

https://scholarsmine.mst.edu/doctoral_dissertations/3094

This thesis is brought to you by Scholars' Mine, a service of the Missouri S&T Library and Learning Resources. This work is protected by U. S. Copyright Law. Unauthorized use including reproduction for redistribution requires the permission of the copyright holder. For more information, please contact scholarsmine@mst.edu.

SHEAR PERFORMANCE AND BEHAVIOR OF LONG CARBON FIBER
REINFORCED CONCRETE

by

BENJAMIN PAUL GLIHA

A DISSERTATION

Presented to the Faculty of the Graduate School of the
MISSOURI UNIVERSITY OF SCIENCE AND TECHNOLOGY

In Partial Fulfillment of the Requirements for the Degree

DOCTOR OF PHILOSOPHY

in

CIVIL ENGINEERING

2018

Approved
Jeffery S. Volz, Co-advisor
Kamal Khayat, Co-advisor
Mohamed Elgawady
Dimitri Feys
Jason Baird

© 2018

BENJAMIN PAUL GLIHA

All Rights Reserved

ABSTRACT

In this study, a laboratory testing program was developed to investigate the shear performance of fiber reinforced concrete beams. Long carbon fibers, to be included with a traditional fresh concrete mix, were developed and their shear performance was evaluated and compared to the performance and behavior of unreinforced concrete, traditionally reinforced concrete, and fiber reinforced concrete (FRC) with other fiber types.

The experimental program consisted of 30 large-scale beams tested for shear performance under monotonic loading. In addition to the large-scale beams, small-scale specimens were constructed of the same materials to correlate large-scale performances to ASTM C1609 testing and to determine if the FRC met the requirements to replace the minimum transverse reinforcement, as required by ACI 318-14. The main parameters investigated were fiber volume fraction, fiber type, and beam depth. Fibers were included at volume fractions between 0.5% and 2.0% for the small-scale testing and 0.5% and 1.0% for the large-scale testing. In addition to the LCFRC specimens tested, specimens including steel fibers and a proprietary, olefin fiber were also tested. The carbon and olefin fibers had an aspect ratio of 32, while the steel fibers had an aspect ratio of 80. The two beam depths tested were 18 in. and 24 in. (457 and 610 mm).

All full-scale, fiber reinforced beams exceeded the ACI 318-14 shear capacities for minimum shear reinforcement. Beam depth did not result in any significant change in the performance of the beams. A mechanistic-based model proposed by the research team reasonably predicted the shear performances of the FRC beams.

ACKNOWLEDGMENTS

This dissertation would not have been possible without the guidance and the help of several individuals who in one way or another contributed and extended their valuable assistance in the preparation and completion of this study.

First and foremost, my utmost gratitude to my advisor, Dr. Jeffery S. Volz, Associate Professor at The University of Oklahoma, the guidance and support he provided me undoubtedly led to the successful completion of this study and consequently this dissertation.

Dr. Kamal Khayat, Dr. Dimitri Feys, Dr. Mohamed Elgawady and Dr. Jason Baird for their inputs and guidance in producing a dissertation that clearly presents the results attained from the study.

The laboratory and research staff at Missouri S&T who provided countless hours in and outside of the lab leading to timely completion of this study, especially John Bullock, Gary Abbott, and Brian Swift.

The Civil Engineering Department staff of Missouri S&T who were always looking to help out in any way and answering all my questions along the way.

My main research colleague, Darwin “Ish” Keener, for his countless hours of dedication to support the completion of this study.

Jamie, for all the nudges, urges, pushes, and kicks to get me across the finish line and the continuous love and support throughout the entire process.

Last but not the least, my family for the continuous support throughout my education and always believing in me.

TABLE OF CONTENTS

	Page
ABSTRACT.....	iii
ACKNOWLEDGMENTS	iv
LIST OF ILLUSTRATIONS	xi
LIST OF TABLES	xvi
SECTION	
1. INTRODUCTION.....	1
1.1. BACKGROUND	1
1.2. OBJECTIVE AND SCOPE OF WORK.....	2
1.3. RESEARCH PLAN	3
1.4. OUTLINE	5
2. LITERATURE REVIEW.....	7
2.1. CARBON FIBERS	7
2.2. FIBER REINFORCED CONCRETE.....	9
2.2.1. Compressive Strength of FRC.....	10
2.2.2. Direct Tension Strength of FRC.....	11
2.2.3. Flexural Strength of FRC	13
2.3. SHEAR THEORY OF PLAIN AND REINFORCED CONCRETE	15
2.3.1. Shear Behavior in Plain Concrete Beams.....	16
2.3.2. Shear Behavior in Reinforced Concrete Beams	20

2.4. SHEAR BEHAVIOR OF FIBER REINFORCED CONCRETE.....	22
2.4.1. Cross Section Shape	24
2.4.2. Beam Size.....	24
2.4.3. Shear Span to Effective Depth Ratio.....	25
2.4.4. Longitudinal Reinforcement Ratio.....	25
2.4.5. FRC Compressive Strength	26
2.4.6. Fiber Volume Fraction	26
2.4.7. Fiber Type	26
2.5. PREDICTION OF SHEAR STRENGTH OF FRC BEAMS	26
2.5.1. Sharma (1986).....	27
2.5.2. Narayanan and Darwish (1987).....	28
2.5.3. Ashour, Hasanain, and Wafa (1992)	29
2.5.4. Khunita, Stojadinovic, and Goel (1999).....	29
2.5.5. Dinh et al. (2011).....	30
3. EXPERIMENTAL PROGRAM.....	31
3.1. OVERVIEW OF THE EXPERIMENTAL PROGRAM.....	31
3.2. REVIEW OF PREVIOUS WORK ON LCFRC.....	33
3.2.1. Impact Testing.....	33
3.2.2. Blast Testing.....	34
3.3. OPTIMIZATION OF FIBER CONTENT, FIBER TYPE, AND MIX DESIGN.....	35
3.3.1. Carbon Fiber Processing	37
3.3.2. Mix Design Refinement	41

3.3.2.1 Batching process	43
3.3.2.2 Mix design 1	44
3.3.2.3 Mix design 2	45
3.3.2.4 Mix design 3	45
3.3.2.5 Mix design 4	45
3.3.2.6 Mix design 5	47
3.3.2.7 Mix design 6	47
3.3.3. Fiber Type Optimization	47
3.4. DESIGN OF LARGE SCALE BEAMS AND TESTED VARIABLES	48
3.4.1. Fixed Parameters of Large-Scale Beams.....	49
3.4.1.1 Shear span to effective depth ratio.....	49
3.4.1.2 Beam size	49
3.4.1.3 Selection of reinforcing bars	51
3.4.1.4 Concrete compressive strength	54
3.4.2. Control Beams.....	55
3.4.3. Varied Parameters of Large-Scale Beams.....	57
3.4.3.1 Fiber volume fraction.....	57
3.4.3.2 Beam depth	58
3.4.3.3 Fiber type	58
3.5. FABRICATION OF LARGE SCALE SPECIMENS	59
3.5.1. Reinforcing Steel.....	59
3.5.2. Formwork	61
3.5.3. Mix Design	62

3.5.4. Casting the Large-Scale Specimens	62
3.6. TESTING AND INSTRUMENTATION	65
3.6.1. ASTM 1609 Test Setup	65
3.6.2. Full-Scale Test Setup.....	66
3.7. MATERIAL PROPERTIES AND TESTING	67
3.7.1. Reinforcing Bars.....	67
3.7.2. Hardened Concrete Properties.....	70
3.7.2.1 Compressive strength.....	70
3.7.2.2 Modulus of elasticity	71
3.7.2.3 Splitting tensile strength	71
3.7.2.4 Flexural strength	71
4. RESULTS OF THE EXPERIMENTAL PROGRAM	73
4.1. PERFORMANCE AND BEHAVIOR OF FRC IN ASTM C1609 TESTING	73
4.1.1. Behavior of Specimens During Mix Design Refinement.....	77
4.1.2. Behavior of Specimens with Varied Parameters	84
4.1.2.1 Physical behavior of ASTM C1609 specimens	84
4.1.2.2 Load-displacement behavior of ASTM C1609 specimens	88
4.1.3. Equivalent Bending Stress, Toughness, and Equivalent Flexural Strength Ratio Behavior of ASTM C1609 Specimens.....	90
4.1.4. Evaluation of ASTM C1609 Results for ACI Requirements	98
4.1.5. Summary of ASTM C1609 Performance.....	99
4.2. PERFORMANCE AND BEHAVIOR OF 18 in. (457mm) DEEP BEAMS..	100
4.2.1. Beam Series B18-PC	104

4.2.2. Beam Series B18-TR.....	108
4.2.3. Beam Series B18-B5-0.5.....	113
4.2.4. Beam Series B18-B5-0.75.....	117
4.2.5. Beam Series B18-B5-1.0.....	122
4.2.6. Beam Series B18-D1-1.0.....	128
4.2.7. Beam Series B18-S-0.75	133
4.3. PERFORMANCE AND BEHAVIOR OF 24 in. (610mm) DEEP BEAMS..	138
4.3.1. Beam Series B24-B5-0.5138.....	138
4.3.2. Beam Series B24-B5-0.75.....	142
4.3.3. Beam Series B24-B5-1.0.....	147
5. ANALYSIS AND DISCUSSION OF RESULTS.....	155
5.1. ANALYSIS OF ASTM C1609 PERFORMANCE AND BEHAVIOR.....	155
5.1.1. Overall Load-Displacement Behavior of Specimens	157
5.1.2. Equivalent Bending Stresses Compared to Fiber Type and Content ...	162
5.1.3. Equivalent Flexural Strength Ratio Compared to Fiber Type and Content	165
5.1.4. Comparison Between ASTM C1609 and Large-Scale Shear Tests.	166
5.1.5. Evaluation of FRC to be Used in Place of Minimum Shear Reinforcement	167
5.2. ANALYSIS OF LARGE-SCALE SHEAR BEAM PERFORMANCE AND BEHAVIOR	170
5.2.1. Overall Load-Displacement and Shear Stress Analysis	171
5.2.2. Failure Modes.....	174
5.2.3. Crack Development and Behavior	175

5.2.3.1 Inclined crack spacing	176
5.2.3.2 Inclined crack angle	177
5.3. EFFECTS OF VARIED PARAMETERS ON LARGE-SCALE SHEAR TESTING	180
5.3.1. Effect of Fiber Volume Fraction	181
5.3.2. Effect of Beam Depth.....	182
5.3.3. Effect of Fiber Type	183
5.4. PREDICTION OF SHEAR PERFORMANCE OF FRC BEAMS	183
5.4.1. Prediction of Shear Performance Based on Previous Research	183
5.4.2. Prediction of Shear Performance Using Mechanics-Based Model	184
5.4.2.1 Prediction of shear force resisted by the compression region ..	186
5.4.2.2 Prediction of shear force resisted by fiber tension.....	190
6. FINDINGS, CONCLUSIONS, AND RECOMMENDATIONS	198
6.1. SUMMARY OF RESEARCH PROGRAM	198
6.2. FINDINGS OF THE RESEARCH PROGRAM	200
6.3. CONCLUSIONS	202
6.4. RECOMMENDATIONS.....	204
BIBLIOGRAPHY.....	205
VITA	209

LIST OF ILLUSTRATIONS

	Page
Figure 2.1. Compressive stress-strain curves for concrete with varying proportion of smooth steel fibers.....	11
Figure 2.2. Tensile stress-strain relationship for different types of SFRC	12
Figure 2.3. Different behaviors of FRC under flexural loading	14
Figure 2.4. Shear failure modes based on varying a/d ratio.....	18
Figure 2.5. Forces resisting shear failure in plain concrete sections	19
Figure 2.6. Stress distribution in longitudinally reinforced concrete beams	21
Figure 2.7. Typical concrete beam failure modes.....	21
Figure 2.8. Shear forces in reinforced concrete section.....	22
Figure 2.9. Distribution of stresses in a FRC beam	25
Figure 3.1. Fibers developed in previous research program	34
Figure 3.2. Total percent weight lost by each panel after blast loading	35
Figure 3.3. Results of previous research program of LCFRC	36
Figure 3.4. Photographs of each fiber variant.....	38
Figure 3.5. Concrete batching process after fiber addition.....	46
Figure 3.6. Beams and cylinders after consolidation.....	46
Figure 3.7. Series B18 beam details.....	55
Figure 3.8. Series B18 cross section details.....	55
Figure 3.9. Series B24 beam details.....	56
Figure 3.10. Series B24 cross section details.....	56
Figure 3.10. Series B18 beam during fabrication	60

Figure 3.11. Reinforcing cage for B18	60
Figure 3.12. Reinforcing cage for B24	61
Figure 3.13. Reinforcing cage and formwork.....	61
Figure 3.14. FRC transfer from concrete mixer to bucket.....	64
Figure 3.15. Concrete during placement into forms	64
Figure 3.16. ASTM C1609 test setup	66
Figure 3.17. Details of large-scale test setup from front.....	68
Figure 3.18. Details of large-scale test setup from side	68
Figure 3.19. Overall large-scale test setup.....	69
Figure 3.20. Strain gauge locations for Beam Series B18	69
Figure 3.21. Strain gauge locations for Beam Series B24	69
Figure 4.1. Typical ASTM C1609 beam after testing	76
Figure 4.2. Example of ASTM C1609 beam cross-section for fiber count documentation	76
Figure 4.3. Example of load-displacement curve with no post-peak hardening.....	77
Figure 4.4. Example of load-displacement curve with post-peak hardening.....	77
Figure 4.5. Distribution of (a) permanent displacement, (b) crack width, (c) crack location for each ASTM C1609 specimen tested during mix design refinement.....	80
Figure 4.6. Load vs. deflection curves of ASTM C1609 tests for mix design refinement.....	81
Figure 4.7. Equivalent stress results for ASTM C1609 testing for mix design refinement.....	83
Figure 4.8. Equivalent flexural strength ratio for ASTM C1609 testing for mix design refinement.....	83

Figure 4.9. Distribution of (a) crack width, (b) crack location, (c) permanent displacement for each ASTM C1609 specimen with varying fiber types and percentages	89
Figure 4.10. Load vs. deflection curves of ASTM C1609 tests, one	92
Figure 4.11. Load vs. deflection curves of ASTM C1609 tests, two.....	93
Figure 4.12. Load vs. deflection curves of ASTM C1609 tests, three.....	94
Figure 4.13. Load vs. deflection curves of ASTM C1609 tests, four	95
Figure 4.14. Equivalent stress results for ASTM C1609 testing	101
Figure 4.15. Equivalent flexural strength ratio results for ASTM C1609 testing.....	101
Figure 4.16. Load versus displacement behavior for beams in Series B18-PC	106
Figure 4.17. Crack behavior of beams in Series B18-PC after failure	107
Figure 4.18. Reinforcement strains for beams in Series B18-PC	108
Figure 4.19. Load versus displacement behavior for beams in Series B18-TR.....	111
Figure 4.20. Crack behavior of beams in Series B18-TR after failure	112
Figure 4.21. Reinforcement strains for beams in Series B18-TR.....	113
Figure 4.22. Load versus displacement behavior for beams in Series B18-B5-0.5	115
Figure 4.23. Crack behavior of beams in Series B18-B5-0.5 after failure	116
Figure 4.24. Reinforcement strains for beams in Series B18-B5-0.5	118
Figure 4.25. Load versus displacement behavior for beams in Series B18-B5-0.75	120
Figure 4.26. Crack behavior of beams in Series B18-B5-0.75 after failure	121
Figure 4.27. Reinforcement strains for beams in Series B18-B5-0.75	123
Figure 4.28. Load versus displacement behavior for beams in Series B18-B5-1.0.....	126
Figure 4.29. Crack behavior of beams in Series B18-B5-1.0 after failure	127
Figure 4.30. Reinforcement strains for beams in Series B18-B5-1.0	128

Figure 4.31. Load versus displacement behavior for beams in Series B18-D1-1.0.....	130
Figure 4.32. Crack behavior of beams in Series B18-D1-1.0 after failure	132
Figure 4.33. Reinforcement strains for beams in Series B18-D1-1.0.....	134
Figure 4.34. Load versus displacement behavior for beams in Series B18-S-0.75	136
Figure 4.35. Crack behavior of beams in Series B18-S-0.75 after failure.....	137
Figure 4.36. Reinforcement strains for beams in Series B18-S-0.75.....	140
Figure 4.37. Load versus displacement behavior for beams in Series B24-B5-0.5.....	141
Figure 4.38. Crack behavior of beams in Series B24-B5-0.5 after failure	144
Figure 4.39. Reinforcement strains for beams in Series B24-B5-0.5	145
Figure 4.40. Load versus displacement behavior for beams in Series B24-B5-0.75.....	147
Figure 4.41. Crack behavior of beams in Series B24-B5-0.75 after failure	149
Figure 4.42. Reinforcement strains for beams in Series B24-B5-0.75	150
Figure 4.43. Load versus displacement behavior for beams in Series B24-B5-1.0.....	151
Figure 4.44. Crack behavior of beams in Series B24-B5-1.0 after failure	152
Figure 4.45. Reinforcement strains for beams in Series B24-B5-1.0	154
Figure 5.1. Load vs. deflection curves of ASTM C1609 tests.....	159
Figure 5.2. Examples of ASTM C1609 specimens after failure.....	160
Figure 5.3. Relationship between fibers crossing crack and post-cracking bending stress	160
Figure 5.4. Load vs. deflection curves of ASTM C1609 tests.....	161
Figure 5.5. Permanent displacement vs. V_f (%) for ASTM C1609 tests	161
Figure 5.6. Equivalent bending stresses vs. V_f (%) for ASTM C1609 testing	164
Figure 5.7. σ_{pc} vs. total fibers for ASTM C1609 testing.....	164

Figure 5.8. δ_{pc} vs. V_f (%) for ASTM C1609 testing	165
Figure 5.9. Equivalent flexural strength ratio (%) vs. V_f (%).....	168
Figure 5.10. Equivalent flexural strength ratio (%) vs. total fibers	168
Figure 5.11. Normalized shear stress vs. equivalent flexural strength ratio	169
Figure 5.12. Normalized shear stress vs. equivalent flexural strength ratio	169
Figure 5.13. Comparison of ASTM C1609 beam performance to ACI 318-14 requirements	170
Figure 5.14. Box plot of maximum shear stresses for each beam series	173
Figure 5.15. Normalized shear stress vs. midspan deflection for large-scale testing	173
Figure 5.16. Inclined crack spacing vs. normalized shear stress	178
Figure 5.17. Inclined crack spacing vs. V_f for the large-scale shear tests	178
Figure 5.18. Normalized shear stress vs. inclined crack angle	179
Figure 5.19. Inclined crack angle vs. V_f for large-scale shear tests.....	179
Figure 5.20. Average inclined crack angle vs. V_f for large-scale shear testing	180
Figure 5.21. Normalized shear stress vs. V_f for each large-scale shear beam series	181
Figure 5.22. Shear strength prediction of FRC beams in this study using proposed equations from previous research.....	185
Figure 5.23. Proposed model to predict shear strength of FRC beams.....	187
Figure 5.24. Normal compressive and shear stress relationship developed by Bresler and Pister (1958).....	189
Figure 5.25. Stress-strain relationships in a RC beam	190
Figure 5.26. Derivation of uniform tensile stresses and crack width relationship.....	191
Figure 5.27. Measured vs. predicted shear stresses for each series based on ASTM C1609 data.....	195
Figure 5.28. Measured vs. predicted loads based on empirical equation	197

LIST OF TABLES

	Page
Table 2.1. Typical properties of various types of carbon fiber	9
Table 3.1. Zoltek 48K carbon fiber tow properties.....	39
Table 3.2. Mix design properties.	42
Table 3.3. Mix design constituents.	42
Table 3.4. Fiber mechanical properties.....	48
Table 3.5. Design parameters of beam Series B18 and B24.....	51
Table 3.6. Shear beam design and construction dimensions	51
Table 3.7. Beam design shear and flexural strength	52
Table 3.8. Properties of fibers included in large-scale test beams.....	58
Table 3.9. Batch weights for each beam series	63
Table 3.10. Summary of reinforcing bar yield strength.....	70
Table 3.11. Summary of large-scale beam compressive strength test results.....	72
Table 3.12. Summary of modulus of elasticity test results at 28 days	72
Table 3.13. Summary of splitting tensile stress test results	72
Table 4.1. Physical behavior for each ASTM C1609 specimen tested during mix design refinement.....	79
Table 4.2. Equivalent bending stress results from ASTM C1609 testing for mix design refinement.....	82
Table 4.3. Physical behavior for each ASTM C1609 specimen tested.....	85
Table 4.4. Equivalent bending stress results from ASTM C1609 testing for fiber development phase.....	95
Table 4.5. Load and failure data for Series B18 and B24 shear beams	102

Table 4.6. Crack behavior data for B18 and B24 series shear beams.....	103
Table 5.1. Average ASTM C1609 results for each set of beams.....	156
Table 5.2. Average response of beam series to large-scale shear testing	171
Table 5.3. Predicted and measured shear strengths for each beam series.....	196

1. INTRODUCTION

1.1. BACKGROUND

Typically, reinforced concrete (RC) sections used for structural applications are subjected to both moment and shear forces. Of the two, shear failure is usually more dangerous due to its unpredictable and sudden failure behavior. RC sections today include transverse steel reinforcement, intended to resist the tensile forces that develop in the web of the section, once inclined cracks propagate. This reinforcement is labor-intensive to install and due to design considerations, leads to areas of congested steel that prohibit proper placement of fresh concrete especially around beam-column connections.

Since the 1960's, fiber reinforced concrete (FRC) has been developed and researched because of its improved properties and behavior compared to that of plain concrete, as well as its potential for reduction in labor costs and steel congestion. Fibers made from steel, glass, synthetic, and natural materials have all been shown to improve certain characteristics of hardened concrete. Of these materials, steel fiber reinforced concrete (SFRC) has been studied extensively for its flexural behavior and shear resistance. Currently, ACI 318-14 "Building Code Requirements for Structural Concrete" allows the use of deformed steel fibers in place of minimum stirrup reinforcement, if the SFRC meets certain requirements. ACI 544.4R-09 "Design Considerations for Steel Fiber Reinforced Concrete" presents current research findings and some equations to use as a design methodology for SFRC in specific applications, but it is clear further research is required to fully understand the capabilities of all FRC materials.

As a result of the work completed by Volz et al. (2009) and the impressive blast and impact results demonstrated by the long carbon fiber reinforced concrete (LCFRC)

developed in the study, further development was undertaken to evaluate the flexural toughness and shear resistance capabilities of the material. The addition of carbon fibers to concrete has been investigated in the past, but little research has been done regarding the structural performance and behavior of carbon fiber reinforced concrete. There is also a need for the development of design parameters for using FRC for structural applications.

1.2. OBJECTIVE AND SCOPE OF WORK

The main *objective* of this study was to further develop the long carbon fibers previously investigated for blast and impact applications to improve the fresh and hardened properties of the LCFRC, as well as understand the shear performance and behavior through small-scale material testing and large-scale shear testing.

The following scope of work was implemented in an effort to attain the objective of the study:

- Review applicable literature
- Develop a research plan
- Further develop long carbon fibers to improve both fresh and hardened FRC properties
- Perform small-scale testing to evaluate changes to fiber processing method, volume fraction, and fiber type
- Design, construct, and test full-scale specimens to failure
- Analyze the information gathered throughout development and testing to provide further insight on the shear performance and behavior of FRC

- Evaluate the LCFRC for use in concrete construction as outlined by ACI 318-14
- Provide a design approach for LCFRC for use as shear reinforcement
- Develop conclusions and recommendations
- Prepare this dissertation to document the details, results, findings, conclusions, and recommendations of this study

1.3. RESEARCH PLAN

The proposed research plan includes seven (7) tasks necessary to successfully complete the study. They are as follows:

Task 1: Review applicable literature. In order to fully understand the topic and to become familiar with previous research related to this subject, all applicable literature must be reviewed. This step establishes the current state of the art, allows for the adoption of test methods, and gives a basis for comparison of results from this study to others.

Task 2: Further develop long carbon fibers through different processing methods commercially available. Previously, a 4-in.-long (102 mm) carbon fiber with an aspect ratio of approximately 32 was developed using a polypropylene backbone to provide rigidity to the carbon fiber tow during mixing. The intention of this task was to evaluate the ability of different processing methods to provide the necessary resiliency and dispersibility properties to the carbon fiber tow for it to handle the mixing of the fresh concrete.

Task 3: Further develop a mix design that provided the necessary paste volume to have a homogenous LCFRC with fiber volume fractions up to 2.0%, while avoiding the use of unnecessary additives and reducing cost of production as much as possible.

Task 4: Perform material and small-scale testing of LCFRC at different volume fractions to understand the impact on performance and ability to comply with ACI 318-14 requirements for use as minimum transverse reinforcement. ASTM C1609 testing was used to evaluate the flexural toughness of the FRC and the results were used to develop the large-scale testing protocol of the study.

Task 5: Develop and perform large-scale shear testing. As current shear provisions for traditional RC are primarily based on empirical data, it was important to understand the performance and behavior of large-scale LCFRC specimens. The large-scale testing was limited to shear testing only and included beams constructed with materials from the local Ready Mix concrete plant to ensure potential use with traditional construction practices. The tested beams were flexurally reinforced to ensure failure due to shear. FRC beams were constructed with different fiber volume fractions, fiber types, and beam depths in order to understand the characteristics of each variable.

Task 6: Analyze the information collected in the study. The material, small, and large-scale tests were analyzed to evaluate the shear performance and behavior of the FRC specimens. The collected data included compressive strength data, ASTM C1609 testing for each set of large-scale specimens, load-deflection data, flexural reinforcement strains, and crack behavior of large-scale specimens. The FRC beams were compared to predicted shear strengths of RC beams containing minimum transverse reinforcement. Finally, a comparison between the collected data and a proposed, mechanics-based model for prediction of shear performance of LCFRC was analyzed to determine the potential for the carbon fibers to serve as minimum shear reinforcement.

Task 7: Develop findings, conclusions, and recommendations based on the results collected in this study.

The dissertation that follows will serve as the evidence of this study for reference of future research work. It will include a literature review, comprehensive review of the experimental program and results collected, as well as conclusions and recommendations from each task included in the study.

1.4. OUTLINE

This dissertation includes six (6) sections, which present a comprehensive overview of the experimental program, as well as detailed results and analysis. The following section details where specific information can be found in this document.

Section 1 includes background information and the motivation for performing the study. It also contains the objective and detailed research plan needed to complete the study.

Section 2 includes a review of all applicable literature used in this study. To date, little research has been conducted in the areas of carbon fiber reinforced concrete for shear applications.

Section 3 details the entire research program. In addition to the fiber development and mix design refinement phases of the research, the large-scale testing included 30 tests performed on full-scale, PC, RC, and FRC beams, as well as material and component testing to establish compressive and flexural strength relationships to the large-scale tests. This section details the fabrication of specimens, testing setups, and data acquisition used throughout the study.

Section 4 presents an extensive overview of the results collected in this study. First, the results of the small-scale testing, used to evaluate the FRC during mix design and fiber refinement phases, are presented. This is followed by an extensive overview of the load-displacement behavior, crack development and behavior, and reinforcement strains collected in the large-scale testing portion of the study.

Section 5 provides an overview of the analysis data collected during the experimental program. The effects of fiber type and volume percentage on the ASTM C1609 performance and behavior are analyzed, as well as the shear performance of the large-scale beams. The relationship of the small-scale testing to the large-scale shear tests is also presented. In addition, the large-scale FRC beam performances are compared to predicted shear strengths of minimally reinforced concrete beams. Finally, a mechanics-based model for the prediction of LCFRC shear performance is presented and compared to the data gathered in this study.

Section 6 concludes this document with a presentation of the findings, conclusions, and recommendations for future research.

2. LITERATURE REVIEW

A significant amount of research has been performed on fiber reinforced concrete (FRC), including studies on the performance of FRC beams undergoing flexural and shear loads. Typically, steel fibers have been used in previous studies due to the maturity in their development, relative acceptance in the construction market, and economical cost versus performance. In recent years, the use of carbon fibers in the aerospace industry, and their subsequent reduction in cost due to improved manufacturing processes, has facilitated wider use in other industries. Also, the length of carbon fibers used in this study were significantly longer than the typical fiber tested to date. This literature review will provide background information on carbon fibers and FRC, as well as give an overview on shear behavior of traditional concrete and FRC.

2.1. CARBON FIBERS

Carbon fibers are extremely thin strands having a micro-graphite crystalline structure with diameters typically ranging from 0.0002 to 0.0005 in. (5.1 to 12.7 μm), approximately 1/10 the diameter of a human hair (Morgan, 2005). The fibers are primarily composed of carbon atoms bonded together in microscopic crystals that are predominantly aligned parallel to the long axis of the fiber. This crystal alignment results in the incredibly high strength-to-weight ratios associated with the material.

In 1996, the American Concrete Institute (ACI) Committee 544 published a report on FRC. This report was first reapproved in 2002 and then again in 2009. In this report, fibers are classified into four types: steel, glass, synthetic, and natural fiber materials. Carbon fiber, the type used in this study, is considered a synthetic fiber material. There are

different types of carbon fiber produced for a variety of industries; Table 2.1 shows typical properties of four different types of carbon fiber.

The two main types of carbon fiber are PAN and pitch fibers. PAN fibers are made from polyacrylonitrile, while pitch fibers are made from coal pitch or petroleum. PAN fibers are generally available in high modulus (HM) and high tensile strength (HT). Pitch fibers are produced as general purpose (GP) or high performance (HP). In the past, carbon fibers were uncommon in civil engineering applications due to their high cost, but as the manufacturing processes improved, the cost decreased, and industry leaders are realizing the beneficial qualities of carbon fiber (ACI 544.1, 2009).

The basic unit of manufactured carbon fiber is the tow (Morgan, 2005). A tow consists of an untwisted bundle of continuous filaments usually containing several thousand fibers. Tow sizes are designated with a number followed by a “K”, which represents how many thousands of filaments are contained in the particular tow. For example, a 25K tow contains 25,000 filaments. Typical tow sizes are 3K, 6K, 12K, and 24K. Other sizes are available at a premium. There are typically two grades of carbon fiber tow produced in the market, aerospace grade and commercial grade. In addition to price, the difference between the two grades is the strength and stiffness, with aerospace grade representing the higher-end product. The final preparation of a carbon fiber tow involves coating the material with a sizing agent, often epoxy-based, to protect the material and allow it to bond with subsequent resins. The amount of sizing depends on the final use of the material but typically ranges from 0.5 to 1.5 percent by weight.

Table 2.1. Typical properties of various types of carbon fiber (ACI 544.1, 2009)

Fiber Type	Equivalent Diameter (in x 10 ⁻³)	Specific Gravity	Tensile Strength (ksi)	Elastic Modulus (ksi)	Ultimate Elongation (%)	Melt, Oxidation, or Decomposition Temperature (°F)
Carbon, PAN HM	0.3	1.6-1.7	360-440	55,100	0.5-0.7	752
Carbon, PAN HT	0.35	1.6-1.7	500-580	33,400	1.0-1.5	752
Carbon, Pitch GP	0.39-0.51	1.6-1.7	70-115	4,000-5,000	2.0-2.4	752
Carbon, Pitch HP	0.35-0.70	1.8-2.15	220-450	22,000-70,000	0.5-1.1	932

2.2. FIBER REINFORCED CONCRETE

Fiber reinforced concrete has been widely researched and has become a prominent material within the civil engineering discipline (ACI 544.1, 2009; ACI 544.2, 2009). Although the focus of this study is on shear performance, FRC is utilized in many other types of construction including slabs on grade, mining, tunneling, and excavation support applications. Steel and synthetic fiber reinforced concrete and shotcrete have been used in lieu of welded wire fabric reinforcement (ACI 554.1, 2009). Although steel is the most common type of fiber used in FRC, other fibers including glass, acrylic, carbon, aramid, nylon, polyester, polyethylene, and polypropylene are used in concrete construction for their beneficial properties.

One key classification of FRC is the aspect ratio of the fibers included in the mix. The aspect ratio of a fiber is the ratio of its length to diameter. In the case of this study, an equivalent diameter can be used to calculate the aspect ratio. Generally, as the aspect ratio

of the fiber increases, the post-peak performance of the fiber improves because it is able to resist pullout from the matrix at higher loads. Increasing the aspect ratio can also be detrimental to the batching process of FRC because the fibers are more susceptible to balling. It is easier for the fibers to be bent over and entangled resulting in non-homogeneous dispersion of the fibers within the matrix (ACI 544.1, 2009).

One of the main reasons for the use of fibers in concrete is to increase the ductility of the section. The ductile behavior of the FRC allows for greater energy absorption and less damage to the section. In addition, as cracks propagate through the section, the fibers pull out of the matrix and this absorbs energy as well. Typically, adding fibers to the mix does not increase the compressive strength, but different fiber types have been shown to increase tensile, flexural, and shear strength (ACI 544.1, 2009).

2.2.1. Compressive Strength of FRC. Studies over the years have shown that the addition of fibers to concrete have had little effect to the ultimate compressive strength of the FRC mixture. There have been studies that have reported slight increases in compressive strength, depending on fiber type. Studies have also reported that compressive strength slightly decreased as the amount of carbon fiber reinforcement increased (Zheng and Feldman 1995). In general, the addition of fibers to the concrete matrix do not provide a benefit to the overall strength until cracks begin to form in the specimen. For concrete in compression, the addition of fibers does not significantly increase the first or post-peak strength. The addition of fibers however, can soften the failure of the specimen after peak strength, allowing it to carry higher stresses at higher strains, instead of losing the ability to carry load after peak strength, as is typical in plain concrete specimens. Figure 2.1 shows typical stress-strain relationships for compression tests of plain concrete compared to steel

fiber reinforced concrete (SFRC), with increasing volume fraction of fibers (ACI 544.4R, 2009).

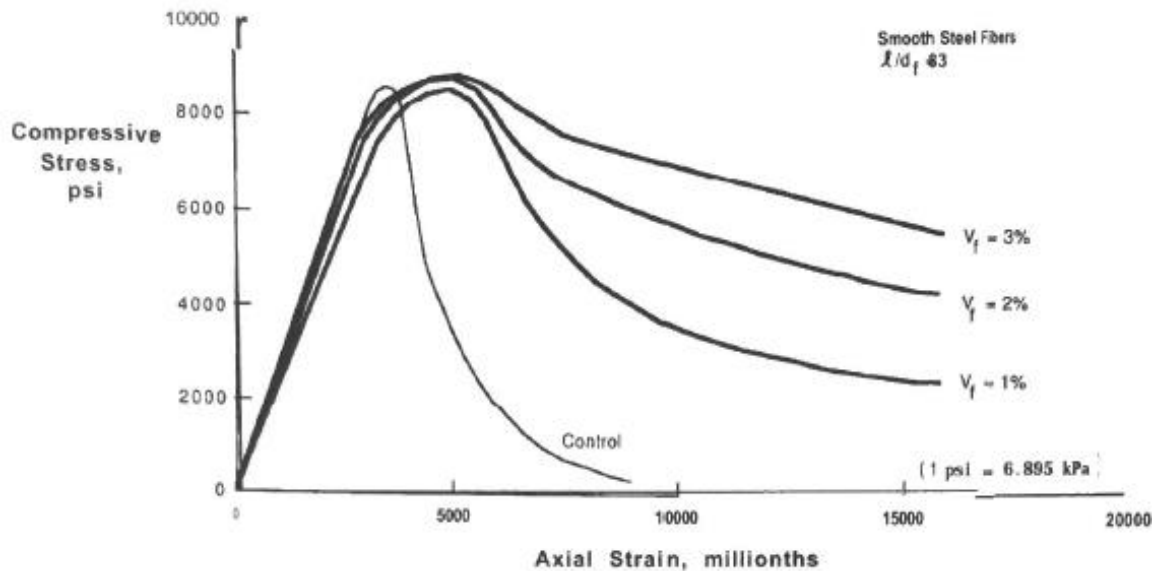


Figure 2.1. Compressive stress-strain curves for concrete with varying proportion of smooth steel fibers (ACI 544.4R, 2009)

2.2.2. Direct Tension Strength of FRC. To date, there is not a standard practice for the measurement of direct tension strength of FRC. This is due to the fact that experiments quantifying the direct tensile strength of FRC are difficult to perform. The results obtained weigh heavily on the test method, stiffness of the testing equipment, gauge length of displacement measurement, number of cracks, and location of cracks in the specimen. It is also difficult to restrain the ends of each specimen when performing the test. Due to these factors, the results of direct tensile tests on FRC are very scattered and difficult to compare from one study to another.

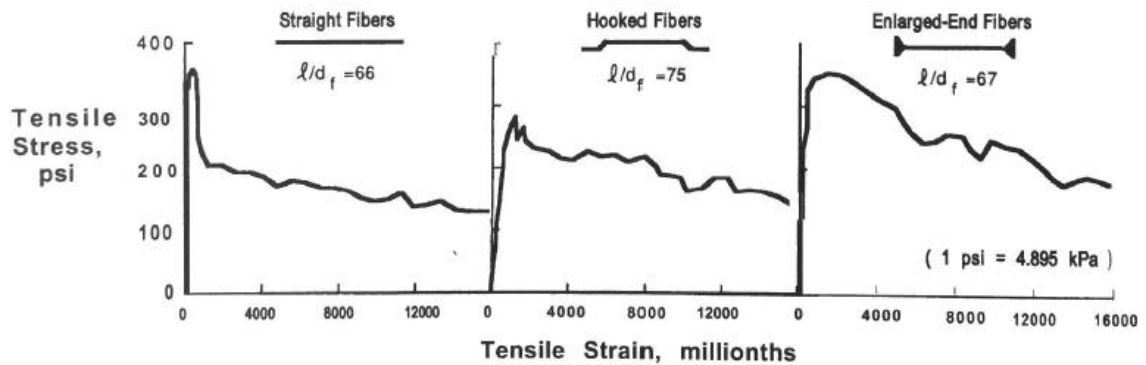


Figure 2.2. Tensile stress-strain relationship for different types of SFRC (ACI 544.4R, 2009)

The main influence in direct tensile performance, similar to the behavior of FRC under compression loading, comes after the cracks form and the fibers are able to sustain load across the cracked concrete section, where plain concrete would no longer be able to carry a load. Figure 2.2 shows the stress strain relationship for tensile tests of straight, hooked, and enlarged-end SFRC. The results obtained from direct tensile tests are able to provide a peak post-cracking stress value, σ_{pc} , or the peak stress that the FRC composite is able to carry after the first crack is formed in the matrix. Tests have shown that as fiber aspect ratio increases, the peak post-cracking stress increases in FRC specimens. The same trend also is typical as fiber volume fraction and bond characteristics increase for FRC specimens.

When comparing bond characteristics, hooked-end and enlarged-end steel fibers have much better capability to bond with the concrete matrix compared to straight fibers. This is due to the mechanical interlock that is formed between the fiber and concrete matrix once the concrete hardens around the discrete fibers. This is also similar for synthetic fiber reinforced concrete (SNFRC). Typically, synthetic fibers are fibrillated in order to increase

their bond characteristics with the concrete matrix. Naaman and Najm (1991) found that increasing the concrete strength also resulted in an increase in the bond strength of plain and hooked-end steel fibers. The study also showed that hooked-end fibers required a higher pull-out force due to the fiber yielding during pull-out of the matrix. The researchers found that increasing the embedment depth for hooked-end steel fibers did not result in a significant increase in the bond strength of the fiber, further reinforcing the prior finding.

2.2.3. Flexural Strength of FRC. Similar to the behaviors discussed above, the enhancement in the flexural strength of the FRC matrix does not result until the first crack is formed. At this point, the fibers sustain the tensile forces in the specimen. The influence of fibers, especially those with high tensile strength, on the flexural strength of fiber reinforced concrete is much more pronounced than with the compressive or direct tensile strength. ACI 544.4R (2009) suggests that two values from flexural tests should be reported, the first being the first-crack flexural strength and the second corresponding to the maximum load achieved after the first crack is formed. Stresses from these loads are calculated according to ASTM C78. Studies have shown that all types of fibers (steel, synthetic, glass, and natural), when added to concrete, can have an effect on the post-peak strength of specimens.

Another important measurement taken from flexural tests of FRC is the toughness. Toughness is a measurement of the energy absorption capacity of the material, or its ability to resist fracture. Figure 2.3 shows two different behaviors typical of FRC during a flexural test. The graph on the left shows a sudden drop in load following the first cracking load, but the material still has the ability to carry some load as the deflection is increased. The graph on the right shows the material's ability to carry an increased load after the first crack

is formed in the specimen. The graph on the right has a much larger area under the load-deflection curve, which corresponds to a much higher toughness value.

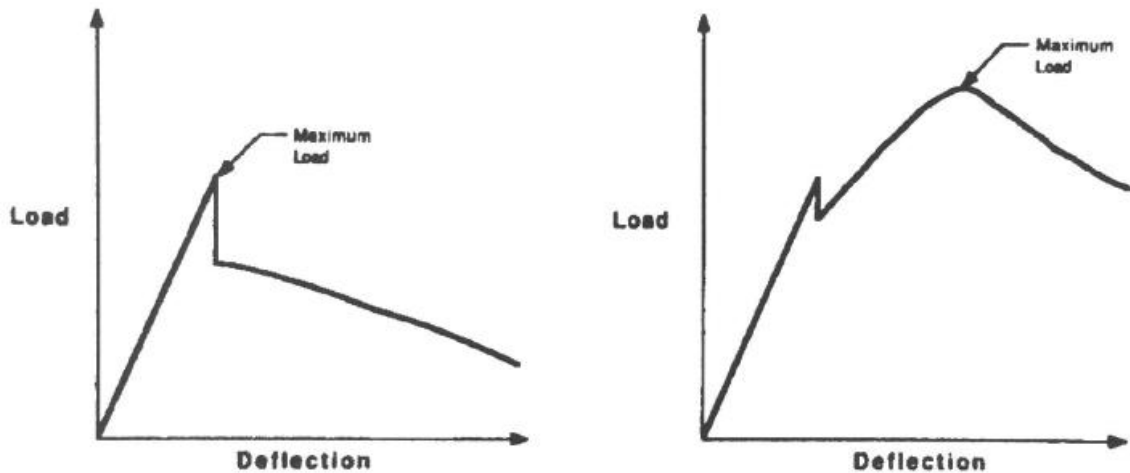


Figure 2.3. Different behaviors of FRC under flexural loading (ACI 544.2R, 2009)

Two different ASTM procedures have been used to perform flexural testing on FRC specimens. ASTM C1018 “Standard Test Method for Flexural Toughness and First-Crack Strength of Fiber-Reinforced Concrete (Using Beam with Third-Point Loading)” is the more historical standard of the two, but the principle is the same as in the ASTM C1609 “Standard Test Method for Flexural Performance of Fiber-Reinforced Concrete (Using Beam with Third-Point Loading), which is the current standard to measure the flexural performance of fiber reinforced concrete. Both standards include small-scale, rectangular specimens, 6 in. x 6 in. x 18 in. or 4 in. x 4 in. x 14 in. (152x152x457 mm or 102x102x356 mm) that are tested under third-point loading. The ASTM C1609 test is controlled using a closed-loop, servo-controlled testing systems in order to precisely control the displacement

and load throughout the entire test. The beam is tested until an average midspan displacement of 1/150 (in.) is reached. The total area underneath the load-displacement curve represents the toughness of the specimen and this value is typically used during development of fibers as a basis for comparison. ACI 318-11 Section 5.6.6.2 permits the use of SFRC for shear resistance provided a minimum fiber percentage and minimum performances from ASTM C1609 tests are met. ACI 318-11 Section 11.4.6.1 permits the use of steel fiber-reinforced concrete used as minimum shear reinforcement provided minimum concrete strengths, beam dimensions, and shear design loads are followed.

Increasing interest in research pertaining to SFRC and ASTM C1609 performance has been seen in recent years, most likely due to the ACI 318-11 provisions. Dinh et al. (2009) showed that increasing volume fractions and aspect ratios of hooked-end steel fibers resulted in an increased flexural toughness in the specimens tested. Kim et al. (2008) investigated the flexural behavior of different fiber types and volume fractions and found that increasing volume fractions resulted an improved ASTM C1609 performance. The researchers also found that fibers that had higher tensile strength and better bond characteristics had increased flexural toughness values. Wille et al. (2012) investigated the effect of beam size, casting style, and support restraint on the specimen during testing and found that all three variables could have significant effect on the overall performance of the specimens.

2.3. SHEAR THEORY OF PLAIN AND REINFORCED CONCRETE

Compared to flexural failure, which for reinforced concrete is already a difficult parameter to model, shear failure proves further difficulty. This challenge is reflected in

the strength reduction factors, ϕ , from ACI 318-11. For tension-controlled sections, ϕ is taken at 0.9, for shear design ϕ is set to 0.75. This reduction is due to the high variability of test data for specimens failing in shear with multiple varied parameters from study to study. Typically, reinforced concrete sections intended for structural support are first designed for flexure and are designed to fail gradually, as a further safety factor in the overall design. Then, the shear design is completed and the transverse steel is proportioned so that the shear resistance, along the entire section, is higher than that of the flexural resistance. This is done because shear failures are typically brittle in nature and occur without any warning (MacGregor and Wight, 2005).

2.3.1. Shear Behavior in Plain Concrete Beams. In this section, the discussion will assume that the sections contain adequate flexural reinforcement to carry the force once flexural cracks form in the section. Without the flexural reinforcement, the section would fail due to flexure prior to the shear forces developing that would lead to cracks and, ultimately, failure.

For consistent width beams and concrete compressive strengths, the main factor determining the failure mechanism is the shear span (a) to depth (d) ratio (a/d). Figure 2.4(a) shows a beam loaded equally at two locations at a distance, a , from the support. Figure 2.4(b) relates the moment at the load point, which is the location of the highest shear force in the section, to the a/d ratio. The nominal moment capacity is represented by a horizontal line because regardless of the shear span length, the moment capacity will remain constant. The shaded region represents the gap in shear resistance delivered by the plain concrete section compared to the nominal moment capacity. This difference is typically accommodated for with mild steel as shear reinforcement, but in recent years steel

fibers have been permitted, provided certain conditions are met (MacGregor and Wight, 2005).

Figure 2.4(b) also shows that as the a/d ratio increases, different failure modes occur. For a/d ratios less than 1, the beams are considered very short or deep. Deep beams follow a strut and tie mode for transfer of forces, in which compression forces are transferred through the concrete between the support and load point, while the longitudinal steel carries the tensile forces. Once the diagonal cracks form in the section, the horizontal forces in the longitudinal steel can no longer be properly transferred and the beam usually suffers an anchorage failure of the longitudinal steel at the support. In the case of short shear spans, a/d between 1.0 and 2.5, diagonal cracks again form, starting at mid depth of the section. Due to the length of the shear span, the forces are able to redistribute slightly, which allows the section to carry an increased load. This failure typically results in crushing of the concrete at the loading point or splitting failure at the longitudinal reinforcement, causing bond failure between the concrete and longitudinal steel.

Once the a/d ratio is greater than 2.5, the predominant shear failure mechanism is diagonal tension due to an increasing width of the critical inclined crack. This failure is typical in beams with a/d ratios up to 6.5. Once the a/d ratio is greater than 6.5 the beams are considered very slender and will fail due to flexure without the formation of any inclined cracks. Figure 2.4(c) shows the same relationship, but with the shear load plotted on the y-axis. The shaded area shows the region between the maximum shear resistance and the available moment capacity (MacGregor and Wight, 2005).

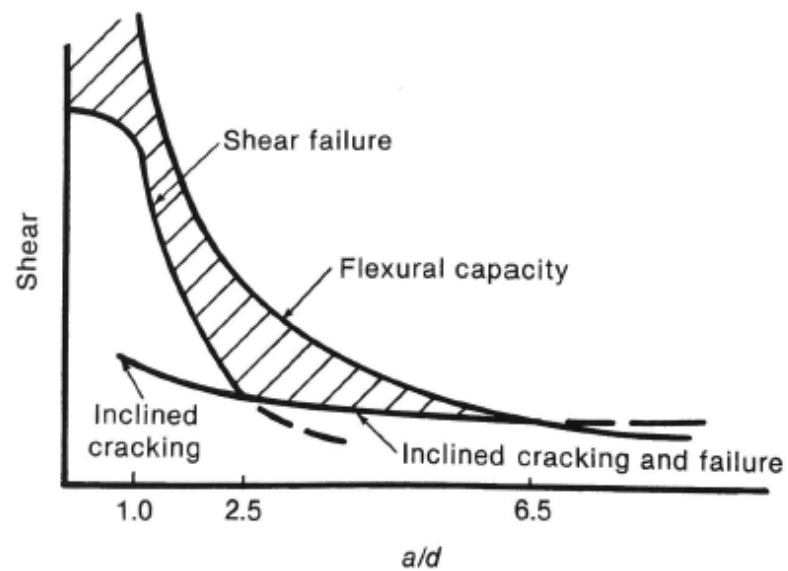
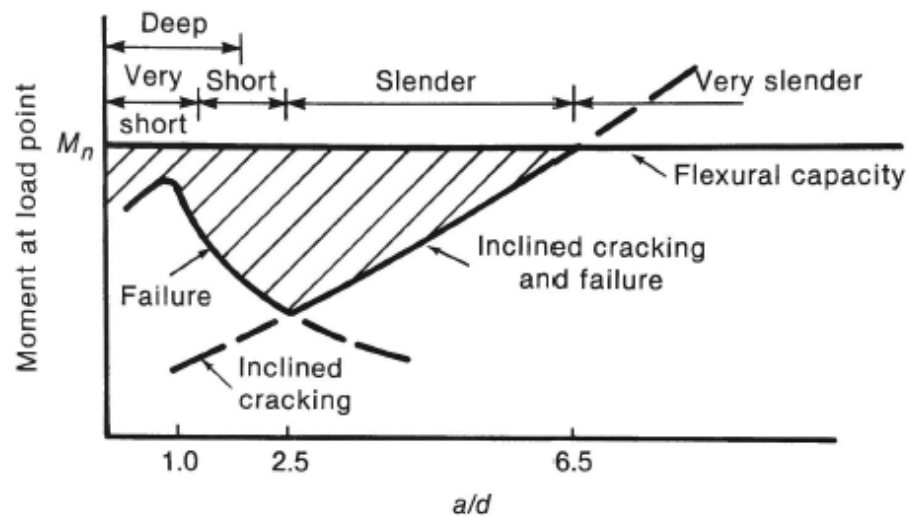
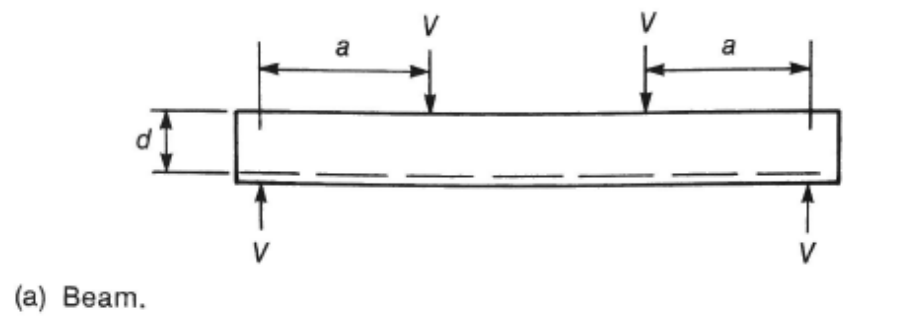


Figure 2.4. Shear failure modes based on varying a/d ratio (MacGregor and Wight, 2005)

In the case of beams with a/d ratios between 2.5 and 6.5, there are multiple forces acting throughout the section to carry the applied load. Figure 2.5 shows all forces presented in a plain concrete section once an inclined crack is formed. The first force, V_{cz} , acts along line A-B and is the shear force carried by the concrete compression zone. The shear force carried by the concrete compression zone is directly affected by the angle of the critical inclined crack and its degree of penetration up through the concrete section. The work of Bresler and Pister (1958) provide the basis for design of shear resistance of the compression zone of a section based off the assumption of idealized stresses that are formed. Figure 2.6. shows the stresses in the concrete compression zone. This approach is further simplified using the Whitney stress block, adopted by ACI in 1956.

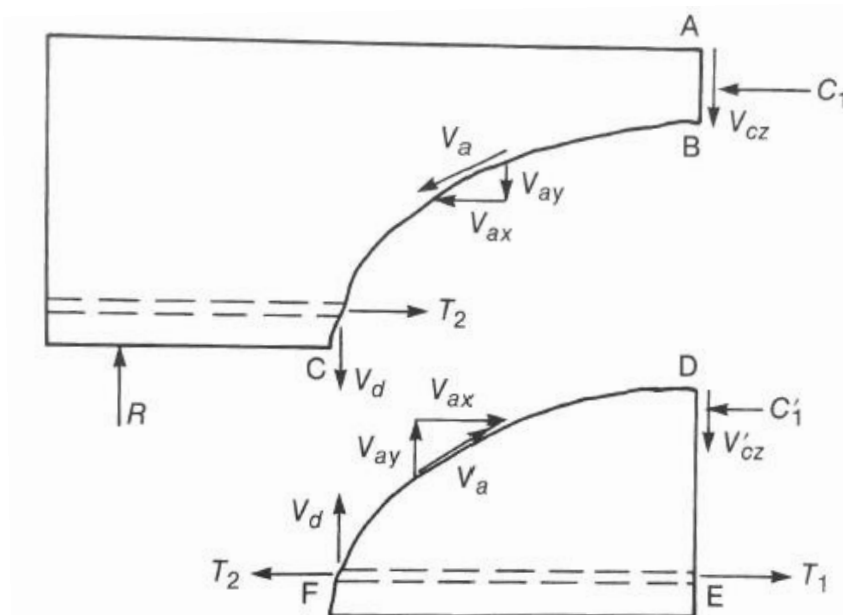


Figure 2.5. Forces resisting shear failure in plain concrete sections (MacGregor and Wight, 2005)

The second force transferring shear in concrete sections without web reinforcement is due to aggregate interlock (V_{ay}). The aggregate interlock forces result from friction between the uneven surfaces of the inclined crack that is formed. Essentially, the aggregate protruding from the concrete matrix prevents the two planes from sliding along each other. As the crack becomes wider, the influence of aggregate interlock on the shear resistance of the section is reduced. If the beam cannot properly redistribute the forces, the beam will fail. The final shear force transfer mechanism is through dowel action of the longitudinal steel, V_d . As the loads on the section are increased, the beam could split along the reinforcement over a short length. In plain concrete sections, all three of these forces interact with each other and stresses are redistributed until all three mechanisms fail. This interaction results in difficulty to accurately determine shear failure mechanisms. Figure 2.7 shows the primary failure modes of plain concrete beams as defined by ACI Committee 426 (1980).

2.3.2. Shear Behavior in Reinforced Concrete Beams. As mentioned previously, typically, plain concrete sections do not contain enough shear resistance to fail prior to flexure. For this reason, mild steel stirrup reinforcement is added to carry the shear forces in the section once inclined cracks are formed. Figure 2.8 shows the forces present in a stirrup-reinforced concrete section. The forces remain unchanged, but the shear force carried by the transverse steel is added as V_s . As shown, the stirrups are spaced at regular intervals to ensure that reinforcement is present at the location of the inclined crack. The stirrups allow the crack width to be controlled to a certain extent, which adds to the ability of aggregate interlock to resist shear forces. This also allows the formation of an increased

number of cracks to be formed increasing the overall capacity of the section (MacGregor and Wight, 2005).

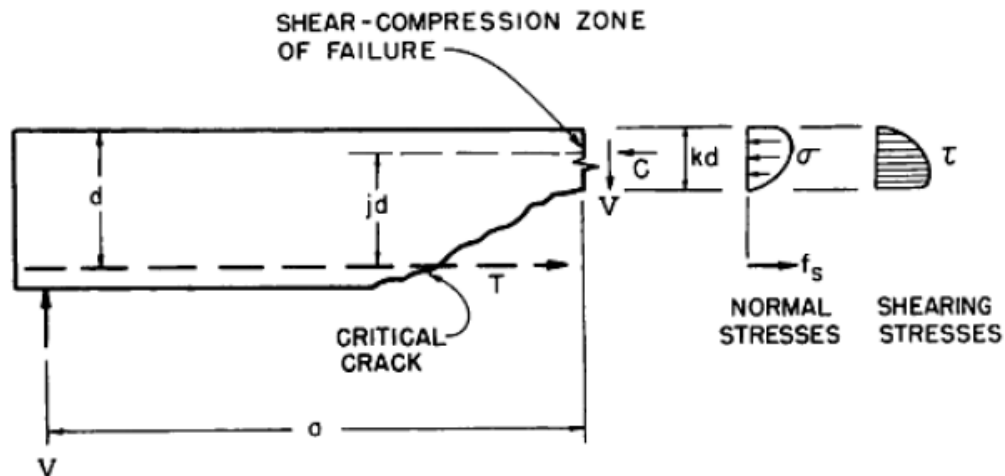


Figure 2.6. Stress distribution in longitudinally reinforced concrete beams (Bresler and Pister, 1958)

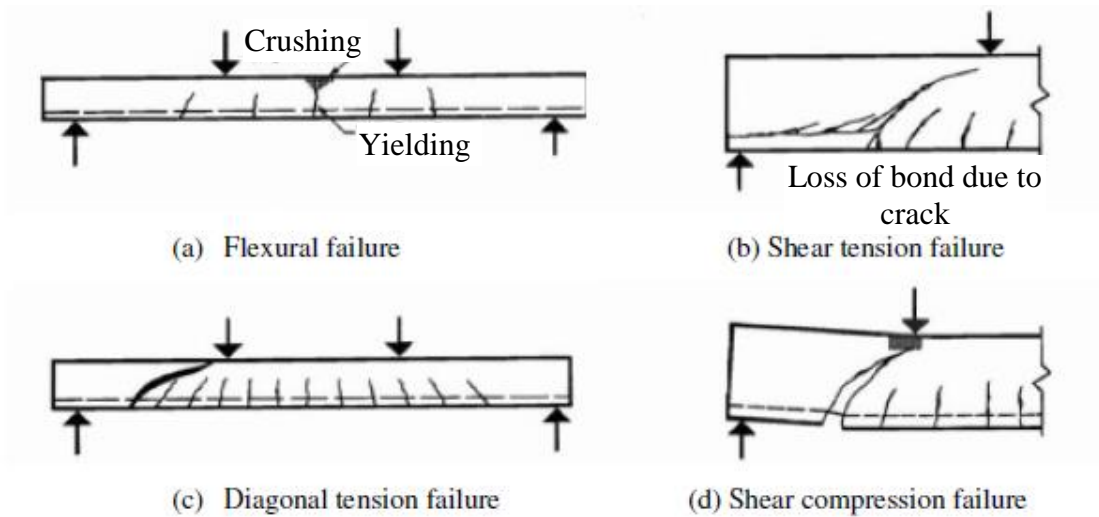


Figure 2.7. Typical concrete beam failure modes (ACI Committee 426, 1980)

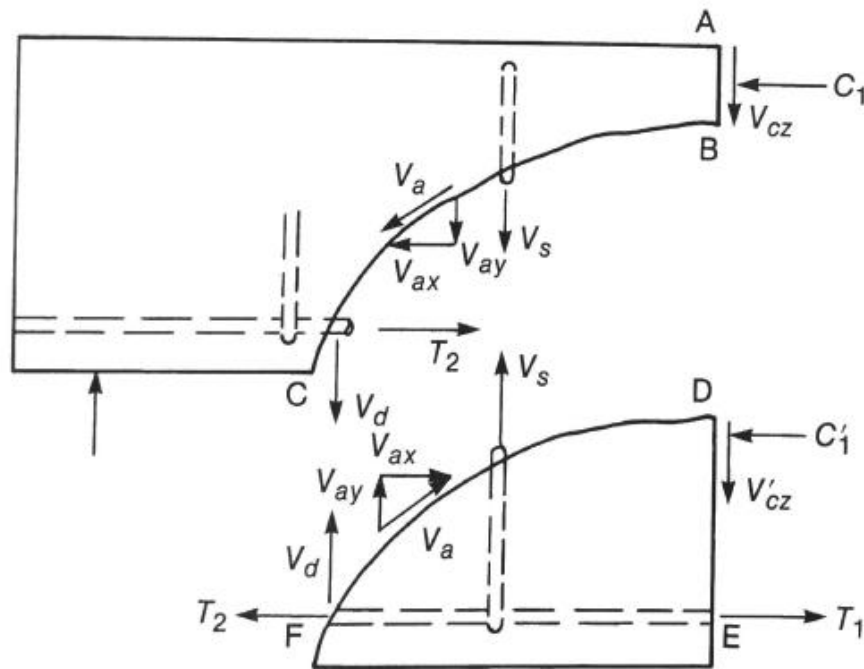


Figure 2.8. Shear forces in reinforced concrete section (MacGregor and Wight, 2005)

2.4. SHEAR BEHAVIOR OF FIBER REINFORCED CONCRETE

Shear behavior of fiber reinforced concrete has been studied since 1972, starting with Batson, Jenkins and Spatney. Subsequently, many studies were undertaken to understand the additional shear resistance provided to concrete beams by the fiber reinforcement. A significant portion of the work completed on the topic of shear behavior of FRC has been with steel fibers. This is due to the maturity of the products and the ability of steel fibers to carry significant forces at relatively low volume fractions. This factor is important when considering the placement of FRC in real-world jobsites, with the potential for beams containing high amounts of steel reinforcement.

In longitudinally-reinforced FRC beams without mild steel transverse reinforcement, fibers provide a similar resistance to that of stirrups, typically in reinforced

concrete sections. The difference is the discrete fibers are distributed randomly throughout the concrete matrix, instead of at distinct points along the length of the beam. As cracks develop in the section, the randomly-oriented fibers bridge the cracks and transfer shear forces similar to the stirrups in a traditionally reinforced concrete section. The presence of the fibers allows for the formation of an increased number of cracks, further enhancing the load-carrying capacity of the section. Figure 2.9 shows the distribution of stresses in a FRC beam. The shear stresses carried by the fibers are represented by a uniform stress acting over an idealized crack of a specific angle, α . The shear forces resisted by the fibers are represented by the stress σ_{fu} , and the resultant force V_f .

While the mechanisms of force transfer and ultimate shear failure may be similar between traditional reinforced concrete and FRC, there are added challenges presented in design. The first challenge is the fact that the fibers need to be randomly oriented throughout the matrix, relatively evenly, to provide equal benefits at all points in the section. When using mild steel, the designer is confident with the location of the reinforcement at specific locations. The designer must also adequately account for the contribution of the fibers to the shear resistance in the section as the cracks develop. This is unlike traditional design, where the engineer would base the design off the shear reinforcement yielding. For this reason, the bond or post-peak cracking strength must be characterized for adequate design of forces carried by the fibers.

Multiple studies have been carried out since the early 1970's to attempt to characterize the shear performance and failure mechanisms of FRC. These studies have included investigations on the following parameters: cross section shape, beam size, shear span to effective depth ratio, longitudinal reinforcement ratio, FRC compressive strength,

fiber volume fraction, and fiber properties. Attempts have been made to correlate the performance to the splitting tensile strength of the concrete, fiber bond characteristics, and most recently flexural performance of small-scale FRC specimens.

2.4.1. Cross Section Shape. Most studies on the shear performance of FRC have focused on rectangular cross-sections. Swamy and Bahia (1985) and Resnbusch and Teutch (2002) investigated the shear performance of rectangular beams compared to T-beams. Swamy and Bahia found that T-beams containing SFRC had a 30% higher shear strength than corresponding rectangular beams. Rosenbusch and Teutsch also showed that T-beams containing SFRC, with the same beam depth as rectangular beams, had 54% higher shear strength.

2.4.2. Beam Size. Most of the research prior to the early 2000's consisted of beams with effective depths less than 12 inches (305 mm). This presents the need for testing of beams with deeper cross-sections to produce data for elements that would realistically be used in practice. This data is critical in providing experimental evidence that a size effect is not significant for FRC beams under shear loads. Noghabai (2000) found there to be a 15% decrease in average ultimate shear stress in SFRC beams by increasing the depth from 16.1 to 22.4 inches (409 to 569 mm). Dinh et al. (2010) tested SFRC beams with a 50% increase in beam depth, 18 inches to 27 inches (457 to 686 mm), and found there to be only a 7% decrease in ultimate load with the deeper beams. Minelli and Plizzari (2013) tested SFRC beams from 15.7 to 39.4 inches (400 to 1000 mm) and found there to be a size effect present for deeper plain concrete beams, but the effect was mitigated by the addition of fibers.

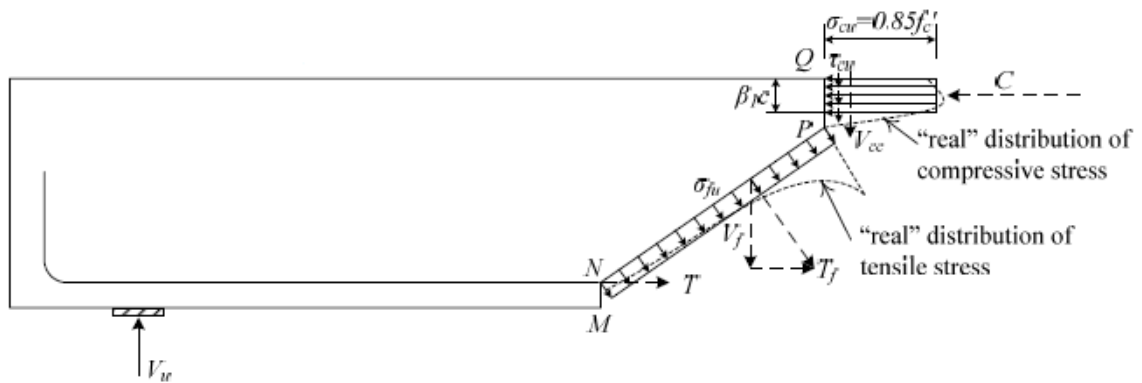


Figure 2.9. Distribution of stresses in a FRC beam (Dinh et al., 2009)

2.4.3. Shear Span to Effective Depth Ratio. Similar to traditional reinforced concrete, a critical shear span to depth ratio needed to be developed for FRC to help distinguish between short and slender beams. Batson et al. (1972) proposed a critical value for shear span to effective depth ratio of 3.0 for SFRC beams. For traditionally reinforced concrete beams, this value is 2.5. Mansur et al. (1986), Ashour et al. (1993), Swamy et al. (1993), Shin et al. (1994), and Kwak et al. (2002) all performed studies on the behavior of SFRC and the relationship of the effective depth to shear span ratio versus shear performance and found that below a ratio of 2.0, the ultimate shear strengths increased rapidly.

2.4.4. Longitudinal Reinforcement Ratio. The effects of longitudinal reinforcement ratio have also been investigated over the years. Ashour et al. (1992) and Swamy et al. (1993) found that increasing the longitudinal reinforcement ratio resulted in higher ultimate shear stresses. This increase was contributed to improved dowel action, leading to a deeper compression zone. This behavior is also typical in traditional reinforced concrete.

2.4.5. FRC Compressive Strength. In general, it has been found that by increasing the compressive strength of FRC, the ultimate shear strength has also increased. Kwak et al. (2002) found that by increasing the compressive strength of the FRC mixture by 50%, there was a corresponding 20% increase in ultimate shear strength. Generally, other parameters should be optimized to drastically increase the shear performance of FRC.

2.4.6. Fiber Volume Fraction. It has been shown that by increasing the fiber volume fraction of SFRC, there is a corresponding increase in the ultimate shear performance as well. The magnitude of this increase is dependent on many factors, but has been shown to diminish with increasing fiber volume fractions. Dinh et al. (2010) showed an increase in performance with increasing fiber content, but the magnitude of increased performance was reduced above a volume fraction of 1.0%. Susetyo et al. (2011) showed similar behavior in rectangular concrete panels with SFRC.

2.4.7. Fiber Type. All of the previous work completed on shear behavior of FRC is primarily based on the use of steel fibers. This presents the need for investigating the performance of other fiber types undergoing shear loading. Regarding SFRC, studies have shown that crimped and hooked-end steel fibers increase the shear performance compared to straight steel fibers. This is due to the need for the deformed fibers to yield prior to pulling out of the concrete matrix, as the straight fibers would, thus increasing the bond characteristics with the concrete.

2.5. PREDICTION OF SHEAR STRENGTH OF FRC BEAMS

Due to the difficulty in modeling shear failure in concrete beams, especially FRC beams, most of the analytical methods use regression analysis to find common variables

affecting the shear performance of FRC. These factors are used based on evaluation of the shear failure mechanisms in the beams and are principally comprised of the shear span to depth ratio, longitudinal reinforcement ratio, fiber aspect ratio, fiber geometry, fiber content, fiber tensile strength, and hardened concrete properties. The following section discusses five representative proposed approaches to predict the performance of FRC beams based on previous research.

2.5.1. Sharma (1986). An empirical expression based on the splitting tensile strength, f_{ct} , and the shear span to depth ratio, a/d , was used by Sharma to predict the ultimate shear strength as shown in Equation 2-1.

$$v_u = (kf_{ct})\left(\frac{a}{d}\right)^{1/4} \quad (\text{Equation 2-1})$$

In Equation 2-1, $k = 2/3$ and the product of k and f_{ct} represent the ultimate direct tensile strength of the SFRC in the study. This result is because Sharma based the equation on the study completed by Wright (1955) who proposed that the direct tensile strength is approximately $2/3$ of the splitting tensile strength. As a result, this expression is not related to the addition of the fibers to the concrete matrix. Also, the role of the longitudinal reinforcement is not accounted for in this equation. Sharma proposed the use of Equation 2-2 to estimate the splitting tensile strength of concrete. Sharma validated his expression against 41 beams with reasonable correlation.

$$f_{ct} = 9.5\sqrt{f'_c} \text{ (psi)} \quad (\text{Equation 2-2})$$

2.5.2. Narayanan and Darwish (1987). In this study, the influence of the splitting tensile strength, f_{ct} , dowel action, through reinforcement ratio, ρ , shear span to depth ratio, a/d , and fiber pullout forces along the inclined crack, v_b , was quantified through Equation 2-3.

$$v_u = eA'f_{ct} + eB'\rho\frac{d}{a} + v_b \text{ (MPa)} \quad \text{(Equation 2-3)}$$

The coefficient, e , used in the first two terms is to account for arch action in the beam and is equal to a value of 1.0 for slender beams ($a/d > 2.8$) and a value of $2.8(a/d)$ for beams with shear span to depth ratios less than 2.8. Using regression analysis, the researchers proposed Equation 2-4 for determining f_{ct} using cube compressive strength, f_{cuf} , and fiber factor, F (Equation 2-5).

$$f_{ct} = \frac{f_{cuf}}{20 - \sqrt{F}} + 0.7 + \sqrt{F} \text{ (MPa)} \quad \text{(Equation 2-4)}$$

$$F = V_f \frac{L_f}{D_f} \beta \quad \text{(Equation 2-5)}$$

The bond factor, represented by β in Equation 2-5, is adopted from the study completed by Narayanan and Kareem-Palanjian (1984) and is equal to a value of 0.5 for round steel fibers, 0.75 for crimped steel fibers, and 1.0 for indented fibers. A' is taken as 0.24, based on a regression analysis of 91 tests, and B' is taken as 80 MPa. The term v_b is the bond stress of all fibers crossing a 45° diagonal line. The fiber bond stress is assumed to act along $\frac{1}{4}$ of the fiber length. The term v_b is estimated using Equation 2-6, where τ is the fiber bond stress, V_f is the fiber volume fraction, L_f is the fiber length, and D_f is the fiber diameter.

$$v_b = 0.41\tau V_f \frac{L_f}{D_f} \beta = 0.41\tau F \quad \text{(Equation 2-6)}$$

The results presented in this study were conservatively acceptable to the proposed model.

2.5.3. Ashour, Hasanain, and Wafa (1992). This research team proposed two different approaches to predicting the shear strength of SFRC. The first approach consisted of modifying an equation from ACI 318 for shear by using factors determined from regression analysis on the parameters $\sqrt{f'_c}$ and $\rho(d/a)$, presented as Equation 2-7.

$$v_u = 0.7 \frac{d}{a} \sqrt{f'_c} + 7 \frac{d}{a} F + 17.2 \rho \frac{d}{a} \text{ (MPa)} \quad \text{(Equation 2-7)}$$

The second approach used by the research team was to modify the equation proposed by Zsutty (1968) to include a fiber factor, F, from Narayanan and Darwish (1987), Equations 2-8 and 2-9.

$$v_u = (2.11 \sqrt[3]{f'_c} + 7F)^3 \sqrt[3]{\rho \frac{d}{a}} \text{ (MPa) for } a/d > 2.5 \quad \text{(Equation 2-8)}$$

$$v_u = \left[(2.11 \sqrt[3]{f'_c} + 7F)^3 \sqrt[3]{\rho \left(\frac{d}{a} \right)} \right] \left(2.5 \frac{d}{a} \right) + v_b \left(2.5 - \frac{a}{d} \right) \text{ (MPa)}$$

for $a/d < 2.5$ (Equation 2-9)

For beams with shear span to depth ratios less than 2.5, the research team took into account the supplementary shear strength of the fiber along the crack with the term v_b . The two approaches were reported to provide good estimates of shear strength for the beams tested in the study.

2.5.4. Khunita, Stojadinovic, and Goel (1999). This research team adopted the fiber factor, F, from the equation proposed by Narayanan and Darwish and estimated the contribution from the compression region, aggregate interlock, and dowel action all in a single term, v_c , as proposed by ACI 318 and shown in Equation 2-10.

$$v_c = 0.167\sqrt{f'_c} \text{ (MPa)} \quad \text{(Equation 2-10)}$$

$$v_u = (0.167\alpha + 0.25F)\sqrt{f'_c} \text{ (MPa)} \quad \text{(Equation 2-11)}$$

In Equation 2-11, α , is an arch action factor equal to $2.5(d/a)$. The expression was reported to be conservative against a wide range of beams with multiple tested variables.

2.5.5. Dinh et al. (2011). This research team proposed an equation based off the contribution from the concrete compression zone and the shear force transferred by the fibers across the critical inclined crack. This approach is very similar to the approach for modeling the behavior of traditional reinforced concrete. The research team proposed Equation 2-12 where A_s is the area of longitudinal steel, f_y is the yield strength of the longitudinal steel, σ_t is the average tensile stress from ASTM C1609 tests, b is the beam width, d is the beam depth, c is the depth of the concrete compression region, and α is the critical inclined crack angle, assumed to be 45° in order to be conservative.

$$v_u = 0.13A_s f_y + \sigma_{t,avg} b(d - c) \cotan(\alpha) \quad \text{(Equation 2-12)}$$

The results of this equation were compared to experimental beams and other research studies and showed positive correlation. In order to use the equation with the absence of ASTM C1609 data, the research team proposed Equation 2-13 to estimate $\sigma_{t,avg}$. Where K was taken to be 400 psi based on an unpublished data set of ASTM C1609 tests on SFRC, L_f is the length of fiber, D_f is the fiber diameter, and V_f is the fiber volume fraction.

$$\sigma_{t,avg} = K \frac{L_f}{D_f} \sqrt{0.0075V_f} \quad \text{(Equation 2-13)}$$

The estimation used for the average tensile strength correlated well the experimental data presented in this study.

3. EXPERIMENTAL PROGRAM

3.1. OVERVIEW OF THE EXPERIMENTAL PROGRAM

As discussed previously, over the past 50 years there has been some research conducted on fiber reinforced concrete beams, but most of the research was limited either to smaller scale test specimens or test specimens containing discrete, steel fiber reinforcement. The intent of this experimental program was to investigate the shear performance of large-scale, “long” carbon fiber reinforced concrete (LCFRC) beams, under monotonic, third point loading. The concrete beams were reinforced with carbon fibers that were developed by a previous research program conducted by Dr. Volz at Missouri S&T and improved upon during the initial stages of this investigation. The performances of the “long” carbon fiber reinforced beams were compared to the performances of beams reinforced with steel fibers, high-modulus polypropylene fibers, and traditional mild steel web reinforcement.

Currently, ACI 318 (2014), “Building Code Requirements for Structural Concrete,” allows for the minimum web shear reinforcements for beams to be replaced with steel fibers given certain criteria are met. The research team is interested in applying the same principle for the long carbon fibers. Although the aspect ratio of the carbon fibers is lower than traditional steel fiber reinforcement, the increased length results in an increased bond length of each individual fiber. That, coupled with an approximate 50% increase in tensile strength gives the LCFRC potential for use in this application. Also, the carbon fibers pose no risk of damage due to corrosion or other harsh environments, where the steel fibers may be more susceptible.

There were multiple targets of this research program. The main goal of this investigation was to determine if it was feasible to use a similar “long” carbon fiber, which showed promising performance under blast and impact loading, for shear applications as well. The research team was interested in the following aspects of the shear application.

1. Is it feasible to design a mix of LCFRC that will be easily mixed and placed in forms to allow for satisfactory consolidation of the concrete and construction of reinforced concrete beams?
2. What are the shear failure mechanisms of the LCFRC beams, what is the ultimate shear strength of the beams, and what is the ductility of the LCFRC beams?
3. How do the results of the LCFRC beams compare when adjusting the fiber content, fiber type, and beam depth?
4. What comparisons and conclusions can be drawn from small scale FRC testing and large-scale shear tests?
5. Does the ASTM C1609 performance meet the requirements for minimum shear reinforcement defined by ACI 318-14?
6. How does the shear performance of the LCFRC beams compare to the theoretical shear strength of traditionally reinforced concrete beams with minimum shear reinforcement as dictated by ACI Committee 318?

This section includes the details associated with the overall experimental program including a review on the previous work done with LCFRC (long carbon fiber reinforced concrete), optimization of fiber content and fiber type, design and construction of the large-scale test beams, details for testing and instrumentation of the large-scale test beams, and the material properties of the LCFRC.

3.2. REVIEW OF PREVIOUS WORK ON LCFRC

During the years 2009 and 2010, Dr. Jeffery Volz and his research team developed and tested a LCFRC that served as the basis for this research program. The team developed two different versions of four inch (101.6 mm) long carbon fiber strands to be mixed with fresh concrete. One fiber was composed of a pre-impregnated carbon fiber fabric that was cut to size from a large sheet; the other fiber was composed of a 48K carbon fiber tow processed in such a way that there was a backbone to give the fiber the rigidity it needed for the mixing process; see Figure 3.1.

The fibers underwent multiple types of testing to determine if their properties would yield a product that would stand up to the mixing process within fresh concrete, as well as provide the increase in performance when compared to traditional reinforced concrete. The testing included scanning electron microscope evaluation, fiber-concrete bond pullout testing, flow cone testing (ASTM C995-01), and beam flexure tests (ASTM C78). These tests provided the data necessary to define the length and width of each fiber type to be used in the larger scale testing.

3.2.1. Impact Testing. Once the dimensions of the fibers were determined, the research team moved to impact testing. Drop-weight impact tests performed on small-scale panels allowed the research team to evaluate the effectiveness of long carbon fiber reinforced concrete (LCFRC) without the enormous undertaking of full-scale blast tests. The 4-ft.-square (1220 mm) by 2-in.-thick (51 mm) specimens were simply supported on all four sides. The testing included plain concrete (no reinforcement) panels, panels reinforced with welded wire reinforcing (WAR), and LCFRC panels.

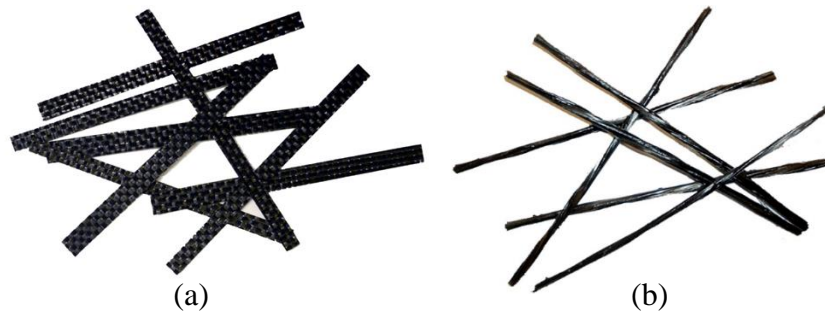


Figure 3.1. Fibers developed in previous research program (a) pre-impregnated carbon fiber fabric (b) carbon fiber tow with backbone

3.2.2. Blast Testing. The blast test specimens included three different types of panels; control panels with traditional reinforcement, panels containing the traditional reinforcement and the “long” carbon fibers made with pre-impregnated carbon fiber sheets, and panels containing the traditional reinforcement and the “long” carbon fibers made with the carbon fiber tow. The panels measured 6-ft.-square in plan (1830 mm), with a thickness of 6.5 in. (165 mm) and were simply supported on the blast frame on all four sides. The panels were exposed to a charge of 85 lbs. (39 kg) of ammonium nitrate/fuel oil (ANFO) and boosters, with a net equivalent weight (NEW) of 75 lbs. (34 kg) of TNT.

The research team found the addition of the carbon fibers to the concrete decreased the amount of damage to the concrete slabs when exposed to impact or blast loading. The results of the blast testing showed that the panels containing the LCFRC had approximately 10 times less damage compared to the control panels containing no carbon fibers; see Figure 3.2 and Figure 3.3.

With the promising results from the blast and impact testing, the research team initiated another iteration of research of LCFRC. The research team used the current data

and development of the fibers to investigate the potential for use as an alternative to traditional shear reinforcement typically used in the construction industry today.

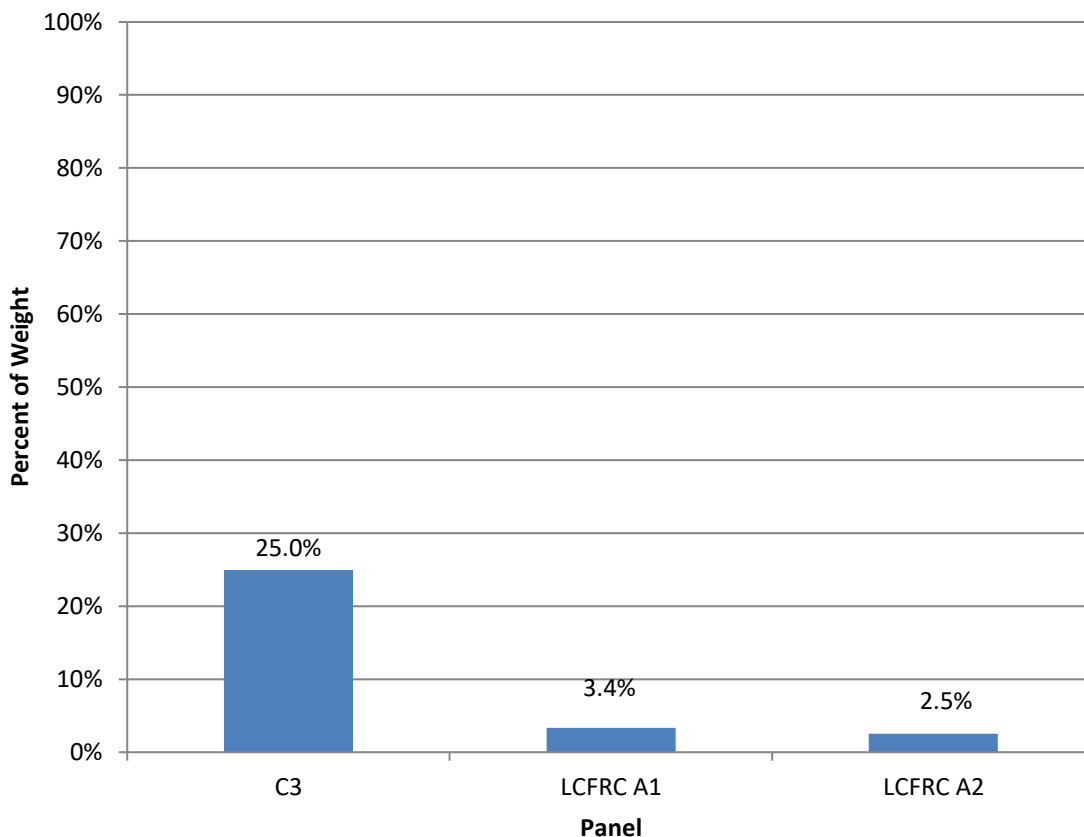


Figure 3.2. Total percent weight lost by each panel after blast loading (C3 – control, A1 and A2 – test panels)

3.3. OPTIMIZATION OF FIBER CONTENT, FIBER TYPE, AND MIX DESIGN

The fiber content, fiber type, and concrete mix design for the previous work on blast resistant concrete were all developed specifically with blast considerations in mind. Commencing the research on shear behavior of LCFRC, the research team determined that

they would improve on the fibers developed for the blast and impact study (Gliha *et al.*, 2011), adjust the fiber content in the mix design, and adjust the mix design of the concrete for the large-scale test beams.

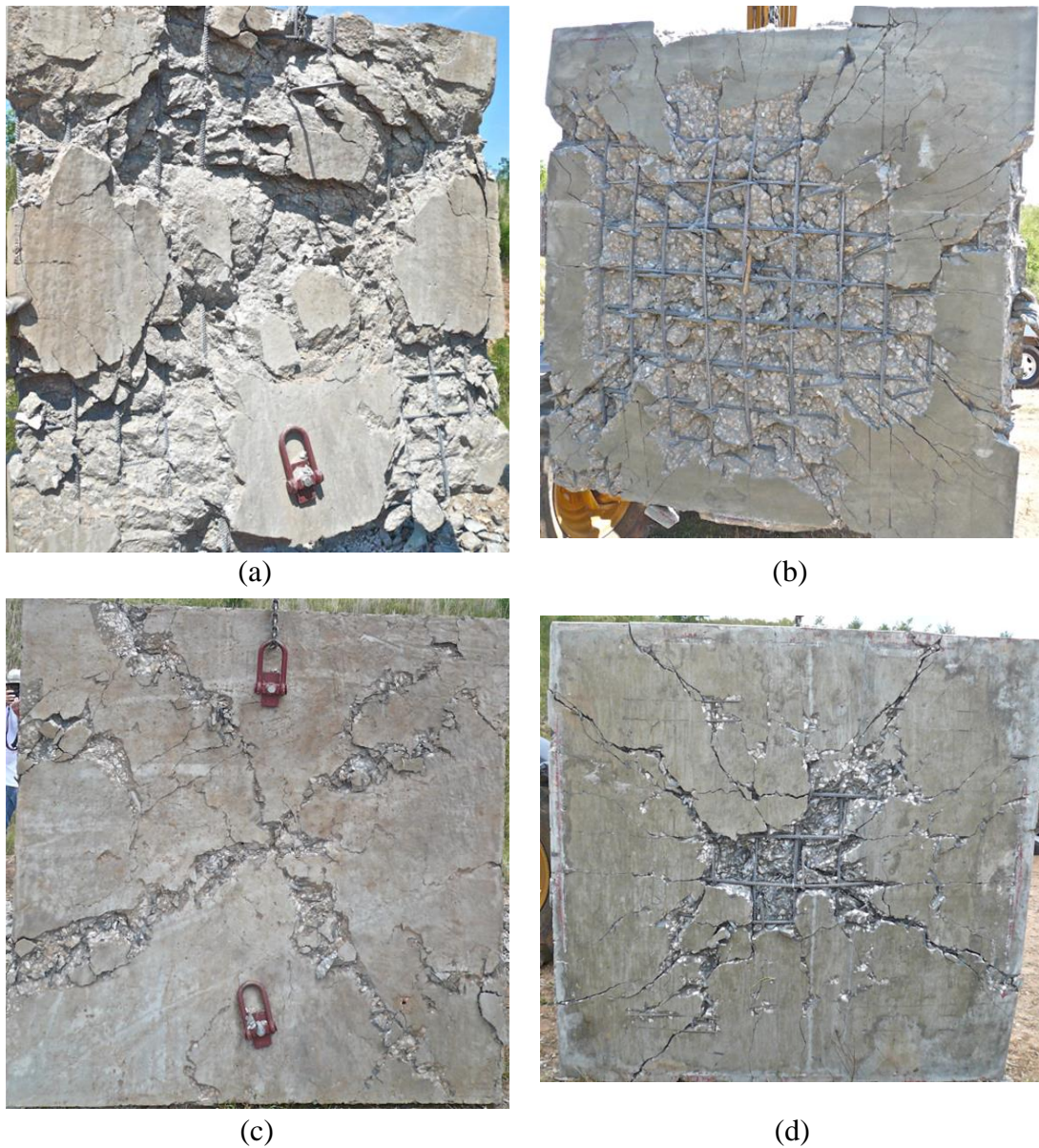


Figure 3.3. Results of previous research program of LCFRC; (a) and (b) show the control panel after blast loading; (c) and (d) show the LCFRC panel after blast loading

The research team decided that the performance of the carbon fiber tow with the backbone both during the batching process and throughout testing surpassed the performance of the pre-impregnated carbon fiber fabric. In an effort to use the best fiber type, content, and concrete mix design, the researchers tested variations to all three variables under ASTM C1609 (2012) Standard Test Method for Flexural Performance of Fiber-Reinforced Concrete (Using Beam with Third-Point Loading) conditions.

The researchers investigated the performance of six carbon fiber processing variations, six separate mix designs, and two different fiber types with C1609 testing to evaluate the performance of each variation. The variations of each are described in detail in the following subsections, with results described within the following sections.

3.3.1. Carbon Fiber Processing. During the initial phases of this research, the investigators attempted to find a processing method for the carbon fiber tow that was more efficient, more economical, and that delivered more consistent results. Figure 3.4 shows the evolution of the six fiber processing methods.

Fibers B1, B2, B3, B4, and B5 processing variations used the same 48K tow, PAN based carbon fiber produced by Zoltek. By keeping the underlying material the same, the researchers could better compare the different processing variations. The properties of the 48K carbon fiber are detailed in Table 3.1. Fiber B3 12K used a 12K tow, PAN based carbon fiber produced by Cytec. Fiber B3 12K was produced because the research team wanted to see the effect of reducing the cross section of the fiber, which would in turn, increase the number of discrete fibers within the cementitious matrix.

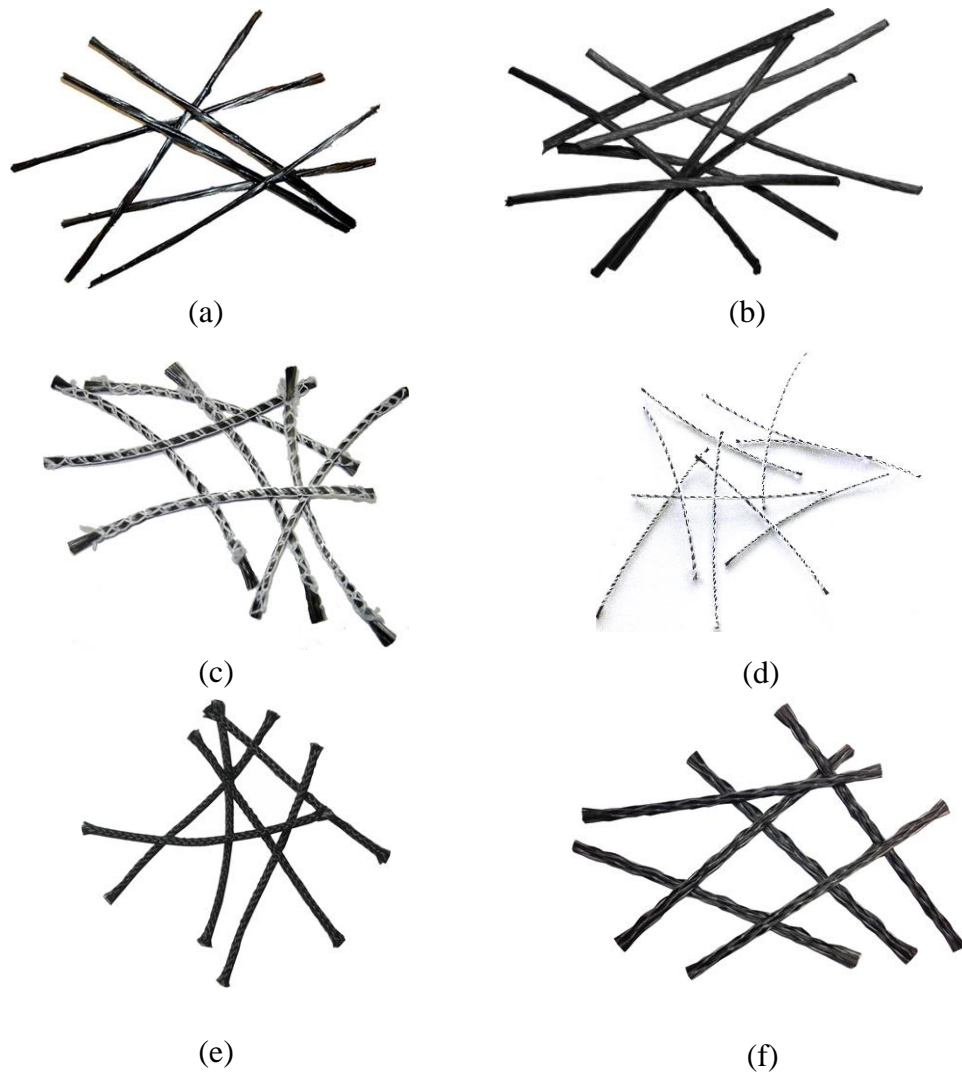


Figure 3.4. Photographs of each fiber variant (a) Fiber B1; (b) Fiber B2; (c) Fiber B3; (d) Fiber B3 12K; (e) Fiber B4; (f) Fiber B5

Fiber B1 consisted of a 48K tow twined around a stiffer polypropylene backbone. During the manufacturing process, a light coating of thermally activated epoxy was applied to the polypropylene immediately prior to twinning with the carbon fiber tow. Once twined, a heat treatment process partially bonded the carbon fibers to the polypropylene core. The end result was a more traditional concrete fiber shape, although appreciably longer in

length, with significantly improved resiliency compared to a raw carbon fiber tow. Due to the extremely high tensile resistance of the carbon fiber tow, the polypropylene backbone did not provide any increase in performance, but was just needed to add to the rigidity of the fiber during the concrete batching process. Without this backbone, the discrete fibers would agglomerate in a large fiber ball. The subsequent processing variations (B2, B3, B4, and B5) used the theory described above when determining the adequacy of the fiber/backbone combination.

Fiber B2 was produced using the same materials that fiber B1 used, but the polypropylene backbone was applied differently. For fiber B2, the polypropylene was placed around the carbon fiber tow, rather than twining the carbon fiber tow around the backbone and was then sectioned into 4 in. (102 mm) lengths. This created a fiber that had a reduction in bond characteristics due to the smooth polypropylene coating surrounding the carbon fibers.

Table 3.1. Zoltek 48K carbon fiber tow properties

Length	4 in. (102 mm)
Aspect Ratio	32
Specific Gravity	1.7
Absorption	3%
Tensile Strength	600 ksi (4,137 MPa)
Tensile Modulus	35 msi (242 GPa)
Alkali, Acid & Salt Resistance	High
Electric Resistivity	0.00061 ohm-in. (0.00155 ohm-cm)
Denier	54,000

Fiber B3 was produced using a 48K carbon fiber tow twined around a stiffer polypropylene backbone, then weaved together with cotton string and sectioned into 4 in. (102 mm) lengths. The weaving allowed for additional stability, kept the fiber from breaking apart during mixing, and allowed the cement paste to thoroughly coat the carbon fiber tow. By allowing the fiber to absorb more of the cement paste during the batching process, the fiber could achieve a superior bond when compared to fiber B2. This fiber type served as the main fiber used in developing the mix designs used in the later stages of this study.

Fiber B3 12K was produced using a 12K carbon fiber tow twined around a stiffer polypropylene backbone, then weaved together with a cotton string and section into 4 in. (102 mm) lengths. The weaving allowed for additional stability, kept the fiber from breaking apart during mixing, and allowed the cement paste to thoroughly coat the carbon fiber tow. This fiber was identical to Fiber B3, except it had $\frac{1}{4}$ the amount of fibers within each discrete fiber. This introduced 4 times the discrete fibers into the concrete matrix. As will be shown in later sections of this dissertation, this fiber type did not have the same performance as Fiber B3. It was concluded by the research team, that, this was a result of the carbon fibers breaking on the rough aggregate and concrete matrix as the test progressed.

Fiber B4 was produced using a 48K carbon fiber tow and stiffer polypropylene backbone, similar to fiber B3, but the carbon fiber and polypropylene were tightly braded to give it rigidity and integrity, and subsequently sectioned into 4 in. (102 mm) lengths. This fiber type possessed good properties for the mixing process, but the braid needed to be so tight that it made it difficult for the cement paste to absorb into the discrete fibers.

Fiber B5 was produced using a 48K carbon fiber tow and eight polyester backbones. During the manufacturing process, a light coating of thermally activated epoxy was applied to the polyester immediately prior to twinning with the carbon fiber tow. Once twined, a heat treatment process partially bonded the carbon fibers to the polyester backbones. Fiber B5 was similar to B3, but it did not have the cotton jacket. Fiber B5 also had eight polyester backbones that were smaller in diameter when compared to the single polypropylene backbone in fiber B3. Due to the even distribution of the backbones in Fiber B5, it provided more stable manufacturing and a better end result. The weave of the polypropylene backbones around the carbon fiber allowed for a larger surface area of the carbon fiber tow to bond to the concrete matrix than any of the other variants. The appearance of Fiber B5 also was superior to Fiber B3 and the research team concluded that it was a product that would perform better in the construction market. Fiber B5 was used in the large-scale shear beams described later in this section.

3.3.2. Mix Design Refinement. Once the research team was satisfied with the development of a superior fiber to fiber B1, which was fiber B3, mix design refinement started. To serve as a basis for comparison, the research team tested all mix designs under ASTM C1609 testing using a fiber content of 1% by volume with fiber B3. The researchers chose 1.0% by volume for the fiber content because it had been demonstrated previously that this fraction produced a mix that was relatively easy to batch and place, as well as containing a high enough fiber content to see a significant increase in post-peak flexural performance. As stated previously, upon the commencement of this study, the researchers determined that the previous mix design should be revised to make it more economical, easier to batch, and easier to place. The previous mix design had a target design strength

of 7,500 psi (51.7 MPa) at 28 days and a water-to-cement (w/c) ratio of 0.38. To improve the design, the team decided to reduce the target design strength to 6,500 psi (44.8 MPa) and increase the w/c ratio. The six mix designs are detailed in Tables 3.2 and 3.3 below.

Table 3.2. Mix design properties

Batch Weights (lb/cu. Yd.)	Mix Design					
	1	2	3	4	5	6
Water	325	325	325	340	340	340
Cement	650	722	855	810	810	810
Coarse agg.	1868	1642	1387	1642	1642	1543
Fine agg.	1031	1196	1340	1087	1087	1254
Glenium 7500 (oz./100# cement)	3	2	3	2	3	3
w/c ratio	0.50	0.45	0.38	0.42	0.42	0.42
Paste volume (%)	34	35	37	37	37	37
Coarse agg. (%)	64	58	51	60	60	55
Fine agg. (%)	36	42	49	40	40	45
Slump before WR (in.)	7	7.75	9.5	7	7	7
Slump after WR (in.)	10	9.5	11	9	10	9

Table 3.3. Mix design constituents

Mix Constituents	Mix Design					
	1	2	3	4	5	6
Cement type I/II	X	X	X	X	X	X
3/4" (19 mm) NMS crushed limestone	X	X	X	X	X	
3/4" (19 mm) NMS crushed limestone (MODOT Grade D)						X
Natural Sand	X	X	X	X	X	X
Glenium 7500	X	X	X	X	X	X

3.3.2.1 Batching process. For the mix design refinement phase, the researchers batched approximately 2.5 cubic feet (0.07 cu. m.) of concrete in a 6 cu. ft. (0.17 cu. m.) electric mixer according to ASTM C192 Standard Practice for Making and Curing Concrete Test Specimens in the Laboratory. For each batch, a slump measurement was taken before the super plasticizer was added to the mix and after it was added to the mix according to ASTM C143 Standard Test Method for Slump of Hydraulic-Cement Concrete. The slump of each mix was taken before and after the super plasticizer was added so that the researchers could consistently produce similar batches after the initial batch and to ensure a similar batch once large-scale beam production commenced, at which time the concrete would be batched at the local ready-mix plant.

Four, 4 in. by 8 in. (102 by 203 mm) concrete cylinders were cast with each batch of concrete to measure the compressive strength of the concrete. The concrete was placed in the molds just before the fibers were added to the mix because it has been shown that the addition of fibers has little significance on compressive strength and the researchers could produce better quality cylinders without the fibers (ACI 544.1R, 2009).

The fibers were added to the concrete once it was fully mixed, while the mixer was turning, see Figure 3.5. They were mixed with the concrete for approximately 5 minutes to ensure the fibers were fully dispersed within the plastic concrete and completely coated in concrete paste. Once the fibers were fully mixed, mixture was placed and consolidated, in two lifts, into six beam forms measuring 6 in. by 6 in. by 20 in. (152 by 152 by 508 mm), see Figure 3.6.

Except for Mix Design 1, all mix designs were stable prior to adding the fibers and allowed for all fibers to be coated with cementitious paste, which is necessary for superior

bond performance. Again, with the exception of Mix Design 1, there was no apparent segregation or excessive bleed water in any of the mix designs used.

Once the specimens were prepared, they were covered for 24 to 48 hours, demolded, and then cured in a moist cure room for 28 days, at which point they were tested. Each mix design had specimens prepared in this manner to serve as a basis for comparison and to allow the researchers to determine which mix design would be used in the large-scale beams. The mix design refinements are detailed in the subsections below, as well as the details of the material testing. The results of this testing phase are discussed in Section 4 of this dissertation.

3.3.2.2 Mix design 1. The first mix design was intended to be far from the mix design previously used for the blast study. The target for creating this mix design was to test the boundaries of the batch constituents with regards to how well the fibers performed during the batching process. The w/c ratio was significantly increased from the initial mix design (0.38 to 0.5). The mix also contained much less cement than the previous design. As a result, it was difficult for the fibers to be fully mixed into the concrete matrix. The researchers also used a higher content of coarse aggregate in this mix compared to the past mixes. By introducing more coarse aggregate in the mix, higher strength can be achieved with less cement, providing a more economical mix. However, an increased amount of coarse aggregate will also provide a harsher mixing environment for the fibers. Even though there was a higher w/c ratio than in the past, the paste content of the mix was reduced. By reducing the paste content in the mix and increasing the coarse aggregate content, there was not enough paste to fully coat all the discrete fibers and a harsher mixing

environment resulted, thus affecting the bond between the fibers and the cementitious matrix.

3.3.2.3 Mix design 2. In the second mix design, more cement was added to the batch. This step did two things, it decreased the w/c ratio from 0.5 to 0.45, but it also increased the volume of paste in the mix from 34% to 35%. By increasing the volume of paste, there is more paste available to fully coat and penetrate into the discrete fibers. As a result, the hardened concrete matrix has a better bond with the fibers and increased performance. In this mix, the coarse aggregate fraction was also reduced from 64% to 58% in order to provide a mix that would not be as harsh on the fibers when compared to mix design 1.

3.3.2.4 Mix design 3. The third mix design incorporated more cement. This again decreased the w/c ratio from 0.45 to 0.38, as well as increased the volume of paste in the mix from 35% to 37%. The researchers also decreased the coarse aggregate fraction to 51%, which was similar to the mix design used in the blast study. The reduction in coarse aggregate content provided a better mix for the fibers, but also reduced the strength of the mix. This was another reason why more cement was added to the mix design.

3.3.2.5 Mix design 4. In an effort to make the mix design more economical, the researchers reduced the cement content from the previous mix, but also increased the water content. The increase in water and reduction in cement resulted in a w/c ratio of 0.42. Not only does this reduce the cost of the mix because of the reduction in cement, it also does not need as much super plasticizer. The researchers also increased the coarse aggregate fraction to 60% to help add to the compressive strength of the material. The paste volume remained consistent at 37%.



Figure 3.5. Concrete batching process after fiber addition



Figure 3.6. Beams and cylinders after consolidation

3.3.2.6 Mix design 5. In this mix design the researchers kept everything constant except the amount of super plasticizer that was added to the mix was increased by 50%. The reason for the increase was to determine the effect of the super plasticizer on the fresh concrete and to understand if this provided a better mix to be used with the fibers.

3.3.2.7 Mix design 6. In this mix design the researchers were interested in the effect of using a coarse aggregate of superior quality on the results of the ASTM C1609 testing. The aggregate that was chosen was the same size as previously used, 3/4 in. (19 mm) NMS, crushed limestone, but this time it was a MoDOT approved aggregate (MoDOT Grade D). This aggregate has tighter constraints on the material, which provides more consistent aggregate and more consistent results in the material testing. The researchers also slightly reduced the coarse aggregate fraction in this mix from 60% to 55%. This mix served as a basis for the large-scale testing in this study due to its superior mixing and placing properties, as well as the performance of the hardened specimens.

3.3.3. Fiber Type Optimization. In recent years, the cost of carbon fiber has been greatly reduced due to its increased use in a wide variety of fields. Although the cost has been reduced, it is still quite high compared to other construction materials and other fiber types. For this reason, the researcher team was interested in exploring other options for the underlying material to produce the discrete fibers. The researchers chose a proprietary material called Innegra S fiber, which is a high-performance olefin fiber. It was much more economical when compared to the carbon fiber, but it also had significantly different tensile properties, see Table 3.4. The tensile strength of the Innegra S fiber is 14% of the carbon fiber and it also has a tensile modulus that is only 6% of the carbon fiber. The

Innegra S fiber also attains a much greater elongation at break than the carbon fiber; 9.5% to 1.94%.

The researchers were interested in the comparison of the Innegra S fiber reinforced concrete to the carbon fiber reinforced concrete because of the different mechanical properties. The goal was to determine the difference in post-peak flexural strength of a much stronger, stiffer carbon fiber to the lower strength, more ductile Innegra S fiber.

Table 3.4. Fiber mechanical properties

	Carbon Fiber	Innegra S
Tensile Strength, ksi (MPa)	660 (4550)	97 (667)
Tensile Modulus, ksi (MPa)	34,000 (234,000)	2150 (14828)
Elongation, %	1.94	9.5
Density, lb/in ³ (g/cc)	0.066 (1.82)	0.030 (0.84)

3.4. DESIGN OF LARGE SCALE BEAMS AND TESTED VARIABLES

The large-scale testing within this study was comprised of 30 rectangular, prismatic beams with two different depths, 18 and 24 in. (457 and 610 mm). Each tested variation consisted of three duplicate beams to allow the researchers to determine the consistency of the beam quality and performance. For the 18 in. (457 mm) deep beams (B18 series), there were three sets of controls; beams containing traditional longitudinal reinforcement and no shear reinforcement, beams containing traditional longitudinal and shear reinforcement, and beams containing traditional longitudinal reinforcement and commonly used steel fibers for shear reinforcement of the web. The B18 series also included three sets of beams containing the B5 carbon fiber with variations in the fiber content, as well as one set of

beams containing the Innegra S fiber. The second series, 24 in. (610 mm) deep beams (B24 series), included three sets of beams containing the B5 carbon fiber with variations in the fiber content. Table 3.5 details the main parameters of each beam series and the details of each parameter are discussed in the following sections.

3.4.1. Fixed Parameters of Large-Scale Beams. To allow for comparisons between the varied parameters within the large-scale testing, the researchers fixed the shear span to effective depth ratio (a/d ratio), beam size, reinforcing details, and concrete compressive strength (f'_c). The details of each are described below.

3.4.1.1 Shear span to effective depth ratio. As it has been shown in previous studies (Batson et al., 1972), traditional reinforced concrete beams with an a/d ratio less than 2.5 can have an increased strength due to a concrete strut between the load and support locations. A previous study researching the effect of steel fiber reinforced concrete demonstrated that an a/d ratio of 3.5 was high enough to minimize the effect of arch action in the concrete, for this reason the researchers decided to use a similar a/d ratio. For Series B18, the research team used an a/d ratio of 3.61 and for Series B24 the researchers used an a/d ratio of 3.45. The goal was to keep the a/d ratio as close as possible between beam series, but due to fabrication and design constraints, this was the closest that could be achieved.

3.4.1.2 Beam size. The beams in Series B18 had a width of 8 in. (203 mm), a total depth of 18 in. (457 mm), and a length of 168 in. (4267 mm). The beams in Series B24 had a width of 8 in. (457 mm), total depth of 24 in. (610 mm), and a length of 192 in. (4877 mm). The researchers used the previous studies discussed in the Literature Review as a basis for choosing the depth of the beams. The investigation included two beam depths,

representing a 30% increase from B18 to B24, to determine the effect on the shear strength of the FRC. The width of the beams was chosen based on the steel arrangement and a beam width-to-fiber length ratio of 2.0.

Due to the capabilities of testing large-scale beams in the Highbay Structures Laboratory at Missouri S&T, the beams were designed to have simply supported end conditions and to be tested under third point loading. As a result of the setup, each beam had two shear spans, which provided the researchers even more variation within the study. Using this constraint, the beams were designed according to ACI 318-11 Building Code Requirements for Structural Concrete. The beam lengths for each series were designed to achieve as close to a 3.5 a/d ratio as possible for their shear span, enough length so that no anchorage failures would occur prior to shear failure, and a distance between load points to satisfy all requirements, as well as the constraints of the test setup. Each end and center section of the beams included transverse reinforcement for confinement surrounding the load points, as well as providing constructability of the steel reinforcement cages. Each beam had longitudinal steel anchorages using 90-degree hooked ends on each reinforcing bar. The details for each beam length are provided in Table 3.6. In the table, the dimensions referenced refer to the following measurements; distance from centerline of load to far edge of loading plate (e), distance between two loading points (m), distance from end of beam to edge of loading plate, used for development length of longitudinal steel (w).

Table 3.5. Design parameters of beam Series B18 and B24

Beam Type	Beam	v_f %	d (in)	a/d	ρ	Fiber Type
Control	B18-PC	N/A	14.75	3.61	3.05	No Fiber
Control	B18-TR	N/A	14.75	3.61	3.05	No Fiber
Control/FRC	B18-S-0.75	0.75	14.75	3.61	3.05	RC80/30BP
FRC	B18-B5-0.5	0.5	14.75	3.61	3.05	B5
FRC	B18-B5-0.75	0.75	14.75	3.61	3.05	B5
FRC	B18-B5-1.0	1	14.75	3.61	3.05	B5
FRC	B18-D1-0.75	0.75	14.75	3.61	3.05	D1
FRC	B24-B5-0.5	0.5	20.05	3.45	2.99	B5
FRC	B24-B5-0.75	0.75	20.05	3.45	2.99	B5
FRC	B24-B5-1.0	1	20.05	3.45	2.99	B5

Table 3.6. Shear beam design and construction dimensions

Dimension	Series B18 (in)	Series B18 (mm)	Series B24 (in)	Series B24 (mm)
d	14.75	375	20.05	509
a/d	3.61	3.61	3.45	3.45
a	53.25	1352	69.14	1756
e	6	152	6	152
m	24	610	24	610
Design w	12	305	12	305
Design Length $= 2*(a+w)+m$	154.5	3924	186.3	4732
Construct Length	168	4267	192	4877
Construct w	15.75	400	11.86	301
l_{dh} (available) = $(w/2)+e-1$	20.75	527	16.86	428

3.4.1.3 Selection of reinforcing bars. Beam series B18 and B24 were both designed with the intent that the beam would fail in shear and not flexure at midspan. The details of the longitudinal reinforcement were kept identical for the control beams and the FRC beams for Series B18 to have a basis for comparison. The reinforcement ratio between

beam Series B18 and B24 was also kept as consistent as possible to have a basis for comparison between beam depths. The reinforcement ratio for Series B18 was 3.05% and the reinforcement ratio for Series B24 was 2.99%.

Equation 3-1, as proposed by Parra-Montesinos (2006) was assumed as the minimum shear strength of the beams containing fibers. For the beam design, the shear capacity was set at 4.5 times the value given by Equation 3-1 to ensure the beams failed in shear and not flexure, where V_c is the shear capacity of the concrete including fibers, b is the beam width, and d is the depth to the centroid of the longitudinal steel. Table 3.7 details the calculation of the shear and flexural strength for beam Series B18 and B24. The expected load due to shear is notated as P_s ; the expected load due to a moment failure is notated as P_m .

$$V_c = 3.5bd\sqrt{f'_c} \quad (\text{Equation 3-1})$$

Table 3.7. Beam design shear and flexural strength

	$\frac{v_u}{\sqrt{f'_c}}$	f'_c	b	d	P_s	M_n	P_m	P_s/P_m
		psi (MPa)	in. (mm)	in. (mm)	kip (kN)	kip-in (kN-m)	kip (kN)	
B18-PC	2.0	6000 (41.4)	8 (203)	14.75 (375)	18.3 (81)	2680 (303)	50.3 (224)	0.36
B18-TR	5.0	6000 (41.4)	8 (203)	14.75 (375)	46.1 (205)	2680 (303)	50.3 (224)	0.91
B18-S	4.5	6000 (41.4)	8 (203)	14.75 (375)	41.1 (183)	2680 (303)	50.3 (224)	0.82
B18-B5	4.5	6000 (41.4)	8 (203)	14.75 (375)	41.1 (183)	2680 (303)	50.3 (224)	0.82
B18-D1	4.5	6000 (41.4)	8 (203)	14.75 (375)	41.1 (183)	2680 (303)	50.3 (224)	0.82
B24-B5	4.5	6000 (41.4)	8 (203)	20.05 (509)	55.9 (249)	4686 (529)	70.4 (313)	0.80

As stated above, the beams were designed according to ACI 318-11 for traditional reinforced concrete beams. The design for Series B18 contained six #7, Grade 60

reinforcing bars in two layers for longitudinal reinforcement and two #4, Grade 60 reinforcing bars for compression reinforcement. The beam flexural strength at yield would occur at a load of 100.6 kip (224 kN), resulting in a load approximately 20% higher than any load predicted to cause shear failure. It should be noted that the shear strength, due its unpredictable behavior could occur higher than the conservative estimate chosen at the planning phases of this study. Figures 3.7 and 3.8 depict Series B18 reinforcement details.

For Series B18, #3, Grade 60 reinforcing bars were chosen for the transverse reinforcement at the ends and between the loading points. At the ends, there were five bars spaced at 2 in. (51 mm) on center. All transverse steel in this study was designed as closed, double leg stirrups. Closed stirrups require greater precision during fabrication, but provide a much more stable reinforcing cage prior to placing the concrete. The purpose of this reinforcing steel was to confine the concrete at the support location to preclude any bearing failure prior to shear failure. The transverse steel at the ends also served as a necessity to construct the reinforcing steel cage. At the center, there were five bars spaced at 6 in. (152 mm) on center. The transverse reinforcement at the center of the beams also provided confinement under the loading points as well as aided in the construction of the beams.

Beams B18-TR also contained transverse reinforcement within each shear span. There were #3, Grade 60 reinforcing bars spaced at 7 in. (178 mm) on center, which was the minimum distance as per the design code requirements. The target was to design, construct, and test a beam with the minimum transverse steel allowed for web reinforcement, but due to code limitations, the minimum allowable spacing forced the design to be four times the required area of steel per inch over the minimum design.

The design for Series B24 contained eight #7, Grade 60 reinforcing bars in three layers for longitudinal reinforcement and two #4, Grade 60 reinforcing bars for compression reinforcement. The beam flexural strength at yield would occur at a load of 140.8 kip (626 kN), resulting in a load approximately 20% higher than the predicted load to cause shear failure in the FRC beams. Figures 3.9 and 3.10 depict Series B24 reinforcement details.

For series B24, #3, Grade 60 reinforcing bars were chosen for the transverse reinforcement at the ends and between the loading points. At the ends, there were five transverse reinforcing bars spaced at 2 in. (51 mm) on center. At the center, there were five bars spaced at 6 in. (152 mm) on center. The transverse reinforcement for Series B24 was included for the same reasons as discussed for Series B18.

3.4.1.4 Concrete compressive strength. As stated earlier in this section, the target compressive strength in the early phases of this study was 6,500 psi (44.8 MPa). Due to the constraints of the beam design, the target compressive strength for the large-scale testing was reduced to 6,000 psi (41.4 MPa) to provide a greater possibility for shear failure to occur. For all beams in Series B18 and Series B24, the design compressive strength was kept consistent, but during testing the compressive strength varied by approximately 15%. This was caused by variations within each batch delivered by the local Ready Mix concrete supplier, as well as variations in the sampling and curing conditions of each batch.

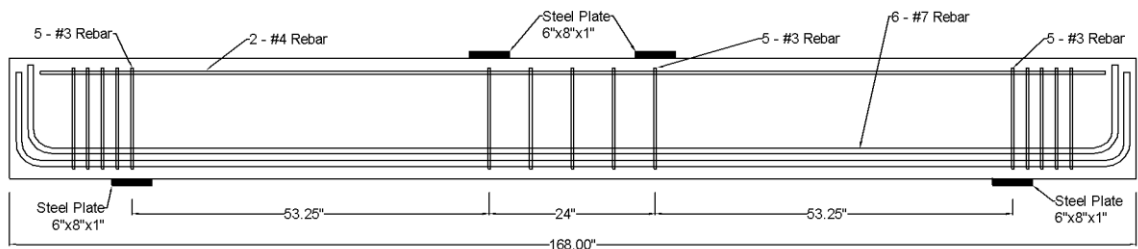


Figure 3.7. Series B18 beam details

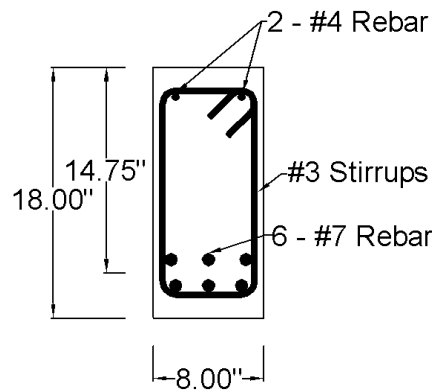


Figure 3.8. Series B18 cross section details

3.4.2. Control Beams. Three sets of control beams were included in the large-scale beam testing. The first set of control beams, B18-PC, contained no transverse reinforcement within the shear test regions. This set of beams served as a basis of comparison between all beam sets to give baseline shear strength of the beam design and concrete matrix. The shear resistance in these beams mainly came from aggregate interlock effect across the inclined cracks as well as shear strength provided through dowel action of the longitudinal steel.

The second set of control beams, B18-TR, contained traditional transverse reinforcement within the shear spans of each beam. The double-leg stirrups were made

with #3, Grade 60 reinforcing bars and spaced at 7 in. (178 mm) on center. Although the intent was to compare the FRC shear strength to the shear strength of the minimum requirement of transverse reinforcement, design and construction limitations required a greater amount of steel. The minimum steel required by the code for the 8 in. by 18 in. (203 mm by 457 mm) beams was 0.0077 in² per inch (0.196 mm² per mm), but the steel included in the B18-TR beams was 0.031 in² per inch (0.787 mm² per mm) due to the maximum spacing requirements of the code.

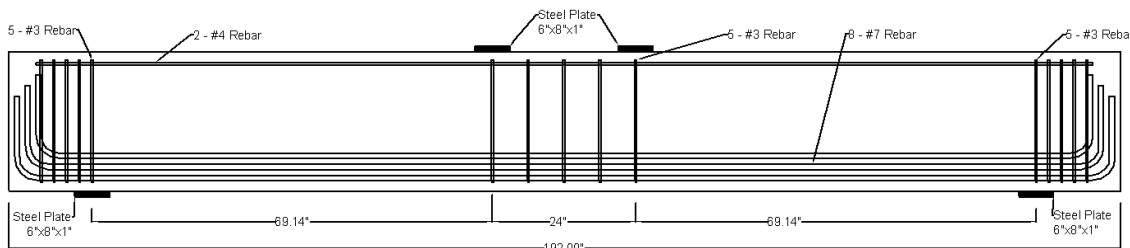


Figure 3.9. Series B24 beam details

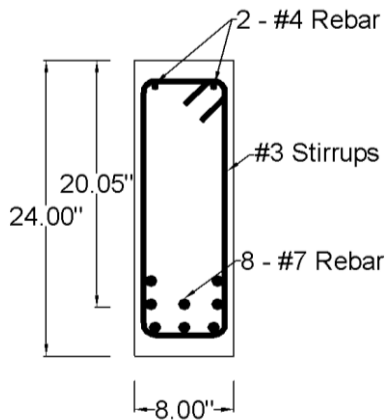


Figure 3.10. Series B24 cross section details

The third set of control beams, B18-S-0.75, contained RC80/30BP hooked-end steel fibers produced by Bekaert. These fibers were chosen because steel fibers are currently accepted in the construction industry and provisions to include steel fibers in place of minimum transverse reinforcement are already included in the current ACI 318 code. The fibers were also tested in a previous study, Dinh et al. (2009), allowing for comparisons of LCFRC to be made to other research done on SFRC. The hooked-end steel fibers were included at 0.75% by volume within the concrete matrix. Table 3.8 compares the properties of the three types of fibers included in the large-scale testing.

3.4.3. Varied Parameters of Large-Scale Beams. With the intent of investigating the potential for the LCFRC to exceed the shear strength requirements for minimum transverse reinforcement as required by ACI 318-14, the fiber volume fraction and beam depth were the varied parameters. The researchers also included one set of Series B18 beams produced with Innegra S fibers to compare the effect of fiber type on the shear behavior.

3.4.3.1 Fiber volume fraction. Based on the results of the ASTM C1609 beam testing and keeping in mind realistic constructability outside of a laboratory environment, carbon fiber volume fractions of 0.5, 0.75, and 1.0% by volume of the concrete mix were chosen for Series B18 and B24. The low fiber volume fractions would make it easier to place the concrete with the longitudinal steel present in the beam forms. The low fiber volume fractions would also keep the cost of the FRC as economical as possible. It was demonstrated during the small-scale testing that fiber volume fractions of 1.5% had superior performance, but the FRC was also much harder to consolidate into the forms. The forms for the ASTM C1609 beams did not include reinforcing steel which provided

an easier condition to consolidate the concrete than with the large-scale beams. The reduction in the fiber volume fraction would also ensure better consolidation around reinforcing bars and an overall, better quality beam.

3.4.3.2 Beam depth. The beam depth was also a parameter that was varied in this study. Series B18 had a total height of 18 in. (457 mm), with an effective depth of 14.75 in. (375 mm). Series B24 had a total height of 24 in. (610 mm), with an effective depth of 20.05 in. (509 mm). By testing the effect of volume fraction of carbon fibers at two different depths, representing a 30% increase in depth from one series to another, it could be determined whether there was a size effect on the performance of LCFRC beams.

3.4.3.3 Fiber type. During the fiber optimization testing, the Innegra S fibers showed promising performance in the ASTM C1609 tests compared to the carbon fiber. For this reason, one set of Innegra S fiber reinforced beams, B18-D1-1.0, were included in the large-scale testing. The inclusion of this variable allowed for comparison between the performances of beams containing fibers with different material properties, as well as comparison to the ASTM C1609 testing.

Table 3.8. Properties of fibers included in large-scale test beams

	Carbon Fiber	Innegra S	RC80/30BP
Length, in. (mm)	4 (102)	4 (102)	1.18 (30)
Aspect Ratio	32	32	79
Tensile Strength, ksi (MPa)	660 (4550)	97 (667)	445 (3070)
Tensile Modulus, ksi (Mpa)	34,000 (234,000)	2150 (14828)	29,000 (200,000)
Density, lb/in ³ (g/cc)	0.066 (1.82)	0.030 (0.84)	0.284 (7.85)

3.5. FABRICATION OF LARGE SCALE SPECIMENS

All large-scale shear test specimens were cast and cured in the Highbay Structures Laboratory at Missouri S&T. The details of the process are described in the following sections.

3.5.1. Reinforcing Steel. The reinforcement within each beam included #3, #4, and #7, Grade 60 deformed rebar that conformed to ASTM A615 Deformed and Plain Billet-Steel Bars for Concrete Reinforcement (2016). The rebar was supplied from Nu Way Concrete Forms, Inc. It was delivered as 20 ft. (6096 mm) straight bars. To complete the construction of the rebar cages for each beam, each bar was cut to length and then bent to the proper shape using a hydraulic rebar bender. This process allowed for each bar and bend to be as identical as possible, which was necessary because of the tight spacing of bars within the forms.

Each cage was suspended upside down during construction to gain the advantage of gravity in aligning each stirrup as it was tied into place. First the top layer of reinforcement was suspended and then five evenly spaced #8 rebar sections, cut to 6.25 in. (159 mm) in length, were laid perpendicular to the longitudinal bars and tied to them. The #8 bars served as 1 in. (25.4 mm) spacers between the layers of longitudinal reinforcement. The subsequent layers of longitudinal reinforcement were then stacked above the spacers. Once the longitudinal steel was tied together, the stirrups were spaced along the length of the cage and the #4 bars used for compression steel were laid into the bottom corners of the transverse reinforcement. All intersections of reinforcing steel were tied together using rebar tie wire in order to construct cages that were virtually identical from one beam to the next. Finally, segments of #3 rebar were tied perpendicular to the transverse reinforcement

to provide the necessary cover on the sides of the beams; and then 1.5 in. (25.4 mm) steel rebar chairs were tied perpendicular to the bottom of the transverse reinforcement to provide for cover on the bottom of the beams. Figure 3.11 shows a beam in Series B18 during fabrication. Figure 3.12 shows a fully constructed cage for B18, and Figure 3.13 shows a fully constructed cage for B24.



Figure 3.10. Series B18 beam during fabrication



Figure 3.11. Reinforcing cage for B18



Figure 3.12. Reinforcing cage for B24

3.5.2. Formwork. Each beam was cast in steel and plywood forms that were secured together using steel keys. The forms were lightly oiled with form release oil prior to lowering the cage into the form. Each cage was lowered into the forms carefully to avoid contact between the rebar and the form release oil. Once the cages were in place, wall ties secured an exact 8 in. (203 mm) width at the top of the form. Figure 3.13 shows the reinforcing steel in the forms, ready for concrete placement.



Figure 3.13. Reinforcing cage and formwork

3.5.3. Mix Design. Based on the testing done during the mix design optimization, Mix Design 6 was chosen for the large-scale testing. The mix consisted of Type I Portland cement, $\frac{3}{4}$ in. (19.1 mm) nominal maximum size, MoDOT Grade D, limestone coarse aggregate, natural river sand, water, and Glenium 7500 super plasticizer. The batch weights for each beam series are shown in Table 3.9. All batch weights are given at a SSD basis for the aggregates.

3.5.4. Casting the Large-Scale Specimens. The large-scale shear test specimens were cast in triplicate. On the day of casting, the moisture content of the aggregates at the local ready-mix plant were measured and the mix design was adjusted accordingly. The concrete was delivered in a standard rotary concrete mixer. Once the truck arrived at the lab, the slump of the concrete was taken and the super plasticizer was added. After the super plasticizer was mixed for 5 minutes in the truck, plastic concrete was sampled for eighteen 4 in. by 8 in. (102 by 203 mm) concrete cylinders and six 6 in. by 12 in. (152 by 305 mm) concrete cylinders to be tested for compressive and split tensile strength of each mix, respectively.

Next, fibers were added to the drum and mixed for approximately five minutes to ensure that they were completely mixed. Each beam casting showed successful mixing of fibers within the concrete. Once the fibers were fully mixed into the concrete, the FRC was loaded into a 0.5 cu. yd. (0.38 m³) bucket and placed into the concrete forms in two lifts. The concrete was consolidated around the rebar using an internal concrete vibrator. Once the concrete was placed, the tops of the beams were finished to level the concrete surface. Six ASTM C1609 beams were also cast with each set of large scale beams, to be tested at 28 days, for correlations to be made between shear strength and post-peak flexural

performance, as well as, determination of code compliance of fibers used for shear reinforcement of concrete elements. Figures 3.14 and 3.15 show typical concrete placement over the course of the large-scale beam fabrication.

Once the surface of the concrete hardened, all beams and small specimens were covered with plastic for approximately 48 hours until they were demolded and cured in laboratory conditions until they were tested. The cylinders for compressive and split tensile strength were match cured in the laboratory environment. The ASTM C1609 beams, along with a set of 3 cylinders, were cured in the moist cure room until they were 28 days old, at which time they were tested.

Table 3.9. Batch weights for each beam series

Batch Weights, lb/cu. yd. (kg/m ³)	Mix Design									
	B18-PC	B18-TR	B18-S-0.75	B18-B5-0.5	B18-B5-0.75	B18-B5-1.0	B18-D1-0.75	B24-B5-0.5	B24-B5-0.75	B24-B5-1.0
Water	340 (202)									
Cement	810 (480)									
Coarse agg.	1543 (915)									
Fine agg.	1254 (744)									
Glenium 7500 (oz./100# cement)	3	3	3	3	3	3	3	3	3	3
Fiber	0	0	321 (190)	13.5 (8)	20.25 (12)	27 (16)	13 (8)	13.5 (8)	20.25 (12)	27 (16)



Figure 3.14. FRC transfer from concrete mixer to bucket



Figure 3.15. Concrete during placement into forms

3.6. TESTING AND INSTRUMENTATION

In order to accurately compare the performances of each variation in the test program, specific test protocols were followed for each type of testing. This section will describe the testing and instrumentation procedure for the ASTM C1609 testing and large-scale beam testing.

3.6.1. ASTM 1609 Test Setup. The research team followed the guidelines of ASTM C1609 (2012) to perform the small-scale evaluation of the fiber variations and mix design changes. The setup consisted of beams measuring 6 in. by 6 in. by 20 in. (152 by 152 by 508 mm), loaded at third points in accordance with ASTM C78. During the test, the beam had a special jig attached to it, which held two LVDT's. The LVDT's were located on either side of the beam at midspan and mid-depth of the beam. The LVDT's were used in conjunction with the data acquisition system (DAQ) to perform a servo-controlled load application, where the net deflection of the center of the beam is measured and used to control the rate of loading and thus, the rate of increase of deflection. For the initial 0.02 inches (0.51 mm) of deflection, the test was run at a speed 0.002 in/min (0.051 mm/min), from there to 0.12 inches (3.0 mm), the test was run at a speed of 0.006 in/min (0.15 mm/min). Rollers were used at all load and support points in order to provide free rotation of the beam during the test. Figure 3.16 shows the typical test setup for the ASTM C1609 test.



Figure 3.16. ASTM C1609 test setup

3.6.2. Full-Scale Test Setup. All the test specimens were tested as simply-supported beams and subjected to a four-point loading. Due to the constraints of the actuators available for testing in the Highbay Structures Laboratory, the test setup required the simultaneous loading of two actuators as shown in Figure 3.17 and Figure 3.18.

Two actuators with a capacity of 140,000 lbf (623 kN) were used to apply load to the beam specimens. The actuators applied the load by simultaneously pushing the spreader beam (W24x55) downwards to distribute the load through the back-to-back channel, which applied the load at two points on the test specimen. The loading frame was designed to withstand at least two times the anticipated maximum load applied to the beams and stiff

enough to prevent displacement within the setup itself. Each test was performed under displacement control and the load was applied in a series of loading steps of approximately 0.05 inches (1.3 mm) per step. The displacement of each test specimen was measured at the mid-point of the beam using a LVDT and plate mounted to the beam.

Electronic measurements of the strain were also taken throughout the entire loading history of the beams, while measurements of the cracks and formations of crack patterns in the beam were taken at the end of each loading step to ensure safety for the research team. Figure 3.19 shows a photograph of the test setup. The strain measurements were taken for each beam at 6 locations. The strain gauges were applied directly to the longitudinal reinforcement prior to placing the concrete. The strain gauges were located at mid-span and mid-points of the shear span on the lowest reinforcing bar on the right and left bars of the longitudinal reinforcement. Figures 3.20 and 3.21 show the locations of the strain gauges for each beam series.

3.7. MATERIAL PROPERTIES AND TESTING

3.7.1. Reinforcing Bars. All reinforcing bars were ordered from the same batch of material to maintain consistency within the full-scale testing program. The test specimens were reinforced with A615, Grade 60 reinforcing bars. The longitudinal bars were #7 for tensile reinforcement and #4 for compression reinforcement. The transverse reinforcement consisted of #3 reinforcing bars. The steel reinforcement was tested according to ASTM A307 “Standard Test Methods and Definitions for Mechanical Testing of Steel Products” to determine the mechanical properties of each size. The results of the tensile testing of the reinforcing bars are summarized in Table 3.10.

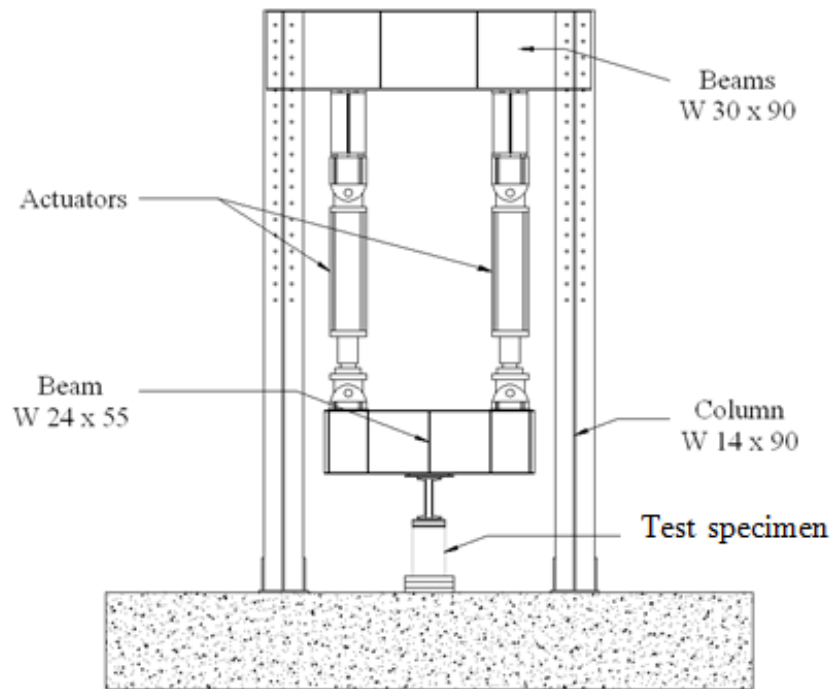


Figure 3.17. Details of large-scale test setup from front

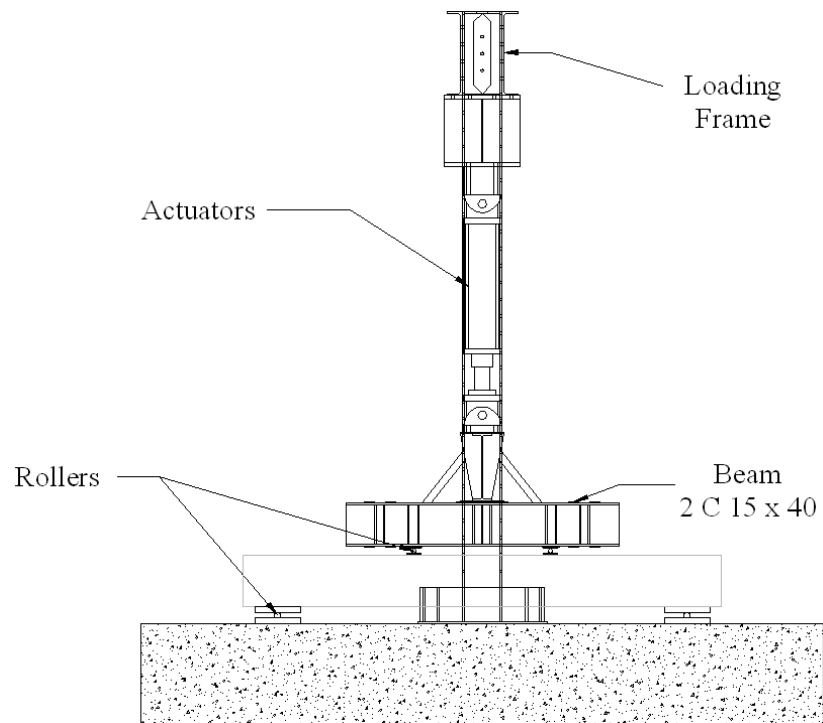


Figure 3.18. Details of large-scale test setup from side



Figure 3.19. Overall large-scale test setup

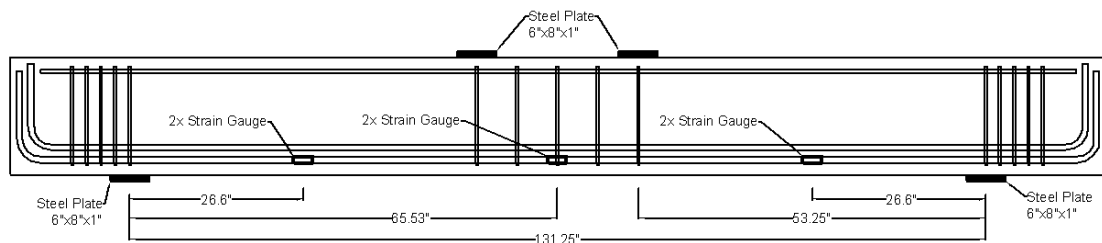


Figure 3.20. Strain gauge locations for Beam Series B18

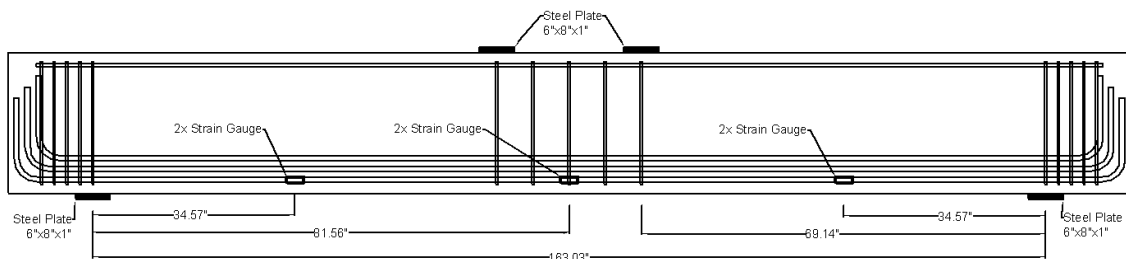


Figure 3.21. Strain gauge locations for Beam Series B24

Table 3.10. Summary of reinforcing bar yield strength

Bar Type	Yield Strength, psi (Mpa)	Modulus of Elasticity ksi, (Mpa)	Ultimate Strength, psi (Mpa)
#3	76,132 (525)	29,600 (204,100)	112,000 (772)
#4	74,192 (512)	29,400 (202,700)	105,400 (727)
#7	71,653 (494)	29,100 (200,600)	106,200 (732)

3.7.2. Hardened Concrete Properties. The compressive strength of the concrete was measured for each set of ASTM C1609 specimens, as well as each set of full-scale beams. For the large-scale test specimens, the modulus of elasticity and splitting tensile strength of the concrete was also measured for select beam sets to gain an understanding of the material properties of each concrete mix. Due to the fact that the mix design remained unchanged for all of the large-scale beam tests, the researchers were confident that the hardened properties of the concrete were very similar with exception to slight deviations in the compressive strength. All relevant ASTM standards were followed when performing the hardened concrete property testing

3.7.2.1 Compressive strength. The compressive strength of each individual mix was tested at multiple ages, including test day of the large-scale specimens and 28-day strength according to ASTM C39 (2011). The testing consisted of three 4 in. by 8 in. (102 mm by 203 mm) concrete cylinders under a uniform compressive load. The cylinders were cast prior to adding fibers to the fresh concrete in order to compare all control mixes to the fiber reinforced concrete mixes. Also, it has been shown that the addition of fibers has limited influence on the overall compressive strength of a given concrete mix. Each cylinder was capped with sulfur capping compound to ensure a flat and level loading

surface. A summary of the compressive strength data for the large-scale beams is shown in Table 3.11.

3.7.2.2 Modulus of elasticity. Concrete cylinders were constructed and tested to evaluate the modulus of elasticity of select concrete mixes. Using ASTM C469 (2002) as a guideline, three 4 in. by 8 in. (102 mm by 203 mm) concrete cylinders were subjected to a uniform compressive load, while measuring deformation of the cylinder throughout the test. Each cylinder was capped with sulfur capping compound to ensure a flat and level loading surface. Table 3.12 contains a summary of the modulus of elasticity of the concrete used for the large-scale beams.

3.7.2.3 Splitting tensile strength. ASTM C496 (2004) was used as a guideline to understand the tensile stress of the different concrete mix designs. Three 6 in. by 12 in. (152 mm by 305 mm) concrete cylinders were subjected to a uniform compressive load through the cylinders' longitudinal axis, as prescribed in the ASTM guideline. Table 3.13 contains a summary of the splitting tensile stress of the concrete used for large-scale testing.

3.7.2.4 Flexural strength. The flexural strength of each fiber reinforced concrete mix was tested using ASTM C1609 (2012) as a guideline. Six 6 in. by 6 in. by 20 in. (152 by 152 by 508 mm) were tested at 28 days in order to have an accurate comparison of the tests completed in the initial mix design and fiber optimization phase to the tests completed during the large-scale beam portion of the research. The results of the tests performed both in the initial phase and large-scale testing phase of the research will be discussed in detail in the next section of this dissertation.

Table 3.11. Summary of large-scale beam compressive strength test results

Beam Set	Days / f'_c (psi)								
	0	1	3	7	8	9	10	12	28
B18-PC	0	3203	4395	5585		5452			6459
B18-TR	0	4175						6671	6870
B18-S-0.75	0	4115	5580	6143					6780
B18-B5-0.5	0			5847	6250				6524
B18-B5-0.75	0	4185	4749	5583					5972
B18-B5-1.0	0	4436	5002	5665					6376
B18-D1-1.0	0	3974	4749	5376					6315
B24-B5-0.5	0	4454		6309	6390				6890
B24-B5-0.75	0	3780	5180		6131				6485
B24-B5-1.0	0	3657	5031	5712			6306		6800
Average	0	3998	4955	5777	6257				6547
Std. Dev.	0	377	348	290	106				277
COV (%)	0	9.4%	7.0%	5.0%	1.7%				4.2%

Table 3.12. Summary of modulus of elasticity test results at 28 days

Beam Set	Modulus of elasticity (ksi)
B18-PC	5342
B18-B5-0.75	4249
B24-B5-0.5	4429

Table 3.13. Summary of splitting tensile stress test results

Beam Set	Days / Splitting Tensile Stress (psi)	
	7	28
B18-PC	374	432
B18-TR	-	-
B18-S-0.75	-	-
B18-B5-0.5	447	495
B18-B5-0.75	389	392
B18-B5-1.0	406	399
B18-D1-1.0	390	-
B24-B5-0.5	428	426
B24-B5-0.75	470	-
B24-B5-1.0	467	434
Average	421	430

4. RESULTS OF THE EXPERIMENTAL PROGRAM

This section provides a full review on the results and behavior of the small and large-scale fiber reinforced concrete beam tests. The ASTM C1609 results obtained during the mix design and fiber optimization process will be discussed first followed by a detailed discussion of the large-scale test beams. The ASTM C1609 discussion will be centered around the load-displacement curves, equivalent beam stresses, and equivalent flexural strength ratio of each beam series, through mix design and fiber development. The large-scale test beams will be analyzed separately with a focus on the load-displacement curves, crack development, and failure behavior of each series, as well as the performance compared to the resistance required by the minimum transverse reinforcement.

4.1. PERFORMANCE AND BEHAVIOR OF FRC IN ASTM C1609 TESTING

To gain a better understanding of the performance of the different concrete mix designs and fiber types, the research team used the ASTM C1609 test to compare the different variables. The beams tested had dimensions of 6 in. by 6 in. by 20 in. (152 by 152 by 508 mm) and were loaded at third points according to the ASTM C1609 guidelines. First, each mix design was evaluated with Fiber B3 to obtain a mix appropriate for the large-scale beam testing. Second, the fiber variants and types were evaluated using the mix design developed in the first stage of the program. The work completed allowed the research team to understand the properties of the fresh FRC over many batches and fiber volume fractions, as well as the performance of each variation. This led to a better understanding of the material and critical information to establish the large-scale beam test program.

Upon completion of each test, when the average midspan deflection of the beam reached 0.12 in. (3.05 mm), the permanent deflection (Δ), average crack width at the tension face (cw), nearest distance to a support from the crack location (a), average beam width at crack location (b), and average beam depth at crack location (d) were recorded. Through the testing, it was also discovered that the location and number of discrete fibers within the beam cross-section at the crack location had a large impact on the ASTM C1609 flexural performance. For this reason, the researchers began to include documentation regarding the number and location of fibers at the crack location to better understand the performance and behavior of each set of ASTM C1609 beams tested. Figure 4.1 shows a typical specimen after testing. Figure 4.2 shows an example of the cross-section of the ASTM C1609 beams after testing, with the location of discrete fibers marked.

Other than the physical measurements taken from the tested specimens, the researchers also obtained the raw data for each beam tested to evaluate the relationships of load and displacement and bending stress versus midspan deflection. A graph of load vs. displacement for all beams was created and used for evaluation, as well as determining specific points along the curves. ASTM C1609 requires the documentation of the following load points; first peak load (P_c), post-cracking peak load (P_{pc}), load at displacement of $L/600$, 0.03 in. (0.762 mm), (P_{600}), load at displacement of $L/150$, 0.12 in. (3.05 mm), (P_{150}), and average midspan deflection at the post-cracking peak load (δ_{pc}). It should be noted, that if the specimen did not exhibit deflection hardening during the test, the post-cracking peak load was determined to be the load corresponding to the first point after cracking. To satisfy the requirements of ACI 318, a condition must be satisfied at a displacement of $L/300$ as well, consequently, the research team also documented the load

at a displacement of $L/300$, 0.06 in. (1.52 mm), (P_{300}). Figures 4.3 and 4.4 show examples of the two different behaviors FRC beams can exhibit during an ASTM C1609 test. In Figure 4.3, after the first crack, the strength of the beam drops steadily with no post-peak strength gain; in Figure 4.4, upon the initial crack, the beam shows an increase in strength (post-peak hardening) prior to eventually dropping in strength until the end of the test.

From the load vs. average midspan displacement plot, the researchers calculated the toughness (T_{150}^D) of each specimen, which is the area under the load vs. displacement curve in units of in-lb. or joules. Corresponding to each recorded load point along the load displacement curves, the researchers then calculated the peak and residual stresses (σ_x) using Equation 1 from ASTM C1609 (2010) and reported the value in psi (Mpa). The equivalent flexural strength ratio ($R_{T,150}^T$) was then calculated using Equation 3 from ASTM C1609 (2010) and reported as a percent. This ratio compares the post-peak flexural strength to the concrete modulus of rupture and is a good measure of comparison between different mix designs, fiber dosages, and variations in fiber properties. Equation 1 from ASTM C1609 (2010) is shown below as Equation 4-1, where the stress corresponding to each location is σ_c , P is the load recorded, L is the length of the span, b is the average width of the beam, and d is the average depth of the beam. Equation 3 from ASTM C1609 is shown below as Equation 4-2.

$$\sigma_c = \frac{PL}{bd^2} \quad (\text{Equation 4-1})$$

$$R_{R,150}^D = \frac{150 * T_{150}^D}{\sigma_c * b * d^2} \quad (\text{Equation 4-2})$$



Figure 4.1. Typical ASTM C1609 beam after testing

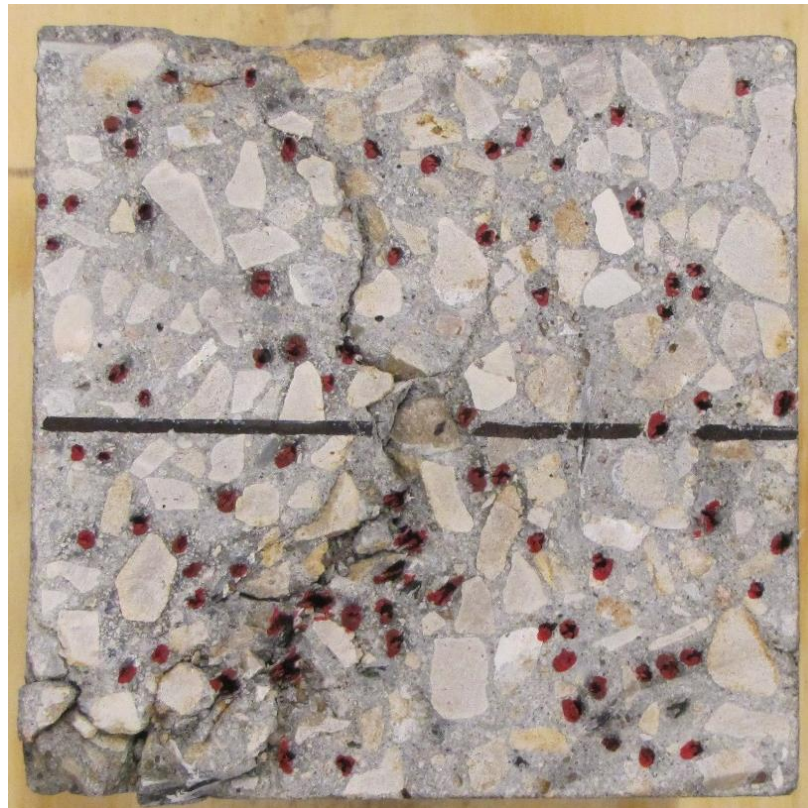


Figure 4.2. Example of ASTM C1609 beam cross-section for fiber count documentation

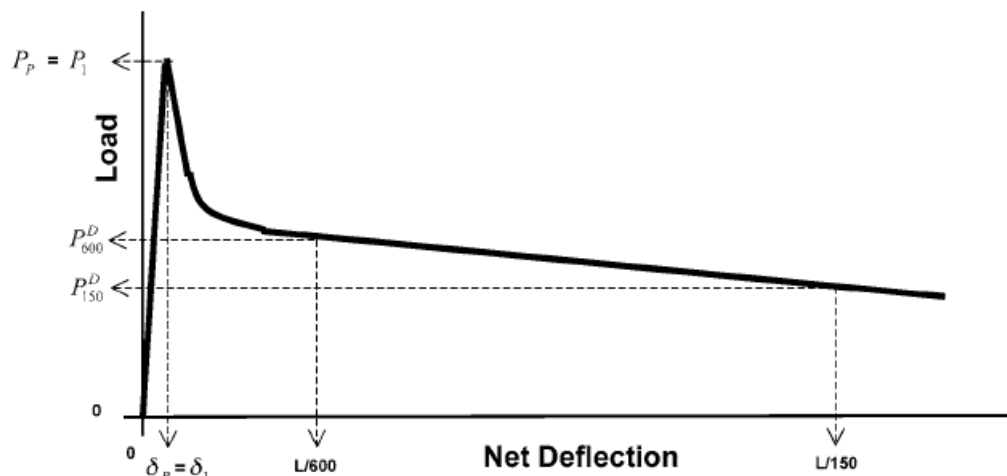


Figure 4.3. Example of load-displacement curve with no post-peak hardening (ASTM C1609 2010)

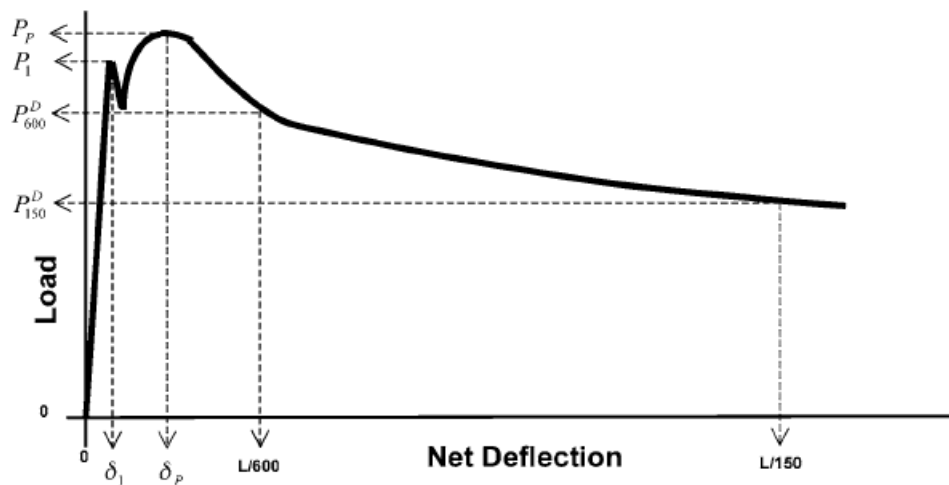


Figure 4.4. Example of load-displacement curve with post-peak hardening (ASTM C1609 2010)

4.1.1. Behavior of Specimens During Mix Design Refinement. Each mix design variation was tested with fiber B3 at 1.0% volume addition of fibers to compare each mix throughout the process. The intention was to find a mix design in which the

requirements of the fresh concrete set by the research team were met, while ensuring positive behavior of the small-scale specimens in the material testing phase that would justify large-scale shear testing.

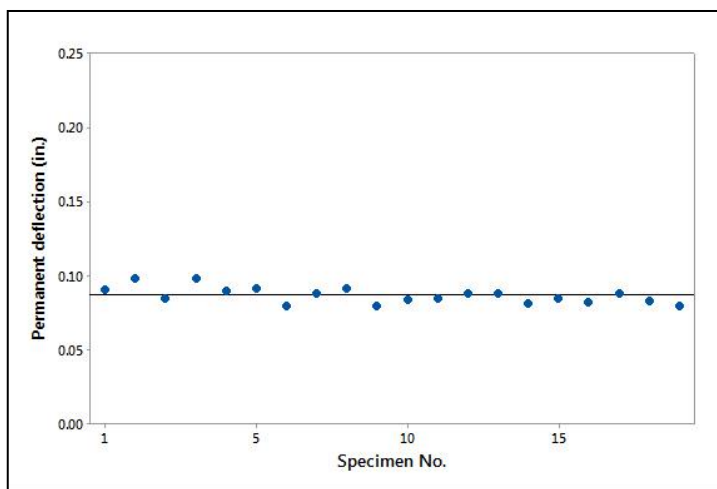
Figure 4.5 illustrates the physical measurement of the specimens taken after completion of each test. The average permanent displacement of the beams was 0.087 in. (2.21 mm), with only a 6% coefficient of variation. This data shows the consistency in performance of the fibers regardless of the changes made to the mix design. The average crack width was 0.137 in. (3.5 mm), which was also relatively consistent. Occasionally, there was spalling at the crack location or more than one crack that formed making it difficult to precisely report the crack width. Finally, the location of the crack was also very consistent at an average distance of 7.9 in. (200.7 mm), which is within the middle third of the beam, ensuring pure flexural loading of the specimens. Table 4.1 lists the physical behavior recorded for each specimen. Mix design 5 did not undergo ASTM C1609 testing because it only represented an increase in amount of super plasticizer used in the mix in order to increase the slump for placing the fresh FRC.

The load versus average midspan deflection curves for each set of specimens are shown in Figure 4.6. For most of the specimens, there is apparent post-peak hardening behavior exhibited. As discussed previously in this section, specific indices for the results were recorded for each specimen to be able to compare the overall behavior, and these results are listed in Table 4.2. They are shown graphically in Figures 4.7 and 4.8. Overall, the peak stress, post-cracking stresses, and equivalent flexural strength ratio did not change drastically with each mix design, showing consistency in the performance of Fiber B3 at a volume fraction of 1.0%. Only 1 out of the 20 specimens tested (M1-B3-3), was able to

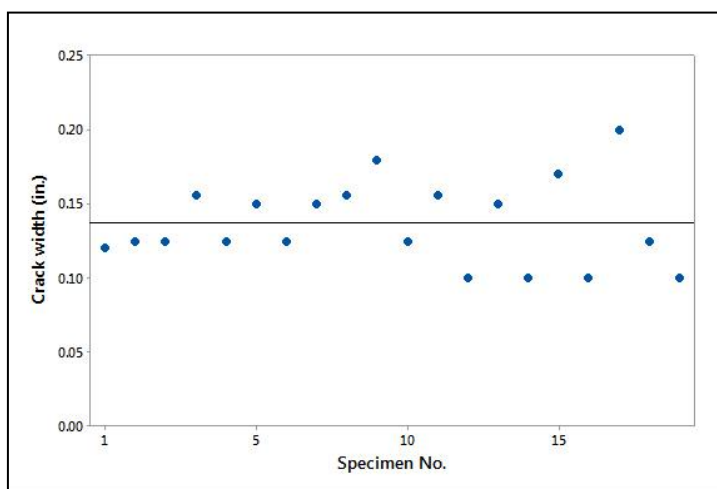
pass the requirements of ACI 318-14 for use as minimum shear reinforcement. The exceptional performance of this beam is most likely due to a heavy concentration of discrete fibers bridging the crack that formed during the test. On average, the beams performed 30% below the requirements at both the average midspan displacement of $L/300$ and $L/150$ for using steel fiber reinforced concrete as shear reinforcement.

Table 4.1. Physical behavior for each ASTM C1609 specimen tested during mix design refinement

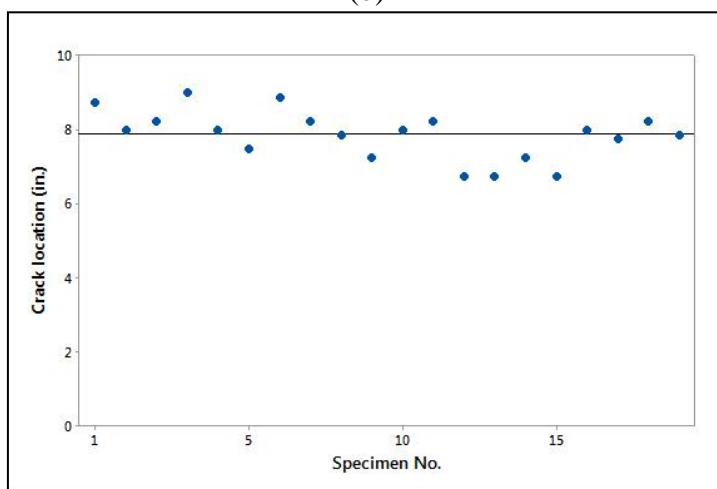
Mix Design	Fiber	v_f (%)	Beam No.	f'_c (psi)	Δ (in.)	cw (in.)	a (in.)	b (in.)	d (in.)
1	B3	1.0	1	4220	0.091	0.120	8.75	6.26	6.03
1	B3	1.0	2	4220	0.098	0.125	8.00	6.26	6.00
1	B3	1.0	3	4220	0.085	0.125	8.25	6.16	6.02
2	B3	1.0	1	5667	0.098	0.156	9.00	6.09	5.98
2	B3	1.0	2	5667	0.090	0.125	8.00	6.03	6.03
3	B3	1.0	1	6256	0.092	0.150	7.50	6.02	5.99
3	B3	1.0	2	6256	0.080	0.125	8.88	6.02	6.08
3	B3	1.0	3	6256	0.088	0.150	8.25	5.99	6.08
3	B3	1.0	4	6256	0.092	0.156	7.88	5.98	6.09
4	B3	1.0	1	4355	0.080	0.180	7.25	6.05	6.04
4	B3	1.0	2	4355	0.084	0.125	8.00	6.06	6.01
4	B3	1.0	3	4355	0.085	0.156	8.25	6.00	5.98
4	B3	1.0	4	4355	0.088	0.100	6.75	6.02	6.00
4	B3	1.0	5	4355	0.088	0.150	6.75	6.01	6.19
6	B3	1.0	1	6447	0.081	0.100	7.25	6.01	5.99
6	B3	1.0	2	6447	0.085	0.170	6.75	6.05	6.01
6	B3	1.0	3	6447	0.082	0.100	8.00	6.06	6.00
6	B3	1.0	4	6447	0.088	0.200	7.75	6.05	6.05
6	B3	1.0	5	6447	0.083	0.125	8.25	6.00	6.07
6	B3	1.0	6	6447	0.080	0.100	7.88	5.99	6.01



(a)



(b)



(c)

Figure 4.5. Distribution of (a) permanent displacement, (b) crack width, (c) crack location for each ASTM C1609 specimen tested during mix design refinement

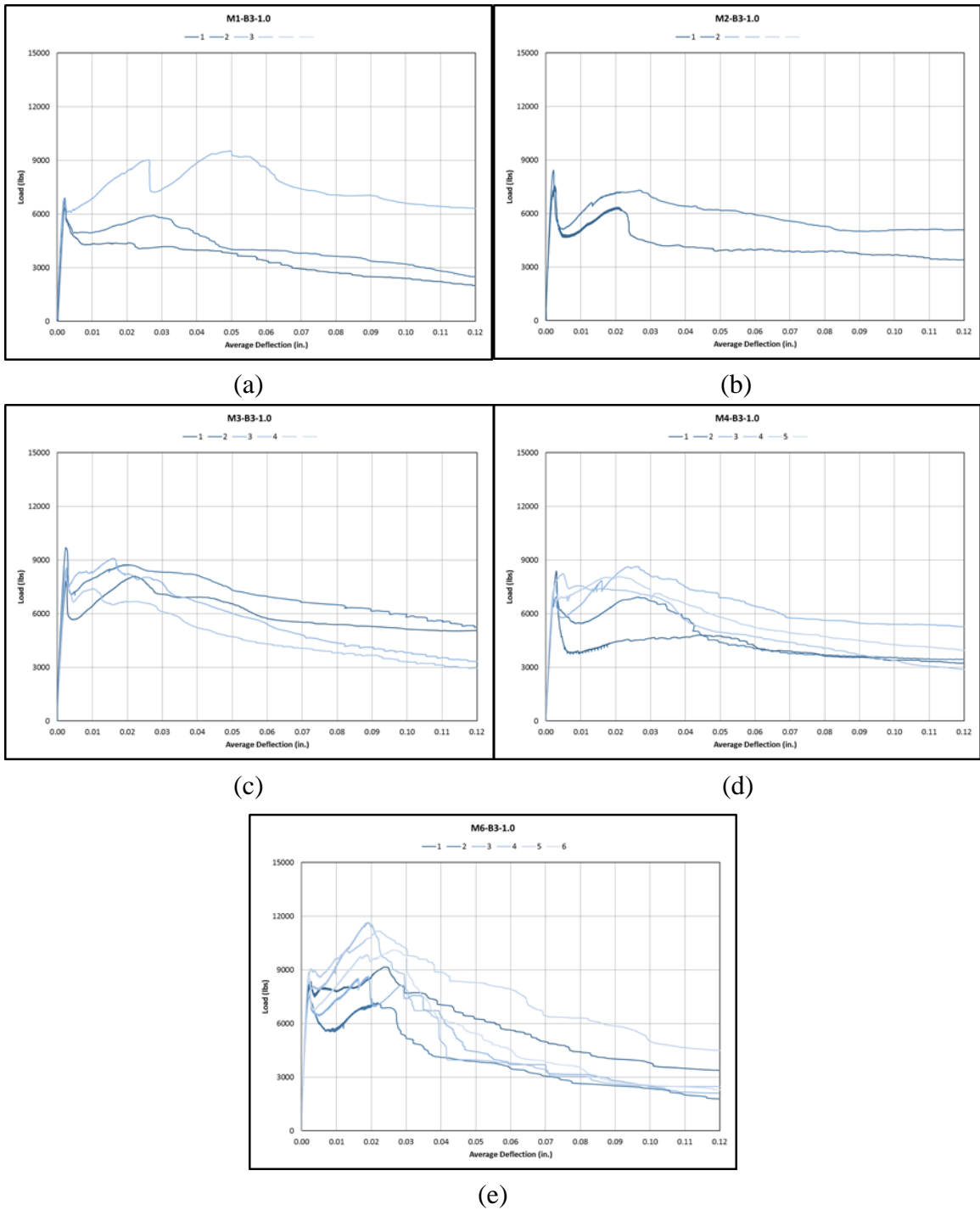


Figure 4.6. Load vs. deflection curves of ASTM C1609 tests for mix design refinement

Table 4.2. Equivalent bending stress results from ASTM C1609 testing for mix design refinement

Mix	Fiber	v_f (%)	Beam No.	σ_c (psi)	σ_{pc} (psi)	σ_{600} (psi)	σ_{300} (psi)	σ_{150} (psi)	δ_{pc} (in.)	T (in- lb)	$R_{T,1}$ 50	ACI 318 90% Req.	ACI 318 75% Req.	Pass ACI Req?
1	B3	1.0	1	545	347	330	268	158	0.0204	402	49%	49%	29%	FALSE
1	B3	1.0	2	521	472	463	318	199	0.0274	497	64%	61%	38%	FALSE
1	B3	1.0	3	645	768	594	694	509	0.0493	902	94%	108%	79%	TRUE
2	B3	1.0	1	625	525	362	327	282	0.0207	506	56%	52%	45%	FALSE
2	B3	1.0	2	692	599	572	487	417	0.0266	394	39%	70%	60%	FALSE
3	B3	1.0	1	653	674	590	478	422	0.0217	722	77%	73%	65%	FALSE
3	B3	1.0	2	785	706	673	564	424	0.0193	843	72%	72%	54%	FALSE
3	B3	1.0	3	738	740	628	439	271	0.0161	680	62%	59%	37%	FALSE
3	B3	1.0	4	685	543	496	349	240	0.0197	567	56%	51%	35%	FALSE
4	B3	1.0	1	684	392	377	341	263	0.0437	486	48%	50%	38%	FALSE
4	B3	1.0	2	571	569	553	333	284	0.0262	567	68%	58%	50%	FALSE
4	B3	1.0	3	605	724	681	539	442	0.0260	770	89%	89%	73%	FALSE
4	B3	1.0	4	685	615	581	391	239	0.0162	605	61%	57%	35%	FALSE
4	B3	1.0	5	621	631	535	409	309	0.0211	678	71%	66%	50%	FALSE
6	B3	1.0	1	697	764	643	470	281	0.0237	695	69%	67%	40%	FALSE
6	B3	1.0	2	680	590	426	287	147	0.0219	468	47%	42%	22%	FALSE
6	B3	1.0	3	698	712	611	306	174	0.0190	554	55%	44%	25%	FALSE
6	B3	1.0	4	880	947	642	307	201	0.0191	640	49%	35%	23%	FALSE
6	B3	1.0	5	822	909	830	644	366	0.0215	899	74%	78%	45%	FALSE
6	B3	1.0	6	796	840	813	377	191	0.0264	627	55%	47%	24%	FALSE

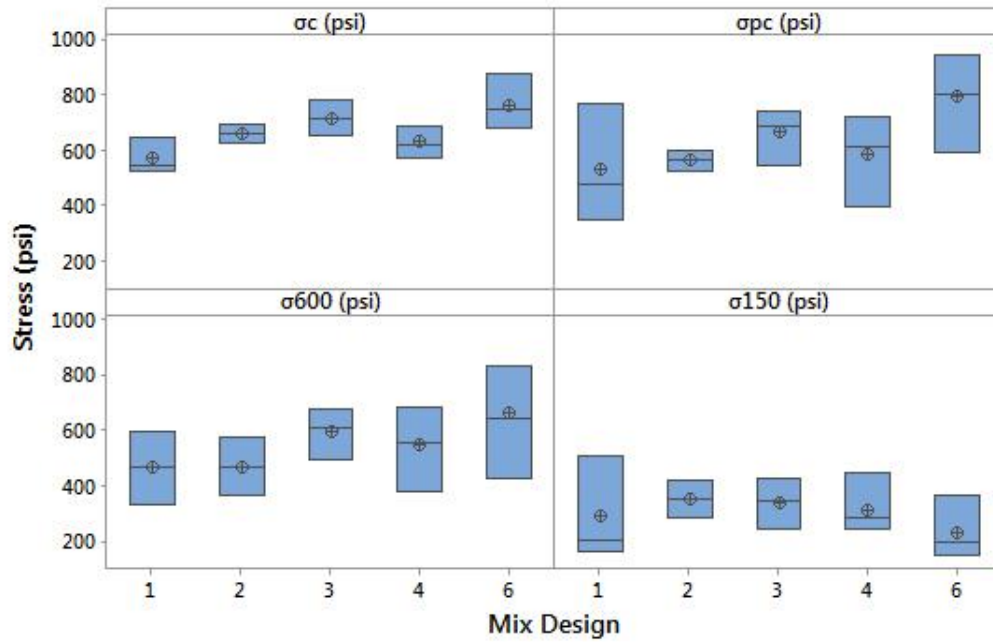


Figure 4.7. Equivalent stress results for ASTM C1609 testing for mix design refinement

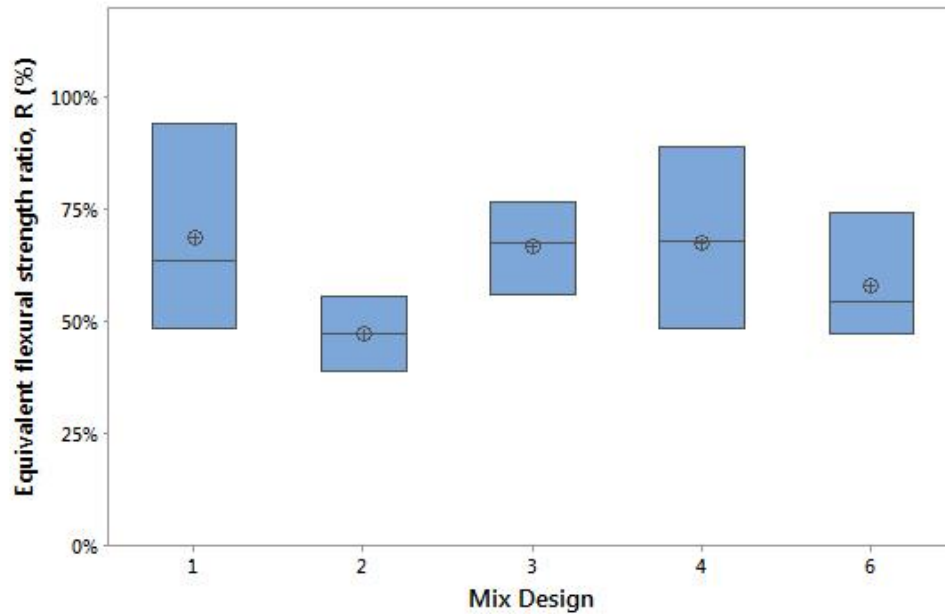


Figure 4.8. Equivalent flexural strength ratio for ASTM C1609 testing for mix design refinement

4.1.2. Behavior of Specimens with Varied Parameters. The following section discusses the results of ASTM C1609 testing with the varied parameters of fiber volume fraction and fiber type. The researchers tested the following fiber and volume fraction variations with mix design six to determine the performance and assist in developing the large-scale shear test program; B3 at 1%, B3 at 1.5%, B3 at 2%, B3(12k) at 1%, B4 at 1%, B5 at 1.5%, D1 at 1.8%, D1 at 2.4%, and a 50/50 blend of B5 and D1 at 1.5%. The Innegra fibers were added at a larger volume fraction compared to the carbon fiber due to the difference in density; the higher percentage corresponds to a similar number of discrete fibers in the mix, which affects the FRC fresh and hardened properties. Fibers D1 at 1.0%, 1.8%, and 2.4% can be compared to the B series of fibers at 0.75%, 1.5%, and 2.0% respectively. Also included in this section are the results from the ASTM C1609 specimens associated with the large-scale beam tests. This allows further comparison of fiber type and volume fraction effects on behavior and performance.

4.1.2.1 Physical behavior of ASTM C1609 specimens. Figure 4.9 illustrates the physical behavior of the specimens measured after completion of the test. The average permanent displacement of the beams was 0.083 in. (2.11 mm), with only an 8% coefficient of variation. As shown on the chart, even though there is a small change in permanent displacement, as the volume percentage of fibers is increased, the permanent deflection decreased for all fiber types. Also, it is shown that the steel fibers resulted in the largest permanent displacement overall, while the Innegra S fibers resulted in the lowest permanent displacement overall. The average crack width was 0.137 in. (3.5 mm) and was also relatively consistent. As mentioned above, occasionally, there was spalling at the crack location or more than one crack that formed making it difficult to precisely report the crack

width. It is interesting to note that the steel fiber reinforced concrete resulted in the largest average crack width, 0.21 in. (5.33 mm), compared to an average of 0.13 in. (3.30 mm) for all the other fiber type and volume percentage variations. Finally, the location of the crack was also very consistent at an average distance of 7.7 in. (195.6 mm), and within the middle third of the beam, ensuring pure flexural loading of the beams. Table 4.3 lists the information recorded for each specimen.

Table 4.3. Physical behavior for each ASTM C1609 specimen tested

Beam Series	Fiber	v_f (%)	Beam No.	f'_c (psi)	Δ (in.)	cw (in.)	a (in.)	b (in.)	d (in.)	Fibers top	Fibers bot	Total Fibers
M6	B3	1.0	1	6447	0.081	0.125	7.25	6.01	5.99	22	20	42
M6	B3	1.0	2	6447	0.085	0.150	6.75	6.05	6.01	16	12	28
M6	B3	1.0	3	6447	0.082	0.125	8.00	6.06	6.00	21	14	35
M6	B3	1.0	4	6447	0.088	0.156	7.75	6.05	6.05	24	16	40
M6	B3	1.0	5	6447	0.083	0.125	8.25	6.00	6.07	19	22	41
M6	B3	1.0	6	6447	0.080	0.100	7.88	5.99	6.01	18	13	31
M6	B3	1.5	1	6010	0.080	0.100	6.75	6.01	6.00	42	47	89
M6	B3	1.5	2	6010	0.079	0.100	7.88	6.05	6.05	46	29	75
M6	B3	1.5	3	6010	0.081	0.125	8.25	6.02	6.01	34	40	74
M6	B3	1.5	4	6010	0.085	0.156	7.50	5.98	6.02	20	18	38
M6	B3	1.5	5	6010	0.081	0.100	7.38	6.05	6.00	15	21	36
M6	B3	2.0	1	7084	0.068	0.125	8.63	5.99	5.95	62	44	106
M6	B3	2.0	2	7084	0.074	0.125	8.00	5.99	6.35	56	67	123
M6	B3	2.0	3	7084	0.080	0.100	6.25	5.92	5.93	50	33	83
M6	B3	2.0	4	7084	0.081	0.125	7.50	5.92	5.90	35	36	71
M6	B3	2.0	5	7084	0.087	0.156	8.75	5.91	6.25	32	38	70
M6	B3	2.0	6	7084	0.068	0.100	7.75	5.95	6.04	43	45	88

Table 4.3. Physical behavior for each ASTM C1609 specimen tested (continued)

Beam Series	Fiber	v_f (%)	Beam No.	f'_c (psi)	Δ (in.)	cw (in.)	a (in.)	b (in.)	d (in.)	Fibers top	Fibers bot	Total Fibers
M6	B3(12k)	1.0	1	6520	0.085	0.125	6.25	6.00	5.99	25	17	42
M6	B3(12k)	1.0	2	6520	0.088	0.180	6.75	6.01	6.00	34	31	65
M6	B3(12k)	1.0	3	6520	0.089	0.200	7.38	5.99	6.01	38	42	80
M6	B3(12k)	1.0	4	6520	0.082	0.125	6.75	5.95	6.04	32	36	68
M6	B3(12k)	1.0	5	6520	0.088	0.156	8.00	6.02	6.01	40	44	84
M6	B3(12k)	1.0	6	6520	0.085	0.150	7.75	6.05	6.00	64	47	111
M6	B4	1.0	1	6360	0.094	0.170	6.50	6.21	6.10	20	10	30
M6	B4	1.0	2	6360	0.099	0.200	6.00	5.97	6.15	12	13	25
M6	B4	1.0	3	6360	0.089	0.188	8.25	5.93	6.07	14	8	22
M6	B4	1.0	4	6360	0.090	0.200	7.25	6.11	6.08	12	15	27
M6	B4	1.0	5	6360	0.097	0.156	6.00	5.83	6.10	8	10	18
M6	B5	1.5	1	7042	0.088	0.127	8.00	6.07	6.14	37	43	80
M6	B5	1.5	2	7042	0.078	0.125	7.75	6.04	6.08	28	20	48
M6	B5	1.5	3	7042	0.083	0.125	8.00	6.08	6.07	31	31	62
M6	B5	1.5	4	7042	0.080	0.100	7.75	6.05	6.06	25	33	58
M6	B5	1.5	5	7042	0.082	0.100	8.00	6.06	6.01	48	27	75
M6	D1	1.8	1	7071	0.064	0.100	6.00	5.93	6.02	52	28	80
M6	D1	1.8	2	7071	0.063	0.125	7.75	5.95	6.35	42	36	78
M6	D1	1.8	3	7071	0.066	0.100	7.00	5.93	6.05	21	34	55
M6	D1	1.8	4	7071	0.060	0.100	7.75	6.01	5.95	44	42	86
M6	D1	1.8	5	7071	0.061	0.100	7.50	6.01	6.29	22	37	59
M6	D1	1.8	6	7071	0.066	0.150	8.25	5.96	5.99	23	34	57
M6	D1	2.4	1	7115	0.059	0.100	7.00	5.99	6.05	48	44	92
M6	D1	2.4	2	7115	0.061	0.125	8.00	5.96	6.25	50	58	108
M6	D1	2.4	3	7115	0.056	0.150	8.25	5.94	5.97	56	61	117
M6	D1	2.4	4	7115	0.063	0.100	8.00	5.95	6.03	51	60	111
M6	D1	2.4	5	7115	0.058	0.125	7.50	5.99	6.40	47	49	96
M6	D1	2.4	6	7115	0.062	0.100	9.00	5.92	6.02	43	51	94
M6	B5/D1	1.5	1	6520	0.075	0.100	7.50	5.95	6.00	41	15	56
M6	B5/D1	1.5	2	6520	0.080	0.125	7.00	5.99	6.05	26	18	44
M6	B5/D1	1.5	3	6520	0.070	0.125	8.00	5.92	6.15	53	12	65
M6	B5/D1	1.5	4	6520	0.072	0.156	8.25	6.01	6.10	38	11	49
M6	B5/D1	1.5	5	6520	0.077	0.100	7.75	6.05	6.01	13	12	25
M6	B5/D1	1.5	6	6520	0.074	0.125	7.50	5.99	6.02	33	16	49

Table 4.3. Physical behavior for each ASTM C1609 specimen tested (continued)

Beam Series	Fiber	v_f (%)	Beam No.	f'_c (psi)	Δ (in.)	cw (in.)	a (in.)	b (in.)	d (in.)	Fibers top	Fibers bot	Total Fibers
B18	B5	0.5	1	7250	0.089	0.150	7.00	6.09	6.04	12	7	19
B18	B5	0.5	2	7250	0.085	0.125	6.50	6.00	6.08	9	13	22
B18	B5	0.5	3	7250	0.087	0.180	8.00	6.16	6.05	10	10	20
B18	B5	0.5	4	7250	0.096	0.125	8.50	6.02	6.18	15	10	25
B18	B5	0.5	5	7250	0.086	0.156	6.25	6.10	6.07	23	16	39
B18	B5	0.5	6	7250	0.084	0.170	9.00	6.13	6.05	5	18	23
B18	B5	0.75	1	6391	0.081	0.125	6.75	6.14	6.00	33	27	60
B18	B5	0.75	2	6391	0.100	0.150	6.75	6.09	6.01	5	12	17
B18	B5	0.75	3	6391	0.087	0.140	6.00	6.06	6.25	14	16	30
B18	B5	0.75	4	6391	0.080	0.135	8.50	6.00	6.05	21	22	43
B18	B5	0.75	5	6391	0.080	0.156	8.00	6.06	6.42	15	16	31
B18	B5	0.75	6	6391	0.082	0.125	7.50	6.05	5.81	15	13	28
B18	B5	1.0	1	6376	0.069	0.125	9.00	6.00	6.00	25	30	55
B18	B5	1.0	2	6376	0.085	0.156	8.50	6.03	6.27	16	14	30
B18	B5	1.0	3	6376	0.077	0.140	8.00	6.03	6.02	25	22	47
B18	B5	1.0	4	6376	0.087	0.125	7.50	6.10	6.07	22	13	35
B18	B5	1.0	5	6376	0.067	0.125	6.75	5.97	6.26	28	16	44
B18	B5	1.0	6	6376	0.097	0.150	8.50	6.05	6.02	14	11	25
B18	D1	1.0	1	6315	0.102	0.100	9.00	5.90	6.20	6	9	15
B18	D1	1.0	2	6315	0.080	0.100	6.00	5.96	6.17	7	13	20
B18	D1	1.0	3	6315	0.086	0.125	9.00	6.03	6.07	7	13	20
B18	D1	1.0	4	6315	0.080	0.125	7.50	5.93	6.06	15	28	43
B18	D1	1.0	5	6315	0.087	0.100	8.75	6.07	6.01	13	12	25
B18	S	0.75	1	6780	0.105	0.190	8.75	6.06	6.11	-	-	-
B18	S	0.75	2	6780	0.108	0.200	8.00	6.03	6.22	-	-	-
B18	S	0.75	3	6780	0.107	0.220	8.50	6.06	5.99	-	-	-
B18	S	0.75	4	6780	0.107	0.210	8.00	5.98	6.33	-	-	-
B18	S	0.75	5	6780	0.107	0.230	8.50	5.96	6.10	-	-	-
B18	S	0.75	6	6780	0.105	0.180	7.75	6.11	5.98	-	-	-
B24	B5	0.5	1	7271	0.096	0.156	8.00	6.09	6.10	12	8	20
B24	B5	0.5	2	7271	0.102	0.175	8.00	6.02	6.10	4	11	15
B24	B5	0.5	3	7271	0.102	0.140	8.75	6.12	6.04	8	11	19
B24	B5	0.5	4	7271	0.087	0.150	8.00	5.92	6.11	14	9	23
B24	B5	0.5	5	7271	0.090	0.125	8.00	6.00	6.05	8	6	14
B24	B5	0.5	6	7271	0.104	0.175	9.00	5.93	6.01	10	15	25

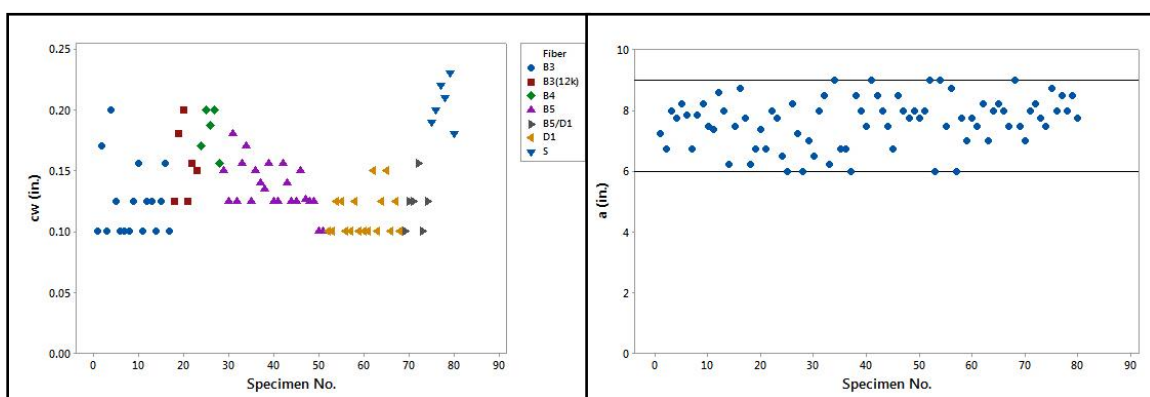
Table 4.3. Physical behavior for each ASTM C1609 specimen tested (continued)

Beam Series	Fiber	v_f (%)	Beam No.	f'_c (psi)	Δ (in.)	cw (in.)	a (in.)	b (in.)	d (in.)	Fibers top	Fibers bot	Total Fibers
B24	B5	0.75	1	7478	0.092	0.125	8.75	6.18	6.12	14	22	36
B24	B5	0.75	2	7478	0.087	0.150	8.75	6.20	6.27	22	18	40
B24	B5	0.75	3	7478	0.083	0.156	9.00	6.15	5.99	12	12	24
B24	B5	0.75	4	7478	0.086	0.100	6.50	6.12	6.24	24	22	46
B24	B5	0.75	5	7478	0.100	0.125	7.00	6.06	6.09	3	10	13
B24	B5	1.0	1	7254	0.089	0.100	7.00	6.09	6.04	10	12	22
B24	B5	1.0	2	7254	0.085	0.125	6.50	6.00	6.08	19	9	28
B24	B5	1.0	3	7254	0.087	0.150	8.00	6.16	6.05	12	12	24
B24	B5	1.0	4	7254	0.096	0.130	8.50	6.02	6.18	6	11	17
B24	B5	1.0	5	7254	0.086	0.150	6.25	6.10	6.07	11	9	20
B24	B5	1.0	6	7254	0.084	0.125	9.00	6.13	6.05	15	13	28

4.1.2.2 Load-displacement behavior of ASTM C1609 specimens. The load versus average midspan displacement curves for each set of specimens is shown in Figures 4.10 through 4.13. For most of the curves, it is apparent that post-peak hardening behavior is exhibited. The exception to this is in the beams containing a low volume fraction of fibers and can be seen specifically in the plots from series B18-B5-05 and B24-B5-0.5. The ASTM C1609 beams from series B24-B5-1.0 also show this trend, but when comparing the number of fibers at the location of the crack, this series contained a number of fibers more indicative of a volume fraction of 0.5%. The related performance of this series to the large-scale shear specimens will be discussed later. Fiber B4 also exhibited a trend of little to no post-peak hardening, which is attributed to the tight weave of the carbon fiber not allowing for as strong of a bond to the cementitious matrix as with Fibers B3, B5, and D1.

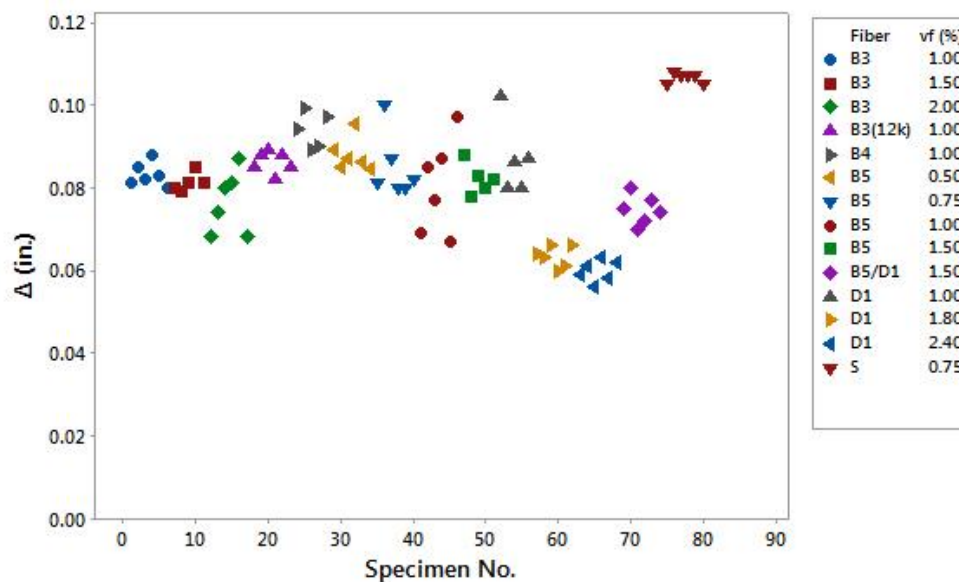
Comparing the behavior of the B series of fibers, it is apparent that Fibers B3 and B5 performed better than Fiber B4, especially within the first 0.06 in. (1.52 mm) of

displacement. Fibers B3 and B5 performed very similarly. For Fibers B3 and B5, as the volume fraction of fiber increased, the amount of post-peak hardening increased. Especially at high volume fractions, multiple cracks were likely to form during the test, further increasing the specimen's ability to sustain higher loads.



(a)

(b)



(c)

Figure 4.9. Distribution of (a) crack width, (b) crack location, (c) permanent displacement for each ASTM C1609 specimen with varying fiber types and percentages

Comparing the B series of fibers to the D series, it is seen that instead of steadily decreasing in load after some post-peak hardening as the B series exhibits, the D series of fibers steadily increases in load, especially at higher volume fractions. This is attributed to the lower tensile modulus of the Innegra fibers compared to the carbon fiber, allowing the fibers to stretch to carry more load, rather than fracture.

The 50/50 blend of Fibers B5 and D1 showed a combination of performance of each of the individual fibers, with a positive increase in post-peak hardening, while maintaining a steady residual load through the last 0.06 in. (1.52 mm) of displacement in the test.

The steel fiber reinforced beams behaved similarly to the beams reinforced with the B3 and B5 series of fibers, with some post-peak hardening, followed by a continuous reduction in load until the end of the test.

4.1.3. Equivalent Bending Stress, Toughness, and Equivalent Flexural Strength Ratio Behavior of ASTM C1609 Specimens. The effect of fiber type and volume fraction on the equivalent bending stress, toughness, and equivalent flexural strength ratio is presented in this section. Table 4.4 lists the recorded and calculated results for each specimen tested with Mix Design 6 and the specimens associated with large-scale shear beams. Figure 4.14 shows the relationship of the average equivalent bending stresses σ_c , σ_{pc} , σ_{600} , σ_{150} with varying fiber type and volume fraction. As was the case with the specimens related to the mix design refinement, there is not much change to σ_c , which is driven mainly by the modulus of rupture of the concrete.

Fiber types B3 and B5 both had very similar values for σ_{pc} at the same volume fraction and a clear trend that as the fiber percentage increased, the post-peak bending stress

increased at a linear rate. Although at 2.0% volume fraction, it was very difficult to place the fresh LCFRC and was at the limit of the usable range of the material. Fiber B4 had an approximately 30% lower post-peak bending stress compared to Fibers B3 and B5 at a volume fraction of 1.0%. Fiber D1 also had a lower post-peak bending stress compared to Fibers B3 and B5 of approximately 30% to 40% depending on the volume fraction. As shown in the load versus displacement curves, the blend of Fibers B5 and D1 provided the benefits of the high post-peak bending stress from the carbon fibers and attained the same approximate value at a volume fraction of 1.0%. The steel fibers performed approximately 25% higher than Fiber B5 at a volume fraction of 0.75%; although it should be noted that the placement of Fibers B5 at 0.75% was much easier than that of the steel fibers at the same volume fraction.

Similar behavior is shown for all beams for the equivalent bending stress at an average midspan displacement of 0.03 in. (0.762 mm). It is shown that the higher additions of Fibers D1 provided a lower benefit to the overall behavior, but more testing should be done to confirm this finding.

The bending stresses at 0.12 in. (3.05 mm) for specimens with Fibers B3 and B5 dropped approximately 60% compared to their post peak bending stress, and were again very similar in value. When comparing Fiber D1 to Fibers B3 and B5, there was a 20% higher performance at a volume fraction of 1.5% and 15% higher performance at a volume fraction of 2.0%. This result is also confirmed in the load displacement curves. As shown in the post-peak stress chart, the blend of Fiber B5 and D1 benefited from the addition of the Innegra fiber. Fiber B5/D1 attained an average value of only 5% below Fiber D1 at a corresponding volume fraction.

Figure 4.15 shows the relationship of the equivalent flexural strength ratio with the varied fiber parameters. This comparison looks at the overall performance of the specimens normalized to their modulus of rupture, providing a good basis to look at the overall effect of the varied parameters. It is interesting to see that, although Fibers B3 and B5 showed strong linear trends for behavior when comparing equivalent stresses, especially through the first 0.06 in. (1.52 mm), the overall effect of their addition diminished as the volume fraction increased. This behavior was also seen in Fiber D1 as well. Generally, the carbon fibers attained a slightly higher equivalent bending stress ratio than the Innegra fibers.

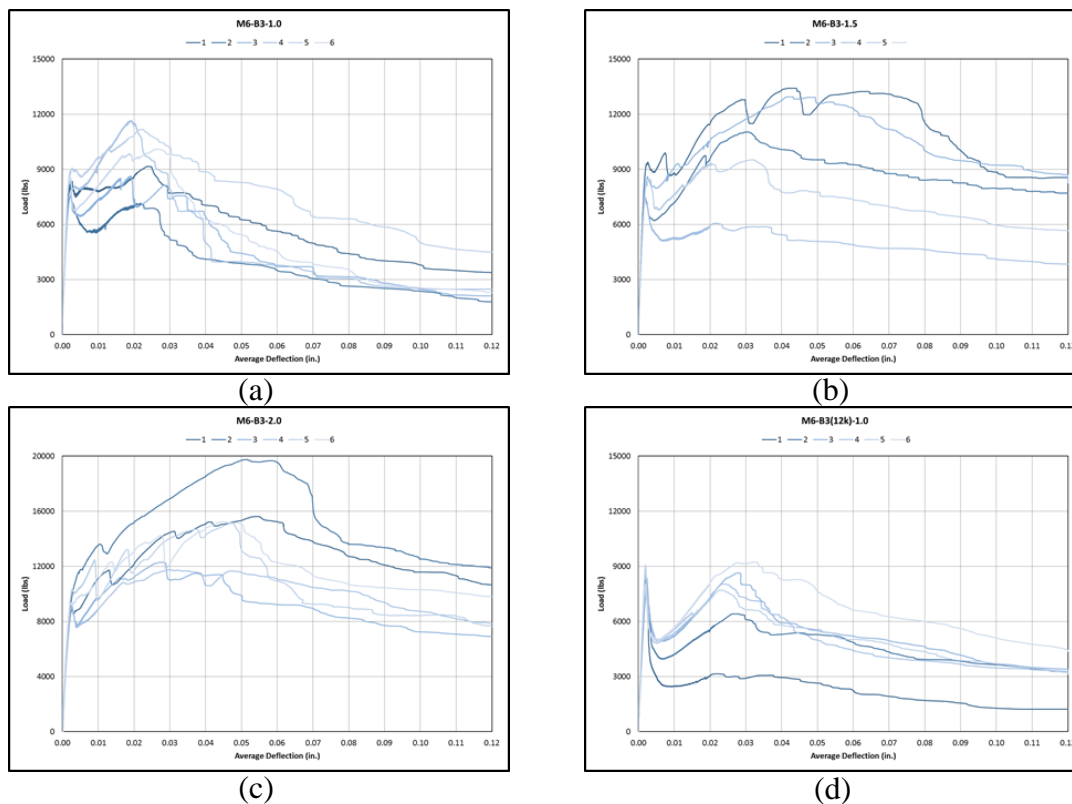


Figure 4.10. Load vs. deflection curves of ASTM C1609 tests, one (a) Fiber B3 @ 1% (b) Fiber B3 @ 1.5% (c) Fiber B3 @ 2% (d) Fiber B3(12k) @ 1%

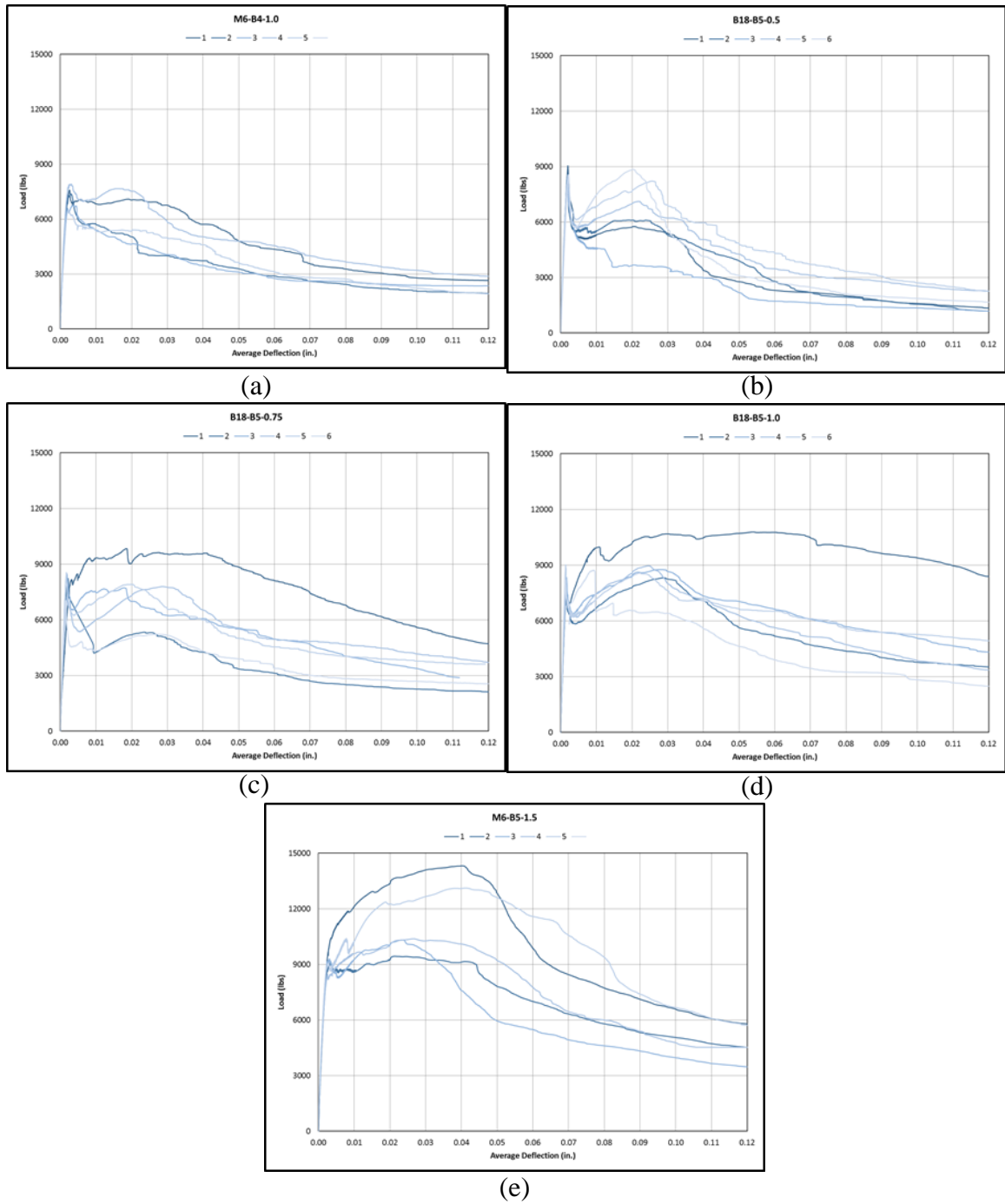
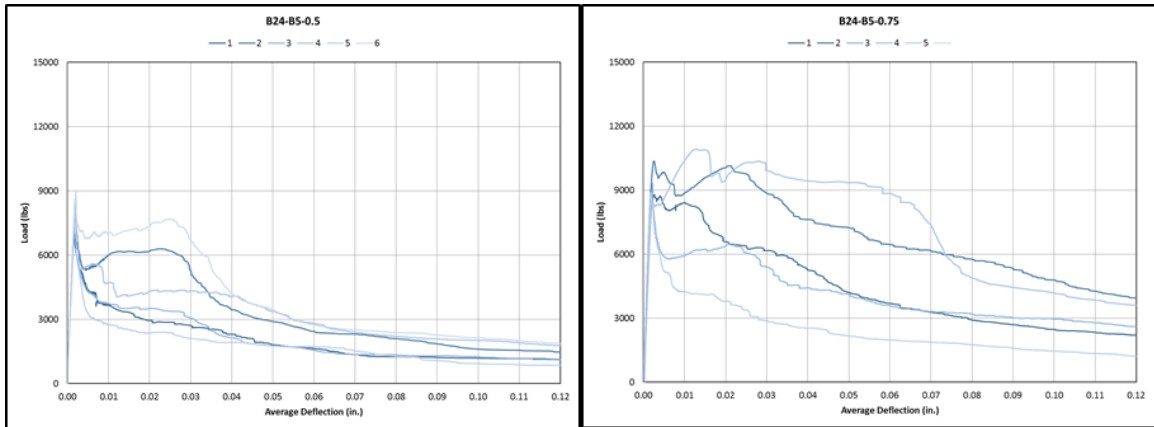
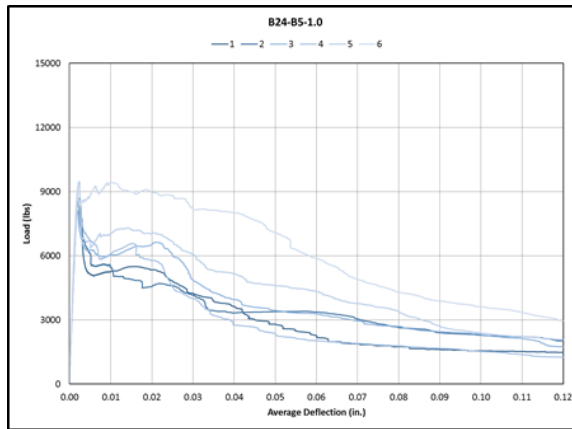


Figure 4.11. Load vs. deflection curves of ASTM C1609 tests, two (a) Fiber B4 @ 1% (b) Fiber B18-B5 @ 0.5% (c) Fiber B18-B5 @ 0.75% (d) Fiber B18-B5 @ 1% (e) Fiber M6-B5 @ 1.5%

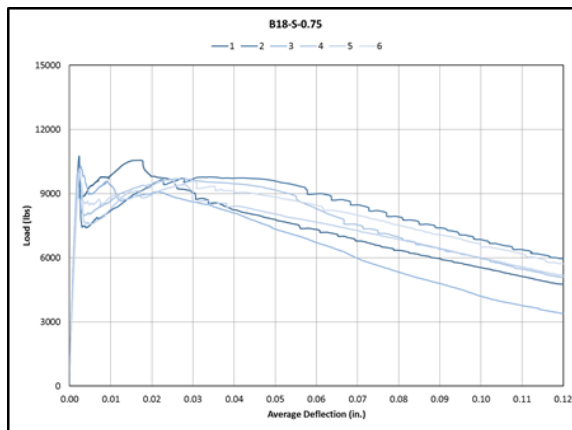


(a)

(b)



(c)



(d)

Figure 4.12. Load vs. deflection curves of ASTM C1609 tests, three (a) Fiber B24-B5 @ 0.5% (b) Fiber B24-B5 @ 0.75% (c) Fiber B24-B5 @ 1% (d) Fiber B18-S @ 0.75%

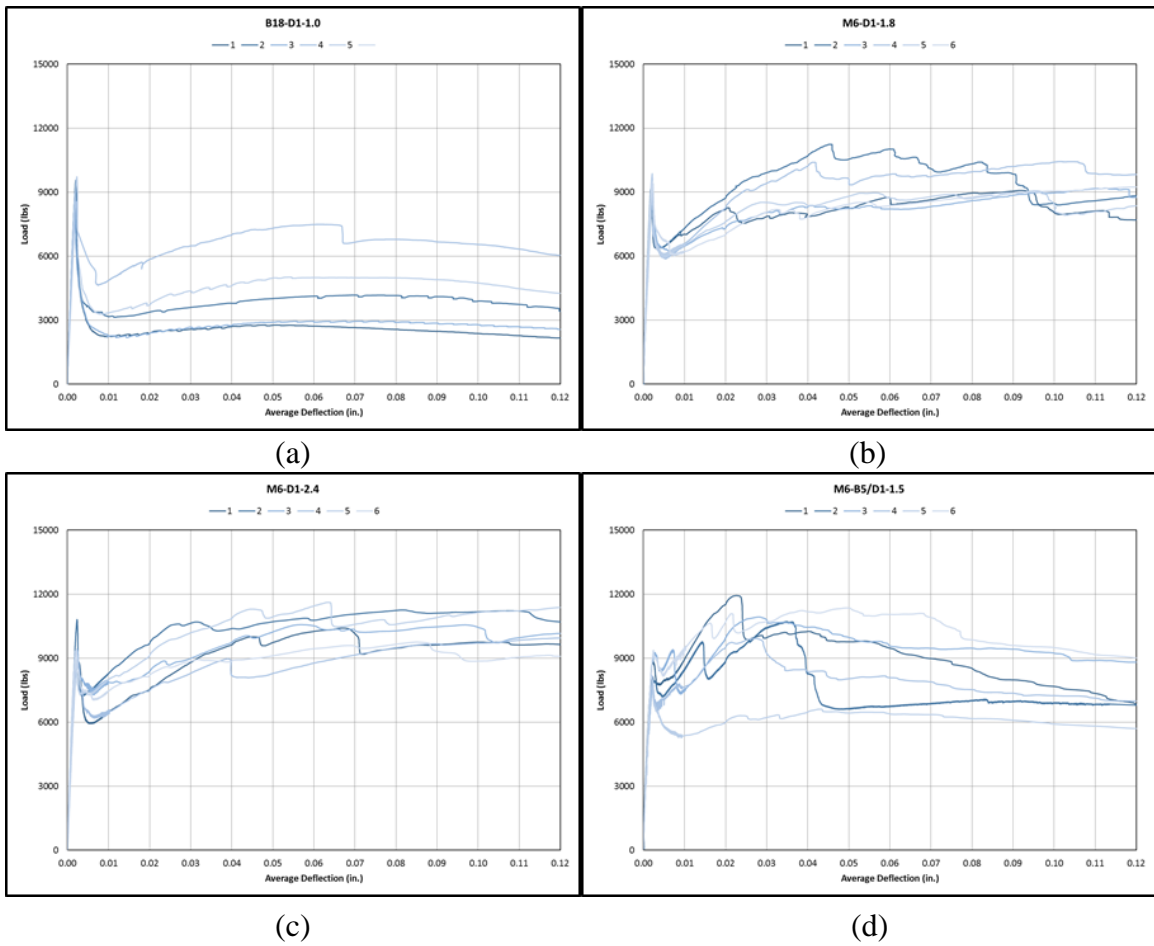


Figure 4.13. Load vs. deflection curves of ASTM C1609 tests, four (a) Fiber B18-D1 @ 1.0% (b) Fiber M6-D1 @ 1.8% (c) Fiber M6-D1 @ 2.4% (d) Fiber M6-B5D1 @ 1.5%

Table 4.4. Equivalent bending stress results from ASTM C1609 testing for fiber development phase

Series	Fiber	v_f (%)	Beam No.	σ_c (psi)	σ_{pc} (psi)	σ_{600} (psi)	σ_{300} (psi)	σ_{150} (psi)	δ_{pc} (in.)	T (in-lb)	$R_{T,150}$	ACI 318 90% Req.	ACI 318 75% Req.	Pass ACI Req?
M6	B3	1	1	697	764	643	470	281	0.0237	695	69%	67%	40%	FALSE
M6	B3	1	2	680	590	426	287	147	0.0219	468	47%	42%	22%	FALSE
M6	B3	1	3	698	712	611	306	174	0.0190	554	55%	44%	25%	FALSE
M6	B3	1	4	880	947	642	307	201	0.0191	640	49%	35%	23%	FALSE
M6	B3	1	5	822	909	830	644	366	0.0215	899	74%	78%	45%	FALSE
M6	B3	1	6	796	840	813	377	191	0.0264	627	55%	47%	24%	FALSE

Table 4.4. Equivalent bending stress results from ASTM C1609 testing for fiber development phase (continued)

Series	Fiber	v_f (%)	Beam No.	σ_c (psi)	σ_{pc} (psi)	σ_{600} (psi)	σ_{300} (psi)	σ_{150} (psi)	δ_{pc} (in.)	T (in-lb)	$R_{T,150}$	ACI 318 90% Req.	ACI 318 75% Req.	Pass ACI Req?
M6	B3	1.5	1	852	1116	1034	1097	711	0.0422	1287	105%	129%	84%	TRUE
M6	B3	1.5	2	680	896	896	752	626	0.0298	1047	104%	111%	92%	TRUE
M6	B3	1.5	3	802	1071	971	1019	720	0.0414	1256	108%	127%	90%	TRUE
M6	B3	1.5	4	622	504	485	406	319	0.0215	589	66%	65%	51%	FALSE
M6	B3	1.5	5	704	786	782	608	468	0.0314	871	85%	86%	66%	FALSE
M6	B3	2	1	850	1326	1226	1294	904	0.0540	1528	127%	152%	106%	TRUE
M6	B3	2	2	943	1471	1260	1456	886	0.0508	1810	119%	155%	94%	TRUE
M6	B3	2	3	794	1063	953	797	596	0.0281	1094	99%	100%	75%	TRUE
M6	B3	2	4	791	1026	1026	966	684	0.0299	1197	110%	122%	86%	TRUE
M6	B3	2	5	891	1178	1094	853	595	0.0468	1282	93%	96%	67%	FALSE
M6	B3	2	6	842	1263	1009	1018	812	0.0446	1412	116%	121%	96%	TRUE
M6	B3(12k)	1	1	707	263	243	187	102	0.0220	268	26%	26%	14%	FALSE
M6	B3(12k)	1	2	660	533	508	404	269	0.0278	549	58%	61%	41%	FALSE
M6	B3(12k)	1	3	695	718	665	433	279	0.0273	629	63%	62%	40%	FALSE
M6	B3(12k)	1	4	709	666	605	366	259	0.0241	586	57%	52%	37%	FALSE
M6	B3(12k)	1	5	752	637	550	415	267	0.0227	606	56%	55%	36%	FALSE
M6	B3(12k)	1	6	662	762	756	548	361	0.0320	785	82%	83%	55%	FALSE
M6	B4	1	1	591	552	526	339	206	0.0189	554	61%	57%	35%	FALSE
M6	B4	1	2	588	459	319	230	155	0.0091	394	45%	39%	26%	FALSE
M6	B4	1	3	556	554	334	228	194	0.0036	399	49%	41%	35%	FALSE
M6	B4	1	4	630	611	464	363	229	0.0156	569	60%	58%	36%	FALSE
M6	B4	1	5	537	462	413	259	159	0.0071	428	55%	48%	30%	FALSE
M6	B5	1.5	1	892	1126	1109	777	455	0.0400	1193	88%	87%	51%	FALSE
M6	B5	1.5	2	734	761	750	564	365	0.0213	846	77%	77%	50%	FALSE
M6	B5	1.5	3	747	829	780	441	279	0.0234	751	67%	59%	37%	FALSE
M6	B5	1.5	4	750	841	832	629	367	0.0266	947	85%	84%	49%	FALSE
M6	B5	1.5	5	849	1079	1041	953	469	0.0412	1194	96%	112%	55%	FALSE
M6	D1	1.8	1	781	760	658	731	645	0.0914	973	87%	94%	83%	TRUE
M6	D1	1.8	2	686	843	744	827	663	0.0450	1128	103%	121%	97%	TRUE
M6	D1	1.8	3	780	762	667	681	727	0.1122	983	87%	87%	93%	FALSE
M6	D1	1.8	4	760	883	796	832	831	0.1011	1120	104%	109%	109%	TRUE
M6	D1	1.8	5	747	686	645	661	633	0.0954	992	84%	88%	85%	FALSE
M6	D1	1.8	6	798	778	679	704	778	0.1199	988	87%	88%	97%	FALSE

Table 4.4. Equivalent bending stress results from ASTM C1609 testing for fiber development phase (continued)

Series	Fiber	v_f (%)	Beam No.	σ_c (psi)	σ_{pc} (psi)	σ_{600} (psi)	σ_{300} (psi)	σ_{150} (psi)	δ_{pc} (in.)	T (in-lb)	$R_{T,150}$	ACI 318 90% Req.	ACI 318 75% Req.	Pass ACI Req?
M6	D1	2.4	1	760	855	723	842	791	0.0670	1090	98%	111%	104%	TRUE
M6	D1	2.4	2	836	870	822	833	827	0.0815	1252	96%	100%	99%	TRUE
M6	D1	2.4	3	801	899	764	894	863	0.0569	1156	102%	112%	108%	TRUE
M6	D1	2.4	4	760	827	690	730	827	0.1199	1041	95%	96%	109%	TRUE
M6	D1	2.4	5	686	852	747	839	835	0.0631	1242	111%	122%	122%	TRUE
M6	D1	2.4	6	787	818	743	792	762	0.0850	1066	95%	101%	97%	TRUE
M6	B5/D1	1.5	1	748	1003	837	796	576	0.0226	1072	100%	106%	77%	TRUE
M6	B5/D1	1.5	2	667	989	854	554	976	0.1142	941	97%	83%	146%	FALSE
M6	B5/D1	1.5	3	756	879	867	770	709	0.0281	1135	101%	102%	94%	TRUE
M6	B5/D1	1.5	4	643	798	743	651	563	0.0273	948	99%	101%	88%	TRUE
M6	B5/D1	1.5	5	677	544	512	526	469	0.0427	733	74%	78%	69%	FALSE
M6	B5/D1	1.5	6	777	941	888	916	748	0.0495	1214	108%	118%	96%	TRUE
B18	B5	0.5	1	732	466	436	186	109	0.0204	375	35%	25%	15%	FALSE
B18	B5	0.5	2	673	495	429	227	96	0.0190	406	41%	34%	14%	FALSE
B18	B5	0.5	3	681	402	282	137	94	0.0050	290	28%	20%	14%	FALSE
B18	B5	0.5	4	633	557	487	272	177	0.0217	498	51%	43%	28%	FALSE
B18	B5	0.5	5	686	658	552	346	182	0.0253	562	55%	50%	27%	FALSE
B18	B5	0.5	6	684	709	452	220	133	0.0201	455	44%	32%	19%	FALSE
B18	B5	0.75	1	663	802	778	661	384	0.0184	912	93%	100%	58%	FALSE
B18	B5	0.75	2	675	437	408	257	174	0.0233	419	42%	38%	26%	FALSE
B18	B5	0.75	3	646	587	474	378	220	0.0178	585	57%	59%	34%	FALSE
B18	B5	0.75	4	595	638	634	406	303	0.0286	647	74%	68%	51%	FALSE
B18	B5	0.75	5	616	569	474	327	261	0.0199	613	60%	53%	42%	FALSE
B18	B5	0.75	6	620	460	454	299	225	0.0268	438	52%	48%	36%	FALSE
B18	B5	1	1	773	897	889	896	698	0.0535	1180	106%	116%	90%	TRUE
B18	B5	1	2	584	631	627	393	267	0.0287	658	71%	67%	46%	FALSE
B18	B5	1	3	686	721	713	546	356	0.0279	776	78%	80%	52%	FALSE
B18	B5	1	4	632	719	643	453	269	0.0245	696	74%	72%	43%	FALSE
B18	B5	1	5	695	661	589	503	380	0.0219	764	71%	72%	55%	FALSE
B18	B5	1	6	700	717	526	320	204	0.0091	544	53%	46%	29%	FALSE
B18	D1	1	1	697	220	205	216	172	0.0510	312	30%	31%	25%	FALSE
B18	D1	1	2	758	331	286	327	271	0.0696	464	40%	43%	36%	FALSE
B18	D1	1	3	724	239	217	235	208	0.0749	337	31%	33%	29%	FALSE
B18	D1	1	4	707	619	536	618	499	0.0618	783	76%	87%	71%	FALSE
B18	D1	1	5	799	412	358	410	350	0.0537	551	47%	51%	44%	FALSE

Table 4.4. Equivalent bending stress results from ASTM C1609 testing for fiber development phase (continued)

Series	Fiber	v_f (%)	Beam No.	σ_c (psi)	σ_{pc} (psi)	σ_{600} (psi)	σ_{300} (psi)	σ_{150} (psi)	δ_{pc} (in.)	T (in-lb)	$R_{T,150}$	ACI 318 90% Req.	ACI 318 75% Req.	Pass ACI Req?
B24	B5	0.5	1	584	332	215	129	87	0.0060	244	28%	22%	15%	FALSE
B24	B5	0.5	2	689	505	421	196	118	0.0225	392	38%	28%	17%	FALSE
B24	B5	0.5	3	668	317	247	126	90	0.0072	252	25%	19%	13%	FALSE
B24	B5	0.5	4	655	455	352	228	145	0.0063	377	39%	35%	22%	FALSE
B24	B5	0.5	5	708	246	173	142	71	0.0067	213	21%	20%	10%	FALSE
B24	B5	0.5	6	757	645	563	230	158	0.0252	470	43%	30%	21%	FALSE
B24	B5	0.75	2	765	748	654	476	291	0.0208	815	66%	62%	38%	FALSE
B24	B5	0.75	1	704	654	480	287	171	0.0099	528	49%	41%	24%	FALSE
B24	B5	0.75	3	760	528	439	293	213	0.0216	494	44%	39%	28%	FALSE
B24	B5	0.75	4	716	824	748	668	273	0.0129	875	77%	93%	38%	FALSE
B24	B5	0.75	5	713	408	231	158	97	0.0062	295	28%	22%	14%	FALSE
B24	B5	1	1	703	445	343	184	120	0.0158	355	34%	26%	17%	FALSE
B24	B5	1	2	707	456	337	273	164	0.0084	409	39%	39%	23%	FALSE
B24	B5	1	3	648	529	388	262	139	0.0210	446	46%	40%	21%	FALSE
B24	B5	1	4	714	514	314	159	99	0.0153	353	32%	22%	14%	FALSE
B24	B5	1	5	758	585	486	347	166	0.0142	527	46%	46%	22%	FALSE
B24	B5	1	6	744	756	655	471	238	0.0091	728	65%	63%	32%	FALSE
B18	S	0.75	1	779	840	719	582	379	0.0166	884	75%	75%	49%	FALSE
B18	S	0.75	2	830	754	748	694	459	0.0342	990	77%	84%	55%	FALSE
B18	S	0.75	3	851	794	713	556	281	0.0089	786	64%	65%	33%	FALSE
B18	S	0.75	4	748	728	724	623	382	0.0258	932	78%	83%	51%	FALSE
B18	S	0.75	5	826	764	705	622	420	0.0277	888	73%	75%	51%	FALSE
B18	S	0.75	6	822	792	788	696	471	0.0237	957	80%	85%	57%	FALSE

4.1.4. Evaluation of ASTM C1609 Results for ACI Requirements. ACI 318-

14 allows for the use of steel fibers as shear reinforcement in place of traditional mild steel, if specific criteria are met. For the ASTM C1609 performance, the specimen must reach at least 90% of the initial cracking strength at a midspan displacement of $L/300$ and 75% of the initial cracking strength at a midspan displacement of $L/150$. The results are shown in Table 4.4. The carbon fibers were able to meet these criteria, on average, for all specimens

tested at volume fractions higher than 1.5%. The Innegra fibers were also able to meet these criteria, on average, for all specimens tested at a volume fraction higher than 1.8%. Although the steel fibers used within this research program are typically used in the construction market today, they were unable to meet the ACI 318 requirements with the parameters the research team chose.

4.1.5. Summary of ASTM C1609 Performance. The ASTM C1609 test was an important step in the development of the long carbon fibers, as well as establishing the parameters for the large-scale shear beam testing. The small-scale tests allowed the research team to identify if there were any influences in the hardened concrete behavior based on changes in the mix design. The research team also gathered important information regarding the effect of the addition of the carbon fibers at different volume fractions. It is a well understood fact that as the volume fraction increases, the performance of the specimens undergoing ASTM C1609 testing will improve, but through many tests, the research team was able to identify that at higher volume fractions, the impact of the fiber addition is reduced compared to lower volume fractions. Also, the effect on fiber type combined with the specific processing method used for the fibers in this research program should be further investigated. The Innegra fibers showed promising performance, especially when blended with the carbon fibers, which could be a worthy balance of cost and performance. The research team was also able to identify that at similar volume fractions, the carbon fiber reinforced concrete had an equal equivalent flexural strength ratio to the steel fiber reinforced concrete, validating further testing. Finally, the research team used the results of the small-scale testing, both fresh and hardened properties, to establish the tested variables for the large-scale beam tests. The lower percentages were

used in order to accommodate better placement of the fresh concrete, with the confidence of a significant increase in shear performance of the FRC.

4.2. PERFORMANCE AND BEHAVIOR OF 18 in. (457mm) DEEP BEAMS

The following sections provide an overview of the behavior of the tested beams with an overall depth of 18 in. (457 mm). Each series will be analyzed separately with an in-depth overview of the load versus deflection and failure behavior, crack behavior and development, midspan deflection, and reinforcement strains. Each beam series will be compared to each other, as well as the control series, in order to evaluate the varied parameters in the study. The research team also used the control beams in this study, along with the ACI 318-14 code, to evaluate the performance of the FRC beams compared to the required calculated resistance. Table 4.5 presents an overview of the loads and failure modes for each beam tested. Table 4.6 presents an overview of the crack behavior for each beam tested. In Table 4.5, v_u was calculated using Equation 4-3, where P_u is the total applied load, b is the beam width, and d is the beam effective depth; Δ is the midspan deflection of the beam at ultimate load. The failure modes referenced in Table 4.5 are as follows: DT – diagonal tension, FC – flexural compression, ST – shear tension, SC – shear compression. In Table 4.6, n is the number of inclined shear cracks in each shear span, Σs is the total spacing of the inclined shear cracks, s is the average spacing between inclined shear cracks, W is the west shear span, E is the east shear span, θ_c is the angle of critical inclined shear crack with respect to the longitudinal axis of the beam.

$$v_u = \frac{P_u}{2*b*d} \quad \text{(Equation 4-3)}$$

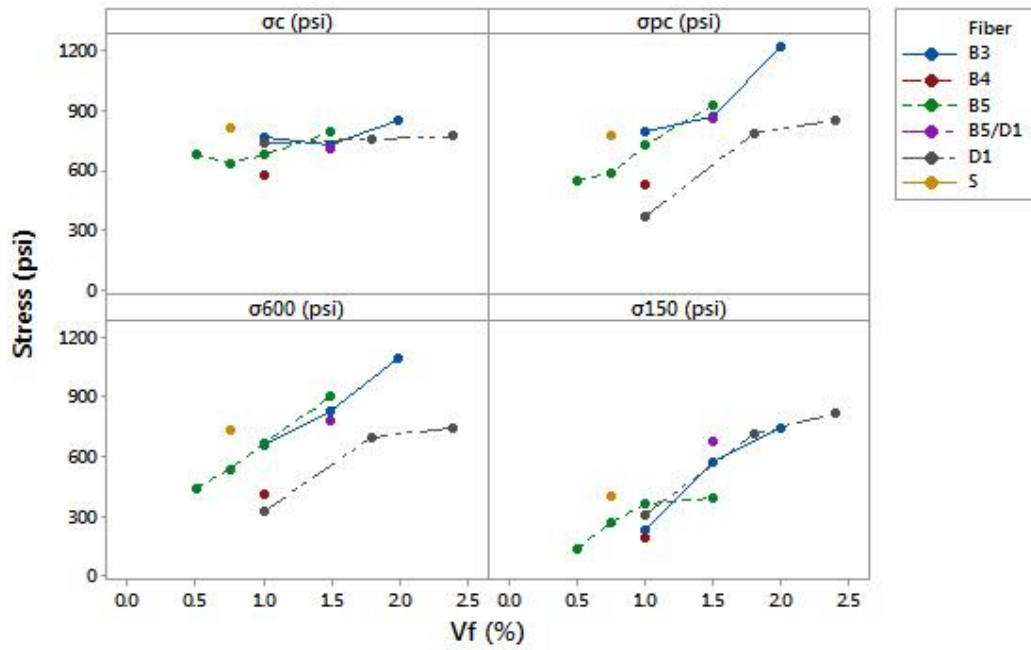


Figure 4.14. Equivalent stress results for ASTM C1609 testing

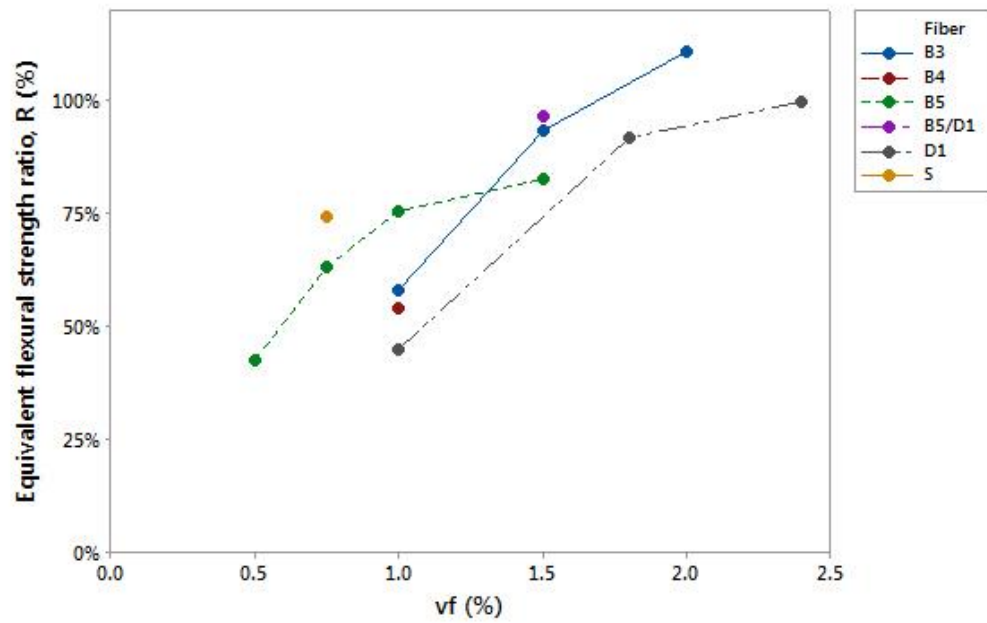


Figure 4.15. Equivalent flexural strength ratio results for ASTM C1609 testing

Table 4.5. Load and failure data for Series B18 and B24 shear beams

Beam	P_u (kips)	v_u (psi)	f'_c (psi)	$v_u/\sqrt{f'_c}$	Failure Mode	Reinf. Yield?	Δ (in.)
B18-PC-1	45.7	194	5452	2.62	DT	N	0.37
B18-PC-2	50.8	215	5452	2.92	DT	N	0.27
B18-PC-3	44.6	189	5452	2.56	DT	N	0.22
B18-TR-1	123.3	522	6143	6.67	FC	Y	1.14
B18-TR-2	114.5	485	6143	6.19	FC	Y	1.04
B18-TR-3	110.5	468	6143	5.97	FC	Y	0.91
B18-B5-0.5-1	72.6	307.6	6250	3.89	DT	N	0.52
B18-B5-0.5-2	74.0	313.6	6250	3.97	DT	N	0.56
B18-B5-0.5-3	71.6	303.4	6250	3.84	SC+DT	N	0.46
B18-B5-0.75-1	69.6	295	5583	3.95	DT	N	0.51
B18-B5-0.75-2	65.3	277	5583	3.70	DT	N	0.45
B18-B5-0.75-3	69	292	5583	3.91	ST+DT	N	0.54
B18-B5-1.0-1	90.4	383	5665	5.09	DT	N	0.75
B18-B5-1.0-2	70.4	298	5665	3.96	ST+DT	N	0.52
B18-B5-1.0-3	83.5	354	5665	4.70	DT	N	0.65
B24-B5-0.5-1	91.4	284.9	6390	3.56	DT	N	0.47
B24-B5-0.5-2	92.2	287.4	6390	3.60	DT	N	0.49
B24-B5-0.5-3	85.8	267.5	6390	3.35	DT	N	0.54
B24-B5-0.75-1	108.7	339	6131	4.33	ST+DT	N	0.64
B24-B5-0.75-2	101.5	316	6131	4.04	DT	N	0.61
B24-B5-0.75-3	92.2	287	6131	3.67	ST+DT	N	0.48
B24-B5-1.0-1	125.1	390	6306	4.91	DT	N	0.68
B24-B5-1.0-2	141.8	442	6306	5.57	DT	N	1.10
B24-B5-1.0-3	117.5	366	6306	4.61	DT	N	0.79
B18-D1-1.0-1	72.2	306	5376	4.17	SC+DT	N	0.64
B18-D1-1.0-2	57.1	242	5376	3.30	SC+DT	N	0.48
B18-D1-1.0-3	59.4	252	5376	3.43	SC+DT	N	0.48
B18-S-1.0-1	101.9	432	6143	5.51	DT	N	0.74
B18-S-1.0-2	84.7	359	6143	4.58	ST+DT	N	0.64
B18-S-1.0-3	93.4	396	6143	5.05	ST+DT	N	0.71

Table 4.6. Crack behavior data for B18 and B24 series shear beams

Beam	W			E			Failure location (E/W)	θ_c (°)
	n	Σs (in.)	s (in.)	n	Σs (in.)	s (in.)		
B18-PC-1	3	9.5	4.8	4	20.0	6.7	E	30
B18-PC-2	1	-	-	3	13.8	6.9	E	31
B18-PC-3	2	11.3	11.3	2	13.5	13.5	E	36
B18-TR-1	5	23.5	5.9	6	29.3	5.9	W	-
B18-TR-2	6	26.0	5.2	5	29.3	7.3	-	-
B18-TR-3	7	31.5	5.3	4	27.0	9.0	-	-
B18-B5-0.5-1	5	28.0	7.0	4	24.8	8.3	E	21
B18-B5-0.5-2	4	18.0	6.0	3	22.5	11.3	W	23
B18-B5-0.5-3	3	22.5	11.3	5	29.5	7.4	E	24
B18-B5-0.75-1	2	22.5	22.5	2	4.5	4.5	E	24
B18-B5-0.75-2	2	15.8	15.8	3	24.8	12.4	E	25
B18-B5-0.75-3	3	26.0	13.0	4	31.5	10.5	E	30
B18-B5-1.0-1	5	36.0	9.0	5	31.5	7.9	W	32
B18-B5-1.0-2	2	11.3	11.3	2	11.3	11.3	E	27
B18-B5-1.0-3	3	27.0	13.5	5	27.0	6.8	W	28
B24-B5-0.5-1	6	36.0	7.2	4	36.0	12.0	W	21
B24-B5-0.5-2	5	30.0	7.5	5	45.0	11.3	E	22
B24-B5-0.5-3	6	39.0	7.8	4	30.0	10.0	E	27
B24-B5-0.75-1	7	42.0	7.0	4	31.0	10.3	E	24
B24-B5-0.75-2	5	30.0	7.5	5	25.5	6.4	W	22
B24-B5-0.75-3	3	21.0	10.5	4	30.0	10.0	E	32
B24-B5-1.0-1	4	36.0	12.0	5	24.0	6.0	E	27
B24-B5-1.0-2	6	29.0	5.8	8	48.0	6.9	E	27
B24-B5-1.0-3	7	33.0	5.5	4	18.0	6.0	E	26
B18-D1-1.0-1	2	11.3	11.3	4	30.5	10.2	W	26
B18-D1-1.0-2	2	23.5	23.5	1	-	-	E	23
B18-D1-1.0-3	4	27.0	9.0	2	11.3	11.3	E	27
B18-S-1.0-1	3	20.3	10.1	9	29.3	3.7	W	22
B18-S-1.0-2	5	22.5	5.6	2	20.3	20.3	E	35
B18-S-1.0-3	4	24.8	8.3	4	22.5	7.5	E	26

4.2.1. Beam Series B18-PC. Beams in Series B18-PC were the control beams, containing no transverse reinforcement. This series provides a baseline shear performance for the concrete mix design used in the study. Although variations can be expected within each series, the data generated within this study was very consistent and the concrete compressive strengths only varied 7% between beam series.

During loading, the first cracks to develop were flexural cracks between the two loading points, at the location of the highest moment. As the test progressed, the flexural cracks spread out towards the supports, relatively evenly spaced. Eventually, an inclined crack formed, and each beam failed relatively soon after in diagonal tension

For Beam 1, the first flexural crack formed at 15 kips (69 kN) and the first inclined crack formed at 31 kips (138 kN). The beam failed at 45.7 kips (203 kN), 47% above the load at the formation of the first inclined crack. For Beam 2, the first flexural crack formed at 15 kips (69 kN) and the first inclined crack formed at 42 kips (187 kN). The beam failed at 50.8 kips (226 kN), 21% above the load at the formation of the first inclined crack. For Beam 3, the first flexural crack formed at 18 kips (80 kN) and the first inclined crack formed at 32 kips (142 kN). The beam failed at 44.6 kips (198 kN), 39% above the load at the formation of the first inclined crack.

The beams in this series had an average failure load of 47 kips (209 kN) with a coefficient of variation (COV) of 7.0%. Considering the beams failed due to shear mechanisms, the data collected is very consistent. Figure 4.16 shows the load versus displacement behavior for each beam in Series B18-PC. Figure 4.17 shows the crack behavior of each beam in Series B18-PC after failure. Prior to failure, Beam 1 developed a

total of 7 inclined cracks within both shear zones, Beams 2 and 3 developed a total of 4 inclined cracks each. The average angle of inclined crack at failure for this series was 32° .

Using equation 11-3 from ACI 318-14, this type of beam should have a normalized shear stress of 2.0. The average of the maximum loads in this series resulted in a normalized shear stress of 2.72, 36% higher than the calculated value. This baseline shear stress for the concrete will be taken into account for the comparison of the FRC performance relative to the ACI requirements.

All beams in Series B18-PC exhibited a linear load-displacement behavior up to the formation of the first flexural crack, at which point the slope decreased and remained constant until failure, with a sudden drop in load as a result of the absence of transverse reinforcement included in the beams. Beam 1 exhibited the highest midspan displacement at failure of 0.37 in. (9.4 mm) even though it did not have the highest load. Beam 2 had a midspan displacement of 0.27 in. (6.9 mm) and Beam 3's midspan displacement at failure was 0.22 in. (5.6 mm).

The reinforcement strains for each beam are shown in Figure 4.18. Due to issues with the data acquisition system for this series, only Beams 1 and 2 received any reinforcement strain data. The research team was only able to collect data from strain gauges 2, 3, and 4. Strain gauge 2 was located at the middle of the west shear span. Strain gauges 3 and 4 were located on opposite sides of the lower level of longitudinal reinforcement at midspan of the beam. It can be seen for both Beams 1 and 2 that the strains were very linear up to the formation of the first flexural crack, at which point strain gauges 3 and 4 had a higher rate of strain increase compared to strain gauge 2. This is due to the higher strain in the longitudinal reinforcement at the center of the beam corresponding to

the location of the highest moment. As shown in the curves, the longitudinal reinforcement did not yield in either beam at the maximum load. It can be assumed the reinforcement did not yield in the third beam in the series as well due to the similarities in load to Beams 1 and 2, as well as the load displacement behavior.

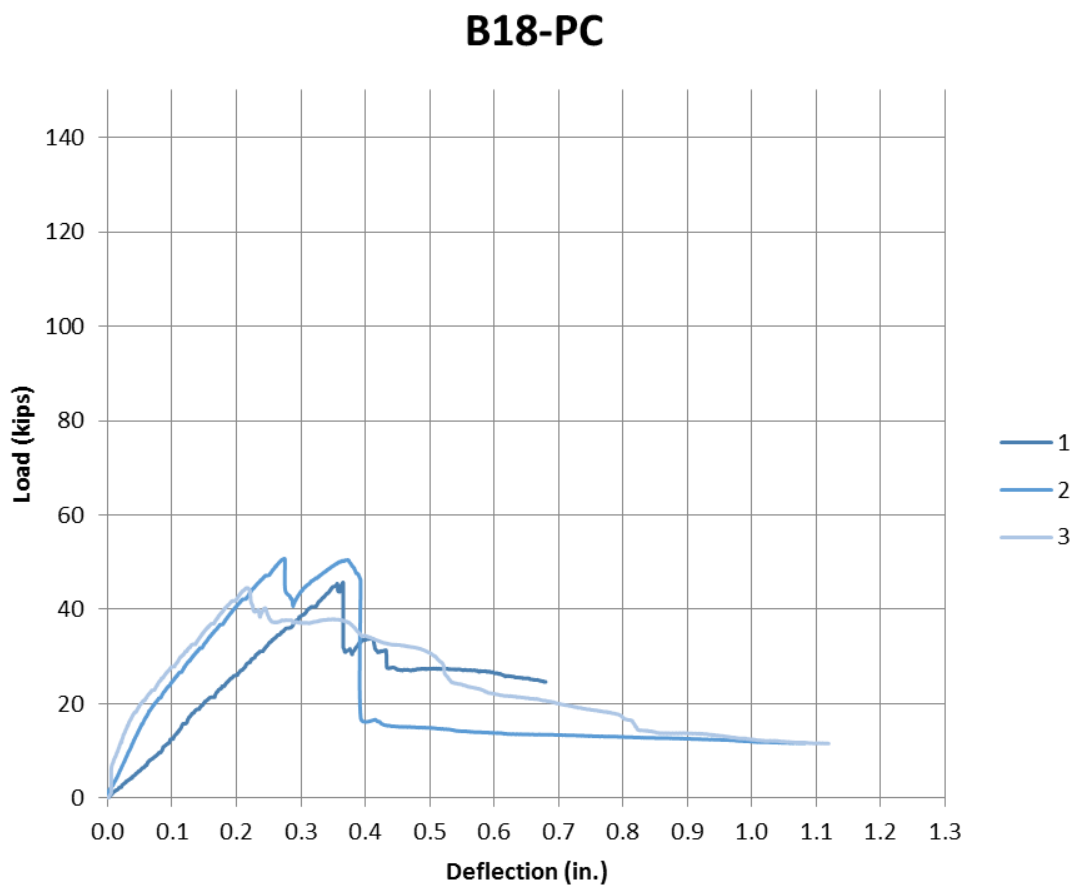
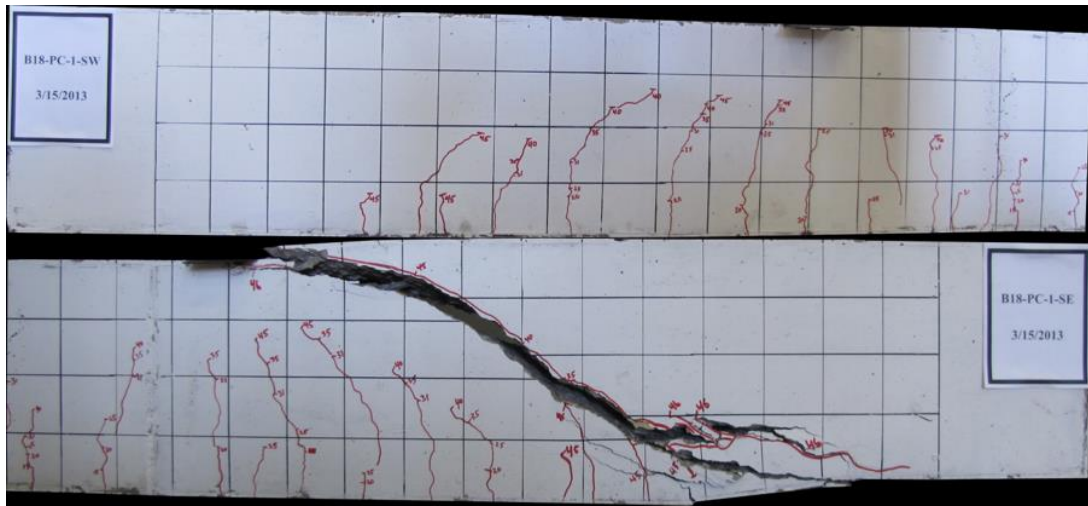
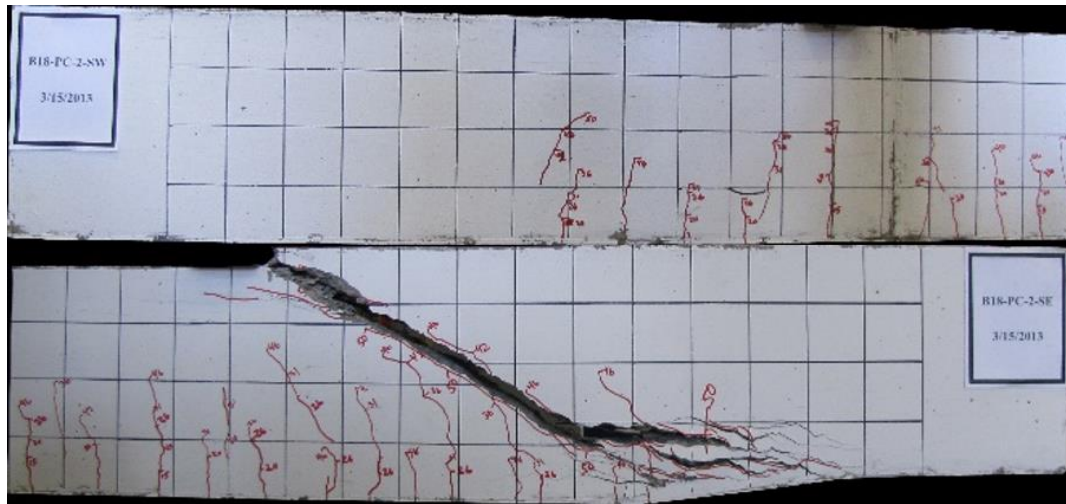


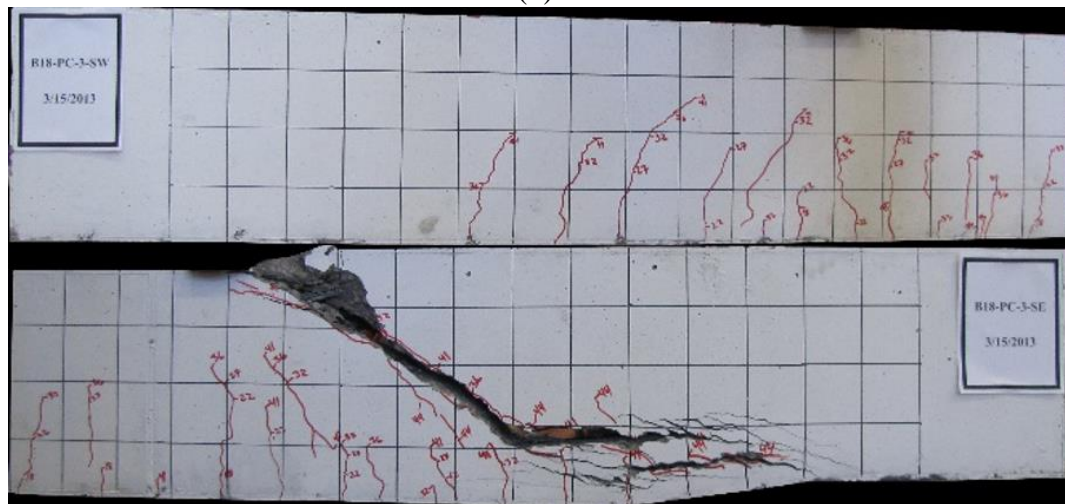
Figure 4.16. Load versus displacement behavior for beams in Series B18-PC



(a)



(b)



(c)

Figure 4.17. Crack behavior of beams in Series B18-PC after failure (a) B18-PC-1 (b) B18-PC-2 (c) B18-PC-3

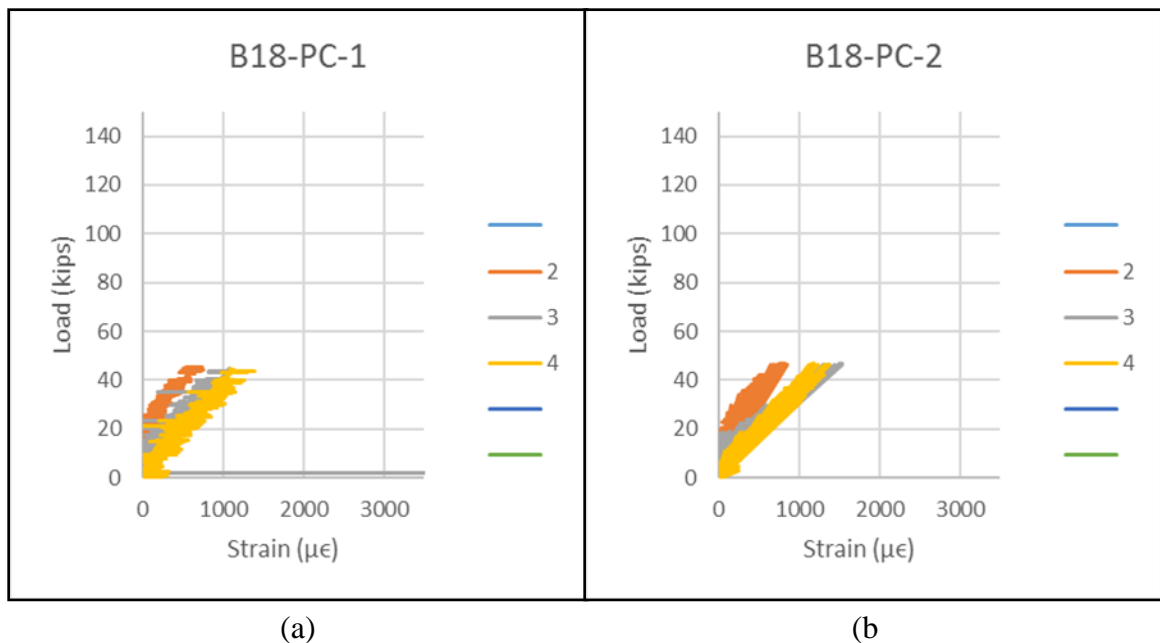


Figure 4.18. Reinforcement strains for beams in Series B18-PC

4.2.2. Beam Series B18-TR. Beams in Series B18-TR were the control beams containing traditional transverse web reinforcement consisting of #3 mild reinforcing steel at 7 in. (178 mm) on center in each shear span. This beam series provide the researchers with a relationship of calculated shear strength of a traditionally reinforced concrete beam to beams constructed and tested with those design parameters. This data allowed further confidence when comparing the performance of the FRC beams to the ACI requirements. The researchers were also able to compare the crack behavior in this series to the FRC beams.

During loading, the first cracks to develop were flexural cracks between the two loading points, at the location of the highest moment. As the test progressed, the flexural cracks spread out towards the supports, relatively evenly spaced. Eventually, inclined

cracks formed within each shear span as the load increased until all three beams failed in flexure due to crushing between the loading points.

For Beam 1, the first flexural crack formed at 20 kips (89 kN) and the first inclined crack formed at 60 kips (267 kN). The beam failed at 123.3 kips (549 kN), 106% above the load at the formation of the first inclined crack. For Beam 2, the first flexural crack formed at 20 kips (89 kN) and the first inclined crack formed at 62 kips (276 kN). The beam failed at 114.5 kips (510 kN), 185% above the load at the formation of the first inclined crack. For Beam 3, the first flexural crack formed at 20 kips (89 kN) and the first inclined crack formed at 40 kips (178 kN). The beam failed at 110.5 kips (492 kN), 176% above the formation of the first inclined crack.

The beams in this series had an average failure load of 116.1 kips (517 kN) with a COV of 5.6%. Due to the similarities in flexural failure mode between each beam in the series, the low COV is expected. This COV falls below that of the beams in the B18-PC series. When considering both equations 11-3 and 11-15 from ACI 318-14 to calculate the total shear strength, V_n , of this section, the predicted load of the beams tested in this series is 107.4 kips (478 kN). On average, the beams in Series B18-TR performed 8% better than the calculated load. Considering the normal variations of shear failure mechanisms, the average tested load is very consistent with the calculations. The equations in ACI 318-14 predict a total load capacity of 59.8 kips (266 kN) for the B18-TR series when containing the code minimum shear reinforcement, which will be used to compare the results of the FRC shear beams to determine adequacy for providing the shear resistance required by code. It should again be noted that the B18-TR beams, as tested, had more than the

minimum shear reinforcement because the maximum stirrup spacing controlled the design, while the #3 stirrups were the smallest bars available.

Figure 4.19 shows the load versus displacement behavior for each beam in Series B18-TR. Figure 4.20 shows the crack behavior of each beam in Series B18-TR after failure. Prior to failure, all beams in Series B18-TR developed a total of 11 inclined cracks.

All beams in Series B18-TR exhibited a linear load-displacement behavior up to the formation of the first flexural crack. Following the first crack, the slope slightly decreased and remained constant until failure, with softening in all of the load-displacement curves prior to failure. Beam 1 showed the most softening, which is most likely due yielding of the longitudinal reinforcement. Beam 1 exhibited the highest midspan displacement at failure of 1.14 in. (29.0 mm), corresponding with the highest load in the series. Beam 2 had a midspan displacement of 1.04 in. (26.4 mm) and the midspan displacement at failure for Beam 3 was 0.91 in. (22.9 mm).

The reinforcement strains for each beam are shown in Figure 4.21. Due to issues with the data acquisition system for this series, Beam 1 only received data on the strain gauge attached to the lower longitudinal reinforcement at midspan. The readings from this strain gauge indicate that the longitudinal reinforcement yielded prior to failure of the beam. Beam 2 acquired data from 9 strain gauges, 3 were attached to the longitudinal reinforcement; one at midspan (channel 8) and 2 at the middle of each shear span (channels 5 and 7). From the graph, it is apparent the longitudinal reinforcement yielded prior to failure at midspan, but not in the shear spans. Strain gauges 2, 3, 4, 6, 9, and 10 were all located along the transverse steel reinforcement to monitor the strain development throughout each test. During the test, the rate of strain applied is greatly increased at around

the load the inclined cracks develop within the shear spans. In Beam 3, 10 strain gauges collected strain data throughout the test. Strain gauge 3 was attached to the bottom level of longitudinal reinforcement at midspan and strain gauges 7 and 9 were located at the same depth in the middle of each shear span. Similar to Beam 2, the strain gauge located at midspan showed that the longitudinal reinforcement yielded prior to failure of the beam. Strain gauges 1, 2, 4, 5, 6, 8, and 10 were all attached to the transverse steel. As seen from the curves, the strain development in the transverse steel was similar to Beam 2, with the rate of strain versus load increasing around the point at which the first inclined cracks developed in the web. The strain gauge data, load-deflection curves, and failure mechanisms all confirm that the beams failed in flexure.

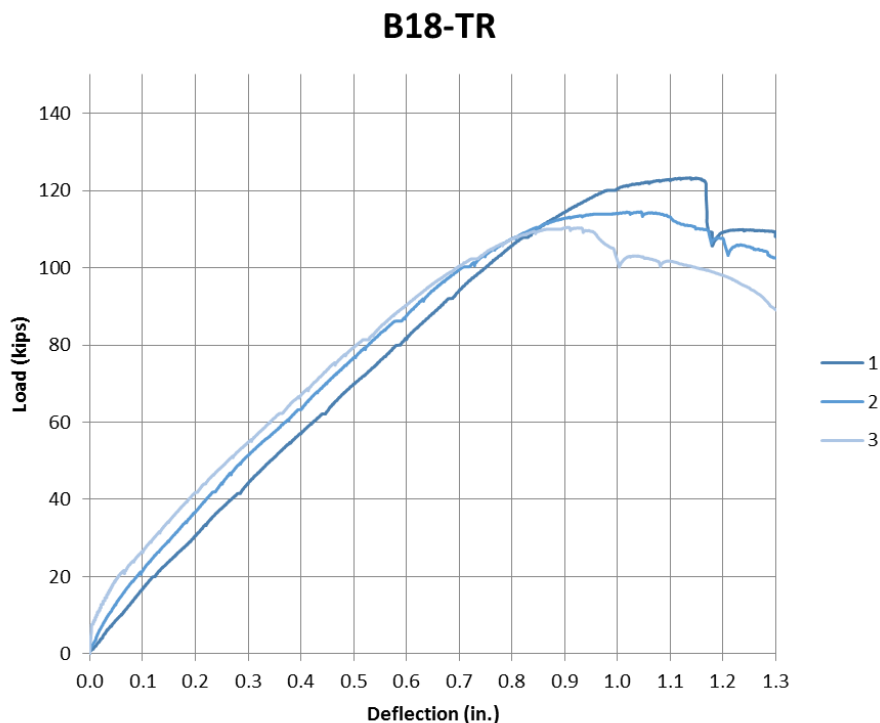
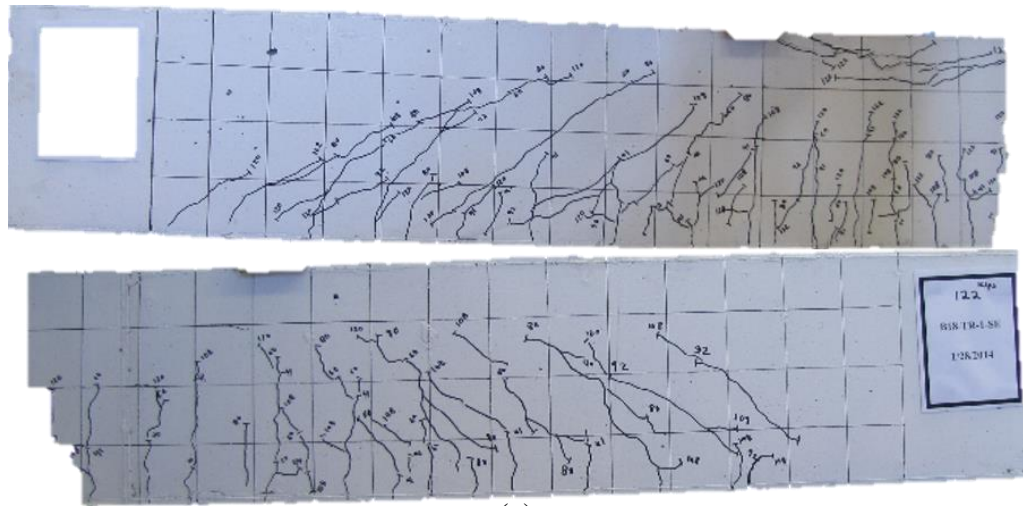
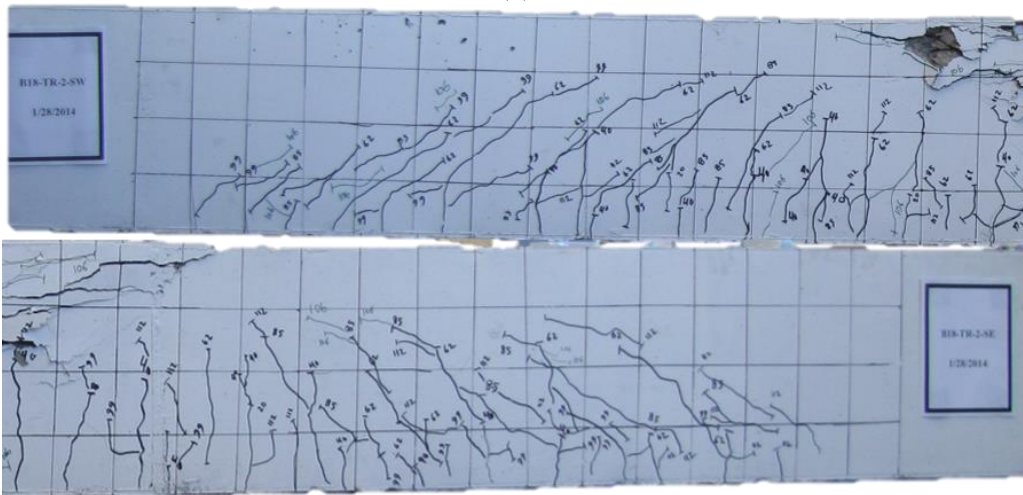


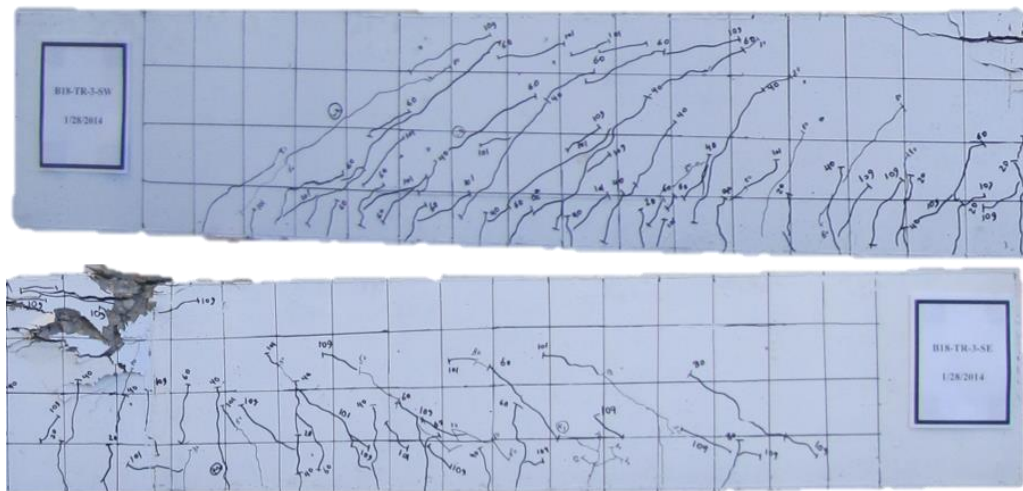
Figure 4.19. Load versus displacement behavior for beams in Series B18-TR



(a)



(b)



(c)

Figure 4.20. Crack behavior of beams in Series B18-TR after failure (a) B18-TR-1 (b) B18-TR-2 (c) B18-TR-3

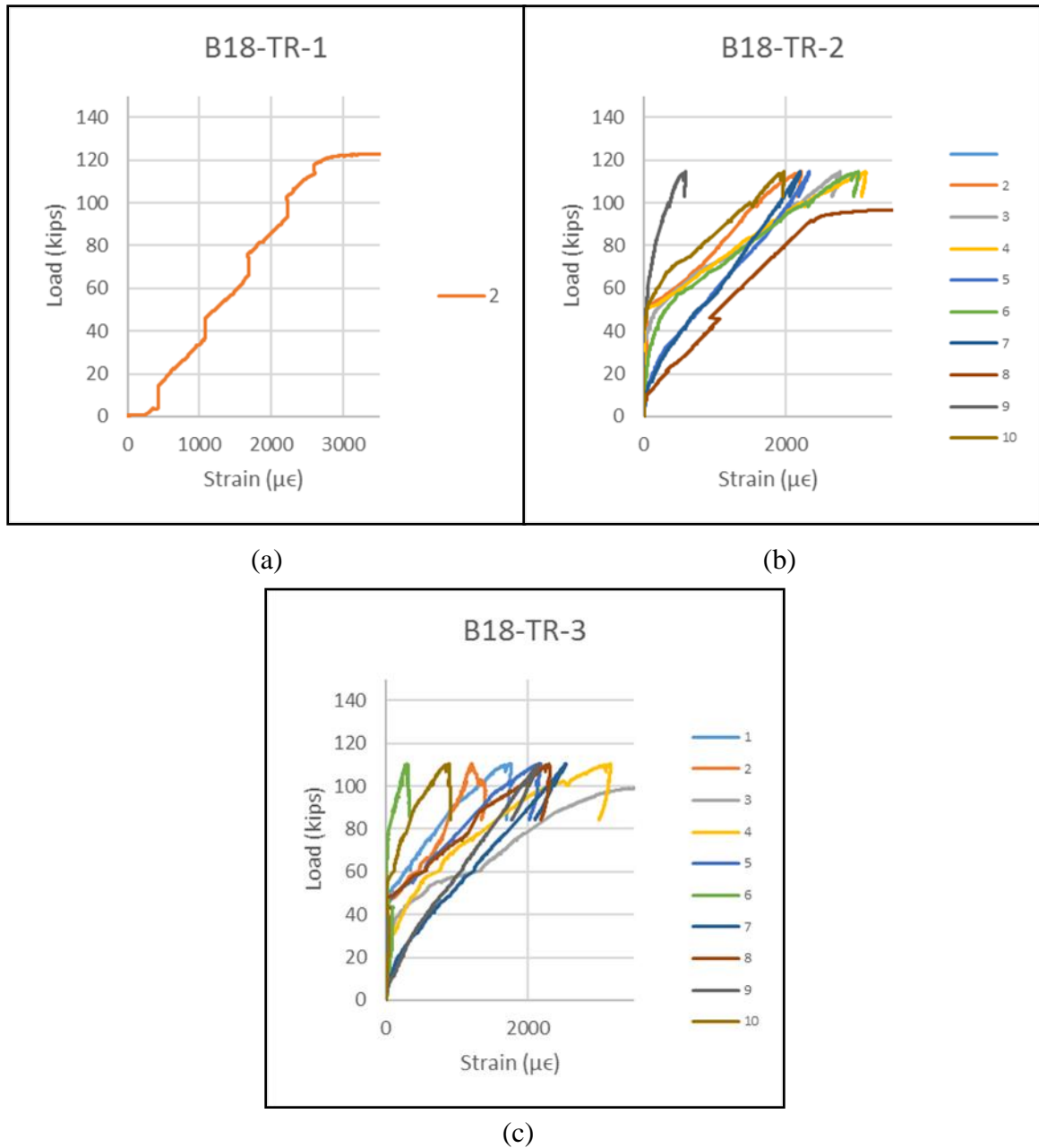


Figure 4.21. Reinforcement strains for beams in Series B18-TR

4.2.3. Beam Series B18-B5-0.5. Beams in Series B18-B5-0.5 contained the lowest level of long carbon fiber addition tested, 0.5% by volume. The results of this beam series will be compared to the behavior and performance of the other levels of fiber

addition, as well as the ability to provide the minimum resistance that would be delivered by traditional transverse steel corresponding to the minimum code requirement.

During loading, the first cracks to develop were flexural cracks between the two loading points, at the location of the highest moment. As the test progressed, the flexural cracks spread out towards the supports, relatively evenly spaced. Eventually, inclined cracks formed within each shear span as the load increased until Beams 1 and 2 failed as a result of diagonal tension, while Beam 3 failed due to a combination of shear-compression and diagonal tension. In Figure 4.23, some concrete crushing under the support can be seen in Beam 3.

For Beam 1, the first flexural crack formed at 26 kips (116 kN) and the first inclined crack formed at 54 kips (240 kN). The beam failed at 72.6 kips (323 kN), 34% above the formation of the first inclined crack. For Beam 2, the first flexural crack formed at 22 kips (98 kN) and the first inclined crack formed at 34 kips (151 kN). The beam failed at 74.0 kips (329 kips), 118% above the load at the formation of the first inclined crack. For Beam 3, the first flexural crack form at 20 kips (89 kN) and the first inclined crack form at 53 kips (236 kN). The beam failed at 71.6 kips (319 kN), 35% above the formation of the first inclined crack.

The beams in this series had an average failure load of 72.7 kips (324 kN) with a COV of 1.7%. This COV falls well below the COV of the failure loads from Series B18-TR. The average normalized shear stress provided by beams B18-B5-0.5 was 3.90. Comparing the results of this series to the calculated shear stress provided by the ACI 318-14 minimum shear reinforcement, the beams provided 14% higher performance than the code minimum.

Figure 4.22 shows the load versus displacement behavior for each beam in Series B18-B5-0.5. Figure 4.23 shows the crack behavior of each beam in Series B18-B5-0.5 after failure. Prior to failure, Beam 1 developed a total of 9 inclined cracks, Beam 2 developed 7 inclined cracks, and Beam 3 developed 8 inclined cracks. On average, this series developed 60% more cracks than the beams in Series B18-PC. The average inclined crack failure angle was 23° , 9° shallower than the average angle formed in the B18-PC series.

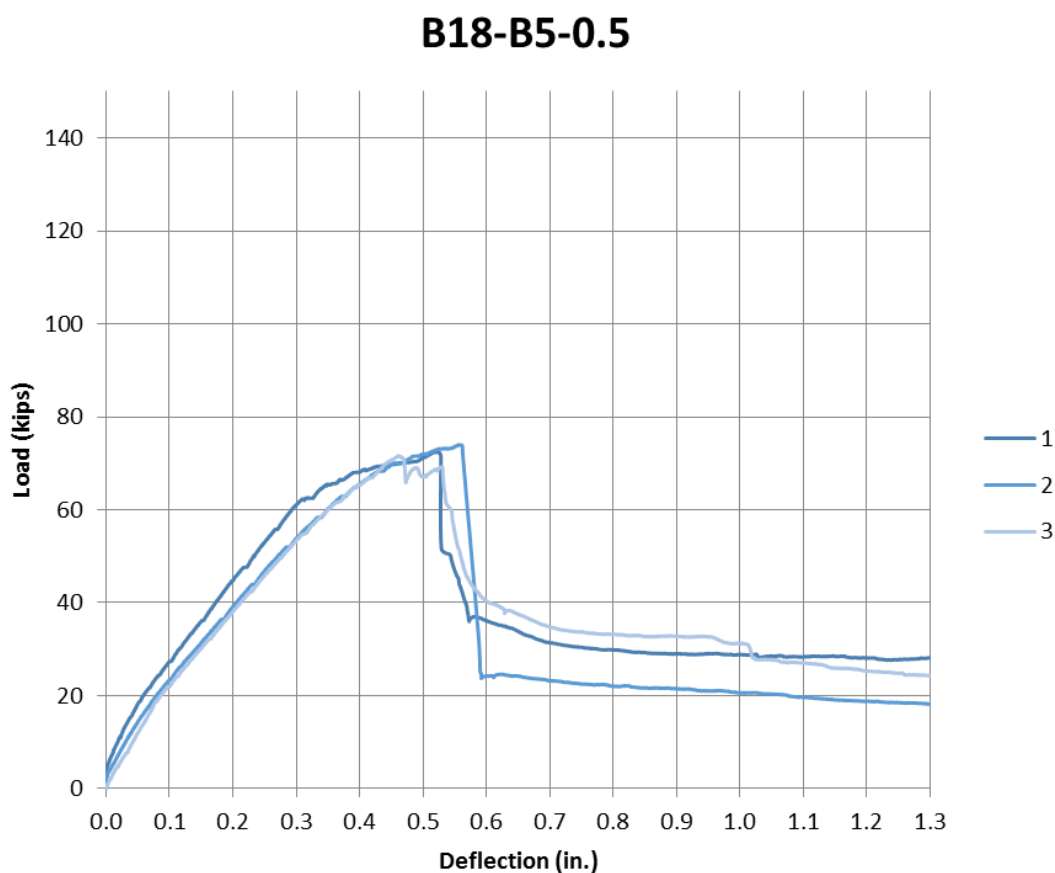
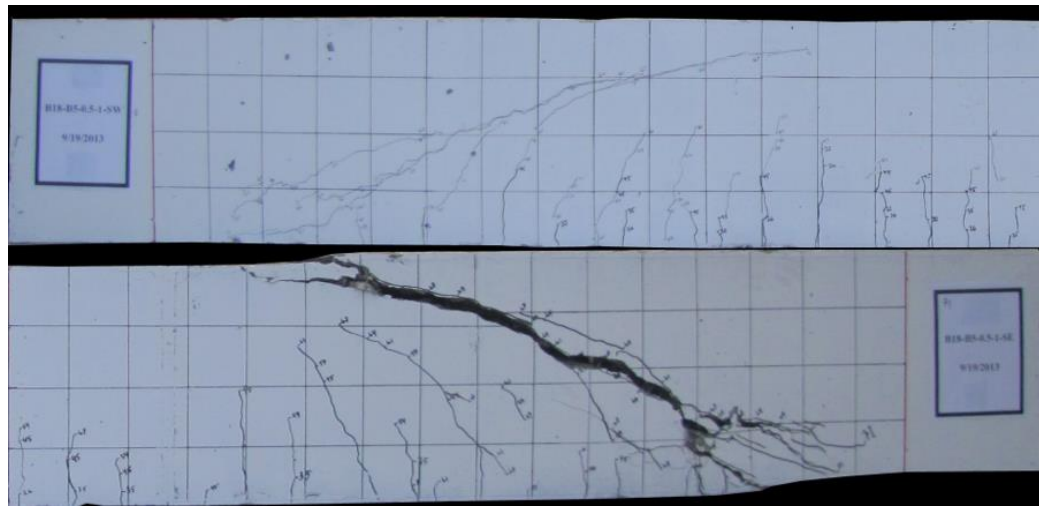
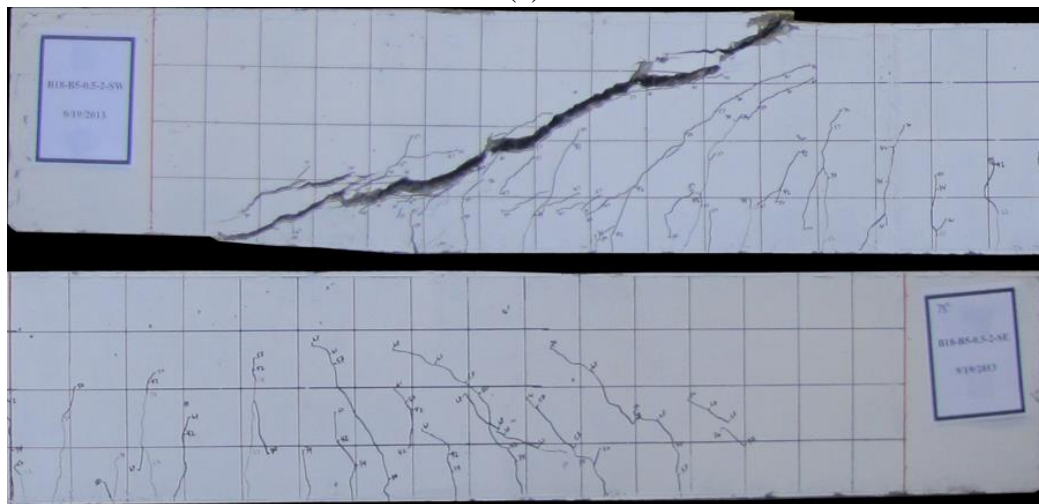


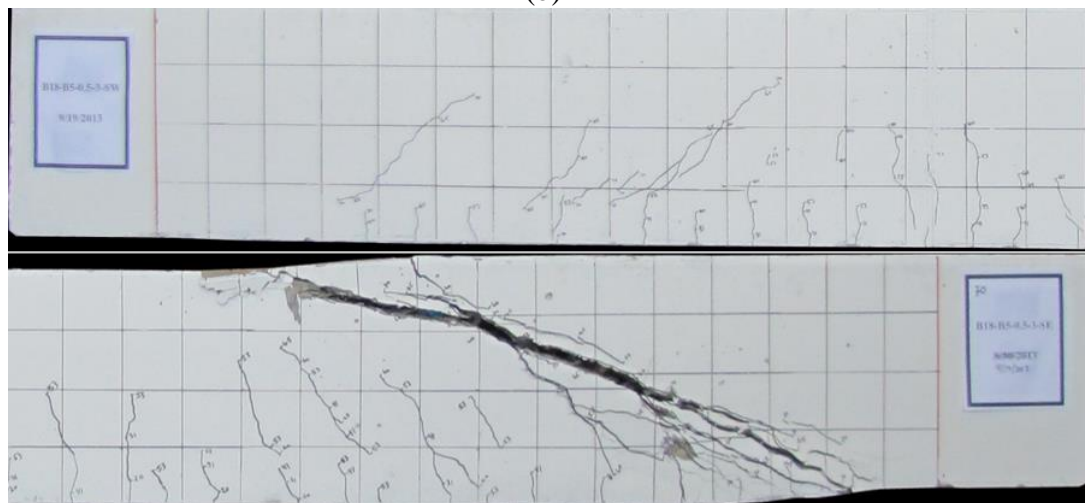
Figure 4.22. Load versus displacement behavior for beams in Series B18-B5-0.5



(a)



(b)



(c)

Figure 4.23. Crack behavior of beams in Series B18-B5-0.5 after failure (a) B18-B5-0.5-1
(b) B18-B5-0.5-2 (c) B18-B5-0.5-3

All beams in Series B18-B5-0.5 exhibited a linear load-displacement behavior up to the formation of the first flexural crack. Following the first crack, the slope slightly decreased and remained constant until failure, with softening in all of the load-displacement curves prior to failure. Beam 1 showed the most softening prior to failure of the beam due to diagonal tension. Beam 1 exhibited a midspan displacement at failure of 0.52 in. (13.2 mm). Beam 2 had a midspan displacement of 0.56 in. (14.2 mm), and the midspan displacement at failure for Beam 3 was 0.46 in. (11.7 mm).

The reinforcement strains for each beam are shown in Figure 4.24. Beam 1 had three strain gauges located at the lower level of reinforcement. Strain gauges 1 and 3 were located at the middle of the shear spans, while strain gauge 2 was located at midspan. From the load versus strain curve, it is apparent that the rate of strain increase after the initial flexural cracks form is higher at midspan compared to that at the middle of the shear spans. Beams 2 and 3 saw similar behavior, with the one difference in strain gauge 3 located at midspan for Beam 2. The strain gauge data indicates that none of the flexural steel yielded in any of the beams prior to shear failure.

4.2.4. Beam Series B18-B5-0.75. Beams in Series B18-B5-0.75 contained 0.75% by volume of fibers B5. The results of this beam will be compared to the behavior and performance of the other levels of fiber addition, as well as the ability to provide the minimum resistance that would be delivered by traditional transverse steel corresponding to the minimum code requirement.

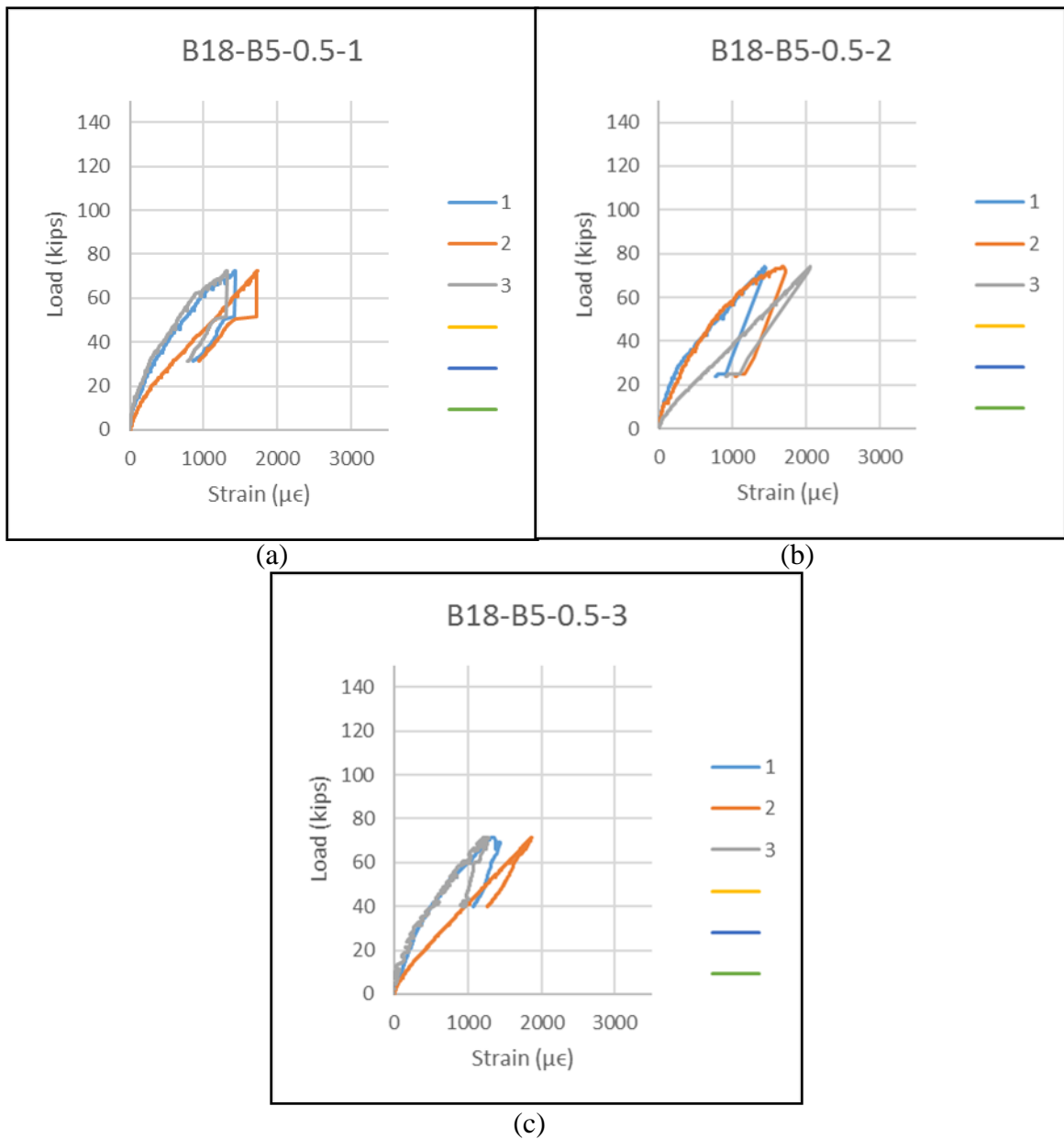


Figure 4.24. Reinforcement strains for beams in Series B18-B5-0.5

During loading, the first cracks to develop were flexural cracks between the two loading points, at the location of the highest moment. As the test progressed, the flexural cracks spread out towards the supports, relatively evenly spaced. Eventually, inclined

cracks began to form within each shear span as the load increased until Beams 1 and 2 failed as a result of diagonal tension, while Beam 3 failed due to a combination of shear-tension and diagonal tension. In Figure 4.26, cracking along the longitudinal reinforcement can be seen in Beam 3.

For Beam 1, the first flexural crack formed at 20 kips (89 kN) and the first inclined crack formed at 40 kips (178 kN). The beam failed at 69.6 kips (310 kN), 74% above the formation of the first inclined crack. For Beam 2, the first flexural crack formed at 19 kips (85 kN) and the first inclined crack formed at 56 kips (249 kN). The beam failed at 65.3 kips (291 kips), 17% above the load at the formation of the first inclined crack. For Beam 3, the first flexural crack form at 21 kips (93 kN) and the first inclined crack form at 53 kips (236 kN). The beam failed at 69.0 kips (307 kN), 30% above the formation of the first inclined crack.

The beams in this series had an average failure load of 68.0 kips (324 kN) with a COV of 3.4%. This COV is slightly above the COV in Series B18-B5-0.5, but still below the value from Series B18-TR. Although this series included a higher volume fraction of fibers, the average normalized shear stress at ultimate load was relatively similar to Series B18-B5-0.5 at 3.85, falling only 1% below the performance of B18-B5-0.5. Comparing the results of this series to the calculated shear stress provided by the ACI 318-14 minimum shear reinforcement, the average normalized shear stress provided by beams B18-B5-0.75 was 3.85, 12% higher than the necessary resistance.

Figure 4.25 shows the load versus displacement behavior for each beam in Series B18-B5-0.75. Figure 4.26 shows the crack behavior of each beam in Series B18-B5-0.75 after failure. Prior to failure, Beam 1 developed a total of 4 inclined cracks, Beam 2

developed 5 inclined cracks, and Beam 3 developed 7 inclined cracks. On average, Series B18-B5-0.75 had a similar number of inclined cracks developed compared to Series B18-PC and three less than the average from Series B18-B5-0.5. The average inclined crack failure angle was 26° . Beams 1 and 2 failed in diagonal-tension and had inclined crack angles of 24° and 25° , respectively, while Beam 3 failed as a result of shear-tension and diagonal-tension and had an inclined crack angle of 30° .

B18-B5-0.75

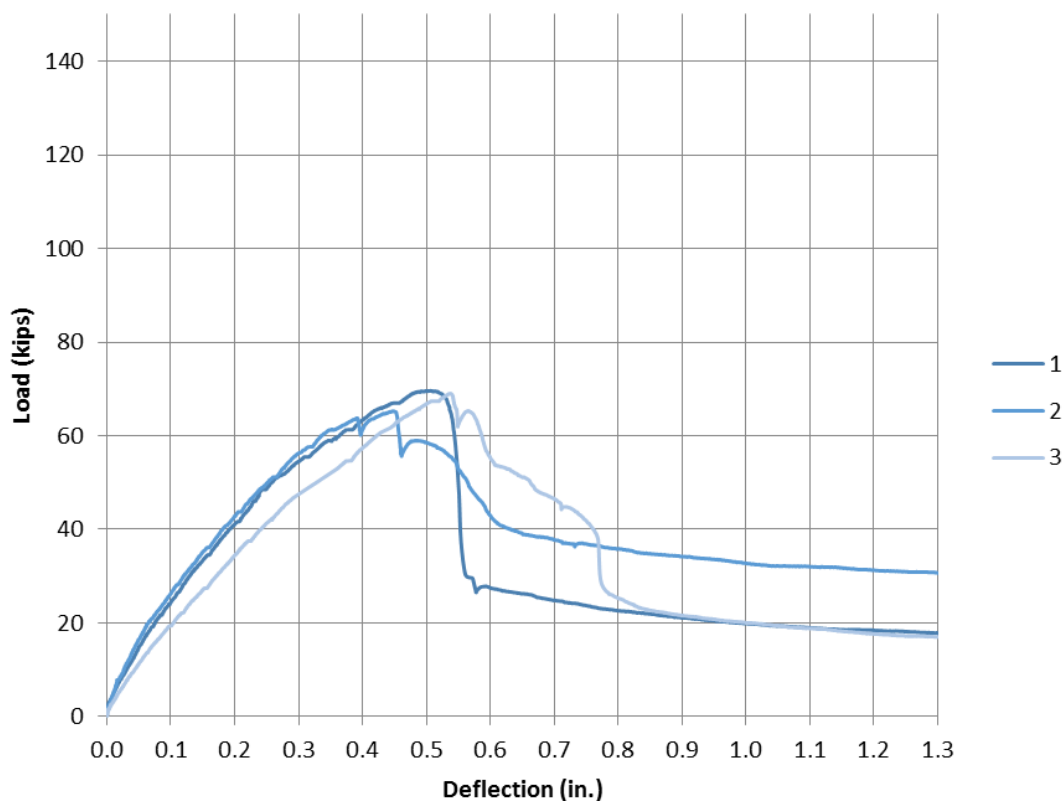
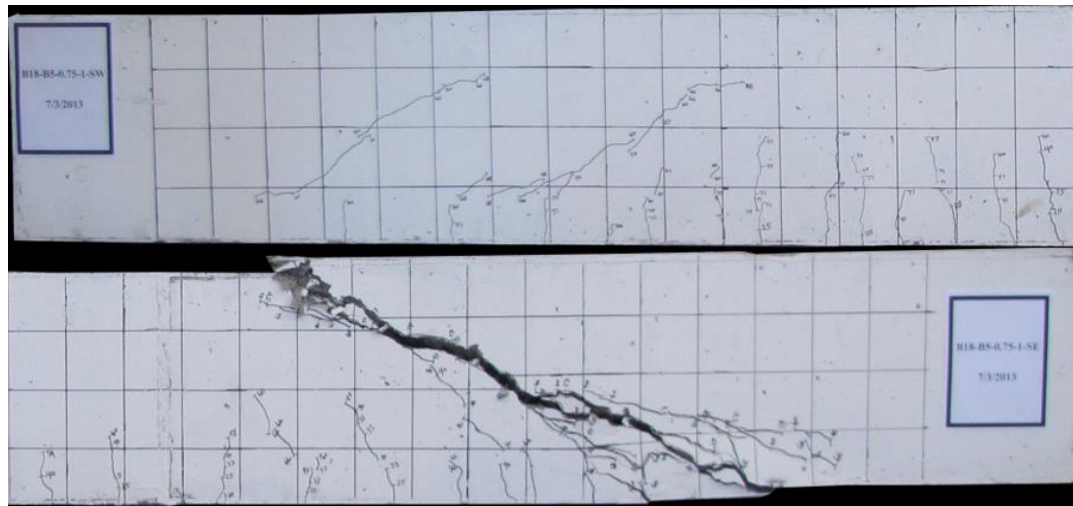
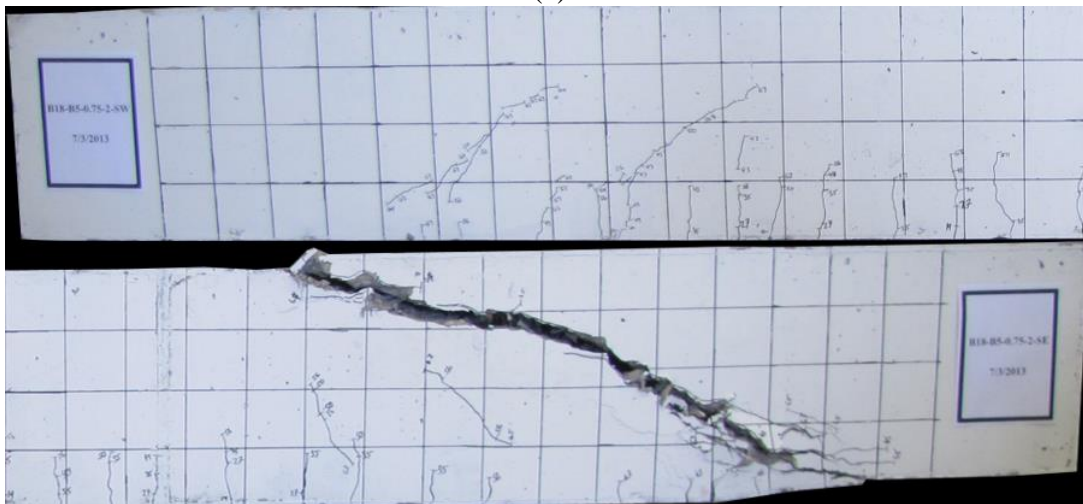


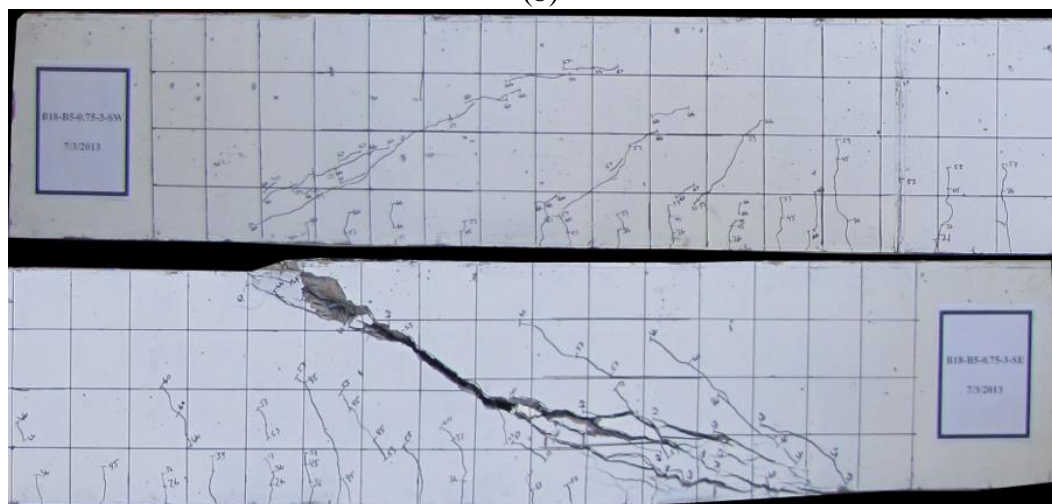
Figure 4.25. Load versus displacement behavior for beams in Series B18-B5-0.75



(a)



(b)



(c)

Figure 4.26. Crack behavior of beams in Series B18-B5-0.75 after failure (a) B18-B5-0.75-1 (b) B18-B5-0.75-2 (c) B18-B5-0.75-3

All beams in Series B18-B5-0.75 exhibited a linear load-displacement behavior up to the formation of the first flexural crack. Following the first crack, the slope slightly decreased, more so in Beam 3 than in Beams 1 and 2, and remained constant until failure, with softening in all of the load-displacement curves prior to failure. Beam 1 showed the most softening prior to failure of the beam. Beam 1 exhibited a midspan displacement at failure of 0.51 in. (13.0 mm). Beam 2 had a midspan displacement of 0.45 in. (11.4 mm), and the midspan displacement at failure for Beam 3 was 0.54 in. (13.7 mm).

The reinforcement strains for each beam are shown in Figure 4.27. Beam 1 had three strain gauges located at the lower level of reinforcement. Strain gauges 1 and 3 were located at the middle of the shear spans, while strain gauge 2 was located at midspan. From the load versus strain curve, it is apparent that the rate of strain increase after the initial flexural cracks form is higher at midspan, compared to that at the middle of the shear spans. Beam 2 showed similar behavior to Beam 1, however only the strain gauge in the East shear span provided data. Beam 3 also showed similar behavior for the strain gauge located at midspan, but strain gauge 3 also showed similar strains to strain gauge 2. This could be due to the formation of cracks along the reinforcing bars on the East shear span, where the strain gauge was located. The strain gauge data indicated that none of the flexural steel yielded in any of the beams prior to shear failure.

4.2.5. Beam Series B18-B5-1.0. Beams in Series B18-B5-1.0 contained 1.0% by volume of fibers B5. This beam series included the highest volume fraction of fibers B5 in the study, but based on the fresh properties of the concrete, the research team is confident a volume fraction of at least 1.25% is feasible.

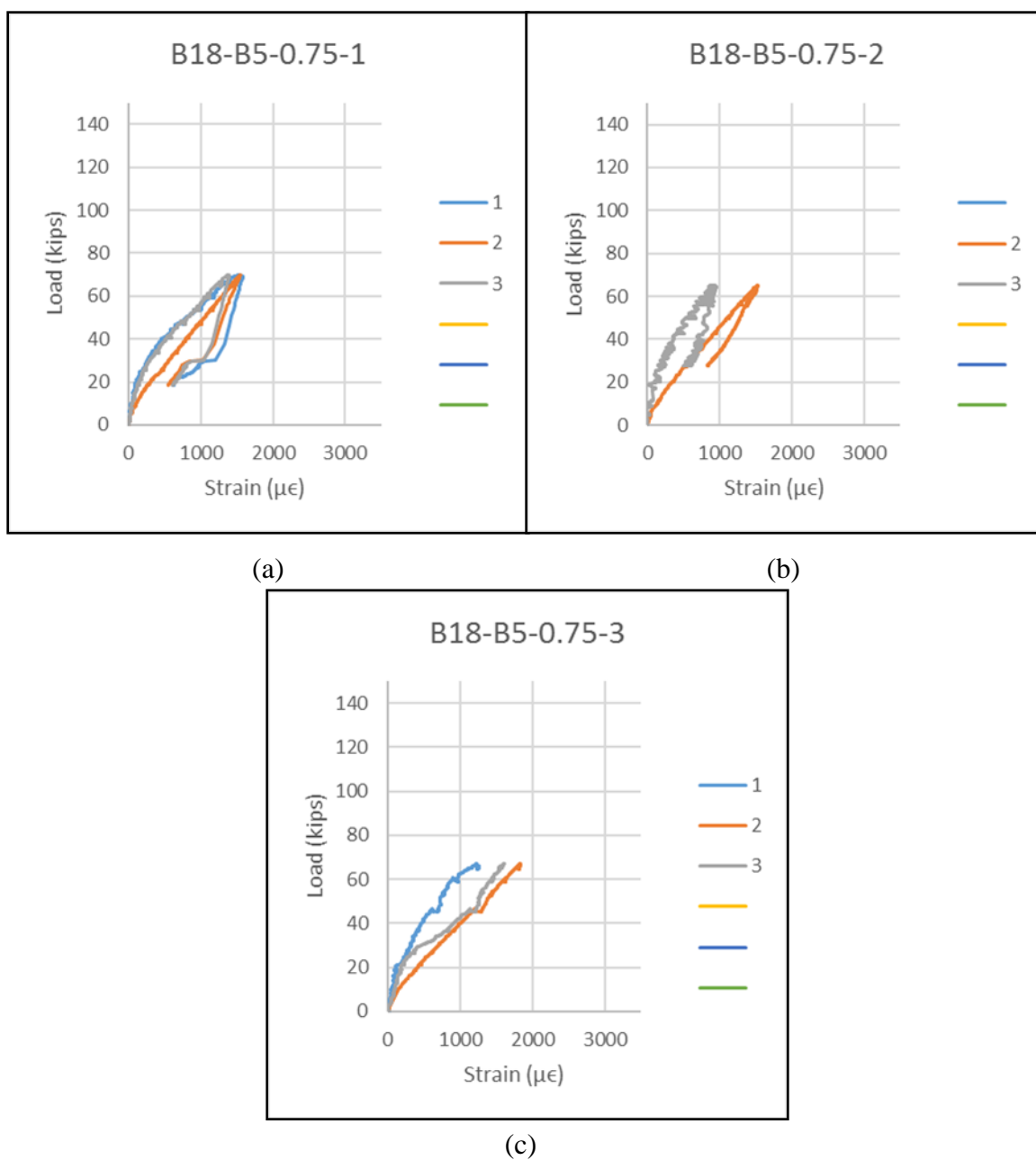


Figure 4.27. Reinforcement strains for beams in Series B18-B5-0.75

Figure 4.28 shows the load versus displacement behavior for each beam in Series B18-B5-1.0. During loading, the first cracks to develop were flexural cracks between the two loading points, at the location of the highest moment. As the test progressed, the

flexural cracks spread out towards the supports, relatively evenly spaced. Eventually, inclined cracks began to form within each shear span as the load increased until Beams 1 and 3 failed as a result of diagonal tension, while Beam 2 failed due to a combination of shear-tension and diagonal tension. In Figure 4.29, cracking along the longitudinal reinforcement can be seen in Beam 2. Some cracking along the reinforcement is also seen in Beam 3, but this occurred well after the maximum load, during post-peak loading of the beam.

For Beam 1, the first flexural crack formed at 21 kips (93 kN) and the first inclined crack formed at 39 kips (174 kN). The beam failed at 90.4 kips (402 kN), 132% above the formation of the first inclined crack. For Beam 2, the first flexural crack formed at 20 kips (89 kN) and the first inclined crack formed at 46 kips (205 kN). The beam failed at 70.4 kips (313 kips), 53% above the load at the formation of the first inclined crack. For Beam 3, the first flexural crack form at 16 kips (71 kN) and the first inclined crack form at 47 kips (209 kN). The beam failed at 83.5 kips (372 kN), 78% above the formation of the first inclined crack. The results from this series presented a much higher ratio between the formation of the first inclined crack and ultimate failure compared to Series B18-PC, on average 87% compared to 36%.

The beams in this series had an average failure load of 81.4 kips (362 kN) with a COV of 12.5%. This COV is higher than both control beams in the series. The higher COV could be a result of multiple cracks opening, due to the higher volume fraction of fibers, leading to increased but more variable performance. This result can be seen especially in Beam 1 of this series. The volume fraction of fibers included in this series lead to a significant increase in normalized shear stress compared to the other beams in this study

with less fibers. The average normalized shear stress in this series equaled 4.58, representing a 19% higher performance than that of Series B18-B5-0.75. Comparing the results of this series to the calculated shear stress provided by the ACI 318-14 minimum shear reinforcement, the average normalized shear stress provided by beams B18-B5-1.0 was 34% higher than the necessary resistance.

Figure 4.29 shows the crack behavior of each beam in Series B18-B5-1.0 after failure. Prior to failure, Beam 1 developed a total of 10 inclined cracks, Beam 2 developed 4 inclined cracks, and Beam 3 developed 8 inclined cracks. On average, Series B18-B5-1.0 developed 40% more cracks Series B18-PC. Beam 1 developed the most cracks prior to failure, which could be attributed to an increased number of fibers bridging the cracks compared to the other beams in the series. The average inclined crack failure angle was 29°.

All beams in Series B18-B5-1.0 exhibited a linear load-displacement behavior up to the formation of the first flexural crack. Following the first crack, the slope slightly decreased, slightly more in Beams 2 and 3 than Beam 1, and remained constant until failure, with softening in all of the load-displacement curves prior to failure. Beam 1 showed the most softening prior to failure of the beam, corresponding with the maximum load in the series. Beam 1 exhibited a midspan displacement at failure of 0.75 in. (19.1 mm). Beam 2 had a midspan displacement of 0.52 in. (13.2 mm), and the midspan displacement at failure for Beam 3 was 0.65 in. (16.5 mm).

The reinforcement strains for each beam are shown in Figure 4.30. All beams in this series contained six strain gauges. Strain gauges 1 and 2 were located on opposite sides of the lower level of longitudinal reinforcement in the middle of the West shear span, strain

gauges 3 and 4 were located at the same depth at midspan of the beam, and strain gauges 5 and 6 were located at the same depth at the middle of the East shear span. All three beams in this series had similar behavior to the other FRC beams tested, with the highest strain located at midspan of the beam and a slightly lower strain at the center of each shear span. The strain gauge data indicated that none of the flexural steel yielded in any of the beams prior to shear failure.

B18-B5-1.0

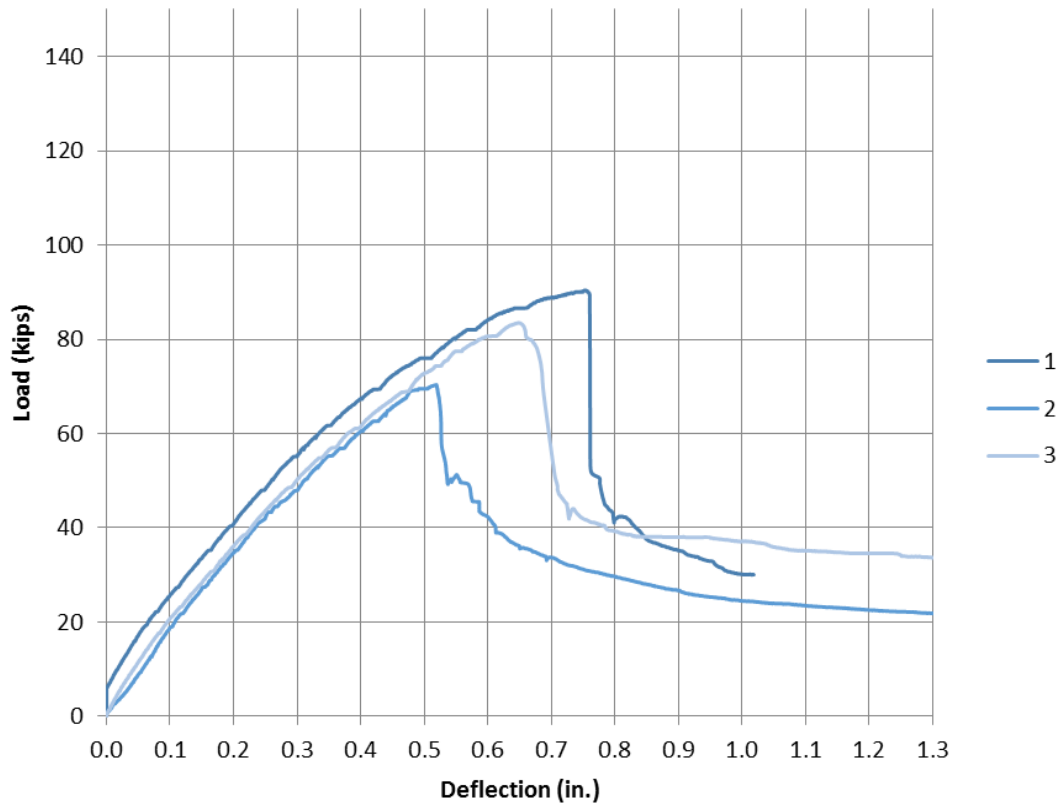
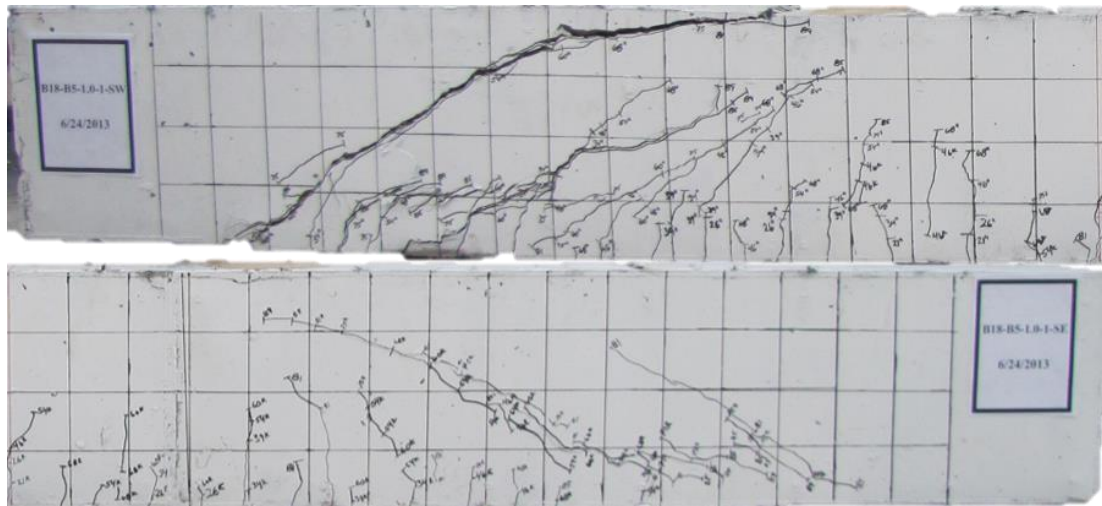
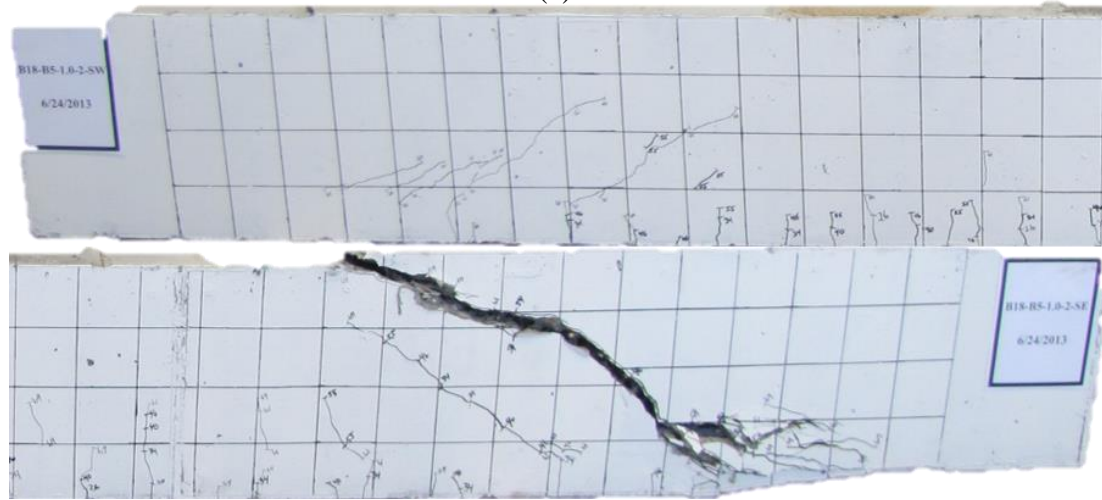


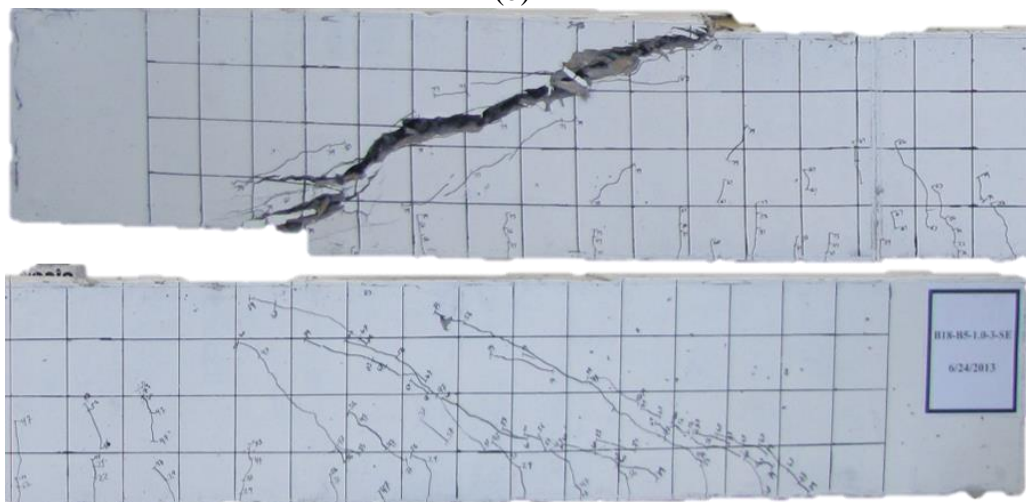
Figure 4.28. Load versus displacement behavior for beams in Series B18-B5-1.0



(a)



(b)



(c)

Figure 4.29. Crack behavior of beams in Series B18-B5-1.0 after failure (a) B18-B5-1.0-1 (b) B18-B5-1.0-2 (c) B18-B5-1.0-3

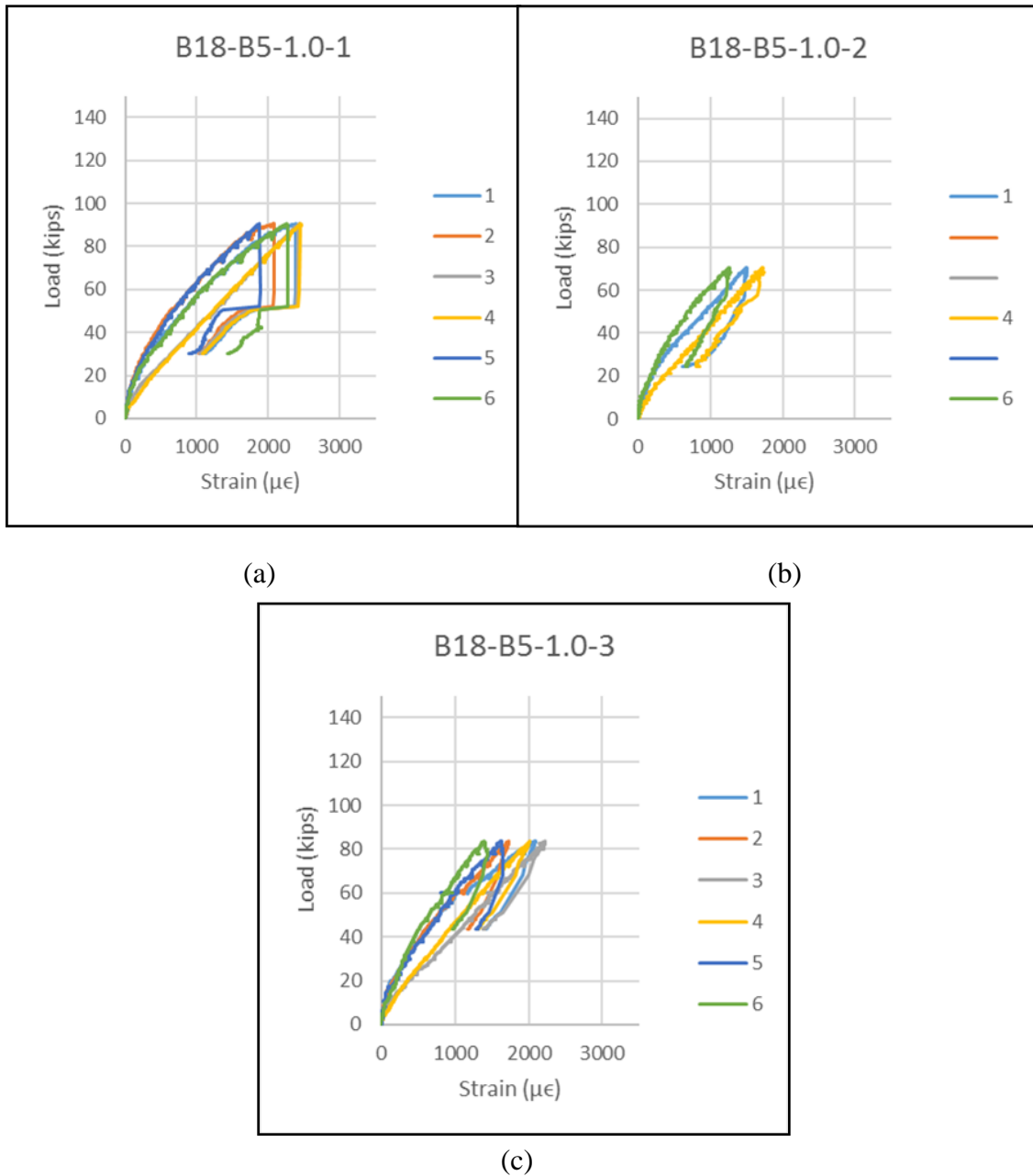


Figure 4.30. Reinforcement strains for beams in Series B18-B5-1.0

4.2.6. Beam Series B18-D1-1.0. Beams in Series B18-D1-1.0 contained 1.0% by volume of fibers D1, which were the fibers manufactured from Innegra S tow material. This beam series contained the same volume fraction of fibers as Series B18-B5-1.0, but

will be compared to the LCFRC beams that contained 0.75% fibers by volume due to the differences in density between the two materials. Compared to Series B18-B5-0.75, this mixture provided similar workability with the fresh FRC, as well as a similar number of discrete fibers within the concrete matrix for shear resistance.

Figure 4.31 shows the load versus displacement behavior for each beam in Series B18-D1-1.0. During loading, the first cracks to develop were flexural cracks between the two loading points, at the location of the highest moment. As the test progressed, the flexural cracks spread out towards the supports, relatively evenly spaced. Eventually, inclined cracks began to form within each shear span as the load increased until all three beams failed as a result of shear-compression and diagonal tension. In Figure 4.32, crushing can be seen under the load point on the side of failure in each of the beams in this series. The concrete compressive strength at testing for this beam series was the lowest out of any in the study and could have led to the shear-compression failure mode seen in each beam in this series. Some cracking along the reinforcement can also be seen, but these cracks opened up during the post-peak loading of the beam.

For Beam 1, the first flexural crack formed at 17 kips (76 kN) and the first inclined crack formed at 47 kips (209 kN). The beam failed at 72.2 kips (321 kN), 54% above the formation of the first inclined crack. For Beam 2, the first flexural crack formed at 18 kips (80 kN) and the first inclined crack formed at 45 kips (201 kN). The beam failed at 57.1 kips (313 kips), 27% above the load at the formation of the first inclined crack. For Beam 3, the first flexural crack form at 20 kips (89 kN) and the first inclined crack form at 41 kips (182 kN). The beam failed at 59.4 kips (264 kN), 45% above the formation of the first inclined crack. On average, the beams in Series B18-D1-1.0 had a maximum load 42%

higher than the formation of the first inclined crack. This is very similar to Series B18-B5-0.75, which had an average value of 40%. Both beam series performed slightly better than Series B18-PC.

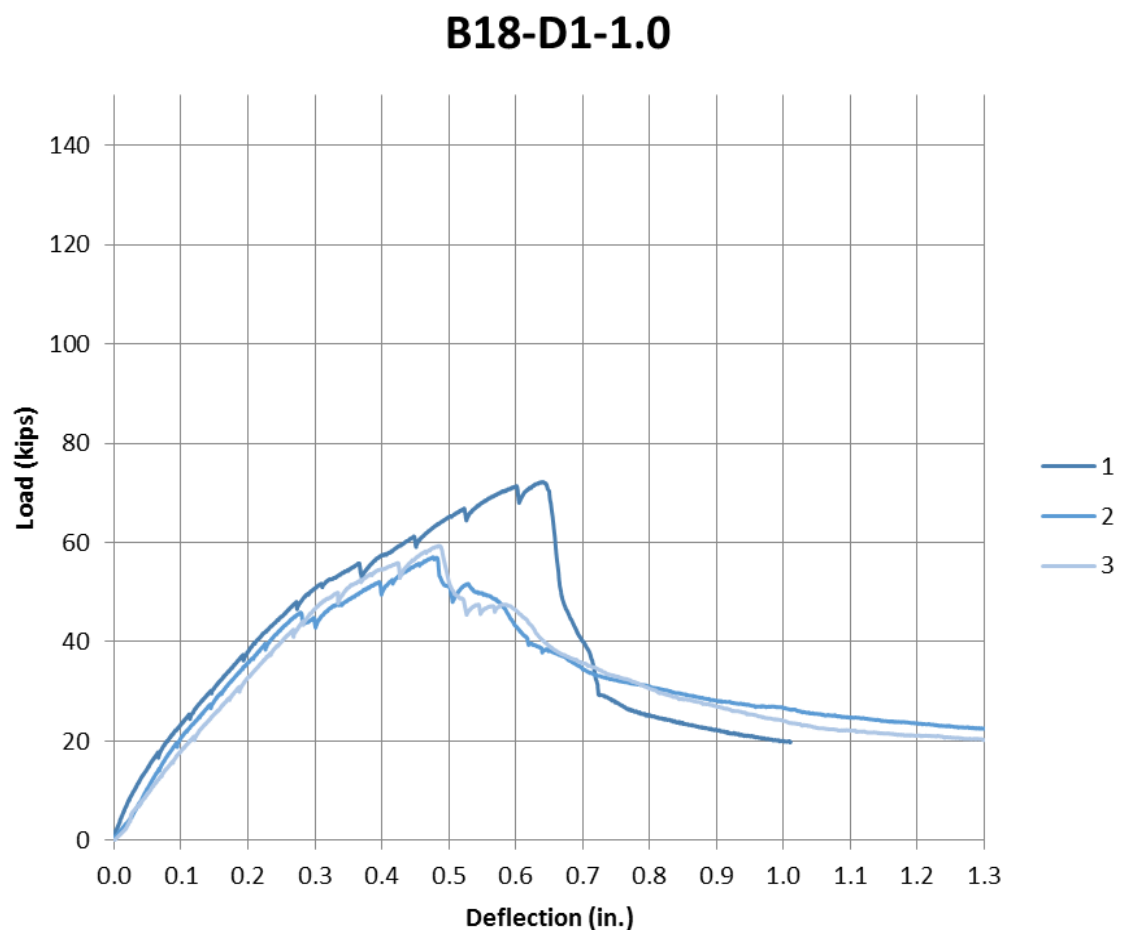


Figure 4.31. Load versus displacement behavior for beams in Series B18-D1-1.0

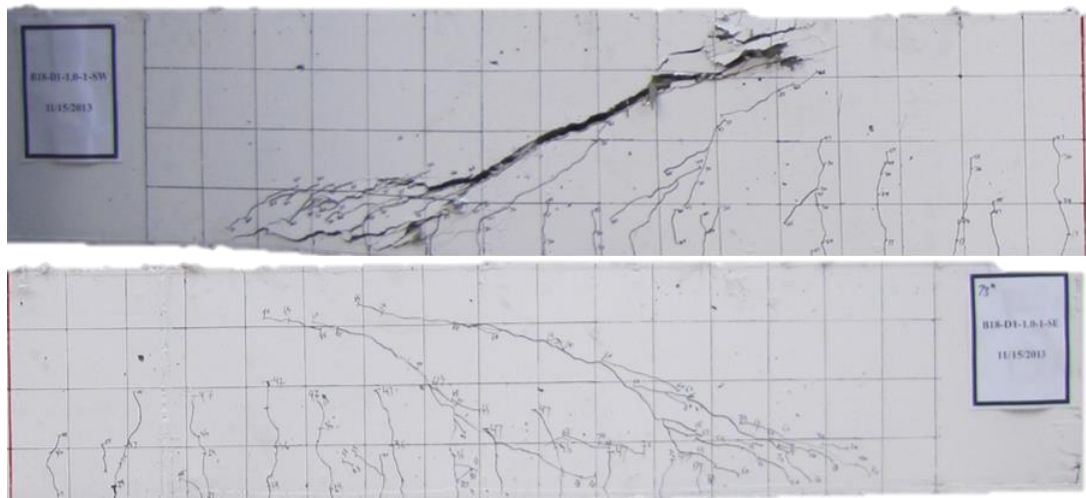
The beams in this series had an average failure load of 62.9 kips (280 kN) with a COV of 12.9%. This COV is higher than both control beams in the series. The higher COV

could be a result of a significant difference in the number of fibers crossing the inclined crack in Beam 1 compared to Beams 2 and 3 and considering that the failure modes and crack behavior were similar between all beams. The average normalized shear stress in this series equaled 3.64, representing a 5% lower performance than that of Series B18-B5-0.75. Comparing the results of this series to the calculated shear stress provided by the ACI 318-14 minimum shear reinforcement, the average normalized shear stress provided by beams B18-D1-1.0 was 6% higher than the necessary resistance.

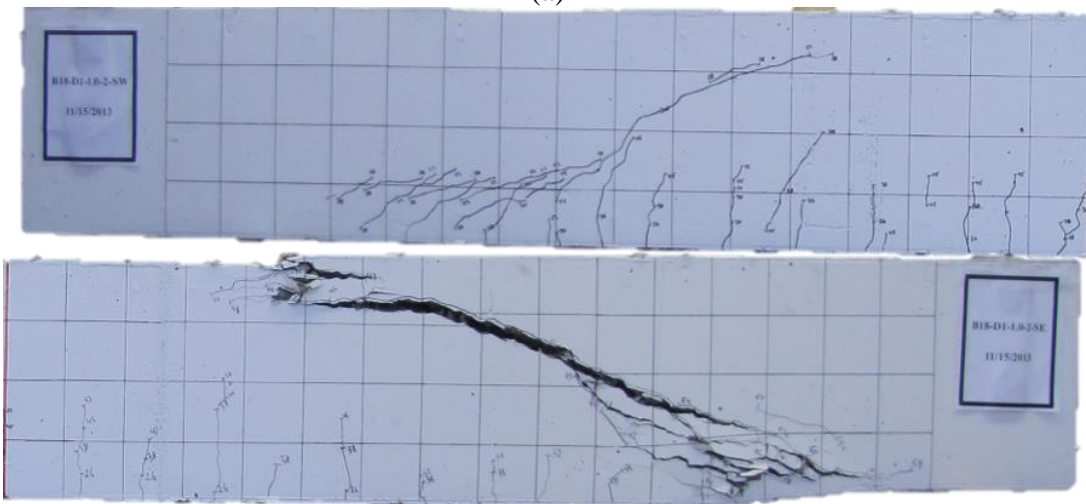
Figure 4.32 shows the crack behavior of each beam in Series B18-D1-1.0 after failure. Prior to failure, Beam 1 developed a total of 6 inclined cracks, Beam 2 developed 3 inclined cracks, and Beam 3 developed 6 inclined cracks. On average, Series B18-D1-1.0 developed an equal number of cracks to Series B18-B5-0.75 and B18-PC. The average inclined crack failure angle was 25° .

All beams in Series B18-D1-1.0 exhibited a linear load-displacement behavior up to the formation of the first flexural crack. Following the first crack, the slope slightly decreased. Upon the formation of the first inclined cracks, the slope for each curve decreased even more and until the beams eventually failed with some softening in the curves prior to failure. Beam 1 exhibited a midspan displacement at failure of 0.64 in. (16.3 mm), which was the highest recorded displacement in the series, also corresponding to the highest load. Beams 2 and 3 had a midspan displacement of 0.48 in. (12.2 mm).

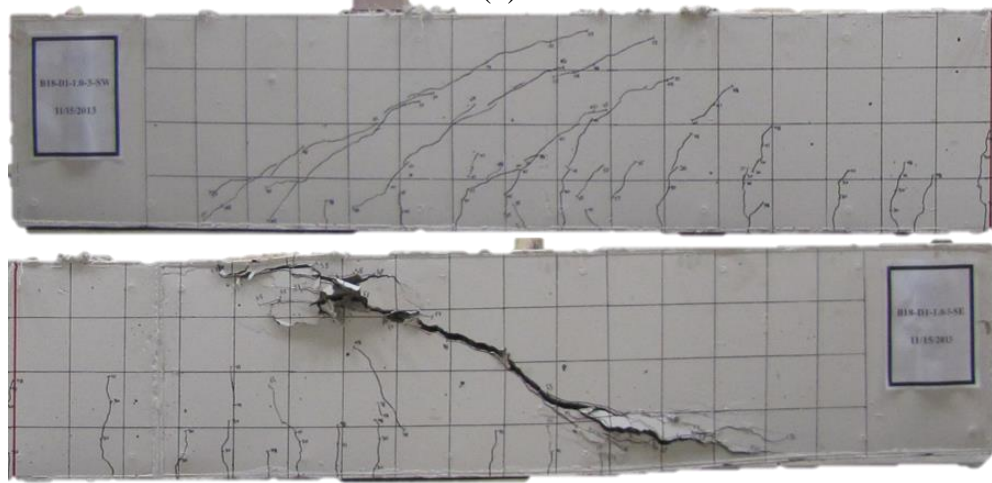
The reinforcement strains for each beam are shown in Figure 4.33. All beams in this series contained three strain gauges. Strain gauges 1 and 3 were located on the lower level of longitudinal reinforcement in the middle of the West and East shear spans, respectively, and strain gauge 2 was located at the same depth at midspan of the beam.



(a)



(b)



(c)

Figure 4.32. Crack behavior of beams in Series B18-D1-1.0 after failure (a) B18-D1-1.0-1 (b) B18-D1-1.0-2 (c) B18-D1-1.0-3

All three beams in this series had similar behavior to the other FRC beams tested, with the highest strain located at midspan of the beam and a slightly lower strain at the center of each shear span. The strain gauge data indicated that none of the flexural steel yielded in any of the beams prior to shear failure.

4.2.7. Beam Series B18-S-0.75. Beams in Series B18-S-0.75 contained 0.75% by volume of Dramix RC80/30BP single hooked-end steel fibers manufactured by Bekaert. This beam series will be compared to the LCFRC beams that contained 1.0% fibers by volume due to the differences in density between the two materials, which led to a much less workable mix for the SFRC at a volume fraction of 0.75% compared to the LCFRC at 1.0%. There has been extensive research conducted regarding the shear capacity of SFRC, and for this reason, this fiber was included in the study to add as a benchmark for FRC currently being researched and tested.

Figure 4.34 shows the load versus displacement behavior for each beam in Series B18-S-0.75. During loading, the first cracks to develop were flexural cracks between the two loading points, at the location of the highest moment. As the test progressed, the flexural cracks spread out towards the supports, relatively evenly spaced. Eventually, inclined cracks began to form within each shear span as the load increased until Beam 1 failed as a result of diagonal tension and Beams 2 and 3 failed due to shear-tension and diagonal tension. In Figure 4.35, cracking along the reinforcement can also be seen in Beams 2 and 3, which lead to the shear-tension failure mode.

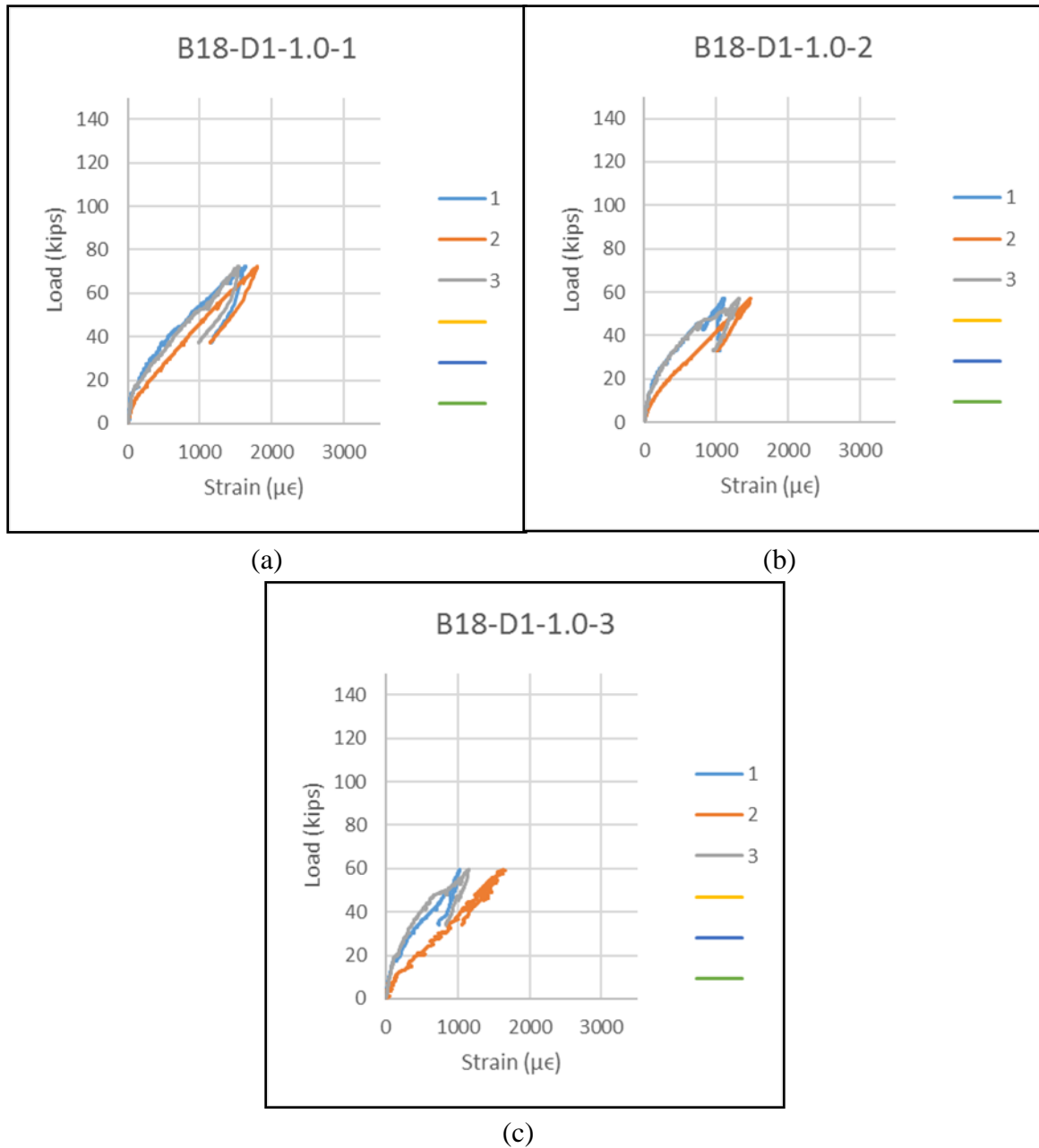


Figure 4.33. Reinforcement strains for beams in Series B18-D1-1.0

For Beam 1, the first flexural crack formed at 17 kips (76 kN) and the first inclined crack formed at 54 kips (240 kN). The beam failed at 101.9 kips (453 kN), 89% above the formation of the first inclined crack. For Beam 2, the first flexural crack formed at 17 kips

(76 kN) and the first inclined crack formed at 51 kips (228 kN). The beam failed at 84.7 kips (377 kN), 66% above the load at the formation of the first inclined crack. For Beam 3, the first flexural crack formed at 20 kips (89 kN) and the first inclined crack formed at 58 kips (257 kN). The beam failed at 93.4 kips (416 kN), 61% above the formation of the first inclined crack. On average, the beams in Series B18-S-0.75 had a maximum load 72% higher than the formation of the first inclined crack, which is slightly below the 87% value for Series B18-B5-1.0%.

The beams in this series had an average failure load of 93.3 kips (415 kN) with a COV of 9.2%. This COV is higher than both control beams in the series and above most of the LCFRC beams tested in this study. The average normalized shear stress in this series equaled 5.05, representing a 5% higher performance than the average of the B18-B5 and B24-B5 series at a volume fraction of 1.0%. Comparing the result of this series to the calculated shear stress provided by the ACI 318-14 minimum shear reinforcement, the average normalized shear stress provided by beams B18-S-0.75 was 47% higher than the necessary resistance.

Figure 4.35 shows the crack behavior of each beam in Series B18-S-0.75 after failure. Prior to failure, Beam 1 developed a total of 12 inclined cracks, Beam 2 developed 7 inclined cracks, and Beam 3 developed 8 inclined cracks. On average, Series B18-S-0.75 developed 9 inclined cracks. The average inclined crack failure angle was 28° .

All beams in Series B18-S-0.75 exhibited a linear load-displacement behavior up to the formation of the first flexural crack. Following the first crack, the slope slightly decreased and remained steady until the beams eventually failed with some softening in the curves prior to failure. Beam 1 exhibited a midspan displacement at failure of 0.74 in.

(18.8 mm), which was the highest recorded displacement in the series, also corresponding to the highest load. Beam 2 had a midspan displacement of 0.64 in. (16.3 mm), and Beam 3 had a midspan displacement of 0.71 in. (18.0 mm).

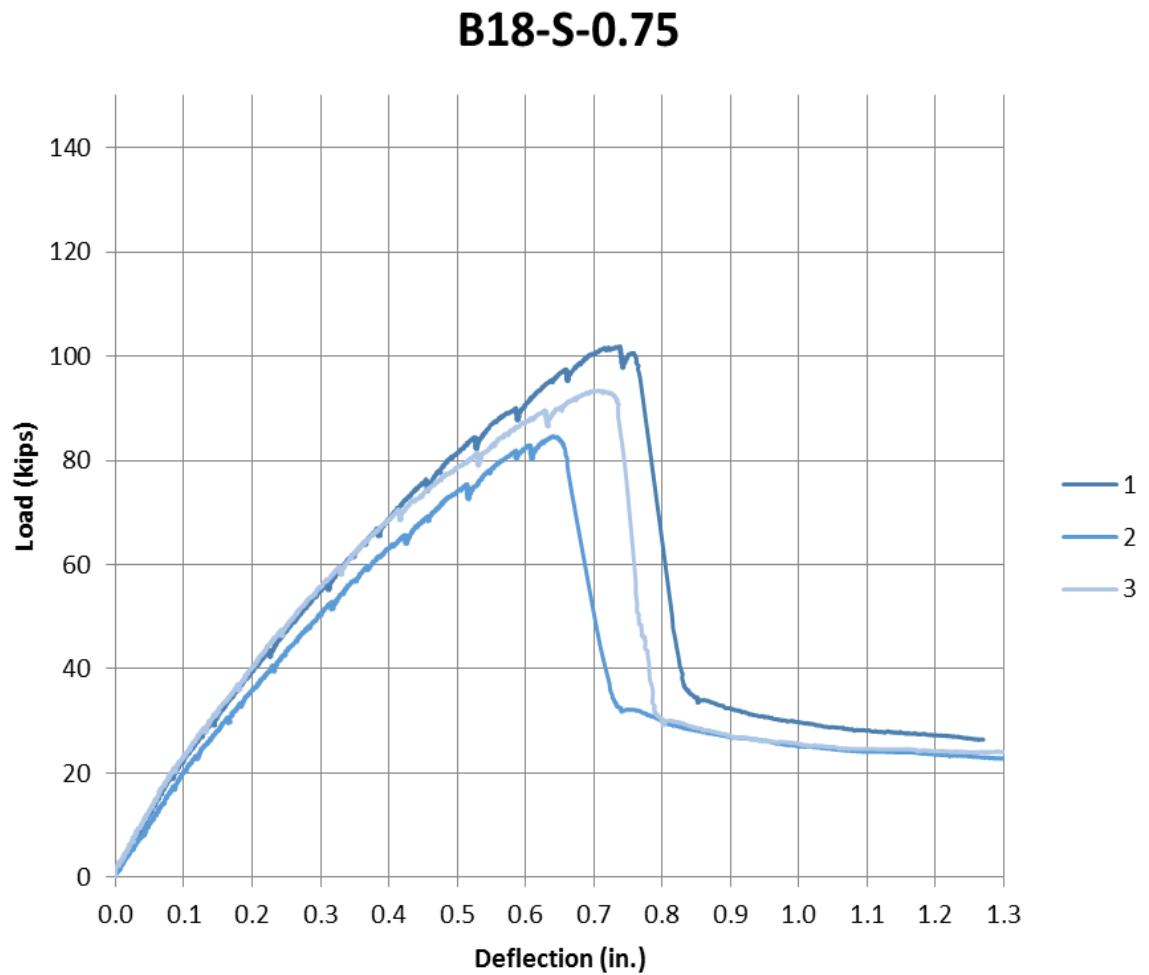
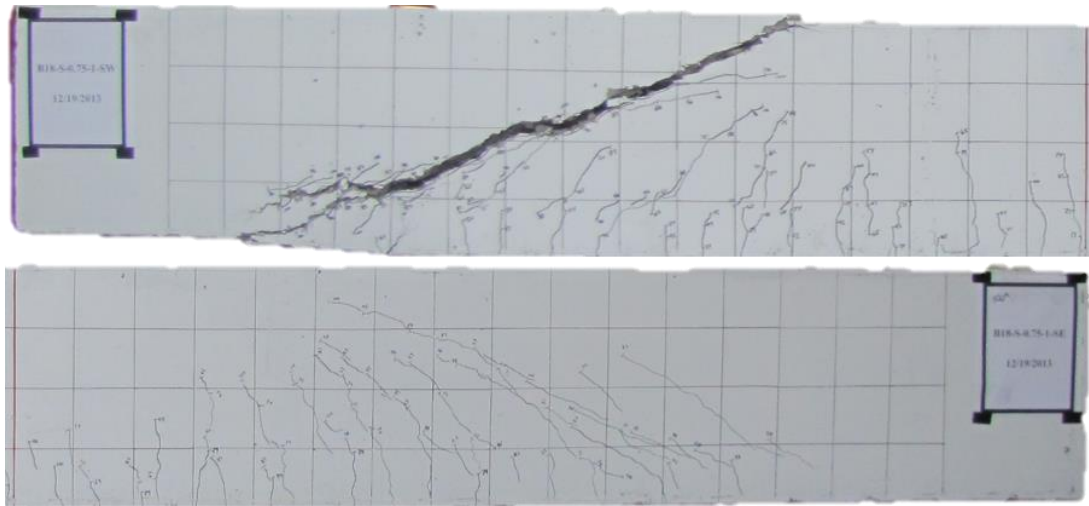
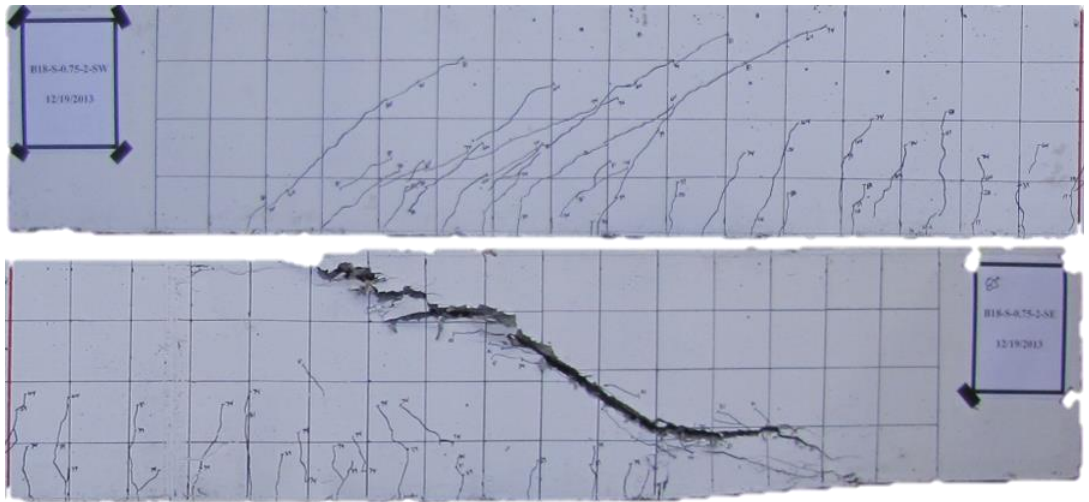


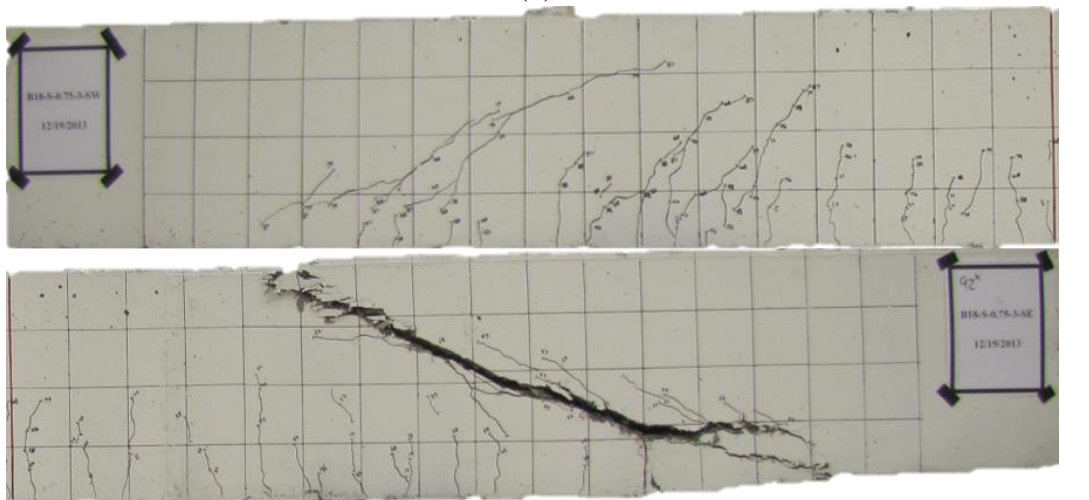
Figure 4.34. Load versus displacement behavior for beams in Series B18-S-0.75



(a)



(b)



(c)

Figure 4.35. Crack behavior of beams in Series B18-S-0.75 after failure (a) B18-S-0.75-1
(b) B18-S-0.75-2 (c) B18-S-0.75-3

The reinforcement strains for each beam are shown in Figure 4.36. All beams in this series contained three strain gauges. Strain gauges 1 and 3 were located on the lower level of longitudinal reinforcement in the middle of the West and East shear spans, respectively, and strain gauge 2 was located at the same depth, at midspan of the beam. All three beams in this series had similar behavior to the other FRC beams tested, with the highest strain located at midspan of the beam and a slightly lower strain at the center of each shear span. The data acquisition failed to collect data from the East shear span in Beam 1 of this series. The strain gauge data indicated that none of the flexural steel yielded in any of the beams prior to shear failure.

4.3. PERFORMANCE AND BEHAVIOR OF 24 in. (610mm) DEEP BEAMS

The following sections provide an overview of the behavior of the tested beams with an overall depth of 24 in. (610 mm). Each series will be analyzed separately with an in-depth overview of the load versus deflection and failure behavior, crack behavior and development, midspan deflection, and reinforcement strains. Each beam series will be compared to each other, as well as the control series, in order to evaluate the varied parameters in the study. The research team also used the control beams in this study, along with the ACI 318-14 code, to evaluate the performance of the FRC beams compared to the required calculated resistance.

4.3.1. Beam Series B24-B5-0.5. Beams in Series B24-B5-0.5 contained the lowest level of fiber addition tested, 0.5% by volume. The results of this beam will be compared to the behavior and performance of the other levels of fiber addition, as well as if there is a depth effect by increasing the beam depth by 33% compared to the B18 series.

During loading, the first cracks to develop were flexural cracks between the two loading points, at the location of the highest moment. As the test progressed, the flexural cracks spread out towards the supports, relatively evenly spaced. Eventually, inclined cracks formed within each shear span as the load increased until all beams failed due to diagonal tension. In Figure 4.38, some concrete spalling can be seen under the load point in Beam 1 and around the longitudinal reinforcement in Beam 2, but this was due the post-peak loading of the beams and handling when removing the beams from the test fixture.

For Beam 1, the first flexural crack formed at 21 kips (93 kN) and the first inclined crack formed at 61 kips (271 kN). The beam failed at 91.4 kips (407 kN), 50% above the formation of the first inclined crack. For Beam 2, the first flexural crack formed at 20 kips (89 kN) and the first inclined crack formed at 53 kips (236 kN). The beam failed at 92.2 kips (410 kips), 74% above the load at the formation of the first inclined crack. For Beam 3, the first flexural crack form at 22 kips (98 kN) and the first inclined crack form at 61 kips (271 kN). The beam failed at 85.8 kips (382 kN), 41% above the formation of the first inclined crack.

The beams in this series had an average failure load of 89.8 kips (400 kN) with a COV of 3.9%. Similar to the beams in Series B18-B5-0.5, this series had an extremely low variation when considering the variability of shear failure mechanisms. This is potentially due to very even distribution of the fibers within the concrete matrix at this volume fraction. Comparing the results of this series to the calculated shear stress provided by the ACI 318-14 minimum shear reinforcement, the average normalized shear stress provided by beams B24-B5-0.5 was 3.50, 2% higher than the necessary resistance. Series B18-B5-0.5

performed 11% better than this series, when comparing normalized shear stresses. Keeping in mind the inconsistencies typical with shear failures, the beams performed very similar.

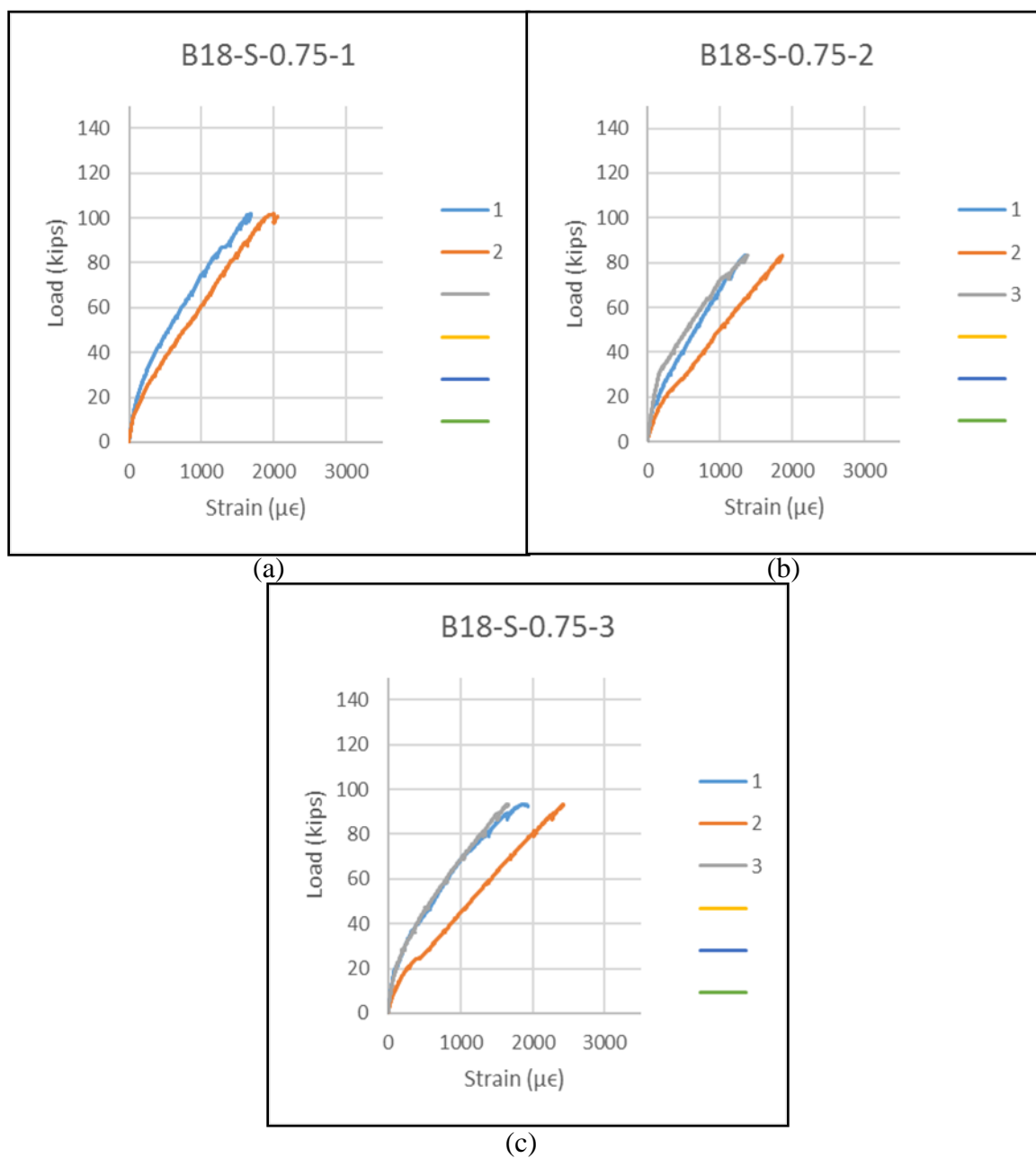


Figure 4.36. Reinforcement strains for beams in Series B18-S-0.75

Figure 4.37 shows the load versus displacement behavior for each beam in Series B24-B5-0.5. Figure 4.38 shows the crack behavior of each beam in Series B24-B5-0.5 after failure. Prior to failure, Beam 1 developed a total of 9 inclined cracks, Beam 2 developed 14 inclined cracks, and Beam 3 developed 11 inclined cracks. On average, this series developed 120% more cracks than the beams in Series B18-PC and 37.5% more than in Series B18-B5-0.5. The average inclined crack failure angle was 23° , the same average crack angle as in Series B18-B5-0.5.

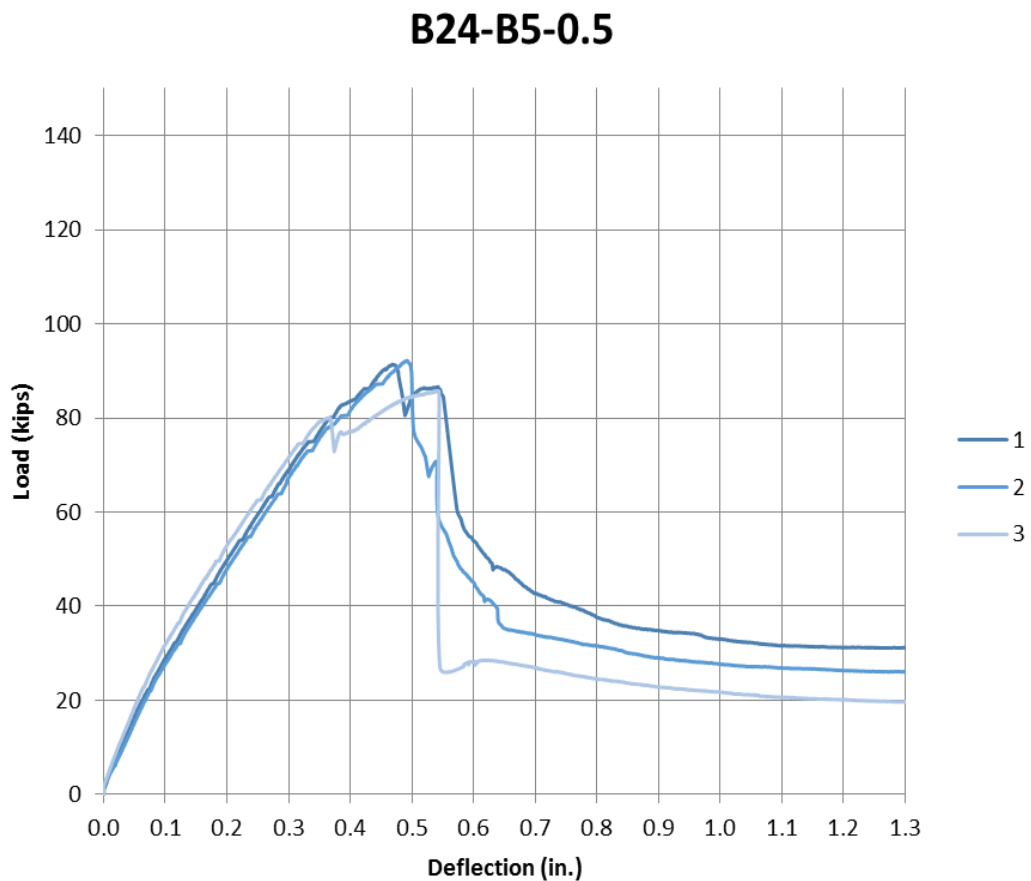


Figure 4.37. Load versus displacement behavior for beams in Series B24-B5-0.5

All beams in Series B24-B5-0.5 exhibited a linear load-displacement behavior up to the formation of the first flexural crack. Following the first crack, the slope slightly decreased and remained constant until failure, with softening in all of the load-displacement curves prior to failure. Beam 3 had a slight load drop around 80 kips (356 kN), but was able to stabilize due to the fibers bridging the crack, and the beam supported an additional 5 kips (22 kN) prior to failure. As a result of this, Beam 2 showed the most softening prior to failure. Beam 1 exhibited a midspan displacement at failure of 0.47 in. (11.9 mm). Beam 2 had a midspan displacement of 0.49 in. (12.4 mm), and the midspan displacement at failure for Beam 3 was 0.54 in. (13.7 mm). The average deflection for the beams in this Series was 0.5 in. (12.7 mm), identical to Series B18-B5-0.5.

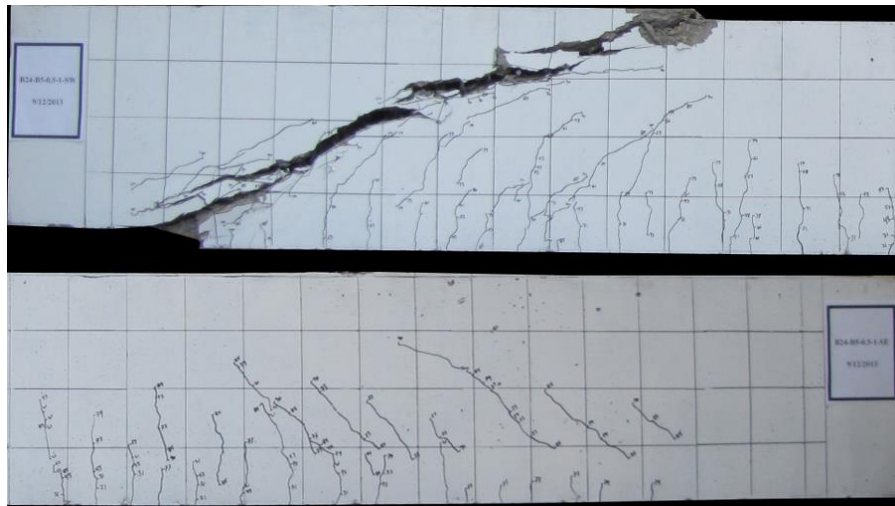
The reinforcement strains for each beam are shown in Figure 4.39. All beams in this series contained three strain gauges. Strain gauges 1 and 3 were located on the lower level of longitudinal reinforcement in the middle of the West and East shear spans, respectively, and strain gauge 2 was located at the same depth at midspan of the beam. All three beams in this series had similar behavior to the other FRC beams tested, with the highest strain located at midspan of the beam and a slightly lower strain at the center of each shear span. The strain gauge data indicated that none of the flexural steel yielded in any of the beams prior to shear failure.

4.3.2. Beam Series B24-B5-0.75. Beams in Series B24-B5-0.75 were the beams tested in this series with the middle level of long carbon fiber addition, 0.75% by volume. The results of this beam series will be compared to the behavior and performance of the other levels of fiber addition, as well as if there is a depth effect by increasing the beam depth by 33% compared to the beams in the B18 series.

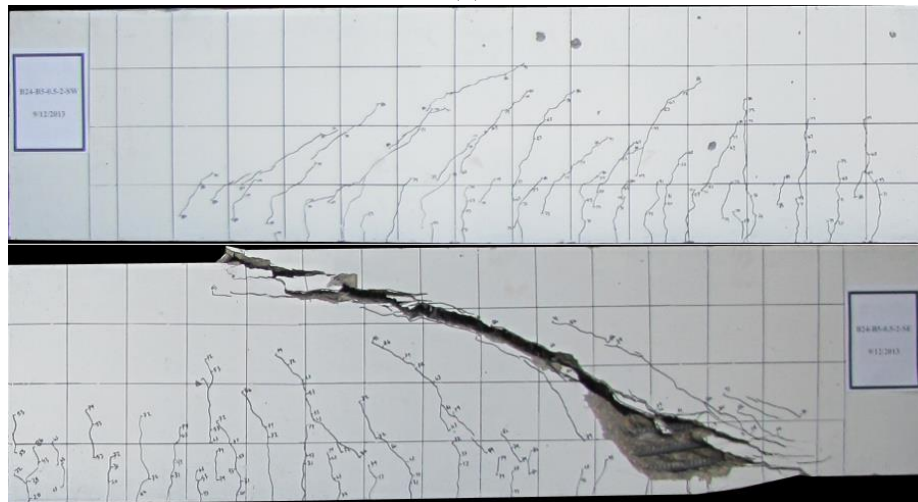
During loading, the first cracks to develop were flexural cracks between the two loading points, at the location of the highest moment. As the test progressed, the flexural cracks spread out towards the supports, relatively evenly spaced. Eventually, inclined cracks formed within each shear span as the load increased until Beams 1 and 3 failed due to shear-tension and diagonal tension and Beam 2 failed due to diagonal tension. In Figure 4.41, cracking can be seen near the longitudinal reinforcement in Beams 1 and 3, indicating the shear tension failure mode. Some cracking is present at the same location in Beam 2, but this is due to the post-peak loading of the test.

For Beam 1, the first flexural crack formed at 28 kips (125 kN) and the first inclined crack formed at 61 kips (271 kN). The beam failed at 91.4 kips (407 kN), 49% above the formation of the first inclined crack. For Beam 2, the first flexural crack formed at 28 kips (125 kN) and the first inclined crack formed at 67 kips (298 kN). The beam failed at 101.5 kips (452 kips), 51% above the load at the formation of the first inclined crack. For Beam 3, the first flexural crack form at 26 kips (116 kN) and the first inclined crack form at 67 kips (298 kN). The beam failed at 92.2 kips (410 kN), 38% above the formation of the first inclined crack.

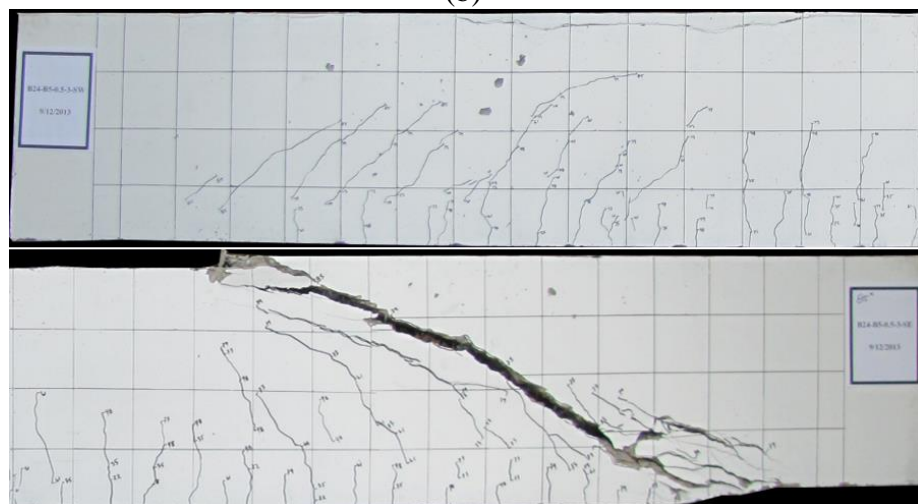
The beams in this series had an average failure load of 100.8 kips (449 kN) with a COV of 8.2%. This variation is higher than the variation presented in Series B18-B5-0.75 by 57%. Comparing the result of this series to the calculated shear stress provided by the ACI 318-14 minimum shear reinforcement, the average normalized shear stress provided by beams B24-B5-0.75 was 4.01, 17% higher than the necessary resistance. Series B24-B5-0.75 only performed 4% better than Series B18-B5-0.75.



(a)



(b)



(c)

Figure 4.38. Crack behavior of beams in Series B24-B5-0.5 after failure (a) B24-B5-0.5-1 (b) B24-B5-0.5-2 (c) B24-B5-0.5-3

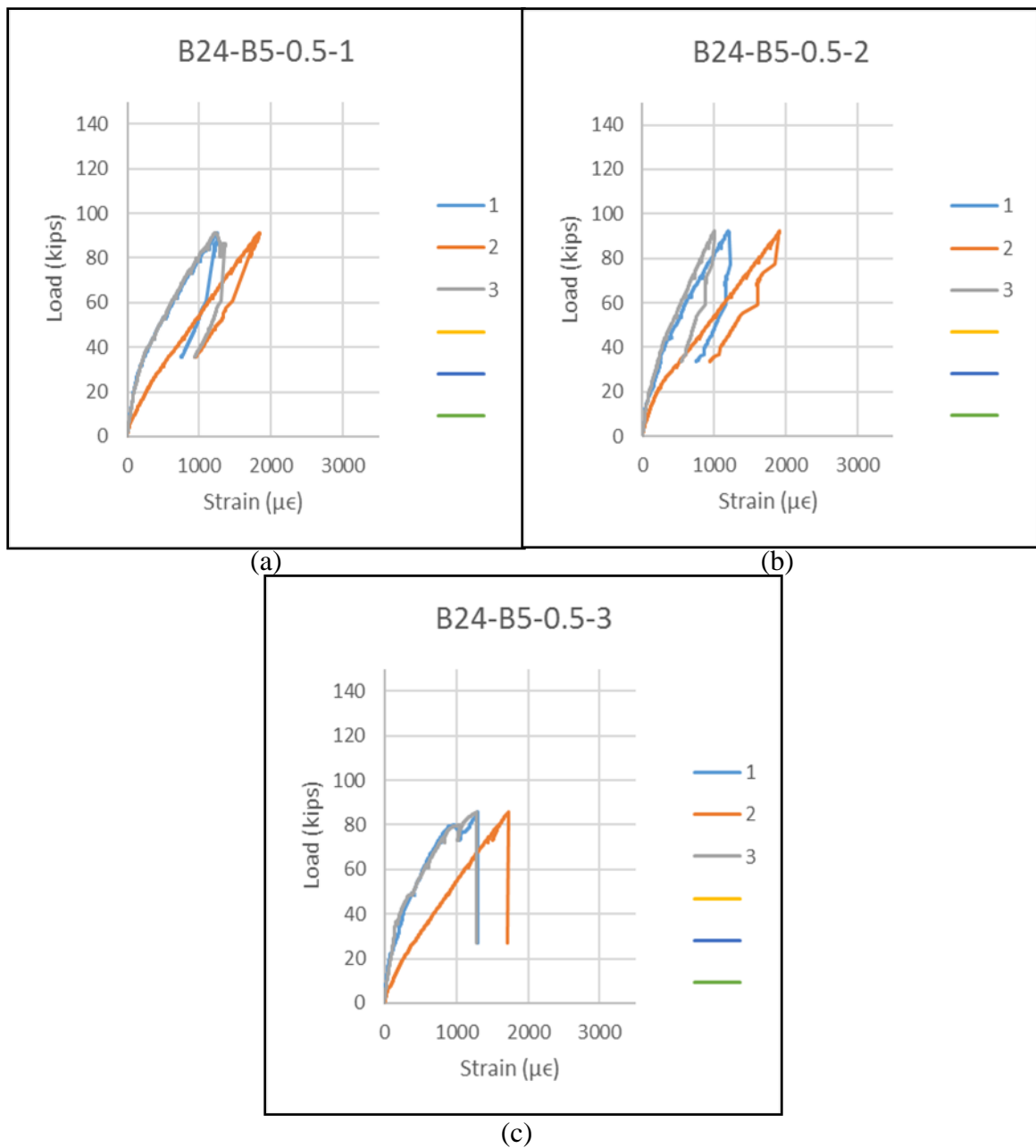


Figure 4.39. Reinforcement strains for beams in Series B24-B5-0.5

Figure 4.40 shows the load versus displacement behavior for each beam in Series B24-B5-0.75. Figure 4.41 shows the crack behavior of each beam in Series B24-B5-0.75 after failure. Prior to failure, Beams 1 and 3 developed a total of 6 inclined cracks and

Beam 2 developed 3 inclined cracks. On average, this series developed the same number of cracks as the beams in Series B18-PC and B18-B5-0.75. The average inclined crack failure angle was 26° , the same average crack angle as in Series B18-B5-0.75.

All beams in Series B24-B5-0.75 exhibited a linear load-displacement behavior up to the formation of the first flexural crack. Following the first crack, the slope slightly decreased and remained constant until failure, with softening in all of the load-displacement curves prior to failure. Beam 3 had a slight load drop around 87 kips (387 kN), but was able to stabilize due to the fibers bridging the crack, and the beam supported an additional 5 kips (22 kN) prior to failure. Beam 1 exhibited a midspan displacement at failure of 0.64 in. (16.2 mm). Beam 2 had a midspan displacement of 0.61 in. (15.5 mm), and the midspan displacement at failure for Beam 3 was 0.48 in. (12.2 mm). The average deflection for the beams in this Series was 0.58 in. (14.7 mm), 16% higher than in Series B18-B5-0.75.

The reinforcement strains for each beam are shown in Figure 4.42. All beams in this series included three strain gauges. Strain gauges 1 and 3 were located on the lower level of longitudinal reinforcement in the middle of the West and East shear spans, respectively, and strain gauge 2 was located at the same depth at midspan of the beam. All three beams in this series had similar behavior to the other FRC beams tested, with the highest strain located at midspan of the beam and a slightly lower strain at the center of each shear span. The strain gauge data indicated that none of the flexural steel yielded in any of the beams prior to shear failure.

B24-B5-0.75

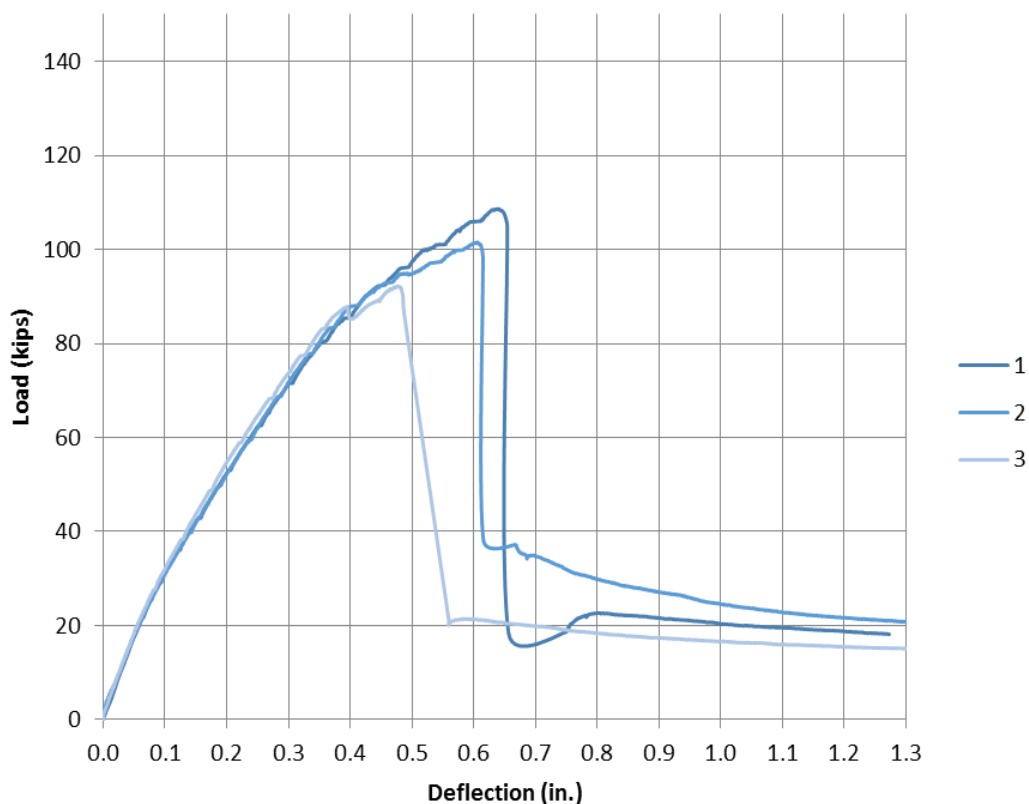


Figure 4.40. Load versus displacement behavior for beams in Series B24-B5-0.75

4.3.3. Beam Series B24-B5-1.0. Beams in Series B24-B5-1.0 were the beams tested in this series with the highest level of carbon fiber addition, 1.0% by volume. The results of this beam will be compared to the behavior and performance of the other levels of fiber addition, as well as if there is a depth effect by increasing the beam depth by 33% compared to the beams in the B18 series.

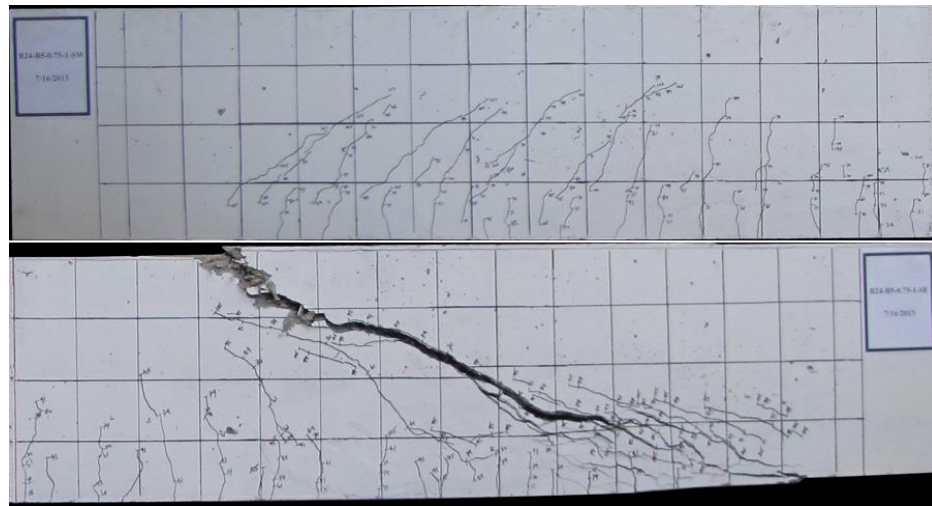
During loading, the first cracks to develop were flexural cracks between the two loading points, at the location of the highest moment. As the test progressed, the flexural cracks spread out towards the supports, relatively evenly spaced. Eventually, inclined

cracks formed within each shear span as the load increased until all beams failed due to diagonal tension. In Figure 4.44, cracking can be seen near the longitudinal reinforcement in each beam, but this is due to the post-peak loading of the test.

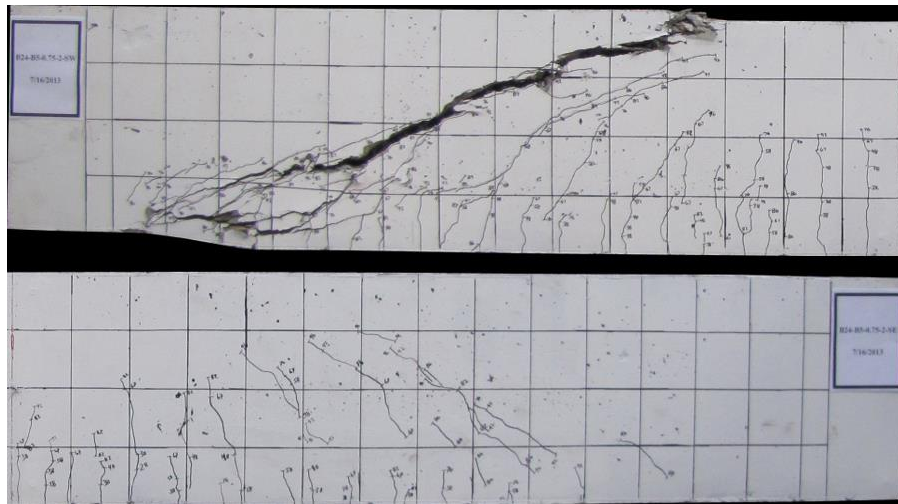
For Beam 1, the first flexural crack formed at 26 kips (116 kN) and the first inclined crack formed at 71 kips (316 kN). The beam failed at 125.1 kips (557 kN), 76% above the formation of the first inclined crack. For Beam 2, the first flexural crack formed at 26 kips (116 kN) and the first inclined crack formed at 67 kips (298 kN). The beam failed at 141.8 kips (452 kN), 111% above the load at the formation of the first inclined crack. For Beam 3, the first flexural crack formed at 28 kips (125 kN) and the first inclined crack formed at 58 kips (258 kN). The beam failed at 117.5 kips (523 kN), 103% above the formation of the first inclined crack.

The beams in this series had an average failure load of 128.1 kips (570 kN) with a COV of 9.7%. This variation is lower than the variation presented in Series B18-B5-1.0 by 22%. Comparing the result of this series to the calculated shear stress provided by the ACI 318-14 minimum shear reinforcement, the average normalized shear stress provided by beams B24-B5-1.0 was 5.03, 47% higher than the necessary resistance. Series B24-B5-1.0 only performed 10% better than Series B18-B5-1.0.

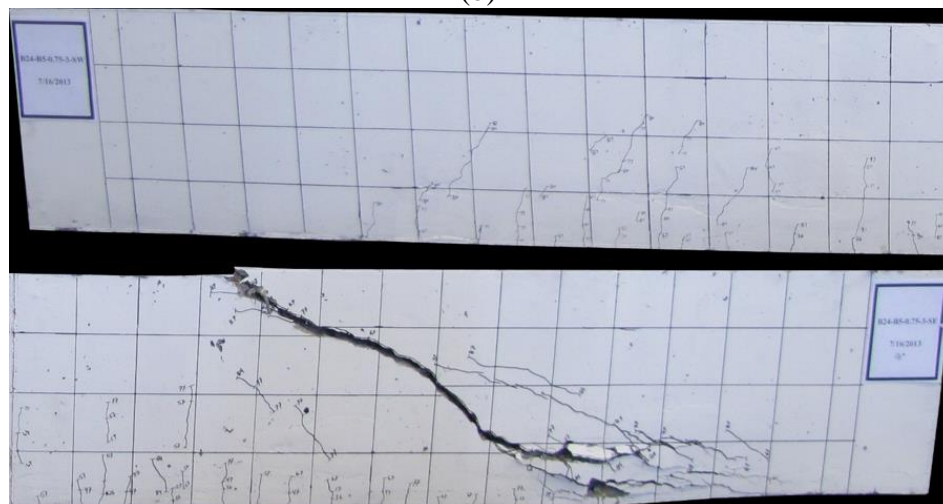
Figure 4.43 shows the load versus displacement behavior for each beam in Series B24-B5-1.0. Figure 4.44 shows the crack behavior of each beam in Series B24-B5-1.0 after failure. Prior to failure, Beam 1 developed a total of 9 inclined cracks, Beam 2 developed 14 inclined cracks, and Beam 3 developed 11 inclined cracks. The average inclined crack failure angle was 27° , only 2° below the average crack angle from Series B18-B5-1.0.



(a)



(b)



(c)

Figure 4.41. Crack behavior of beams in Series B24-B5-0.75 after failure (a) B24-B5-0.75-1 (b) B24-B5-0.75-2 (c) B24-B5-0.75-3

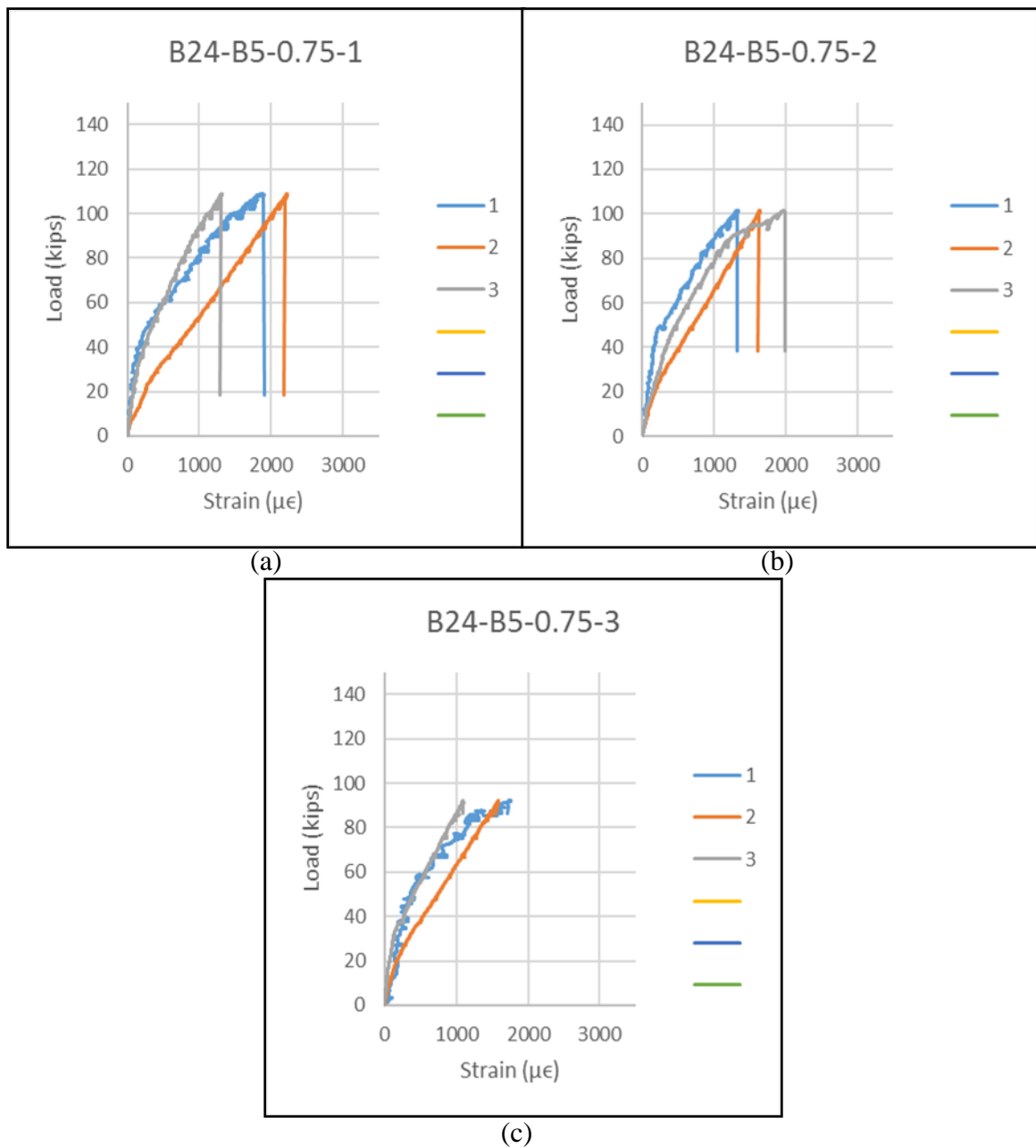


Figure 4.42. Reinforcement strains for beams in Series B24-B5-0.75

All beams in Series B24-B5-1.0 exhibited a linear load-displacement behavior up to the formation of the first flexural crack. Following the first crack, the slope slightly decreased and remained constant until failure, with softening in all of the load-

displacement curves prior to failure. Beam 1 exhibited a midspan displacement at failure of 0.68 in. (17.3 mm). Beam 2 had the highest midspan displacement of 1.10 in. (27.9 mm), which corresponded to the highest load in the series. The midspan displacement at failure for Beam 3 was 0.79 in. (20.1 mm). The average deflection for the beams in this Series was 0.86 in. (14.7 mm), 34% higher than in Series B18-B5-1.0.

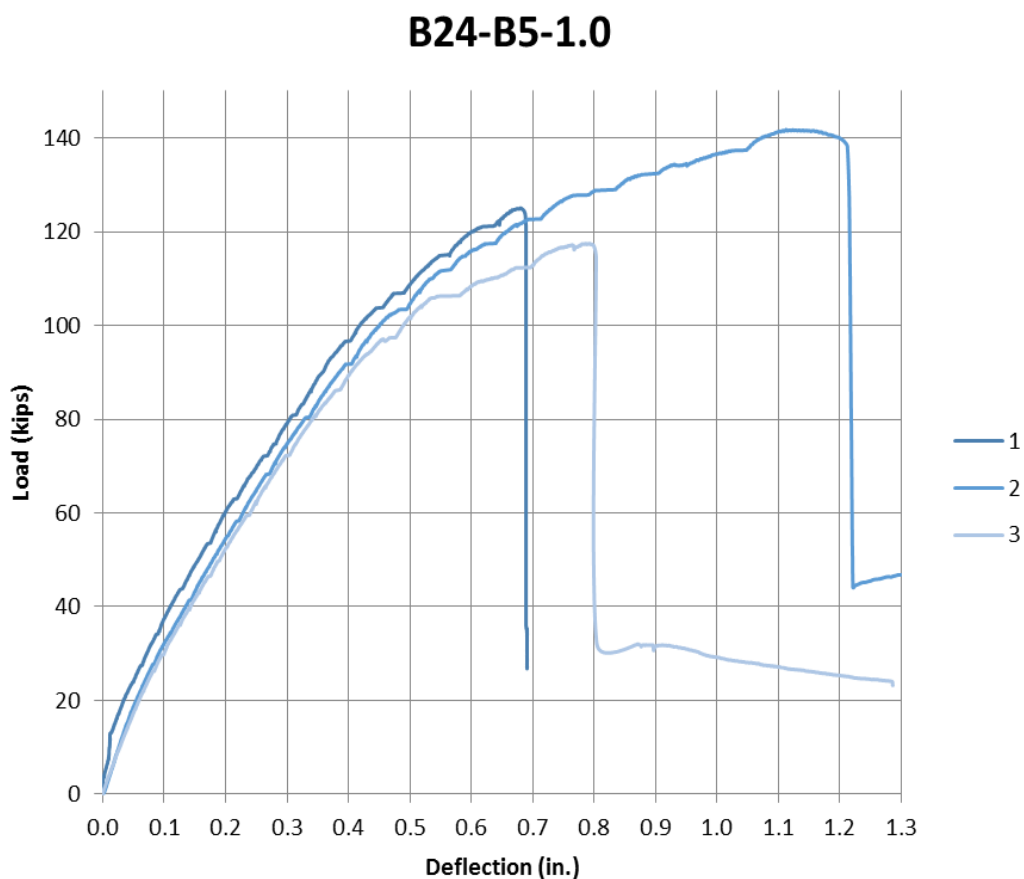
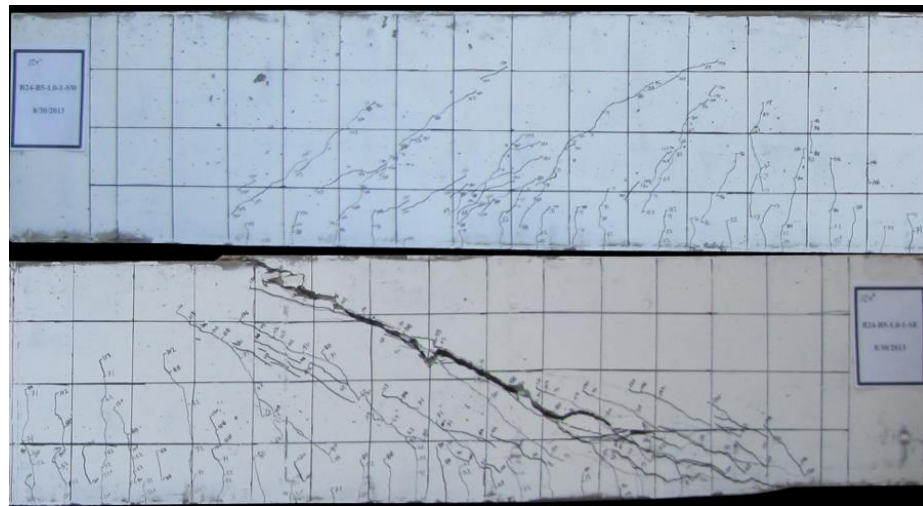
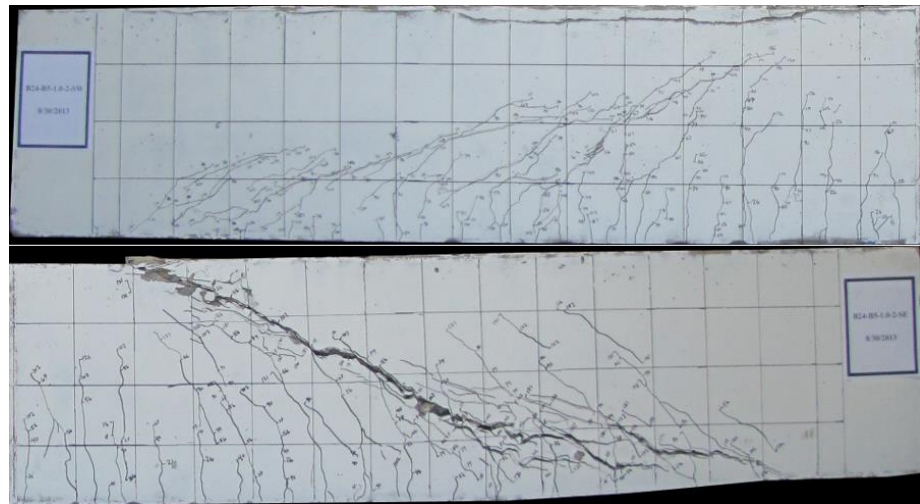


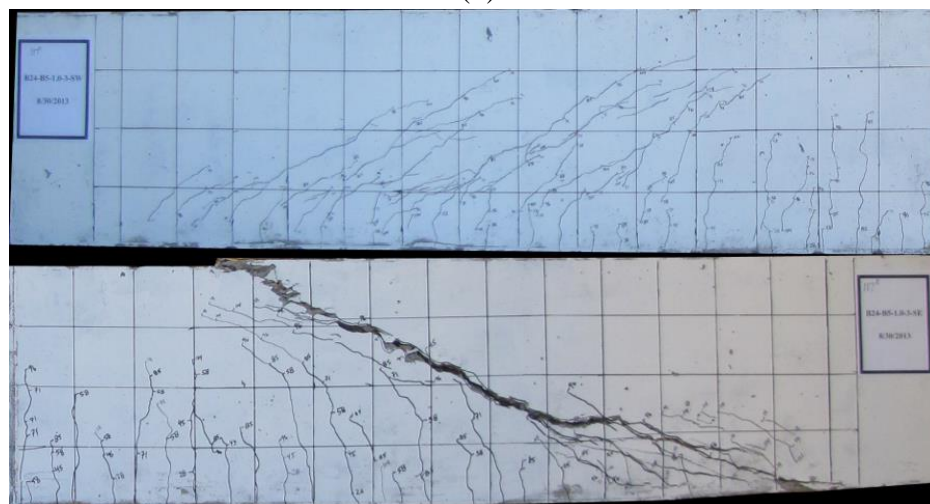
Figure 4.43. Load versus displacement behavior for beams in Series B24-B5-1.0



(a)



(b)



(c)

Figure 4.44. Crack behavior of beams in Series B24-B5-1.0 after failure (a) B24-B5-1.0-1 (b) B24-B5-1.0-2 (c) B24-B5-1.0-3

The reinforcement strains for each beam are shown in Figure 4.45. All beams in this series included three strain gauges. Strain gauges 1 and 3 were located on the lower level of longitudinal reinforcement in the middle of the West and East shear spans, respectively, and strain gauge 2 was located at the same depth at midspan of the beam. All three beams in this series had similar behavior to the other FRC beams tested, with the highest strain located at midspan of the beam and a slightly lower strain at the center of each shear span. The strain gauge data indicated that none of the flexural steel yielded in any of the beams prior to shear failure.

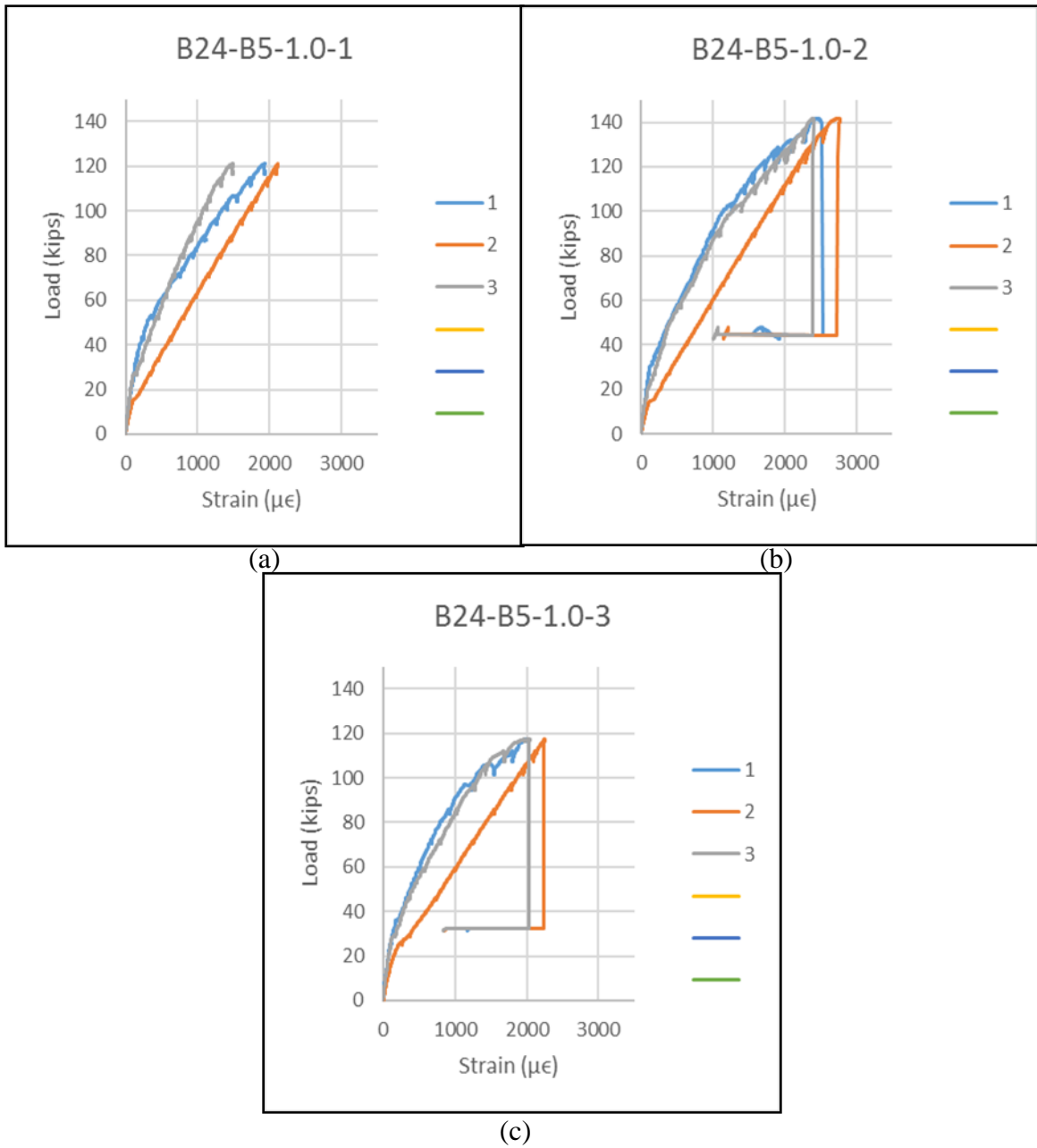


Figure 4.45. Reinforcement strains for beams in Series B24-B5-1.0

5. ANALYSIS AND DISCUSSION OF RESULTS

In this section, the results from the experimental program will be discussed and analyzed. First, an overview of the ASTM C1609 results will be presented, along with any correlations that can be drawn between the ASTM C1609 specimens and the large-scale shear testing. The results will then be analyzed with respect to the capability of the FRC as a suitable replacement for the ACI minimum shear reinforcement. Second, an analysis of the overall behavior of the large-scale shear specimens will be discussed, including a global overview of the shear performance, crack patterns and behavior, and beam deflection. Then, the effects of the varied parameters will be discussed, including fiber volume fraction, fiber type, and beam depth. The section will close with a comparison of the FRC performance to a mechanics-based model for prediction of shear performance.

5.1. ANALYSIS OF ASTM C1609 PERFORMANCE AND BEHAVIOR

In the following sections, the overall ASTM C1609 performance will be analyzed. The main discussion points will be centered around the overall load-displacement behavior and trends between the equivalent flexural strength ratios, equivalent bending stresses, volume fraction of fibers, and total fibers. Also, comparisons between ASTM C1609 testing and the large-scale shear tests will be drawn, along with the suitability of the FRC tested for minimum transverse reinforcement. The average results for each set of ASTM C1609 beams tested is presented in Table 5.1.

Table 5.1. Average ASTM C1609 results for each set of beams

Mix	Fiber	v_f (%)	f'_c (psi)	σ_c (psi)	σ_{pc} (psi)	σ_{600} (psi)	σ_{300} (psi)	σ_{150} (psi)	δ_{pc} (in.)	T (in- lb)	R (%)	ACI 318 90% Req.	ACI 318 75% Req.	Pass ACI Req?	Total Fibers	Δ (in.)
1	B3	1.0	4220	570	529	462	426	289	0.0324	600	69	73	49	F	-	0.091
2	B3	1.0	5667	658	562	467	407	349	0.0237	450	47	61	53	F	-	0.094
3	B3	1.0	6256	715	666	597	457	339	0.0192	703	67	64	48	F	-	0.088
4	B3	1.0	4355	633	586	545	402	308	0.0266	621	67	64	49	F	-	0.085
6	B3	1.0	6447	762	793	661	399	227	0.0219	647	58	52	30	F	36	0.083
6	B3	1.5	6010	732	875	834	777	569	0.0333	1010	94	104	77	T	62	0.081
6	B3	2.0	7084	852	1221	1095	1064	746	0.0424	1387	111	124	88	T	90	0.076
6	B3 (12k)	1.0	6520	697	597	554	392	256	0.0260	571	57	57	37	F	75	0.086
6	B4	1.0	6360	581	528	411	284	189	0.0108	469	54	49	32	F	24	0.094
6	B5	1.5	7042	794	927	902	673	387	0.0305	986	83	84	48	F	65	0.082
6	D1	1.8	7071	759	785	698	739	713	0.0942	1031	92	98	9%	T	69	0.063
6	D1	2.4	7115	772	853	748	822	818	0.0789	1141	100	107	106	T	103	0.060
6	B5 / D1	1.5	6520	711	859	784	702	673	0.0474	1007	96	98	95	T	48	0.075
B18	B5	0.5	7250	681	548	440	231	132	0.0186	431	42	34	19	F	25	0.088
B18	B5	0.75	6391	636	582	537	388	261	0.0225	602	63	61	41	F	35	0.085
B18	B5	1.0	7120	678	724	664	519	362	0.0276	770	75	75	52	F	39	0.080
B24	B5	0.50	7271	677	417	329	175	111	0.0123	325	32	26	16	F	19	0.097
B24	B5	0.75	7478	732	632	510	377	209	0.0143	601	53	51	28	F	32	0.090
B24	B5	1.0	7254	712	548	421	283	154	0.0140	470	44	39	2	F	23	0.088
B18	D1	1.0	7170	737	364	320	361	300	0.0622	489	45	49	41	F	25	0.087
B18	S	0.75	6780	809	779	733	629	399	0.0228	906	74	78	49	F	-	0.107

5.1.1. Overall Load-Displacement Behavior of Specimens. From the 112 C1609 specimens tested in this research program, some basic trends can be drawn from the load-displacement curves presented in Section 4. First of all, it can be seen in the curves, and in Table 5.1, that σ_c was very consistent across all groups of specimens, with a COV of only 10%. Taking into consideration the differences in concrete compressive strength at testing, this is very stable and confirms a well-known fact that the fibers in a FRC specimen do not contribute greatly to the first cracking stress, but carry load once a crack is formed.

A majority of the specimens tested, regardless of fiber type, were able to display some level of post-peak hardening in the load-displacement curve. The beams that did not exemplify this behavior typically came from groups with a lower volume fraction of fibers or beams with less discrete fibers crossing the flexural crack that was formed during the test. When comparing the curves in Figure 5.1, it is seen that the B24-B5-1.0 series is very similar to Series B24-B5-0.5, even with twice the volume fraction of fibers. When investigating the fibers crossing the crack in each specimen, Series B24-B5-0.5 contained an average of 19 fibers, compared to an average of 23 fibers for Series B24-B5-1.0. This shows how critical it is to have even fiber dispersion within the fresh concrete, in order to fully benefit from the fiber addition. During the fresh placement of Series B24-B5-1.0, there were no indications of any differences from any other large-scale pours. However, the low fiber count could be attributed to using the first portion of concrete out of the truck for the ASTM C1609 specimens, which may have not been mixed as well as the rest of the concrete in the truck.

Another observation of the load-displacement curves that can be drawn is that some individual beams gained a much higher σ_{pc} compared to the others within the group. Upon

investigation, correlations can be drawn corresponding to the fiber type and number of fibers crossing the crack and number of crack(s) formed within the test. Generally, the B3 and B5 variants of fibers were able to attain the highest post-cracking loads, especially at higher volume fractions. As seen in Tables 4.3 and 4.4, the highest σ_{pc} recorded, 1471 psi, corresponded with the beam containing the largest number of fibers crossing the crack, 123, (M6-B3-2.0-2). Figure 5.2 shows the crack patterns of two beams; M6-B3-2.0-2 and M6-B3-2.0-3, with 123 and 83 fibers respectively. Clearly, there is a considerable increase in the cracking behavior in Beam 2 from this series, which also corresponds to the highest number of fibers crossing the crack. Generally, as the number of fibers crossing the crack increased, the post-peak load increased as well, this can be seen in Figure 5.3.

Comparing the load-displacement behavior between fiber types, there were clear differences between the B series and D series of fibers. The first, already mentioned above, is that the carbon fibers are capable of gaining higher post-peak hardening behavior and, correspondingly, higher σ_{pc} values than the Innegra fibers. The second difference is the shape of the curves of the Series B and D fibers. For the B series, there is a second peak after the initial cracking load, typically within the first half of the test, followed by a steady decline of load capacity until the end of the test. The tests completed on the D series show a much different behavior. Instead of showing a peak within the first half of the test, the D series beams exhibited a slight load drop after the first crack with a gradual increase in load until the end of the test. This difference in behavior is exhibited in Figure 5.4 This difference could be due to either differences in bond between the carbon and Innegra fibers and the concrete matrix or the relative difference in ultimate strength and modulus between the fiber types. Further investigation is needed to determine the driving factor, but when

comparing the behavior of the steel fiber beams, they are analogous to the LCFRC beams. The tensile strength and modulus of the steel fibers are within the same magnitude of the carbon fibers, much higher than the properties of the Innegra fibers, further driving the hypothesis regarding material strength differences. When combining the B5 and D1 fibers, at a 50/50 proportion, the load-displacement curve shows a balance between the behavior of both fibers. The beams are able to gain post-peak hardening, similar to the B series of beams, while maintaining a higher load at the end of the test, similar to the D series of beams. Examples of this can be seen in Figure 5.4.

The last comparison drawn from the load-deflection curves is the permanent deflection of the beams after the test. Figure 5.5 shows the trends according to each fiber type. Generally, as the volume fraction increased, the permanent deflection of the beam decreased. The D series fibers had a slightly lower displacement compared to the B series, at similar volume fractions. The combination of fibers B5 and D1 was slightly above the average of each series containing the respective fiber individually.

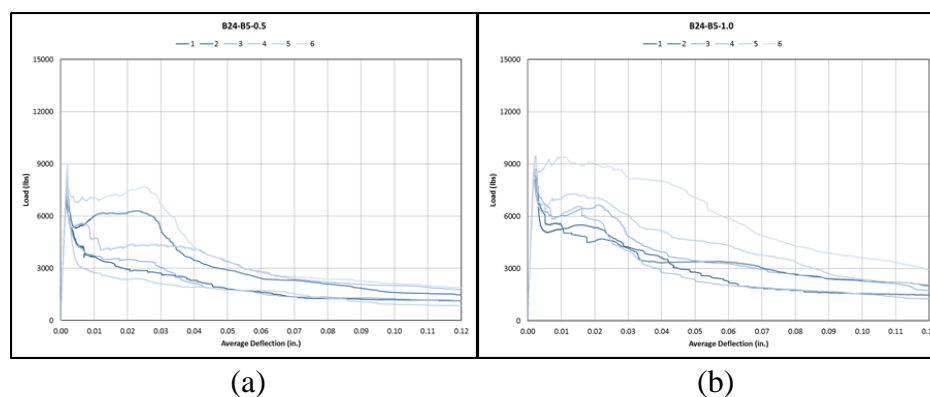


Figure 5.1. Load vs. deflection curves of ASTM C1609 tests (a) Fiber B24-B5 @ 0.5%
(b) Fiber B24-B5 @ 1.0%



(a)



(b)

Figure 5.2. Examples of ASTM C1609 specimens after failure (a) M6-B3-2.0-2 – single crack (b) M6-B3-2.0-3 – multiple cracks

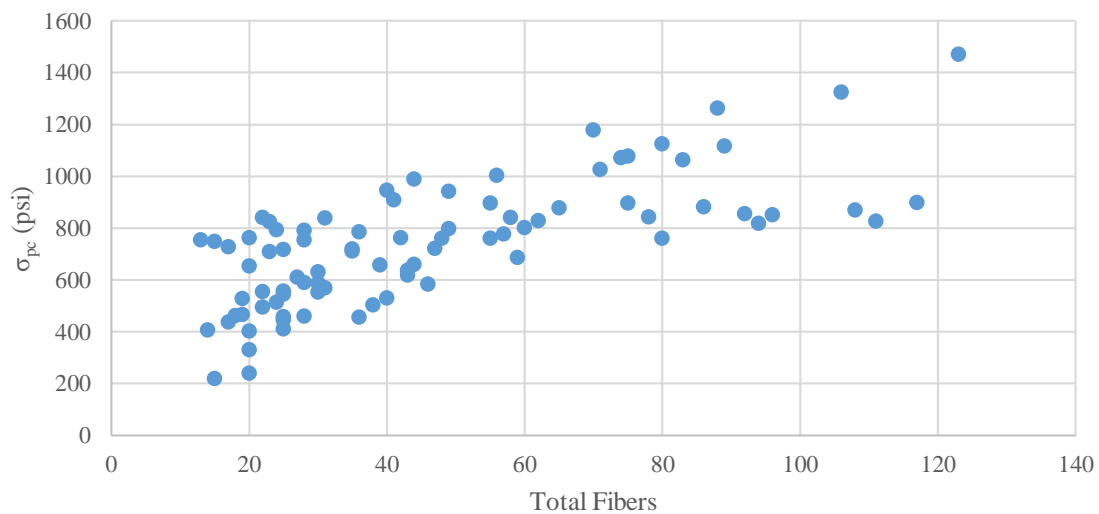


Figure 5.3. Relationship between fibers crossing crack and post-cracking bending stress

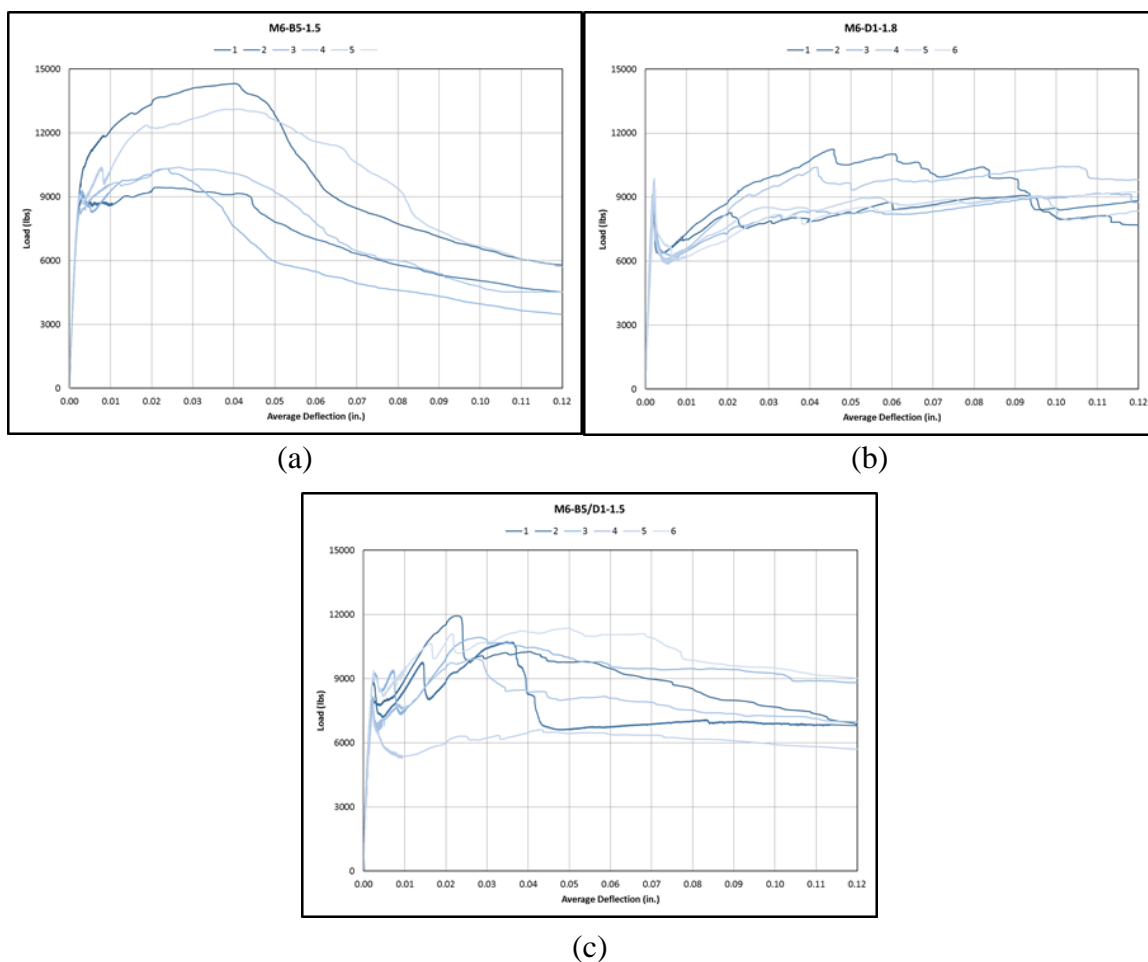


Figure 5.4. Load vs. deflection curves of ASTM C1609 tests (a) M6-B5-1.5 (b) M6-D1-1.8 (c) M6-B5/D1-1.5

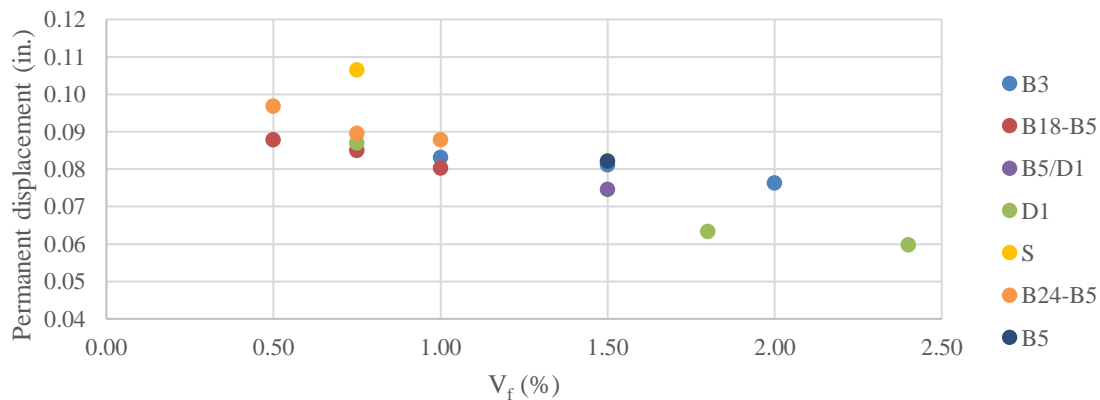


Figure 5.5. Permanent displacement vs. V_f (%) for ASTM C1609 tests

5.1.2. Equivalent Bending Stresses Compared to Fiber Type and Content. As discussed in the previous section, the equivalent bending stresses, at key points throughout the test, were calculated in order further understand performance of each specimen. The average values for each group of beams are recorded in Table 5.1. Figure 5.6 graphically shows the relationship of equivalent bending stresses σ_c , σ_{pc} , σ_{600} , and σ_{150} versus volume fraction and fiber series.

From Figure 5.6, it is clear that the first peak bending stress did not vary with regard to fiber type or volume fraction. This consistency is due to the fibers adding strength only once the cracks develop in the beams. The concrete compressive strength varied 13% between each beam series, while σ_c only varied 10%.

Once the crack was formed in each beam, the behavior of the FRC is displayed. It is shown in Figure 5.6 that as the volume fraction of fibers is increased, σ_{pc} increases as well. For the B series of fibers, this increase was relatively linear between a volume fraction of 0.5% and 2.0%. This trend was similar for the beams tested with Fiber D1, but as seen in the load-displacement curves, at similar volume fractions, they were not able to reach the same post-peak strength. Also, it appears that at a higher volume fraction, the addition of Fiber D1 has a diminishing effect. Figure 5.7 shows a comparison of σ_{pc} to the total fibers in each beam. It is clear from the graph that there is a linear trend between the number of fibers crossing the crack and σ_{pc} for the beams containing B3 and B5 fibers. However, as the total number of fibers increases for beams containing fibers D1, they appear to follow a logarithmic trend. Once the bending stress is approximately 900 psi (6.2 Mpa), the FRC does not gain much benefit by adding additional fibers. This could be due to the material strength differences between the two materials. Fiber B4 responded similarly to the

trendline for Fibers D1, this is most likely due to the lower bond between Fiber B4 and the concrete matrix. The steel fibers at a volume fraction of 0.75% performed at the same level as Fibers B3 and B5 at a volume fraction of 1.0%. The blend of Fibers B5 and D1 performed similarly to B3 at a volume fraction of 1.5%.

Comparable trends for fiber volume fractions and types were seen for σ_{600} as were seen with σ_{pc} . But, once the displacement of the test reached 0.12 in. (3.05 mm), the behavior of the specimens changed. There was still an increase in the performance of groups of beams as the fiber volume fraction increased. However, similar to the beams containing Fiber D1, the beams containing Fibers B3 and B5 showed a lessening increase in performance as the volume fraction rose above 1.5%. Also, as a result of the D1 beams retaining higher loads at the end of the test, on average, each volume fraction (1.0%, 1.8%, and 2.4%) attained higher σ_{150} values compared to B3 and B5 beams (0.75%, 1.5%, and 2.0%). Subsequently, the blend between B5 and D1 reached an average of only 6% below Fiber D1 at a volume fraction of 1.8%, but 74% above Fiber B5 at a volume fraction of 1.5%.

The last observation taken from the bending stresses is a comparison of deflection of each specimen at σ_{pc} versus volume fraction and fiber type. Figure 5.8 shows that as the fiber volume fraction increased, there is a slight increase in δ_{pc} . This is most likely due to the tendency for beams containing more fibers to form more than one crack during the test, thus increasing its post-peak load-carrying capacity and increasing the deflection at which it occurs. It can also be seen in this chart that at similar volume fractions, the D1 fibers reached higher δ_{pc} values, demonstrating its ability to maintain a more consistent load throughout the test compared to the carbon and steel fibers.

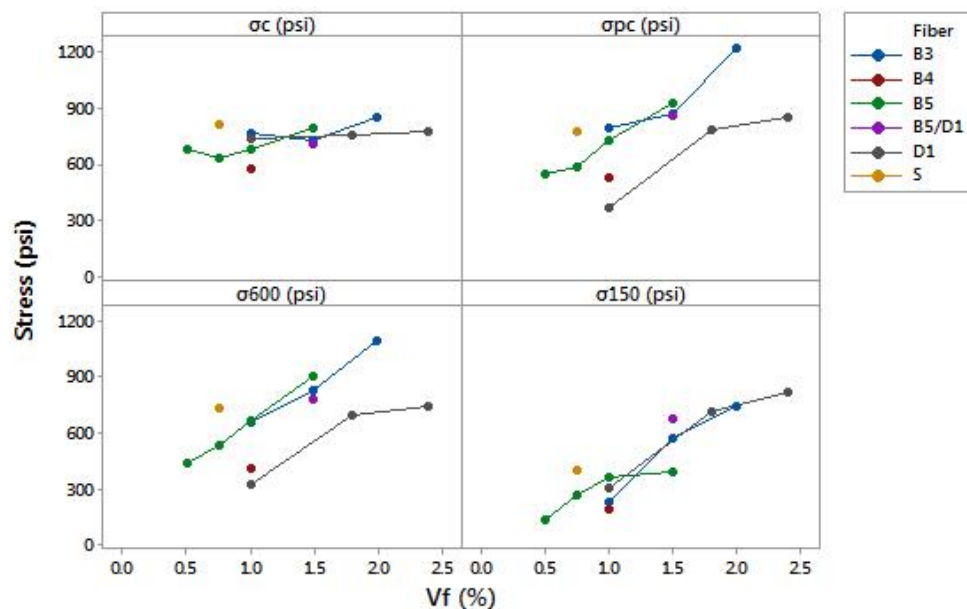


Figure 5.6. Equivalent bending stresses vs. V_f (%) for ASTM C1609 testing

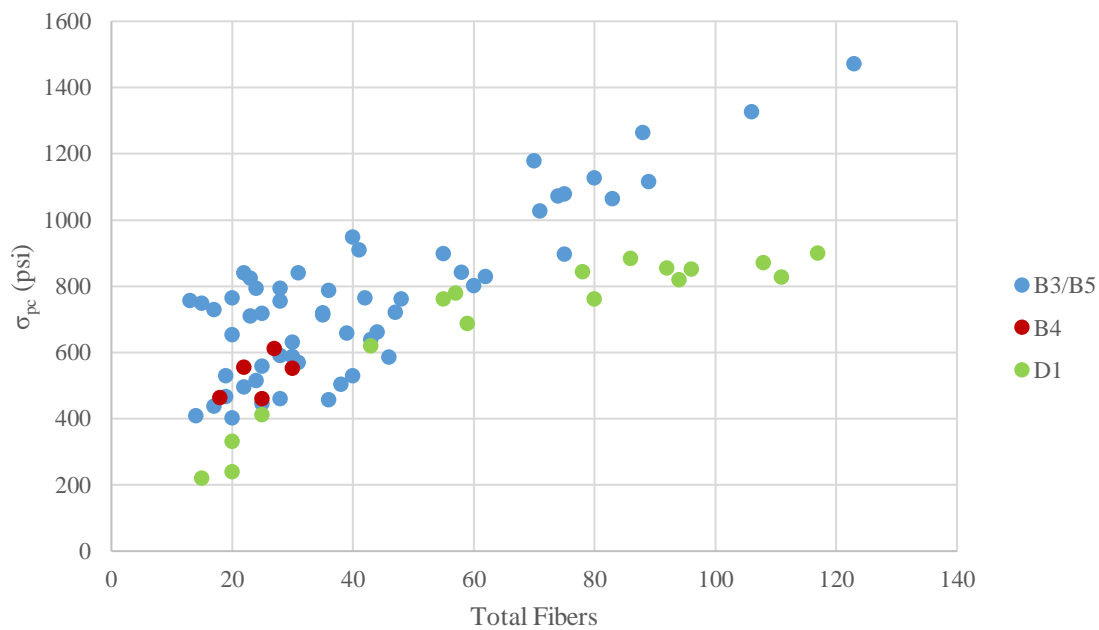


Figure 5.7. σ_{pc} vs. total fibers for ASTM C1609 testing

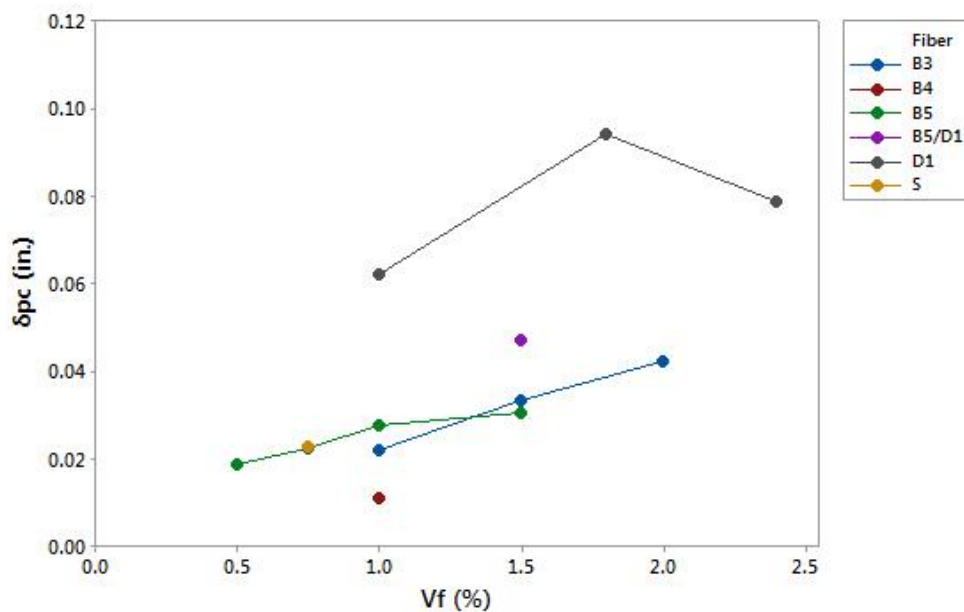


Figure 5.8. δ_{pc} vs. V_f (%) for ASTM C1609 testing

5.1.3. Equivalent Flexural Strength Ratio Compared to Fiber Type and

Content. The final, critical value for comparison among the ASTM C1609 tests is the equivalent flexural strength ratio, which is a ratio between the toughness of the beam and the first-peak load. This essentially normalizes the area under the load-displacement curve for each beam to its first-peak load. Overall beam performance can be easily compared with this ratio because it does not identify specific points along the stress-deflection curve to compare, rather it compares overall behavior of the FRC throughout the entire test.

Figure 5.9 shows that, similar to other measures already discussed, as the fiber volume fraction increases, the performance of the beam is increased as well. Fibers B3 and B5 exhibited similar behavior between volume fractions of 0.5% and 2.0%, but as the

volume fraction increased, the performance gain diminished. Series B18 and B24 beams were separated to show the effect of discrete fibers crossing the crack. Between a volume fraction of 0.5% and 1.0%, Series B18 shows a strong linear trend, but Series B24 appears to lose performance at the 1.0% level compared to 0.75% and 0.5%. When taking the number of fibers crossing the crack into consideration, the apparent outlier from the trend disappears. Figure 5.10 shows a comparison of total fibers at the crack location to equivalent flexural strength ratio. It can be seen in the chart that the B24-B5-1.0 series had a similar number of fibers crossing the crack to those series at 0.5%, with comparable performance. The B3 and B5 beams had almost identical trends as the fiber volume fraction increased from 0.5% to 2.0%. It is worthy to note, that although the blend of Fibers B5 and D1 performed somewhere within the average of each individual beam series for each measure compared above, at comparable volume fractions of 1.5% and 1.8% respectively, Series B5/D1 performed significantly better than the trend for either B5 or D1 alone.

5.1.4. Comparison Between ASTM C1609 and Large-Scale Shear Tests.

Corresponding to each set of large-scale beams constructed and tested, a set of 6 ASTM C1609 beams were cast in order to attempt to draw correlations between the small-scale material tests and the large-scale application testing. To compare all fiber types, Figure 5.11 shows the relationship between the average equivalent flexural strength ratio and the normalized shear stress for each series. The graph shows that most beams fall along the trendline starting at a normalized shear stress of 2.7. If all series are included in this chart, the R^2 value equals 0.6, but removing the outlier, B24-B5-1.0 (due to discrete fiber count), the R^2 value increases to 0.86. This trend is further displayed in Figure 5.12. This graph shows that for all C1609 beam series tested in this study that attained equivalent strength

ratios above 30%, the full-scale beams were able to perform above a theoretical beam reinforced with the minimum transverse reinforcement according to ACI 318-14.

5.1.5. Evaluation of FRC to be Used in Place of Minimum Shear Reinforcement. All beams tested with various fiber types and volume fractions were evaluated to determine if they would achieve the limits set by ACI 318-14, Section 5.6.6, to replace the minimum transverse reinforcement in traditional reinforced concrete beams.

According to the regulation, the ratio of σ_{300} to σ_c must be greater than or equal to 0.9 and the ratio of σ_{150} to σ_c must be greater than or equal to 0.75. The average ratios for each criterion are listed in Table 5.1 and presented graphically in Figure 5.13.

It is shown that the beams containing 1.5% or more of the carbon fibers were able to meet this criterion. The Innegra fibers were also able to meet the criteria at volume fractions of 1.8% and 2.4%. The steel fibers, at a volume fraction of 0.75%, were not able to meet this criterion. Although the beams containing 0.5% to 1.0% LCFRC were not able to meet the criteria set forth by ACI 318-14, as discussed in the previous section, they were still able to achieve the shear resistance necessary for the minimum transverse reinforcement.

As shown in the multiple fiber types tested with positive results in the large-scale shear testing, the ACI 318-14 criteria for the use of steel fiber reinforced concrete as minimum shear reinforcement is very conservative. With further research and testing, it may be possible to adapt the criteria for wider use of FRC in place of minimum shear reinforcement.

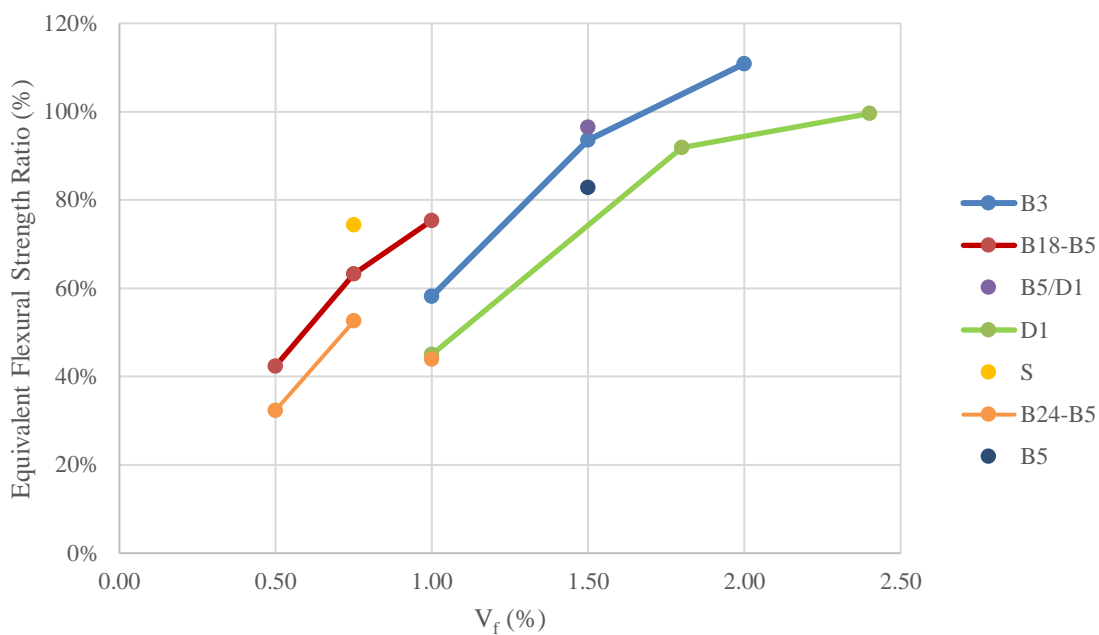


Figure 5.9. Equivalent flexural strength ratio (%) vs. V_f (%)

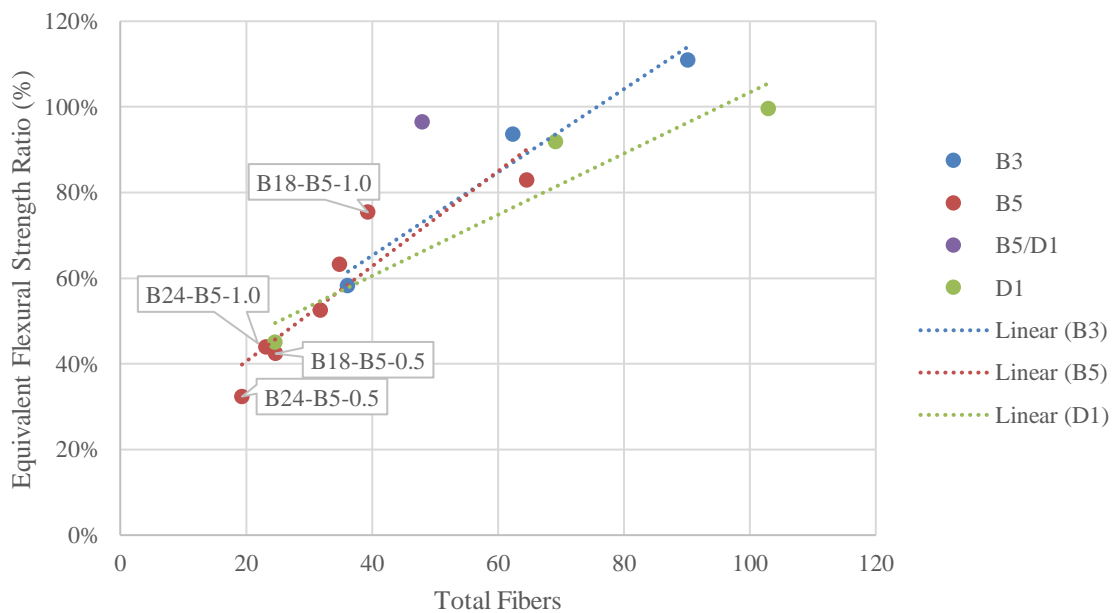


Figure 5.10. Equivalent flexural strength ratio (%) vs. total fibers

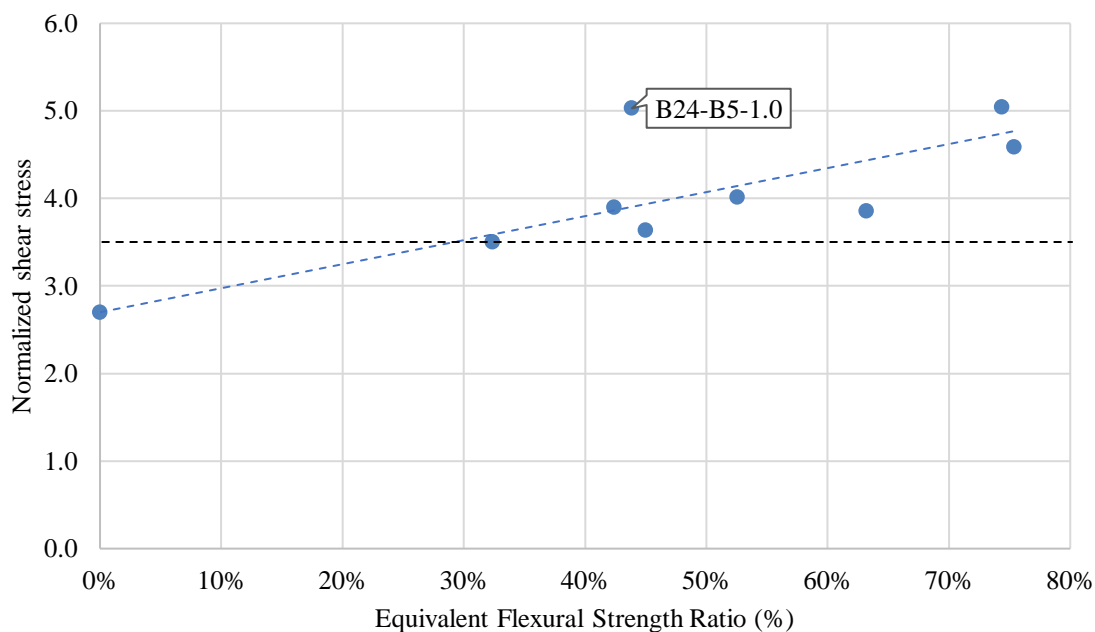


Figure 5.11. Normalized shear stress vs. equivalent flexural strength ratio

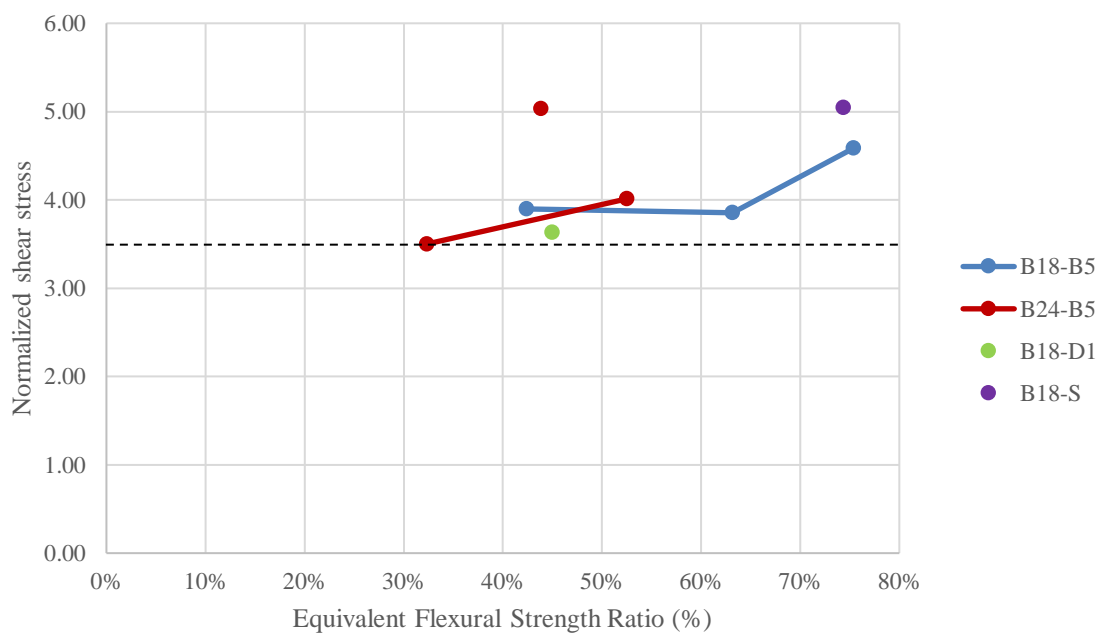


Figure 5.12. Normalized shear stress vs. equivalent flexural strength ratio

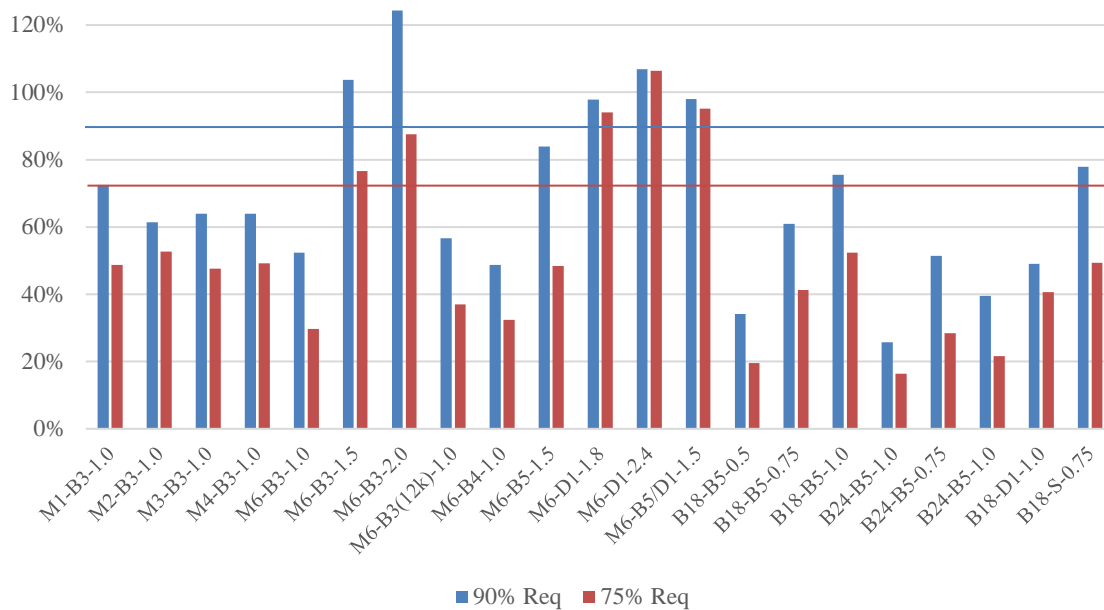


Figure 5.13. Comparison of ASTM C1609 beam performance to ACI 318-14 requirements

5.2. ANALYSIS OF LARGE-SCALE SHEAR BEAM PERFORMANCE AND BEHAVIOR

In the following sections, the overall performance and behavior of the large-scale shear beams will be discussed. The main points reviewed will be the overall load-displacement behavior, shear stresses, failure modes, and crack development and behavior. Table 5.2 lists the fiber percentage, average ultimate failure load, COV, average shear stress, compressive strength at testing, average normalized shear stress, average midspan displacement at failure, average total number of inclined cracks, and average angle of the critical inclined shear crack, respectively.

Table 5.2. Average response of beam series to large-scale shear testing

Beam	V_f (%)	P_u (kips)	COV (%)	v_u (psi)	f'_c (psi)	$v_u/\sqrt{f'_c}$	Δ (in.)	Total N	Avg. θ_c (°)
B18-PC	0	47.0	7.0	199	5452	2.70	0.29	5.0	32
B18-TR	0	116.1	5.6	492	6143	6.28	1.03	11.0	-
B18-B5-0.5	0.5	72.7	1.7	308	6250	3.90	0.51	8.0	23
B18-B5-0.75	0.75	68.0	3.4	288	5583	3.85	0.50	5.3	26
B18-B5-1.0	1.0	81.4	12.5	345	5665	4.58	0.64	7.3	29
B24-B5-0.5	0.5	89.8	3.9	280	6390	3.50	0.50	10.0	23
B24-B5-0.75	0.75	100.8	8.2	314	6131	4.01	0.58	9.3	26
B24-B5-1.0	1.0	128.1	9.7	399	6306	5.03	0.86	11.3	27
B18-D1-1.0	1.0	62.9	12.9	267	5376	3.64	0.53	5.0	25
B18-S-0.75	0.75	93.3	9.2	395	6143	5.05	0.70	9.0	28

5.2.1. Overall Load-Displacement and Shear Stress Analysis. Each set of three, large-scale beams were loaded monotonically until failure, at which point the ultimate load and displacement of the test was recorded. The ultimate loads were converted in shear stresses using Equation 4-3. A box plot of the ultimate loads for each series of beams tested is shown in Figure 5.14. The control series of plain concrete, without transverse reinforcement, supported an average shear stress of 199 psi (1.4 Mpa) at failure. The minimum average shear stress achieved by the LCFRC beams was 1.4 times greater than the control beams tested, resulting from Series B24-B5-0.5. The maximum average shear stress achieved by the LCFRC beams was 2.0 times greater than the control beams tested, resulting from Series B24-B5-1.0. Series B18-D1-1.0 performed 1.34 times better than the control series, and the beams from Series B18-S-0.75 performed the same as those from Series B24-B5-1.0.

As shown in Figure 5.14, the lowest variation came from Series B18-B5-0.5 (1.7%), followed closely by Series B24-B5-0.5 (3.4%). This variation was even lower than the

series containing traditional mild steel as transverse reinforcement, Series B18-TR. The highest variations tended to come from the beam series containing the higher volume fractions of fibers, with Series B18-D1-1.0 having the largest variation of 12.9%. This result is believed to be due to multiple cracks forming and opening within the beams that contained the larger volume fractions of fibers, which engaged a larger portion of the fiber-reinforced concrete and the inherent variability in fiber dispersion within beams in these series. Considering the high degree of variability commonly associated with shear failure mechanisms in concrete, the variations resulting from the tests in this study show reliability within the data.

When comparing the overall load-displacement behavior of each series in the figures presented in Section 4, the FRC beams containing carbon, Innegra, and steel fibers all exhibited some softening in the curve prior to ultimate failure. This was not the case with the control specimens, Series B18-PC, which presented sudden drops at ultimate load, just after linear load-displacement behavior. The overall midspan displacements versus normalized shear stresses are presented in Figure 5.15. There is a clear link between the load at failure and the midspan displacement, with an R^2 value of 0.9 from the trendline on the graph. Series B18-PC attained displacements between 0.2 and 0.4 in. (5.1 and 10.2 mm), while the FRC beams reached displacements from 0.45 to 1.1 in. (11.4 and 27.9 mm). The beams containing mild steel reinforcement attained displacements between 0.9 and 1.15 in. (22.9 and 29.2 mm).

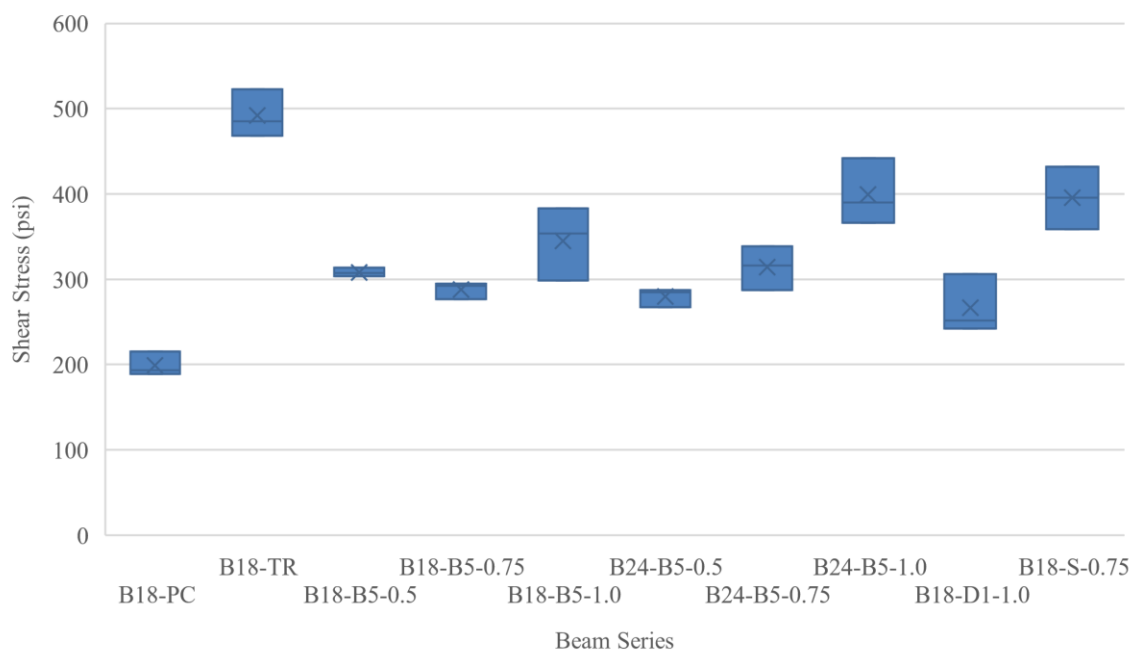


Figure 5.14. Box plot of maximum shear stresses for each beam series

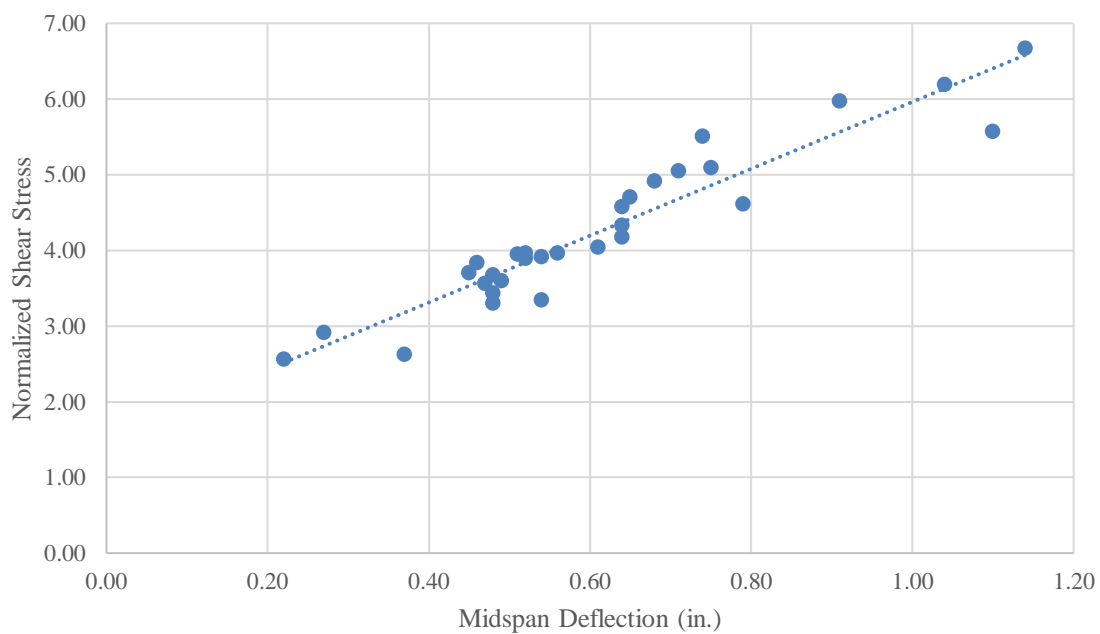


Figure 5.15. Normalized shear stress vs. midspan deflection for large-scale testing

5.2.2. Failure Modes. The failure modes of each beam are presented in Table 4.5. Of the 30 beams tested, there were 4 failure modes throughout the study, diagonal tension, combination shear-tension and diagonal tension, combination shear-compression and diagonal tension, and flexural failure due to crushing. Each shear failure mode resulted in a critical diagonal crack, under which the RC and FRC beams could no longer resist the stresses crossing the section.

For the diagonal tension failure mode, the critical crack propagated from the point of loading to the support with the greatest width occurring around mid-depth of the beam. The critical inclined crack was typically the outermost crack from the load point. This type of failure mode occurred in the control beams without transverse reinforcement, as well as about 60% of the FRC beams. Similar to this failure mode was the failure due to combination shear-tension and diagonal tension. Again, the critical crack started around mid-depth of the section, propagating to the load point, but on the other end of the crack, cracks along the reinforcing bars developed propagating towards the support. This failure mode occurred in approximately 30% of the beams tested.

The beams reinforced with the Innegra fibers all exhibited failure due to combination shear-compression and diagonal tension. In contrast to the previous two failure modes, the critical inclined crack opened from the top of the longitudinal reinforcement propagating upwards toward the loading point, but at failure, the concrete under the support failed due to crushing. The beams in this series had the lowest compressive strength at testing, which could have potentially led to this failure mode as a result. It should be mentioned that the beams in this series performed approximately 10%

below the average of the two B series at a volume fraction of 0.75%, but more testing would need to be done to confirm this trend.

The final failure mode for the beams in this study was a result of failure from crushing due to flexure. All three beams from Series B18-TR failed in this manner. As the load increased, more inclined cracks developed along the two shear spans, along with an increasing number of flexural cracks, beginning at the extreme tension face of the section. Eventually, cracks formed between the loading points, in a semi-circle pattern, and the beam failed soon after due to crushing of the concrete between the load points and yielding of the longitudinal reinforcement at midspan.

Through all of the shear failures, all beams in Series B18-PC, B18-B5-0.5, B24-B5-1.0, and B18-D1-1.0 failed in an identical manner. That being said, when the beams failed due to different failure modes within the same series, there was no trend that could be drawn in terms of ultimate load capacity. For that reason, all shear failures were analyzed together.

5.2.3. Crack Development and Behavior. Throughout each beam tested in this study, the first crack to form was as a result of flexure, within the middle third of the beam. The load at initial crack for the B18 beams ranged from 15 to 26 kips (67 to 116 kN). For the B24 series, the load at initial crack ranged from 20 to 28 kips (89 to 125 kN). Subsequent to the formation of the first shear crack, an increasing number of flexural cracks developed along the bottom section of the beam starting in the middle and expanding out to the support. Eventually, the flexural cracks reached a point between the longitudinal reinforcement and mid-depth of the beam, where they became inclined towards the point of loading. At this time, diagonal cracks around mid-depth of the beam were also

developing. The crack patterns of each beam in this study are shown throughout Section 4. As the load increased, an increasing number of diagonal and flexural cracks formed, at progressively closer spacing.

The B18-PC beams developed an average of 5 cracks in total between the two shear spans, prior to failure. Compared to the other beams in the study, this was the lowest average number of inclined cracks formed within a series. Series B18-D1-1.0 and B18-B5-0.5 developed approximately the same number of cracks, on average. Overall, the beams in the B24 series developed an average of 10 cracks versus an average of 7 for the LCFRC B18 beams. The LCFRC beams formed one more crack, on average, than the SFRC beams. Series B25-B5-1.0 was able to develop the same number of inclined cracks as Series B18-TR, with 11 total cracks. This behavior indicates beneficial shear crack development behavior of the LCFRC beams, especially at higher volume fractions.

5.2.3.1 Inclined crack spacing. The total spacing between all inclined cracks and average spacing of the inclined cracks formed in each beam were presented previously in Table 4.6. Inclined cracks were included in this count if they passed mid-depth of the section. In some FRC beams, typically those with higher volume fractions, multiple cracks developed from, and around, one main crack, due to the addition of the fibers in the concrete matrix. In these cases, only one crack was reported. Once the total number of cracks in each shear span were counted and the distance measured, the distance was divided by the number of cracks to determine the average spacing between the cracks.

Figure 5.16 shows the relationship between inclined crack spacing and normalized shear stress for each beam tested. From the data, it is shown that as the normalized shear stress increases, there is a decrease in the average spacing of the inclined cracks in the

section. This is usually due to the formation of an increasing number on inclined cracks, allowing the section to maintain higher load-carrying capacities. Figure 5.17 shows the relationship between inclined crack spacing and fiber volume fraction. The only observation that can be made is that at higher volume fractions, there is an increasing variability in average spacing of inclined cracks.

5.2.3.2 Inclined crack angle. Upon failure, the angle of the critical inclined crack was measured in each beam to determine if any correlations could be made. The results for each beam are reported in Table 4.6 and the averages for each series are reported in Table 5.1 The crack angle versus normalized shear stress for each beam tested is shown in Figure 5.18. Overall, the shallowest average angle of inclined crack was a result of shear-compression and diagonal tension failure, at 25° . A failure due to diagonal tension occurred at an average angle of 26° and a combination failure due to shear-tension and diagonal tension had the highest average angle of 29° .

Figure 5.19 shows the relationship between inclined crack angle and volume fraction for each beam tested. Similar to the finding in the previous section, as the fiber volume fraction increases, there is a higher variability in the angle of the critical inclined crack. Figure 5.20 shows the relationship between average inclined crack angle and fiber volume fraction for each series in this study. Series B18-PC presented the highest average inclined crack angle out of all the beams tested, at 32° . For all FRC beams tested, as the fiber volume fraction increased from 0.5% to 1.0%, the average angle of inclined crack increased as well.

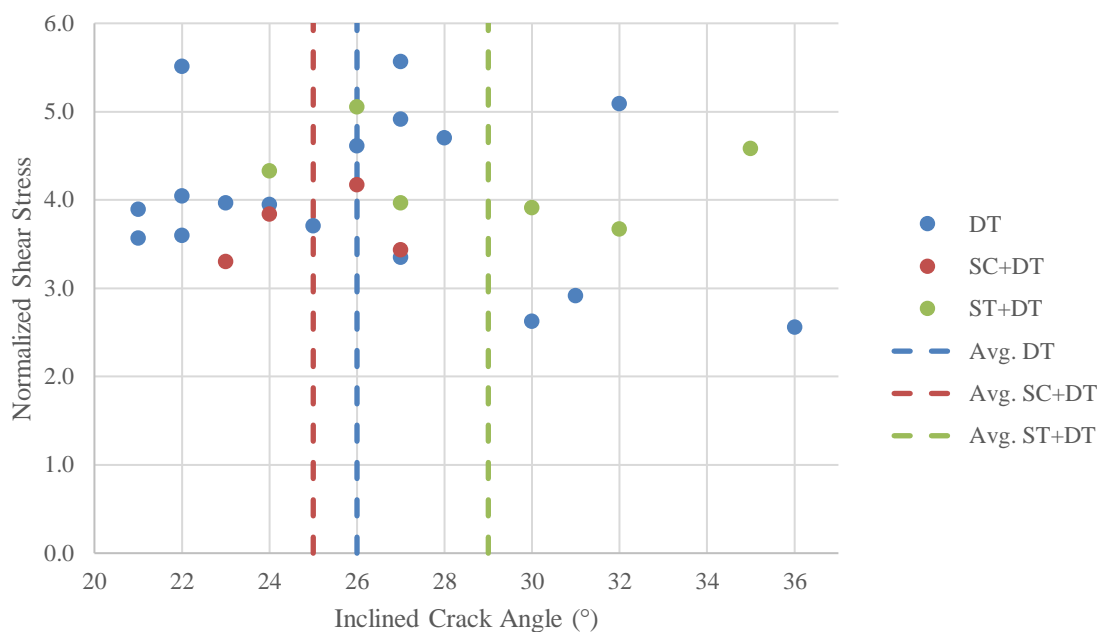


Figure 5.18. Normalized shear stress vs. inclined crack angle

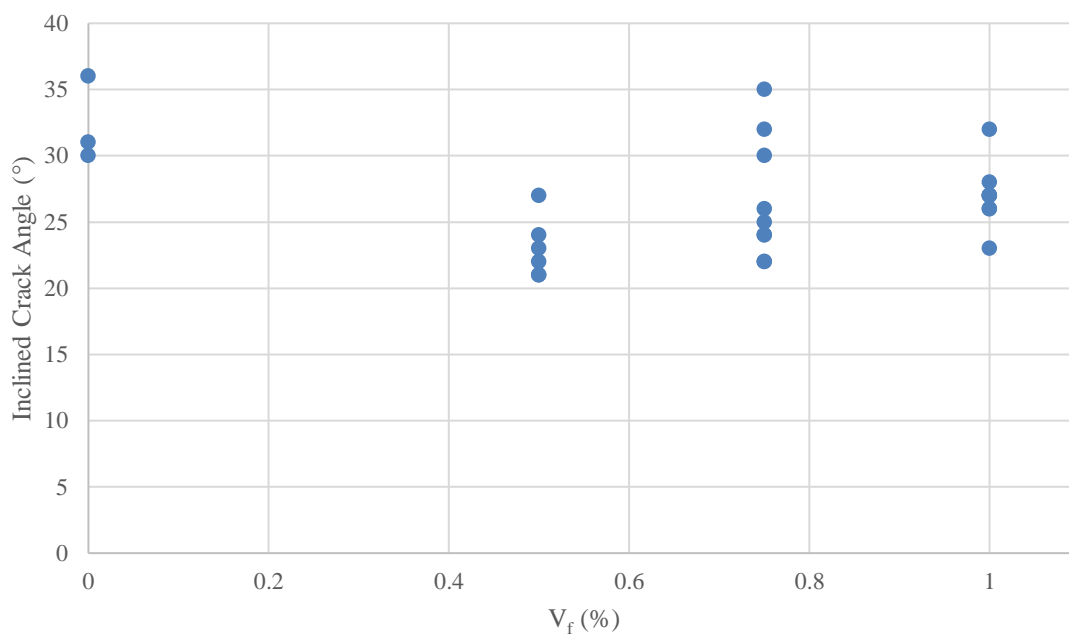


Figure 5.19. Inclined crack angle vs. V_f for large-scale shear tests

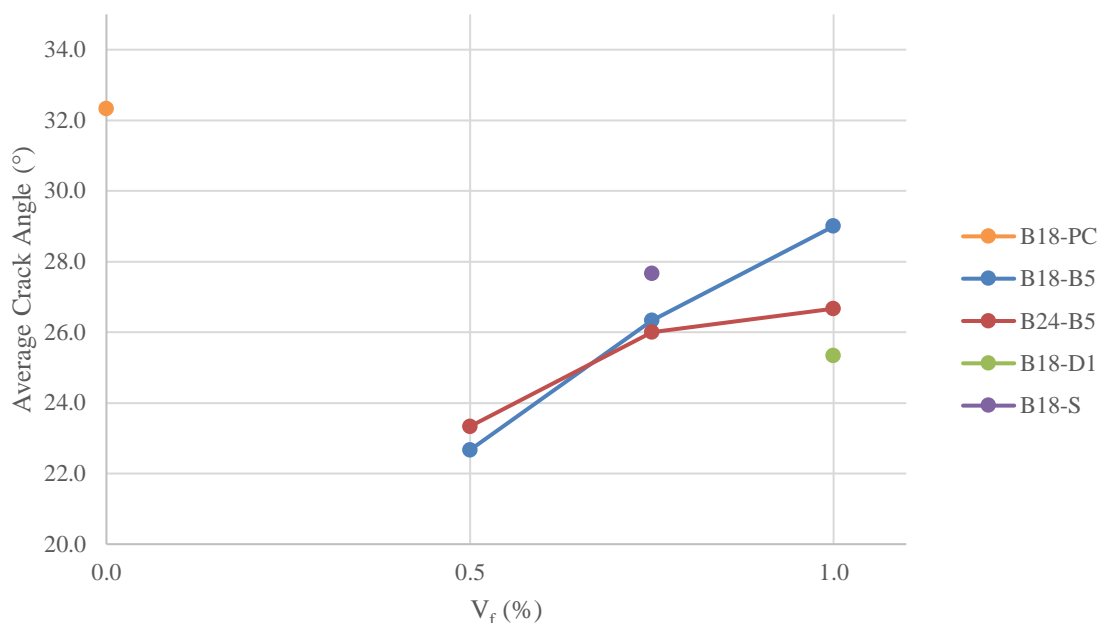


Figure 5.20. Average inclined crack angle vs. V_f for large-scale shear testing

5.3. EFFECTS OF VARIED PARAMETERS ON LARGE-SCALE SHEAR TESTING

The following sections discuss the effects of varying the fiber volume fraction, beam depth, and fiber type within this study. Figure 5.21 shows the relationship between fiber volume fraction and average normalized shear stress for each beam series. This figure will illustrate the main discussion points in the following sections.

In some studies, an equivalent fiber factor is used to compare results instead of volume fraction. The equivalent fiber factor is a product of the fiber aspect ratio and the volume fraction. In this study, the research team decided to compare the results based on fiber volume fraction. For reference, Fiber B5 at 1.0% has an equivalent fiber factor of 32, while the steel fibers at 0,75% have a factor of 60.

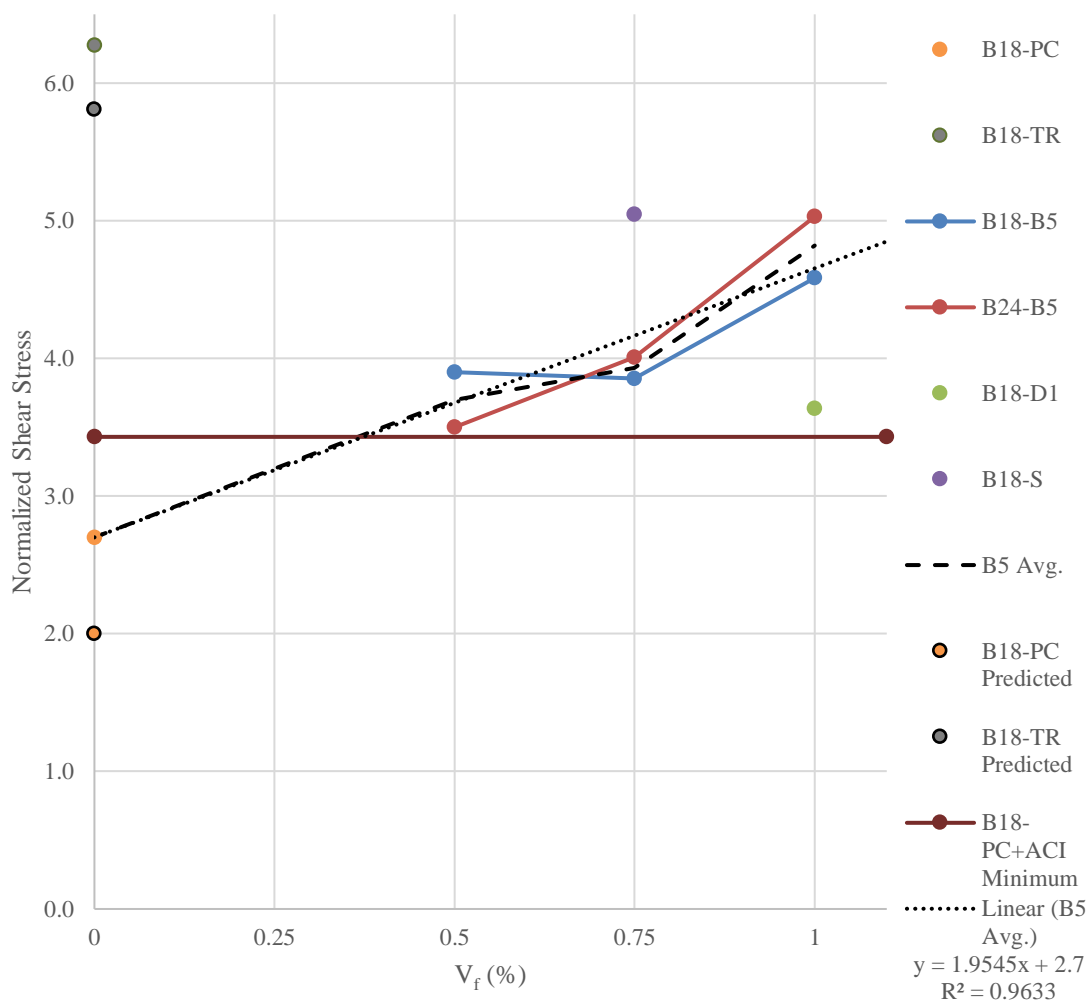


Figure 5.21. Normalized shear stress vs. V_f for each large-scale shear beam series

5.3.1. Effect of Fiber Volume Fraction. From Figure 5.21, it is apparent that as the fiber volume fraction is increased, the shear performance increases as well. The lowest average normalized shear stress resulted from Series B24-B5-0.5, still performing 30% better than the beams with no transverse reinforcement. Of the synthetic fibers tested, Series B24-B5-1.0 had the highest performance, with an average normalized shear stress of 5.03, 1.86 times the performance of Series B18-PC. The SFRC beams had a similar performance

to Series B24-B5-1.0 for the same volume fraction, with a normalized shear stress of 5.05. On average, between both beam depths, the B5 beams performed 1.4, 1.5, and 1.8 times better than Series B18-PC at volume fractions of 0.5%, 0.75%, and 1.0%, respectively. Observing the R^2 of 0.96 from the trendline on the graph, there is a strong correlation between the normalized shear stress performance of the LCFRC beams, when starting the trendline at 2.7, which is the average normalized shear stress of Series B18-PC. Calculating the shear stress provided by the minimum transverse shear reinforcement required by code yielded a normalized shear stress value of 3.43, when adding the concrete component from the control beams. As a result of the testing, on average, all FRC beams provided a normalized shear stress greater than required by code for minimum transverse reinforcement.

5.3.2. Effect of Beam Depth. The two selected depths for beams included in this study were 18 and 24 in. (457 and 609 mm). This allowed the research team to determine if there was a size effect on the LCFRC by increasing the depth 33% from Series B18 to B24. Comparing the two curves in Figure 5.21 for fibers B5 at varying depths, it is apparent that the beams performed similarly at the same fiber volume fractions. At volume fractions of 0.5%, 0.75%, and 1.0%, the LCFRC beams varied by 10.8%, 4.1%, and 9.4%, with the B18 series performing better at the 0.5% volume fraction and the B24 series performing better at the 0.75% and 1.0% volume fractions. As a result, the findings in this study indicate that beam depth has a negligible effect on normalized shear stress of FRC for beam depths up to 24 in. (609 mm). This finding confirms similar findings from the study done on SFRC by Dinh et al. (2009).

5.3.3. Effect of Fiber Type. From the results shown in Figure 5.21, it appears that regardless of the fiber type used in this study, at comparable volume fractions (based on workability or number of discrete fibers), the FRC beams performed similarly. Series B18-D1-1.0 performed 8% below the average of the Fiber B5 series beams at 0.75%. Series B18-S-0.75% performed 5% better than the average of the Fiber B5 series beams at 1.0%. Utilizing the ASTM C1609 results, the performance of the D1 fibers is similar to B5 at lower volume fractions, but appears to have a slight decrease in utility at higher volume fractions. Due to the major dissimilarities between the synthetic and steel fibers in terms of length and bond characteristics, it is interesting that they both provide similar shear resistance within the varied parameters, as well as, equivalent flexural strength ratios from ASTM C1609 testing, at comparable volume fractions. Comparing the SFRC results from this study to Dinh et al. (2009), for the same fiber type and similar testing conditions, the average normalized shear stress was 5.05 versus 6.0, representing a 20% better performance than the results in this study but still within expected variations for shear testing.

5.4. PREDICTION OF SHEAR PERFORMANCE OF FRC BEAMS

5.4.1. Prediction of Shear Performance Based on Previous Research. As discussed in Section 2, a majority of the research completed on shear performance and behavior of FRC has been undertaken with SFRC. Figure 5.22 shows the correlation between the measured performance of beams in this study versus predicted performance based on equations proposed by previous research discussed in Section 2. When a point falls above the 45-degree line, the equation underestimates the performance of the beam,

when the point falls below the line, its performance is overestimated. As shown in the graphs, the equation proposed by Sharma (1986) overestimated the ultimate shear stress, except in the beams that attained higher ultimate shear stresses. The equations proposed by Narayanan and Darwish (1987), Ashour, Hasanain, and Wafa (1992), and Khunita, Stojadinovic, and Goel (1999) all underestimated the performance of the beams in this study, especially the beams that reached higher ultimate shear stresses. As a result, these equations are conservative in terms of predicting the shear failure of LCFRC beams. (Due to the similarities in the performances between the LCFRC and the hooked-end steel fibers in this study, β was taken as 0.75 in the equations presented by Narayanan and Darwish (1987), Ashour, Hasanain, and Wafa (1992), and Khunita, Stojadinovic, and Goel (1999).)

None of the equations proposed in the studies included in this section relate the performance of large-scale shear tests to the performance of ASTM C1609 specimens. In the following section, a mechanics-based model using the results of ASTM C1609 testing is adapted from the research completed by Dinh et al. (2009). It will be shown that the prediction of shear performance based on ASTM C1609 results attained in this study provides a stronger correlation to the data.

5.4.2. Prediction of Shear Performance Using Mechanics-Based Model. The following section presents a mechanics-based model previously proposed by Dinh et al. (2009) using unreinforced concrete theory and ASTM C1609 results to predict the performance of FRC beams without stirrup reinforcement. Figure 5.23 shows the assumed behavior of the critical inclined crack and the distribution of stresses and strains in the section.

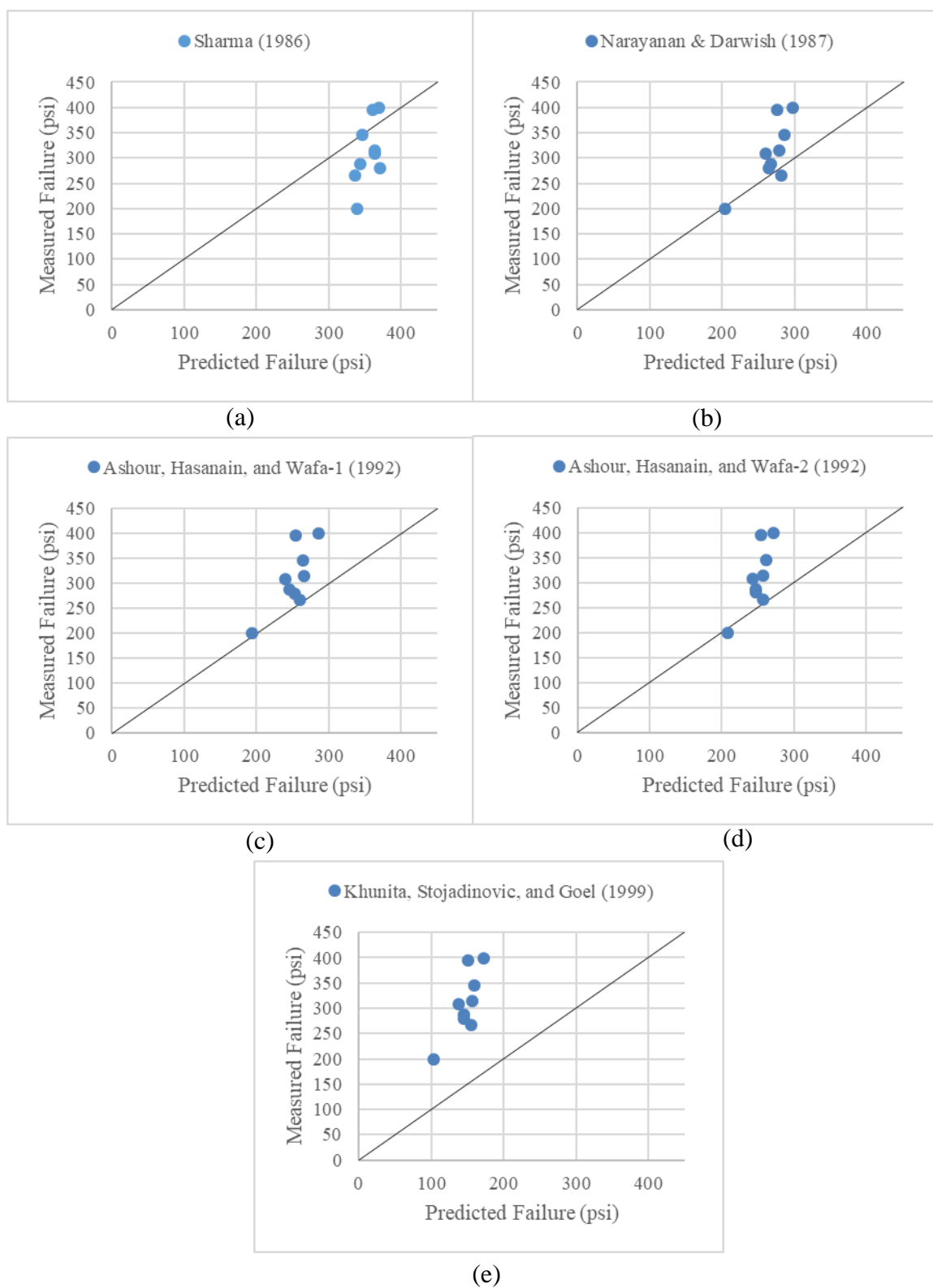


Figure 5.22. Shear strength prediction of FRC beams in this study using proposed equations from previous research

The approach assumes that an inclined shear crack, of width, w , extends from the top of the longitudinal reinforcement (Point N), at an angle, α , to the depth of the neutral axis (Point P), at the outer edge of the loading plate. At this location, the strain in the centroid of the reinforcement is ϵ_s and the strain in the extreme compression fiber is ϵ_{cm} . It is then assumed that the shear forces developed in the section are from the concrete, through the compression zone of the beam, between Points P and Q, and fiber tension, across the inclined shear crack, between Points N and P. Shear resistance due to aggregate interlock and dowel action are neglected due to their assumed minimal contribution. The ultimate shear strength is represented by Equation 5-1, where V_{cc} is the predicted shear force resisted by the compression region and V_f is the predicted shear force resisted by fiber tension.

$$V_u = V_{cc} + V_f \quad (\text{Equation 5-1})$$

For the beams in this study, α is taken as 40° , which provides a conservative estimate, based on the data collected, but due to the uncertainties with shear failure behavior, it provides an added factor of safety.

5.4.2.1 Prediction of shear force resisted by the compression region. The prediction of the shear force carried through the compression region of the concrete is based on Bresler and Pister's model (1955 and 1958) for predicting shear strength of plain concrete beams, containing no shear reinforcement. In their study, tubular specimens were subjected to axial compression and torsion at each end of the specimen. The researchers presented a failure criterion for concrete subjected to normal compressive stress, σ_{cu} , and shear stress, τ_{cu} , as shown in Equation 5.2

$$\frac{\tau_{cu}}{f'_c} = 0.1[0.62 + 7.86 \left(\frac{\sigma_{cu}}{f'_c}\right) - 8.46 \left(\frac{\sigma_{cu}}{f'_c}\right)^2]^{1/2} \quad (\text{Equation 5-2})$$

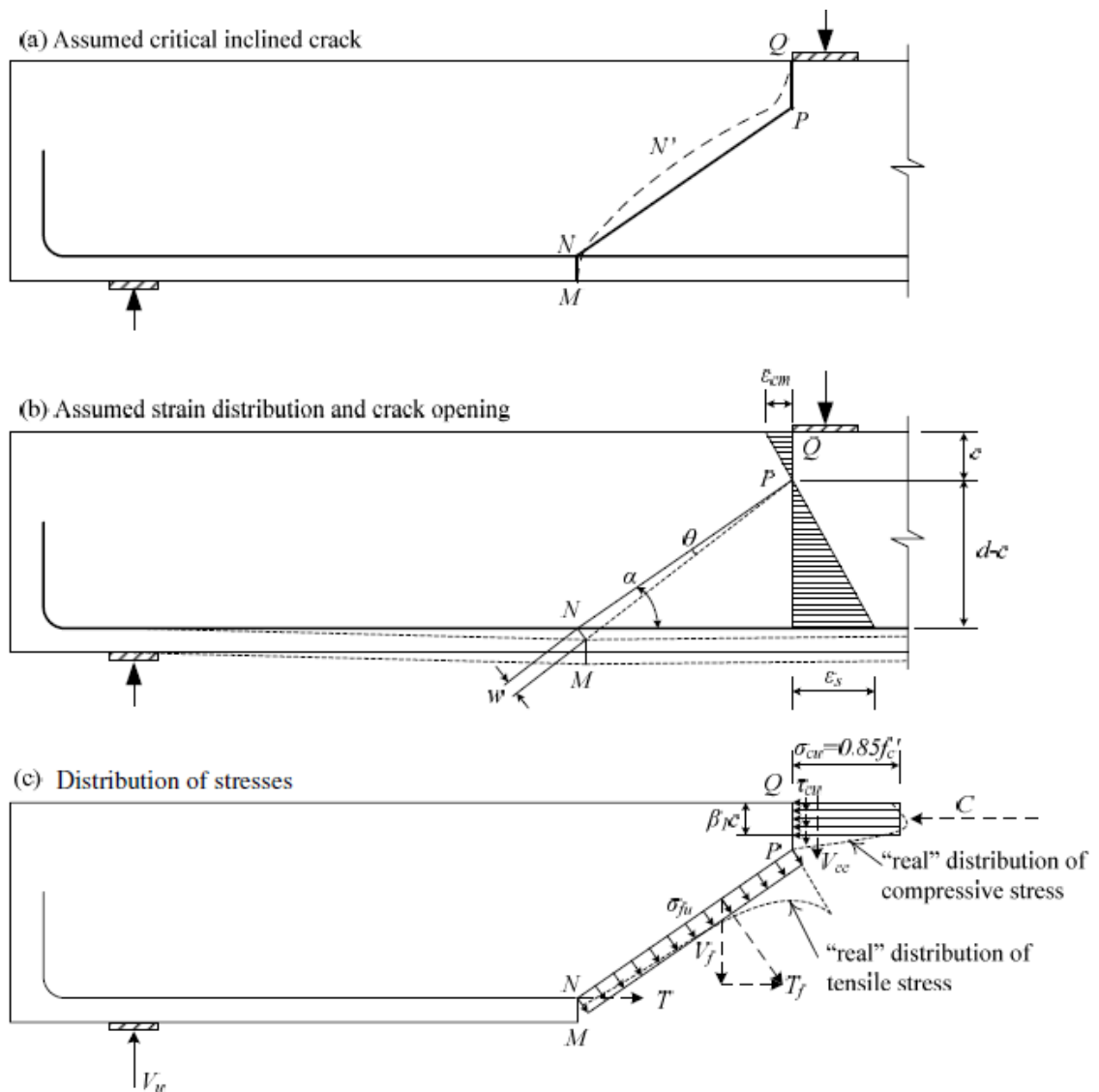


Figure 5.23. Proposed model to predict shear strength of FRC beams (Dinh et al., 2009)

Figure 5.24 shows the relationship, found by Bresler and Pister (1958), between the normal compressive stress and a coincident shear stress. When the concrete is in pure compression (i.e., no shear stress present), their equation predicts a compressive strength equal to f'_c . When the concrete is under a compressive stress between $0.39f'_c$ and $0.54f'_c$, their equation predicts an approximately consistent shear strength of $0.16f'_c$.

Bresler and Pister (1958) then used the above failure criterion to predict the shear strength of unreinforced concrete beams without stirrup reinforcement. The assumed uniform compressive stress at failure, σ_{cu} , is shown in Equation 5-3. The uniform compressive stress, calculated using Equation 5-3, is assumed to act over the depth of the compressive region, c in Figure 5.23b. The depth is calculated using the equation of equilibrium in the reinforced concrete section, assuming the longitudinal reinforcement has yielded.

$$\sigma_{cu} = \frac{3900 + 0.35f'_c}{3200 + f'_c} f'_c \quad (\text{Equation 5-3})$$

In order to simplify the approach, the model proposed by Dinh et al. (2009) used Whitney's Stress Block to estimate the normal compressive stress through the section of the beam in compression, where σ_{cu} is equal to the product of 0.85 and the concrete compressive strength. The longitudinal reinforcement ratio, ρ , is limited to 2% in order not to overestimate the shear performance of beams containing a high amount of flexural steel. Due to the constraints of the experimental setup, the beams were flexurally reinforced to ensure shear failure prior to flexural failure. For this reason, the area of steel in the beams has been artificially reduced to a corresponding ρ of 2% in order to compare measured strength to predicted resistance. With the above assumption, the depth of a uniform stress

block, c , is calculated using Equation 5-4, where A_s is the area of longitudinal steel, f_y is the yield strength of the longitudinal steel, f'_c is the concrete compressive strength, and b is the beam width.

The variable β_1 is calculated according to Equation 5-5 and is used as a factor to reduce the depth of the uniform compressive stress block. This is due to the fact that the stress acting across the section is not truly uniform, as represented by the Whitney's Stress Block in Figure 5.25(c). Finally, V_{cc} is then the product of the shear stress (τ , based on the Bresler and Pister relationship to equal $0.11f'_c$), β_1 , c , and the beam width, b . V_{cc} is shown in Equation 5-6.

$$c = \frac{A_s f_y}{0.85 \beta_1 f'_c b} \quad (\text{Equation 5-4})$$

$$\beta_1 = 1.05 - 0.05 \frac{f'_c}{1000} \quad (\text{Equation 5-5})$$

$$V_{cc} = (0.11 f'_c) * \beta_1 * c * b \quad (\text{Equation 5-6})$$

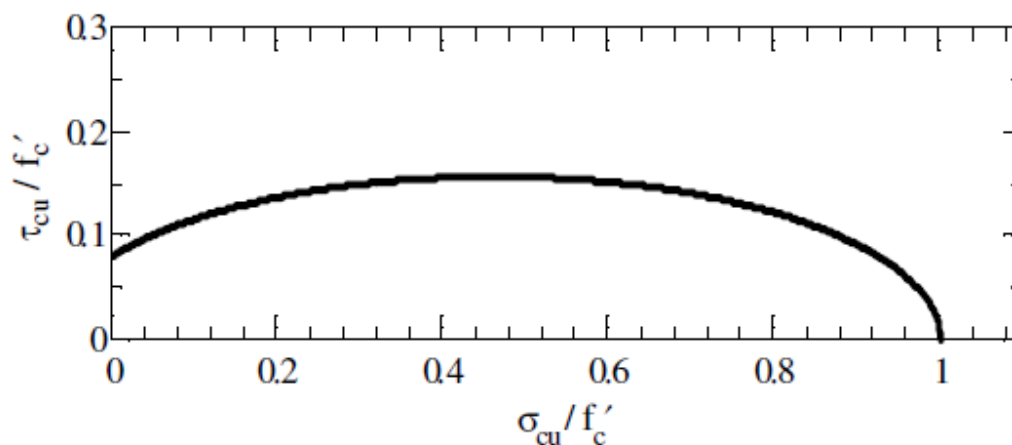


Figure 5.24. Normal compressive and shear stress relationship developed by Bresler and Pister (1958)

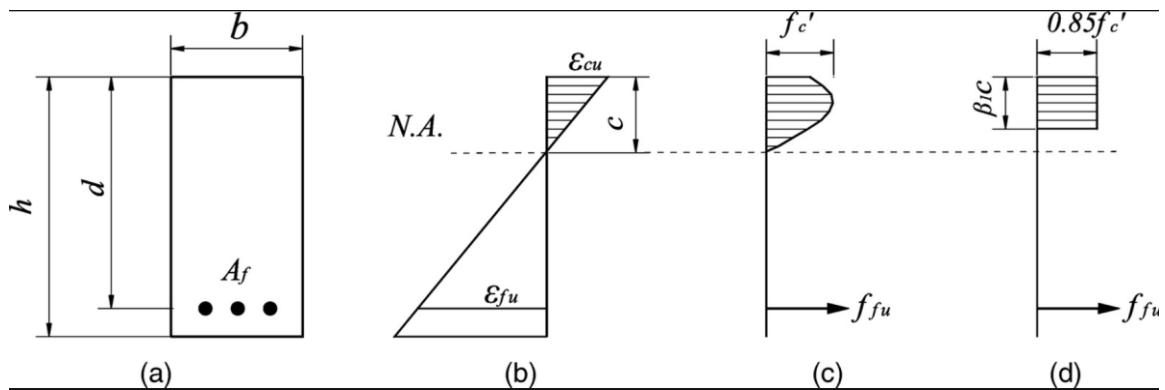


Figure 5.25. Stress-strain relationships in a RC beam (a) typical reinforced concrete section (b) typical strains across reinforced concrete section (c) typical stresses across reinforced concrete section (d) typical stresses across reinforced concrete section represented by Whitney's stress block

5.4.2.2 Prediction of shear force resisted by fiber tension. The contribution of the beam's shear resistance due to fiber tension is shown in Figure 5.23(c). The shear force resisted by fiber tension across the inclined shear crack is estimated as follows. The approach proposes an average tension stress acting along the crack from the top of the reinforcement to the bottom of the compression region of the beam, represented by Equations 5-7 and 5-8, where σ_{fu} is the equivalent uniform tensile stress. The equivalent uniform tensile stress can be determined from ASTM C1609 material testing, assuming that the forces acting along the inclined shear crack and the crack formed in the ASTM C1609 beams behave consistently.

$$V_f = T_f \cos \alpha = \sigma_{fu} b (d - c) \cot \alpha \quad (\text{Equation 5-7})$$

$$T_f = \sigma_{fu} b \frac{d-c}{\sin \alpha} \quad (\text{Equation 5-8})$$

The data collected in the ASTM C1609 testing is used to plot the result of each specimen, but instead of plotting load versus deflection data, the loads are converted into

equivalent uniform tensile stresses and the deflections are converted into crack widths at the extreme tension fiber, based on Figure 5.26. When calculating the forces in the cracked section, it is assumed that the uniform compressive stress is equal to $0.85f'_c$. Equation 5-9 is used to determine the moment at the cracked section, and the depth of the compression region in the beam, c , is calculated using Equation 5-10. Equation 5-11 is used to determine the moment in the center section based on a beam loaded at third points. This moment can also be used to calculate the uniform tensile stress in the beam using Equations 5-12 and 5-13.

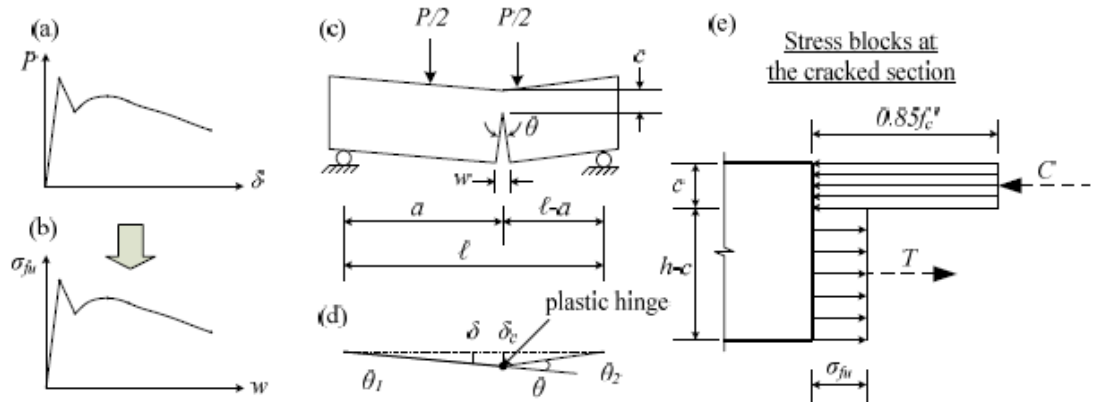


Figure 5.26. Derivation of uniform tensile stresses and crack width relationship (Dinh et al., 2009)

$$M = C x \frac{h}{2} = (0.85f'_c bc)x \frac{h}{2} \quad \text{(Equation 5-9)}$$

$$c = \frac{2M}{0.85f'_c bh} \quad \text{(Equation 5-10)}$$

$$M = \frac{P}{2} x \frac{l}{3} \quad \text{(Equation 5-11)}$$

$$M = T x \frac{h}{2} = \left(\sigma_{fu} b (h - c) \right) x \frac{h}{2} \quad (\text{Equation 5-12})$$

$$\sigma_{fu} = \frac{2M}{bh(h-c)} \quad (\text{Equation 5-13})$$

Data for each specimen in this study was generated using the equations above and used to calculate the shear forces in the large-scale beams resisted by fiber tension, as related to crack width. In the absence of crack width measurements, at the location of failure for the large-scale beams, the research team recorded the equivalent uniform tensile stresses at the maximum post-peak stress, beam displacement of L/600, beam displacement of L/300, beam displacement of L/150 in order to determine which value best predicted the large-scale beam performance.

Table 5.3 shows the data used to calculate the predicted shear strengths of each series and the comparison made to the tested values. Figure 5.27 shows a representation of the measured versus predicted loads for each series according to the maximum post peak stress, stress at L/600, and stress at L/300. As shown in the chart, the predicted shear load, based off ASTM C1609 stresses at a midspan displacement of L/600, fits well with the data generated in this study. The ratio of measured-to-predicted shear stresses spans from 0.88 to 1.34, but the stress from Series B24-B5-1.0 is slightly underrepresented by the ASTM C1609 data, which is why the model overpredicts the performance by such a large factor. Series B18-B5-0.75 was overpredicted by the model by the greatest margin, with a value of measured-to-predicted of 0.88. The steel fiber beams performed 1.02 times the predicted performance of the model. Overall, an average of each volume fraction for the LCFRC beams were evaluated, with measured versus predicted ratios of 1.02, 0.92, and 1.03 for volume fractions of 0.5%, 0.75%, and 1.0%, respectively. This signifies a good fit for the

prediction model of the shear performance of the large-scale shear beams in this study to the data collected. The reason B5-0.75 is slightly overpredicted is the low performances of the large-scale beams, compared to the trend, as well as slightly high ASTM C1609 results, compared to the other series. Further investigations should be done on the Innegra fibers to verify the validity of the model over a larger set of data, but the single data point provided by the beams reinforced with the Innegra fibers exactly predicted the performance of the large-scale beams.

From the data presented above and the correlation of the trendline in Figure 5.27, it was determined that the equivalent uniform tensile stress at a displacement of $L/600$ for the C1609 tests best predicts the ultimate shear strength from the data generated in this study and should be used in the model to predict the contribution of shear resistance from the FRC. A similar approach was proposed by Dinh et al. (2009), but, those researchers took the equivalent uniform tensile stress at the post-peak location along the curve.

Using the proposal above is beneficial if there are small-scale, C1609 beams fabricated alongside the beams that will be used in a real-world condition. For that reason, Dinh et al. (2009) proposed Equation 5-14 in situations when small-scale beams are not fabricated, where σ_{fu} is estimated based on fiber aspect ratio, fiber volume fraction, and a constant generated from empirical data. For hooked-end steel fibers, at volume fractions similar to the range in this study, K was proposed to be 400 psi. Figure 5.28 shows the relationship between the measured and predicted shear strengths based on a K values ranging from 400 to 900 psi. The aspect ratio for both the carbon and Innegra fibers was 32, the steel fibers had an aspect ratio of 80.

When comparing the different curves generated, it is apparent that using a $K = 800$ in Equation 5-14 provides the best estimate of shear performance for the LCFRC. This prediction fits well with the data collected in this study, with a range of measured-to-predicted values from 0.88 to 1.13. Series B24-B5-1.0 had the highest value, 1.13. When comparing the data, it is a result of the high performance of this series compared to the average trend. The second to highest value recorded was from Series B18-B5-0.5, with a value of 1.01; the model predicted the performance of this series the best. Overall, the average of the LCFRC beams produced a measured-to-predicted ratio of 0.96, 0.92, and 1.06 at volume fractions 0.5%, 0.75%, and 1.0%, respectively, showing reasonable prediction capabilities of the model, although it does appear that the model has a tendency to under predict the performance to a greater degree at higher volume fractions. In design, this would provide a greater safety factor for the engineer, which would be beneficial considering there was higher variation in the data at higher fiber volume fractions. It should be noted that the K value proposed by Dinh et al. (2009) was generated from a number of ASTM C1609 beams, while the K generated in this study is based on empirical data from 15 beams fit to Equation 5-14.

$$\sigma_{fu} = K * \frac{L_f}{D_f} \sqrt{0.0075V_f} \quad (\text{Equation 5-14})$$

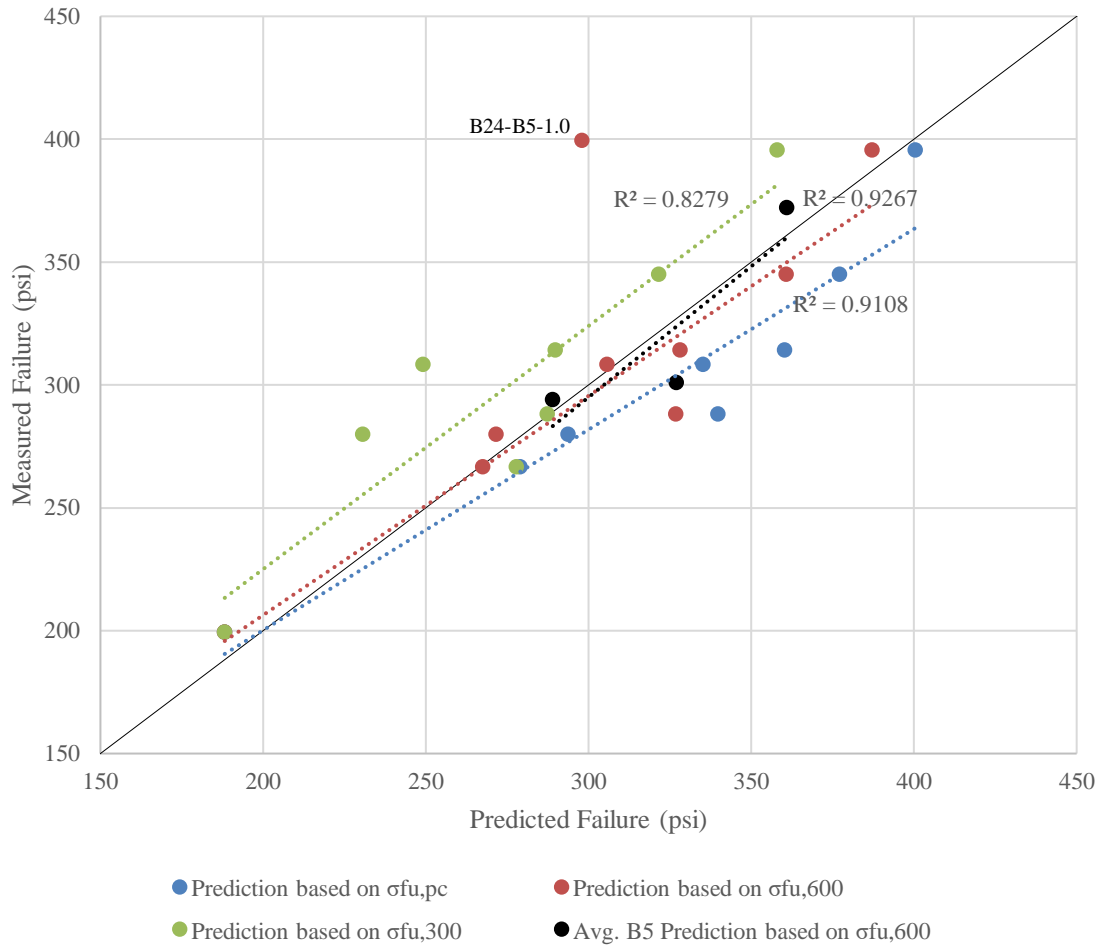


Figure 5.27. Measured vs. predicted shear stresses for each series based on ASTM C1609 data

Table 5.3. Predicted and measured shear strengths for each beam series

Series	P/2 (kips)	β_1	c (in.)	V_c (kips)	σ_{fupc} (psi)	$\sigma_{fu,600}$ (psi)	$\sigma_{fu,300}$ (psi)	$\sigma_{fu,150}$ (psi)	V_{fupc} (kips)	$V_{r,600}$ (kips)	$V_{r,300}$ (kips)	$V_{r,150}$ (kips)	V_{upc} (kips)	$V_{u,600}$ (kips)	$V_{u,300}$ (kips)	$V_{u,150}$ (kips)	meas. / pred. (pc) (%)	meas. / pred. (L/600) (%)	meas. / pred. (L/300) (%)
B18-PC	24	0.78	5.95	22									22.2	22.2	22.2	22.2	1.06	1.06	1.06
B18-B5-0.5	36	0.74	5.47	22	196	157	82	49	17.3	13.9	7.2	4.3	39.6	36.1	29.4	26.6	0.92	1.01	1.24
B18-B5-0.75	34	0.77	5.86	22	212	193	138	93	17.9	16.4	11.7	7.9	40.1	38.6	33.9	30.1	0.85	0.88	1.00
B18-B5-1.0	41	0.77	5.81	22	262	239	185	131	22.3	20.4	15.7	11.1	44.5	42.6	38.0	33.3	0.91	0.96	1.07
B24-B5-0.5	45	0.73	7.21	30	143	114	60	41	17.5	14.0	7.4	5.0	47.1	43.6	37.0	34.6	0.95	1.03	1.21
B24-B5-0.75	50	0.74	7.38	30	234	191	140	77	28.2	23.0	16.9	9.3	57.8	52.6	46.5	38.9	0.87	0.96	1.08
B24-B5-1.0	64	0.73	7.26	30	197	150	100	55	23.9	18.2	12.2	6.7	53.5	47.8	41.8	36.4	1.20	1.34	1.53
B18-D1-1.0	31	0.78	6.01	22	129	113	127	107	10.7	9.4	10.6	8.9	32.9	31.6	32.8	31.1	0.96	1.00	0.96
B18-S-0.75	47	0.74	5.53	22	286	268	228	155	25.1	23.5	20.0	13.6	47.3	45.7	42.3	35.8	0.99	1.02	1.10
B5-0.5	294 (psi)												315	289	240		0.93	1.02	1.23
B5-0.75	301 (psi)												350	327	289		0.86	0.92	1.04
B5-1.0	372 (psi)												378	361	322		0.98	1.03	1.16

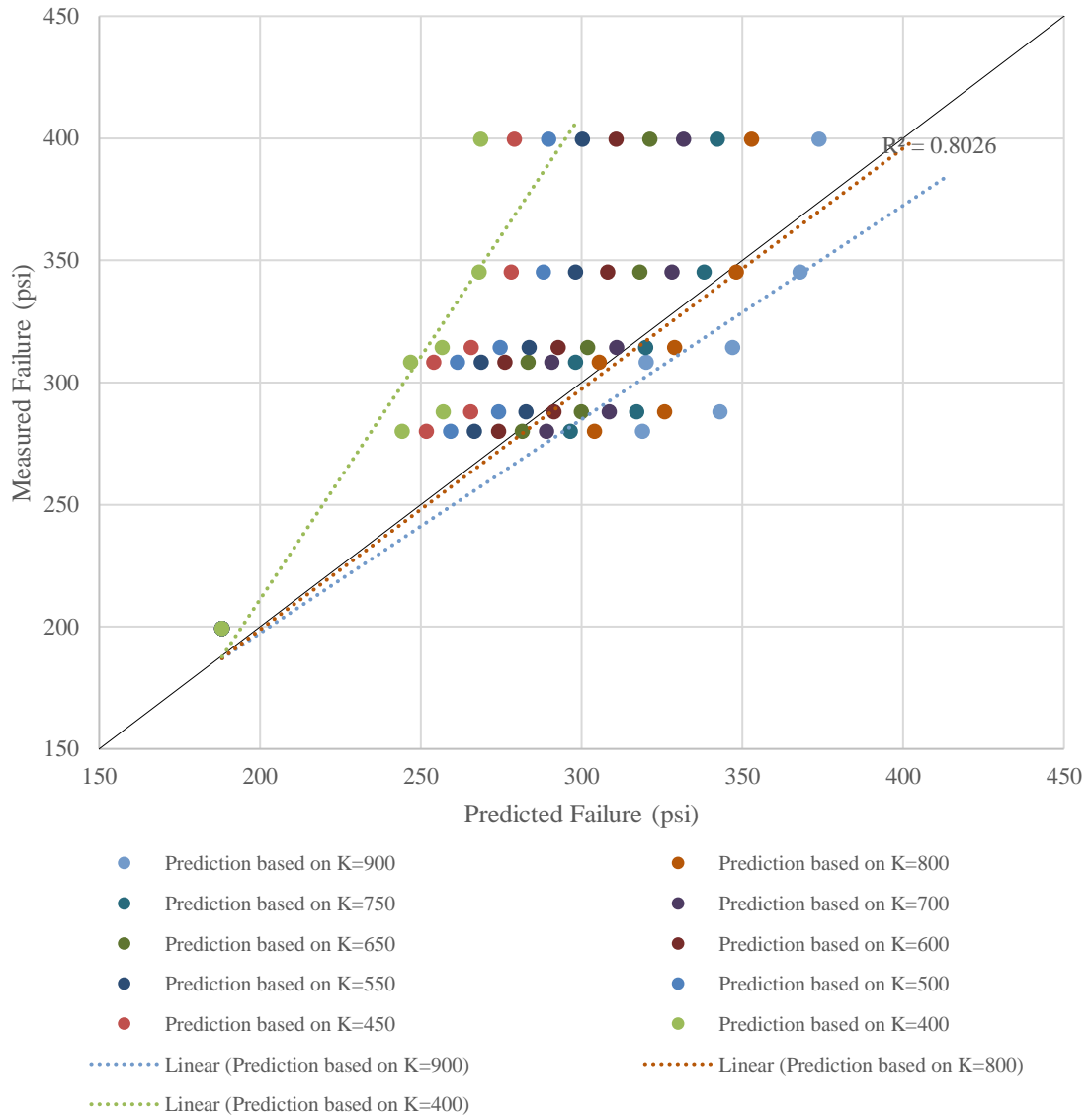


Figure 5.28. Measured vs. predicted loads based on empirical equation

6. FINDINGS, CONCLUSIONS, AND RECOMMENDATIONS

6.1. SUMMARY OF RESEARCH PROGRAM

At the onset of the research program, the research team aimed to further develop the LCFRC previously developed and tested for blast and impact loading, and investigate the material's potential for use in shear applications of structural concrete members. At the moment, steel fiber reinforced concrete is a widely used material in the construction market and has been adopted for use by ACI 318-14 "Building Code Requirements for Structural Concrete." Given specific criterion are met, SFRC is allowed to replace the minimum transverse steel required for shear reinforcement. Given the fact that steel fibers are the only fiber type allowed to replace traditional mild steel shear reinforcement, the research team initiated a research program to evaluate the potential for LCFRC to also be used as replacement of minimum transverse steel.

The research team began by refining the mix design used in the previous research program, in efforts to reduce the strength and potential cost of the mix, while maintaining the fresh properties of the mix design that allow for uniform fiber distribution and placement of the FRC. Once the mix design was established, six carbon fiber variants were evaluated at varying volume fractions, using ASTM C1609 testing to compare the performance and behavior. The results of the ASTM C1609 testing were used to select the variant to be used in the large-scale shear testing. Different fiber types were also evaluated in the small-scale testing phase to assess the performance of fibers with different material properties. The ASTM C1609 testing was also used to determine if each set of specimens passed the current ACI 318-14 criteria to be allowed for use as minimum shear reinforcement.

The research team determined that Fiber B5 possessed the best properties, with regard to the fresh and hardened concrete, and selected it to be used in the large-scale shear testing. The large-scale shear tests included 30 simply-supported beams that were tested to failure under monotonic loading. There were ten beam series tested, with three replicate beams included in each series to determine the consistency in the performance of the FRC. Each beam tested had two shear spans, with an approximate shear span-to-effective depth ratio of 3.5. The beams were flexurally reinforced to ensure shear failure prior to failure due to flexure, with a reinforcement ratio of approximately 3%. The target compressive strength for the beams tested was 6000 psi (41 Mpa), with an actual tested range between 5400 and 6400 psi (37 to 44 MPa).

The studied parameters within this research program were fiber volume percentage, fiber type, and beam depth. A total of 21 out of the 30 beams tested had a beam depth of 18 in. (457 mm), with the remaining nine having a depth of 24 in. (610 mm). There were two control series of the 18 in. (457 mm) deep sections, one without any transverse steel reinforcement and one containing #3 rebars at 7 in. (179 mm) on center, to compare with the performance and behavior of the FRC beams. There were nine LCFRC beams tested at each depth containing volume fractions of 0.5%, 0.75%, and 1.0%. At the 18 in. (457 mm) depth, there were two additional series, one containing single-hooked end steel fibers at volume fraction of 0.75% and the other containing twined Innegra S fibers, produced in the same method as the carbon fibers in this study. The carbon and Innegra fibers had an aspect ratio of 32, while the steel fibers had an aspect ratio of 80. At the same time as the large-scale beams were cast, six ASTM C1609 beams were cast to determine the

performance compared to ACI requirements for transverse reinforcement, as well as evaluate the trends between the small-scale and large-scale testing.

6.2. FINDINGS OF THE RESEARCH PROGRAM

Based on the small-scale testing, the research team was successfully able to develop a superior long carbon fiber, as well as further refine the mix design, which provided suitable performance in terms of both fresh and hardened concrete properties. The results showed that regardless of the changes made to the mix design, the performance of Fiber B3 at a volume fraction of 1.0% remained consistent. In general, as the volume fraction of fibers increased, the corresponding ASTM C1609 performance increased, in terms of σ_{pc} , σ_{600} , σ_{150} , and the equivalent flexural strength ratios. It was shown that the load-displacement behavior of the carbon fibers and Innegra fibers was drastically different, while providing a similar average equivalent flexural strength ratio. A combination of the two fiber types resulted in an increased flexural strength ratio and improved load-displacement behavior compared to each fiber used individually. The SFRC had similar load-displacement behavior to the LCFRC.

Of the carbon fiber variants tested, it was found that for Fibers B3 and B5, at volume fractions above 1.5%, the ASTM C1609 performance achieved the requirements necessary to use the fibers as replacement for the minimum transverse steel according to ACI 318-14. A similar finding was discovered for the Innegra fibers at volume fractions of 1.8% and 2.4%. The SFRC specimens at a volume fraction of 0.75% did not meet the requirements of ACI 318-14.

The large-scale testing resulted in ultimate shear stresses of the carbon fiber-reinforced beams between 288 and 399 psi (2 and 2.8 Mpa). The ultimate shear stress for the beams reinforced with Innegra fibers was 267 psi (1.8 Mpa), and with SFRC, the ultimate shear stress was 395 psi (2.7 Mpa). These ultimate shear stresses correspond to normalized shear stresses of 3.85 to 5.03 for the LCFRC, 3.64 for the Innegra fibers, and 5.05 for the SFRC. The plain concrete specimens had an average normalized shear stress of 2.7, while the specimens containing traditional transverse reinforcement had an average normalized shear stress of 6.28.

Similar to the small-scale testing, the results showed that as the fiber volume fraction increased, the corresponding average normalized shear stress increased. This finding was displayed in both the 18 in. and 24 in. (457 and 610 mm) deep sections. The results also showed that at higher volume fractions, the benefit of performance slightly decreased, compared to lower volume fractions. The results from the Innegra and steel fiber reinforced concrete beams provided similar shear resistance to the carbon fiber reinforced beams at comparable volume fractions. The addition of the fibers to the concrete resulted in improved load-deflection behavior and crack development within the beams.

All FRC beams tested provided shear resistance higher than the predicted normalized shear strength of a minimally reinforced concrete beam. In contrast to this finding, none of the average results from the ASTM C1609 specimens cast with the large-scale specimens were able to achieve the ACI requirements for allowing fibers in place of transverse steel. It was shown that the ASTM C1609 specimens, regardless of fiber type, achieved an average equivalent beam strength ratio above 30%, providing the necessary

shear resistance in the large-scale testing of corresponding specimens. All fibers tested in this study achieved this result at volume fractions of 0.5% and above.

Using both the results from the small and large-scale testing, a mechanistic model was proposed to predict the shear performance of large-scale LCFRC beams (up to 24 in. (610 mm) deep). The model proposed a total shear stress of the LCFRC beams as a sum of the contribution of the shear resistance provided by the concrete compression region and the fibers crossing the critical inclined crack. The average tensile stress provided by the fibers was calculated using the results from the ASTM C1609 testing. The model corresponded well with the measured values from the large-scale beams in this study.

6.3. CONCLUSIONS

The following conclusions were taken from the results of the research program.

- a) Long carbon fibers developed in this study measuring 4 in by 0.125 in. (102 by 3.2 mm) can be used in concrete mixtures at up to 2.0% volume addition when placed without reinforcing steel and up to 1.5% with the presence of reinforcing steel.
- b) Fibers comprised of Innegra S material, undergoing similar processing treatments to the carbon fibers developed, can be used at comparable volume fractions as the carbon fibers.
- c) The placement of SFRC at a volume fraction of 0.75% was similar to the placement of the LCFRC at 1.0%.
- d) An increase in volume fraction of the long carbon fibers results in improved ASTM C1609 behavior and performance for volume fractions between 0.5% and 2.0%. This

- strength gain is also exhibited with the Innegra S fibers, but at higher volume fractions, less performance increase is seen.
- e) The ACI 318-14 requirements for replacement of transverse steel with SFRC can be met for concrete mixes containing carbon and Innegra fibers at volume fractions above 1.5% and 1.8%, respectively.
 - f) An increase in volume fraction of the long carbon fibers results in improved shear resistance of FRC members between volume fractions of 0.5% and 1.0%.
 - g) Innegra and steel fibers, at comparable volume fractions to the long carbon fibers, provide similar shear resistance to the carbon fibers tested in this study.
 - h) Beam depth did not represent a significant factor in the shear performance of the LCFRC beams.
 - i) Long carbon fibers, long Innegra fibers, and steel fibers at volume fractions above 0.5% provide a higher supplementary shear resistance than that predicted using ACI 318-14 regulations as a guide.
 - j) Although at the volume fractions used in the large-scale testing, the FRC did not meet the ACI requirements for use as minimum shear reinforcement, the tested values for all series were higher than the predicted shear strength of a minimally reinforced beam.
 - k) The ACI 318-14 requirements for SFRC to be used in place of minimum transverse reinforcement may not truly evaluate the necessary behavior for FRC to be used in concrete construction.
 - l) A mechanistic model proposed showed the shear capacity of LCFRC beams can be predicted using a combination of the ASTM C1609 results and the shear failure

criterion recommended by Bresler and Pister for concrete without transverse reinforcement, with remarkable fit to the data.

- m) Based on the results presented, macro-synthetic fibers with similar tensile strength, modulus of elasticity, bond characteristics, and aspect ratio to the synthetic fibers used in this study could be allowed for use as minimum shear reinforcement by ACI 318.

6.4. RECOMMENDATIONS

Based on the findings of this study, the research team proposes the following recommendations for future investigation.

- a) Further ASTM C1609 testing of carbon and Innegra fibers to increase the database for historical testing of the materials and to further understand the differences between load-displacement behavior and ultimate performances.
- b) Further development of long synthetic fibers using a combination of materials to take advantage of individual properties and potential performance increases, as well as cost reduction of the product.
- c) Additional large-scale shear testing of long synthetic fiber reinforced concrete to build on the knowledge gained from this study, as well as further understand the shear performance and behavior capabilities of long synthetic fiber reinforced concrete.
- d) Expanded application testing of long synthetic fibers to understand the potential of the material and differences in performance and behavior to SFRC.

BIBLIOGRAPHY

- ACI Committee 318. (2011). *Building Code Requirements for Structural Concrete and Commentary*, American Concrete Institute, Farmington Hills, MI, 465.
- ACI-ASCE Committee 426 (1973). *The Shear Strength of Reinforced Concrete Members*. ACI Journal Proceedings, 70(7), 471-473.
- ACI Committee 544. (1989). *Report on Fiber Reinforced Concrete (Reapproved 2009)*. American Concrete Institute, Farmington Hills, MI.
- ACI Committee 544. (1989). *Measurement of Properties of Fiber Reinforced Concrete (Reapproved 2009)*. American Concrete Institute, Farmington Hills, MI.
- ACI Committee 544. (1988). *Design Considerations for Steel Fiber Reinforced Concrete (Reapproved 2009)*. American Concrete Institute, Farmington Hills, MI.
- Ashour, S. A., Hasanain, G. S., and Wafa, F. F. (1992). "Shear Behavior of High-Strength Fiber Reinforced Concrete Beams." *ACI Structural Journal*, 89(2), 176-184.
- ASTM A370, "Standard Test Methods and Definitions for Mechanical Testing of Steel Products," ASTM International.
- ASTM A615, "Standard Specification for Deformed and Plain Carbon-Steel Bars for Concrete Reinforcement," ASTM International.
- ASTM C39, "Standard Test Method for Compressive Strength of Cylindrical Concrete Specimens," ASTM International.
- ASTM C78, "Standard Test Method for Flexural Strength of Concrete (Using Simple Beam with Third-Point Loading)," ASTM International.
- ASTM C143, "Standard Test Method for Slump of Hydraulic-Cement Concrete," ASTM International.
- ASTM C192, "Standard Practice for Making and Curing Concrete Test Specimens in the Laboratory," ASTM International.
- ASTM C469, "Standard Test Method for Static Modulus of Elasticity and Poisson's Ratio of Concrete in Compression," ASTM International.
- ASTM C496, "Standard Test Method for Splitting Tensile Strength of Cylindrical Concrete Specimens," ASTM International.

- ASTM C1609/1609M. (2006) "Standard Test Method for Flexural Performance of Fiber-Reinforced Concrete (Using Beam with Third-Point Loading)." ASTM International, West Conshohocken, PA.
- Batson, G., Jenkins, E., and Spatney, R. (1972). "Steel Fibers as Shear Reinforcement in Beams." *ACI Journal Proceedings*, 69(10), 640-644.
- Bresler, B., and K.S., Pister. (1958). "Strength of Concrete under Combined Stresses." *ACI Journal Proceedings*, 55(9), 321-345.
- Casanova, P., and Rossi, P. (1999). "High-Strength Concrete Beams Submitted to Shear: Steel Fibers versus Stirrups." *ACI Special Publication*, 182, 53-68.
- Cho, S.-H., and Kim, Y.-I. (2003). "Effects of Steel Fibers on Short Beams Loaded in Shear." *ACI Structural Journal*, 100(6), 765-774.
- Cucchiara, C., La Mendola, L., and Papia, M. (2004). "Effectiveness of Stirrups and Steel Fibres as Shear Reinforcement." *Cement and Concrete Composites*, 26(7), 777-786.
- Dinh, H. H., Parra-Montesinos, G. J., and Wight, J. K. (2010). "Shear Behavior of Steel Fiber Reinforced Concrete Beams without Stirrup Reinforcement." *ACI Structural Journal*, 107(5), 597-606.
- Dinh, H. H., Parra-Montesinos, G. J., and Wight, J. K. (2011). "Shear Strength Model for Steel Fiber Reinforced Concrete Beams without Stirrup Reinforcement." *ASCE Journal of Structural Engineering*, 137(10), 1039-1051.
- Dwarakanath, H. V., and Nagaraj, T. S. (1991). "Comparative Study of Predictions of Flexural Strength of Steel Fiber Concrete." *ACI Structural Journal*, 88(6), 714-720.
- Fanella, D. A., and Naaman, A. E. (1985). "Stress-Strain Properties of Fiber Reinforced Mortar in Compression." *ACI Journal Proceedings*, 82(4), 475-483.
- Han, S.-M., Kong, J.-S., Kim, S.-W., Kang, S.-T., and Park, H.-G. (2004). "Shear and Flexural Behavior of I-Shaped RC Beams Made of Steel Fiber Reinforced Cementitious."
- Hota, S., and Naaman, A. E. (1997). "Bond Stress-Slip Response of Reinforcing Bars Embedded in FRC Matrices under Monotonic and Cyclic." *ACI Structural Journal*, 90(5), 525-537.

- Khuntia, M., Stojadinovic, B., and Goel, S. C. (1999). "Shear Strength of Normal and High-Strength Fiber Reinforced Concrete Beams without Stirrups." *ACI Structural Journal*, 96(2), 282-289.
- Kim, S.-W., Kang, S.-T., Koh, K.-T., Kim, D.-G., and Han, S.-M. (2004). "Shear and Flexural Behavior of Rectangular Beams Made of Steel Fiber Reinforced Cementitious Composite."
- Kwak, Y.-K., Eberhard, M. O., Kim, W.-S., and Kim, J. (2002). "Shear Strength of Steel Fiber-reinforced Concrete Beams without Stirrups." *ACI Structural Journal*, 99(4), 530-538.
- Li, V. C., Ward, R., and Hamza, A. M. (1992). "Steel and Synthetic Fibers as Shear Reinforcement." *ACI Materials Journal*, 89(5), 499-508.
- Lim, D. H., and Oh, B. H. (1999). "Experimental and Theoretical Investigation on the Shear of Steel Fibre Reinforced Concrete Beams." *Engineering Structures*, 21(10), 937-944.
- Mansur, M. A., Ong, K. C. G., and Paramasivam, P. (1986). "Shear Strength of Fibrous Concrete Beams Without Stirrups." *ASCE Journal of Structural Engineering*, 112(9), 2066-2079.
- Minelli, F. and Plizzari, G.A. (2013). "On the Effectiveness of Steel Fibers as Shear Reinforcement." *ACI Structural Journal*, 110(3), 379-389.
- Morgan, P., Carbon Fibers and Their Composites (Materials Engineering), CRC Press, May 20, 2005, 1200 pp.
- Naaman, A. E. (1985). "Fiber Reinforcement for Concrete." *Concrete International*, 7(3), 5.
- Naaman, A. E., and Najm, H. (1991). "Bond-Slip Mechanisms of Steel Fibers in Concrete." *ACI Materials Journal*, 88(2), 135-145.
- Narayanan, R., and Darwish, I. Y. S. (1987). "Use of Steel Fibers as Shear Reinforcement." *ACI Structural Journal*, 84(3), 216-227.
- Parra-Montesinos, G. J. (2006). "Shear Strength of Beams with Deformed Steel Fibers." *Concrete International*, 28(11), 57-66.
- Shah, S., and Rangan, B. V. (1971). "Fiber Reinforced Concrete Properties." *ACI Journal Proceedings*, 68(2), 126-35.

- Sharma, A. K. (1986). "Shear Strength of Steel Fiber Reinforced Concrete Beams." *ACI Journal Proceedings*, 83(4), 624-628.
- Susetyo, J., Gauvreau, P., and Vecchio, F. J. (2011). "Effectiveness of Steel Fibers as Minimum Shear Reinforcement." *ACI Structural Journal*, 108(4), 488-496.
- Swamy, R. N., and Bahia, H. M. (1985). "Effectiveness of Steel Fibers as Shear Reinforcement." *Concrete International*, 7(3), 35-40.
- Wafa, F. F., and Ashour, S. A. (1992). "Mechanical Properties of High-strength Fiber Reinforced Concrete." *ACI Materials Journal*, 89(5), 449-455.
- Wight, J. K., and MacGregor, J. G. (2005). *Reinforced Concrete: Mechanics and Design*, Pearson Prentice Hall.
- Wille, K. and Parra-Montesinos, G.J. (2012). "Effect of Beam Size, Casting Method, and Support Conditions on Flexural Behavior of Ultra-High-Performance Fiber-Reinforced Concrete." *ACI Materials Journal*, 109(3), 379-388.
- Zheng, Z., and Feldman, D., (1993). *Third Canadian Symposium on Cement and Concrete*. Ottawa, Canada.

VITA

Benjamin Paul Gliha was born in Hartford, Connecticut. He attended elementary schools in the East Hampton School District and graduated from East Hampton High School in May 2005. The following August he entered The Pennsylvania State University and in May of 2009 received the degree of Bachelor of Science in Civil Engineering. He entered Missouri University of Science and Technology in August 2009 and received a Master of Science Degree in Civil Engineering in May 2011. He returned to Missouri University of Science and Technology in August 2012 and received a Doctor of Philosophy Degree in Civil Engineering in May 2018.